

**HYDRAULICALLY FRACTURED WELLS
IN HETEROGENEOUS RESERVOIRS:
INTERACTION, INTERFERENCE,
AND OPTIMIZATION**

D. Nathan Meehan

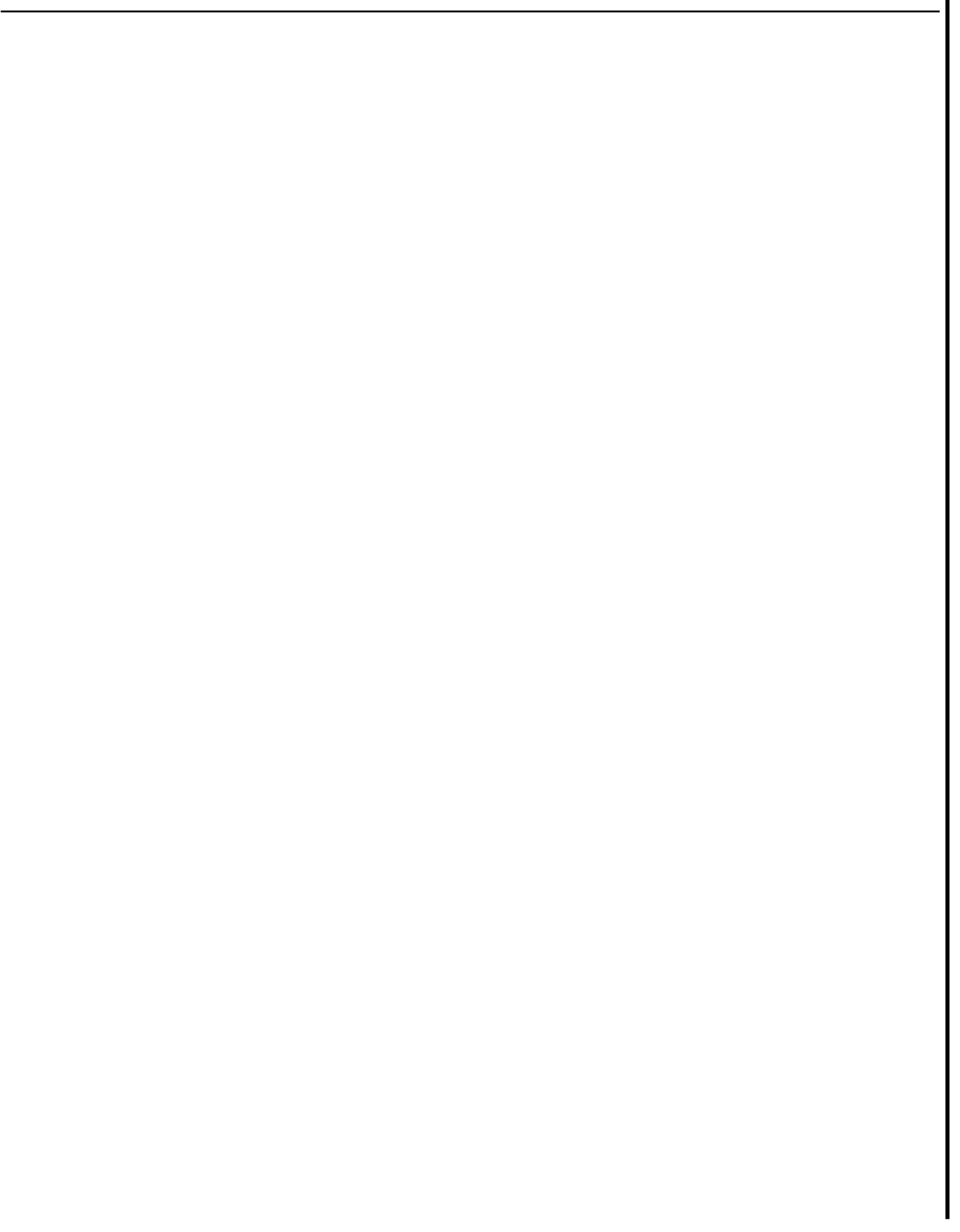
July 1989

Reservoir Simulation Industrial Affiliates

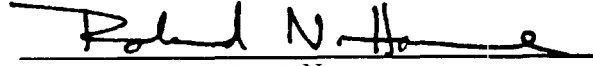
HYDRAULICALLY FRACTURED WELLS IN
HETEROGENEOUS RESERVOIRS: INTERACTION,
INTERFERENCE, AND OPTIMIZATION

A DISSERTATION
SUBMITTED TO THE DEPARTMENT OF PETROLEUM ENGINEERING
AND THE COMMITTEE ON GRADUATE STUDIES
OF STANFORD UNIVERSITY
IN PARTIAL FULFILLMENT OF THE REQUIREMENTS
FOR THE DEGREE OF
DOCTOR OF PHILOSOPHY

By
D. Nathan Meehan, P.E.
July, 1989



I certify that I have read this thesis and that in my opinion it is fully adequate, in scope and in quality, as a dissertation for the degree of Doctor of Philosophy.



Roland N. Horne
(Principal Adviser)

I certify that I have read this thesis and that in my opinion it is fully adequate, in scope and in quality, as a dissertation for the degree of Doctor of Philosophy.



Henry J. Ramey, Jr.

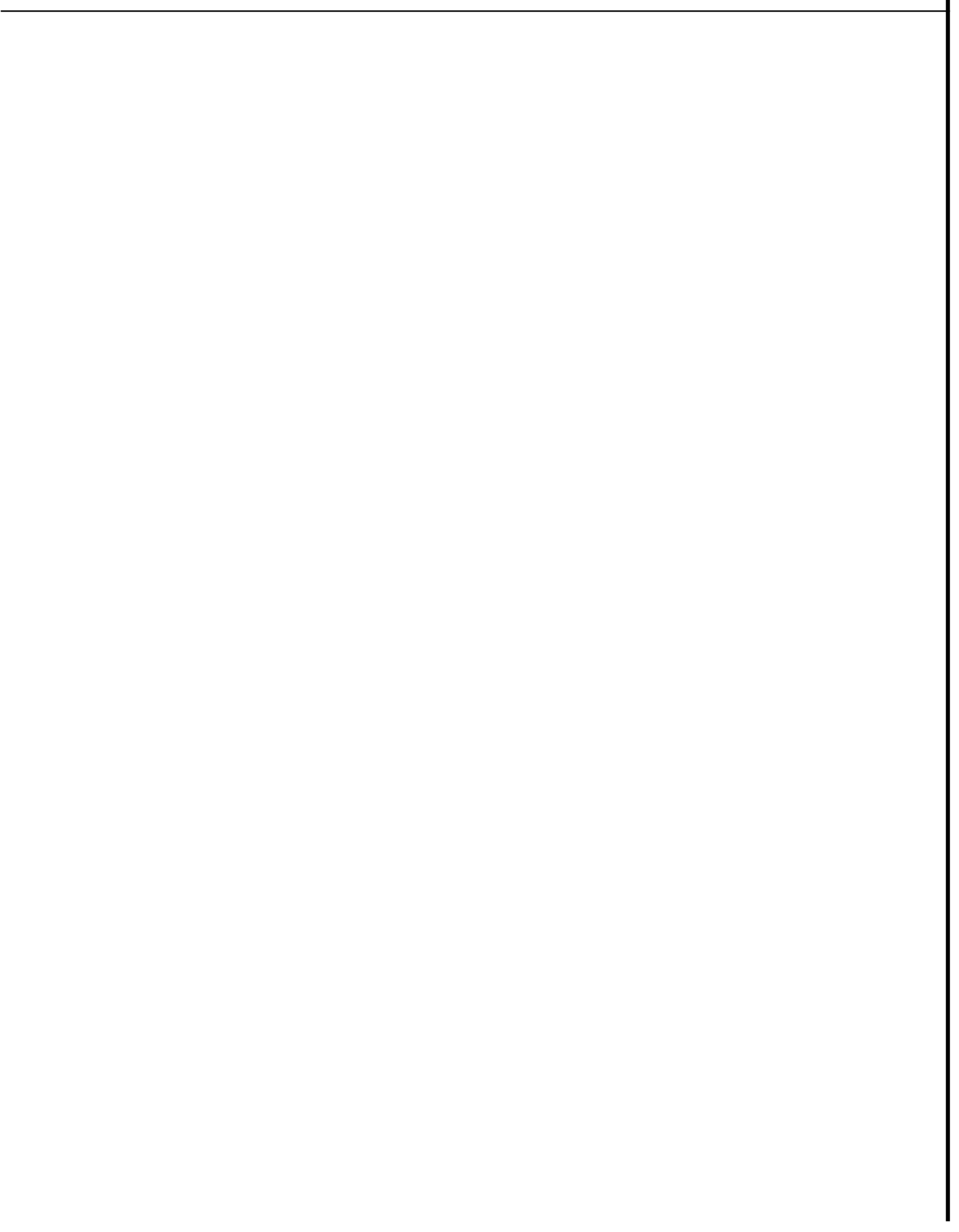
I certify that I have read this thesis and that in my opinion it is fully adequate, in scope and in quality, as a dissertation for the degree of Doctor of Philosophy.



AndrC G. Journal
(Applied Earth Sciences)

Approved for the University Committee on Graduate Studies:

Dean of Graduate Studies



Abstract

Many petroleum reservoirs employ hydraulic fracturing for well completions. Reservoir flow patterns are significantly altered by these fractures. As more wells are drilled and longer fractures are created, the influence of the fractures on production and well testing responses increases. Existing approximate solutions to this interference problem have limited applicability. This is especially true for reservoirs with moderate permeability or ones with very long hydraulic fractures, both of which are likely to have small dimensionless fracture flow capacity. Additionally, existing solutions fail to account for reservoir heterogeneities. Efforts at characterization of reservoir heterogeneities have concentrated on fluid displacement projects. Little effort has been spent on using reservoir characterization for optimizing hydraulic fracture length, well spacing, and well location selection.

This dissertation presents techniques for the design and analysis of interference tests when the active and observation well are both hydraulically fractured. These techniques are based on a new mathematical solution. This solution allows any value of dimensionless fracture conductivity, including infinite conductivity. The solution is presented in Laplace space; fracture skin, wellbore storage, naturally fissured matrix behavior, etc. are readily included. Any rate or pressure schedule of the active well can be analyzed.

Compass orientation of the wells' hydraulic fractures can be determined from an interference test. Relative fracture lengths, conductivities, and azimuth significantly affect well performance. The economic value of knowing hydraulic fracture azimuth can also be determined. Performance of a hydraulically fractured well near a large natural fracture or another hydraulically fractured well may also be evaluated. Values

of fracture conductivity and fracture length for each fracture can not be determined uniquely from the interference response and must be determined separately.

In addition to the new analytic solutions, geostatistical techniques are used to generate conditionally simulated permeability fields. These permeability distributions honor local data, are unbiased, and retain the variance of the desired field. Flow simulations using finite difference methods illustrate the importance of the spatial correlation and the level of heterogeneity in these fields.

e Primary Contributions

- e Conditions for which finite conductivity fractures influence interference tests are delineated.
- e A method for design and analysis of such tests including storage, skin, changing rates, natural fissures, etc. is presented.
- e A new method for determining the value of knowing fracture azimuth is presented.
- e Effects of reservoir heterogeneities on well performance, interference testing, and economic optimization are illustrated.
- e Economic optimization of anisotropic heterogeneous systems with finite conductivity, hydraulically fractured wells is presented. Economic importance of knowing hydraulic fracture azimuth is quantified.

Acknowledgements

First and foremost, I am indebted to my lovely bride Jan for her encouragement and support for this effort. She made it possible and kept me going. It is hard to imagine what good sports my daughters have been; dragged from a comfortable home to a cramped Escondido apartment, they occasionally complained (as did I), but mainly grew and matured under this new experience. I particularly appreciate our faculty for their help and encouragement. Hank Ramey **was as** much a reason for me to come back to school **as** he was an inspiration to me here. I learned more in the office of the petroleum industry's *éminence grise* than in any of my classes. Roland Horne, my principal advisor was more help to me than he realizes. He never seemed to believe that I couldn't do it. Khalid **Aziz** always treated me **as a** peer rather than a student, and is responsible for helping me to travel and broaden my thinking about this problem as well **as** my career. André Journel encouraged my efforts in reservoir characterization, and inspired the International Geological Congress paper. Many other faculty members were helpful both in learning new things and in surviving the trek. Especially significant to me were Lynn Orr, Avrami Grader, Bill Brigham, and Steve Wheelwright. Richard Pascale convinced me of things I had wanted to believe for years. More than any other, his course has inspired my life aspirations.

Before I came back to school, Vince Matthews gave me two bits of advice—first, to work on the problem *I* wanted to do, and second, to learn from the other students **as** they could teach me **as** much as the faculty. The first piece of advice was the same counsel the faculty here gave. The second has proved very true, and I am indebted to my friends here. Chris White and Jeff Wingard salvaged me from initial self-destruction. Evandro Nacul, Jitendra Kikani, and Mike Riley helped me a great deal.

Chick Wattenbarger was a friend and supporter all the time. Proofreaders include my wife, Jan, Chick Wattenbarger, Mohan Srivastava, Martha Meaney, and others. Ed Isaaks provided several PostScript programs used for most of the Figures. Angharad Jones made hundreds of slides for the defense, multiple presentations to SCRF, and three papers which have resulted from this research.

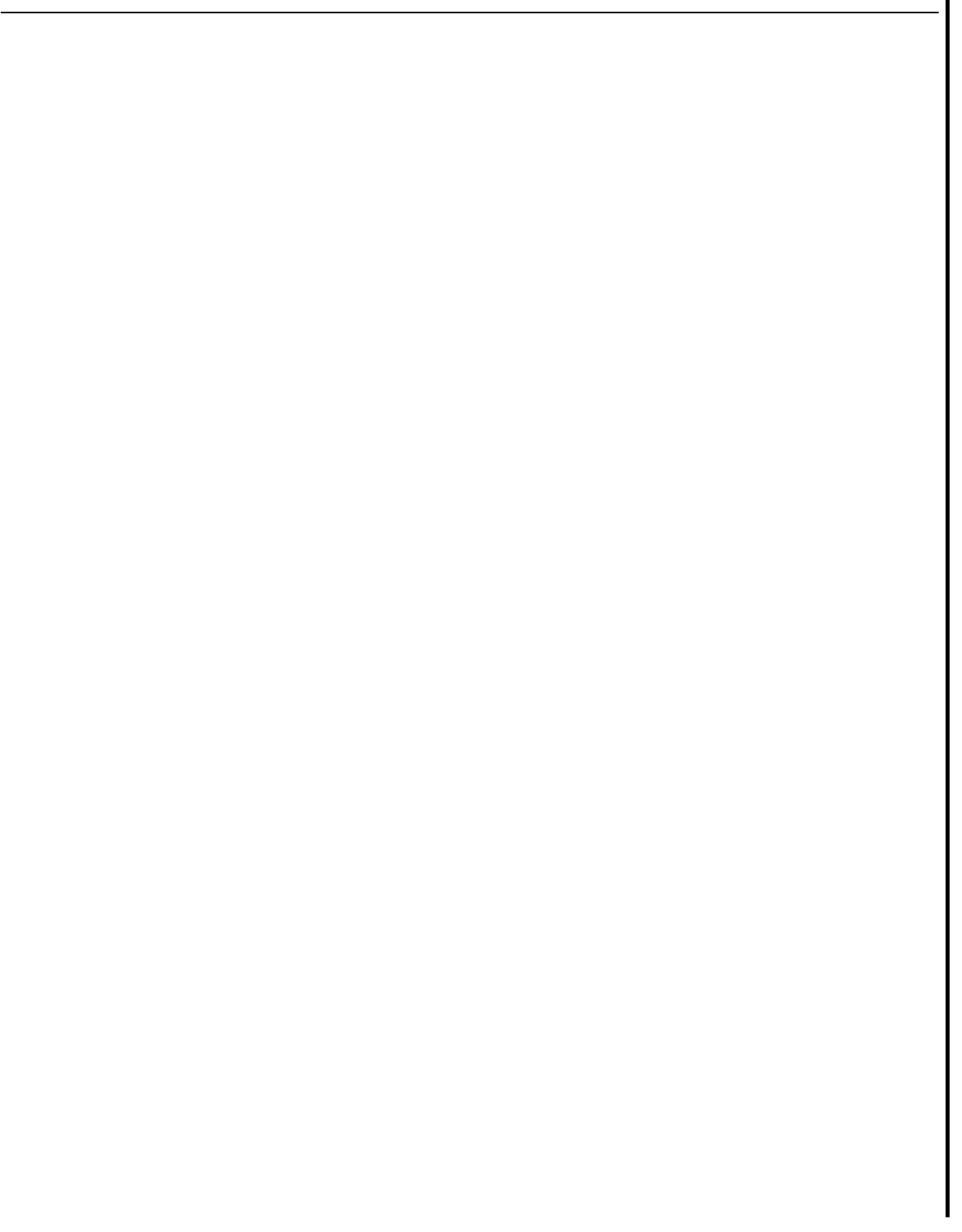
M. Scott Kraemer of Union Pacific Resources (retired) taught me to go after the things I wanted to do in life without sweating the small stuff, and that it was all small stuff. Union Pacific Resources has been generous in supporting me and employing me when I ran out of money. They also supported the portion of my research done at MIT with Prof. Michael Cleary. The Stanford Center for Reservoir Forecasting (SCRF) provided support for this research.

Dedication

I came to Stanford hoping for and expecting many things. I have not been disappointed; however, I received a bonus making **all** the rest pale.

This dissertation is dedicated to:

Daniel Nathan Meehan



Contents

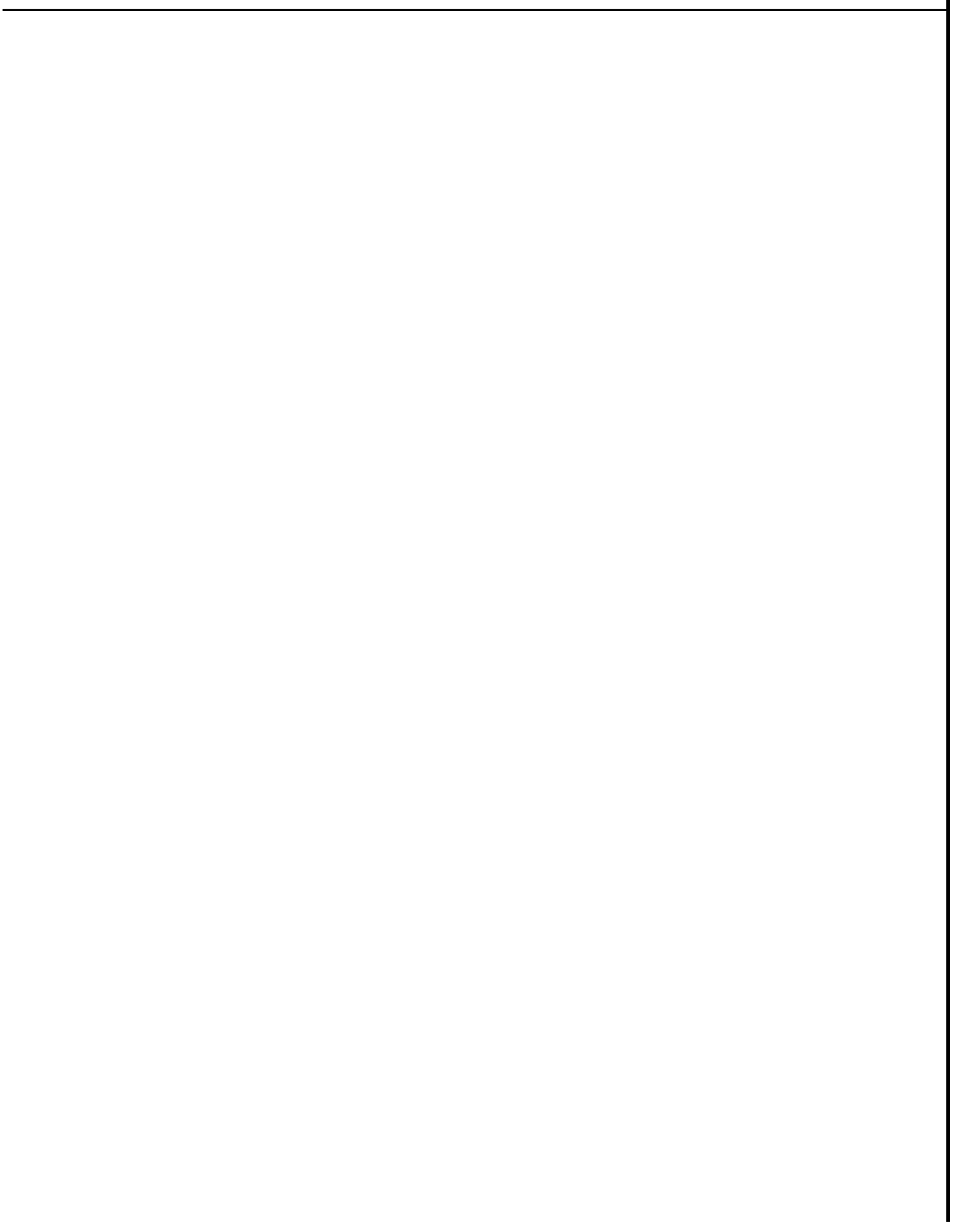
Abstract	iv
Acknowledgements	vi
Dedication	viii
1 Introduction	1
1.1 Central Themes	2
1.2 Background	3
1.2.1 A Quick View	4
1.2.2 Reservoir Heterogeneities	5
1.3 Interference of Hydraulically Fractured Wells in Heterogeneous Formations	7
1.4 Problem Statement	8
2 Fracturing and Fracture Azimuth	9
2.1 Hydraulic Fracturing Mechanics	9
2.1.1 Types of Damage	11
2.1.2 When Hydraulic Fracturing is Applicable	12
2.1.3 Fracture Design	13
2.2 Determining Fracture Azimuth	14
2.2.1 Seismic Methods	15
2.2.2 Methods Requiring Cores	18
2.2.3 Direct Observation Methods	20

2.2.4	Pressure Analysis Methods	31
2.2.5	Other Methods	32
2.3	Field Results	34
2.4	Chapter Summary	38
3	Flow Equations and Solutions	39
3.1	Fundamentals	39
3.2	Derivation For the Dimensionless Pressure Drop Due to a Uniform Flux Fracture	41
3.3	Infinite-Acting Solutions	44
3.3.1	Analytic Solution	45
3.3.2	Closed Boundary Solutions	48
3.3.3	SomeResults	49
3.3.4	Rectangular Boundaries	50
3.4	Anisotropic Case	50
3.5	Infinite Conductivity Fractures	52
3.6	Extension to Finite Conductivity Wells	53
3.6.1	Derivation of Laplace Transformation Model for Finite Conductivity Fractures	54
3.6.2	Discretization and matrix formulation	59
3.6.3	Integrating the Modified Bessel Function	60
3.6.4	Inversion Procedure	61
3.6.5	Verification and Example Results	62
3.7	Interference results	65
3.8	Numerical Simulation	66
3.8.1	Uniform Flux Fractures	71
3.8.2	Infinite Conductivity Fractures	74
3.8.3	Drainage Patterns	76
3.8.4	Performance Results	76
3.9	Chapter Summary	87

4	Interference and Interaction	89
4.1	Historical Approach	89
4.2	Interference With Two Fractures	90
4.3	Extension to Finite Conductivity Wells	92
4.3.1	Derivation of Laplace Transformation Model for Interference Testing with Infinite Conductivity Fractures	92
4.3.2	Some Results	94
4.3.3	Interference Between a Finite Conductivity Fracture Intersect- ing the Observation Well and a Line Source Active Well	97
4.4	Interference Between Two Finite Conductivity Hydraulically Fractured Wells	102
4.4.1	Semianalytic Solution	103
4.4.2	Modifications for Different Fracture Lengths, Conductivities	106
4.4.3	Effects of Azimuth and Spacing	107
4.4.4	Effects of Different Fracture Lengths and Conductivities	114
4.4.5	Interference With Two Active Wells	120
4.4.6	Interference With a Constant Pressure Active Well	123
4.5	Verification Comparisons, Example Problem	123
4.6	Early Behavior	127
4.7	Chapter Summary	132
5	Economic Optimization	138
5.1	Historical Methodology	139
5.1.1	Waterflooding and EOR; Historical Efforts	140
5.2	Value of Knowing Fracture Azimuth	141
5.3	Economics	142
5.4	Example Economics	144
5.4.1	Optimizing Spacing and Fracture Length	145
5.4.2	Economic Examples — Effect of Azimuth	148
5.4.3	Economic Sensitivity to Permeability Anisotropy	153
5.5	Chapter Summary	155

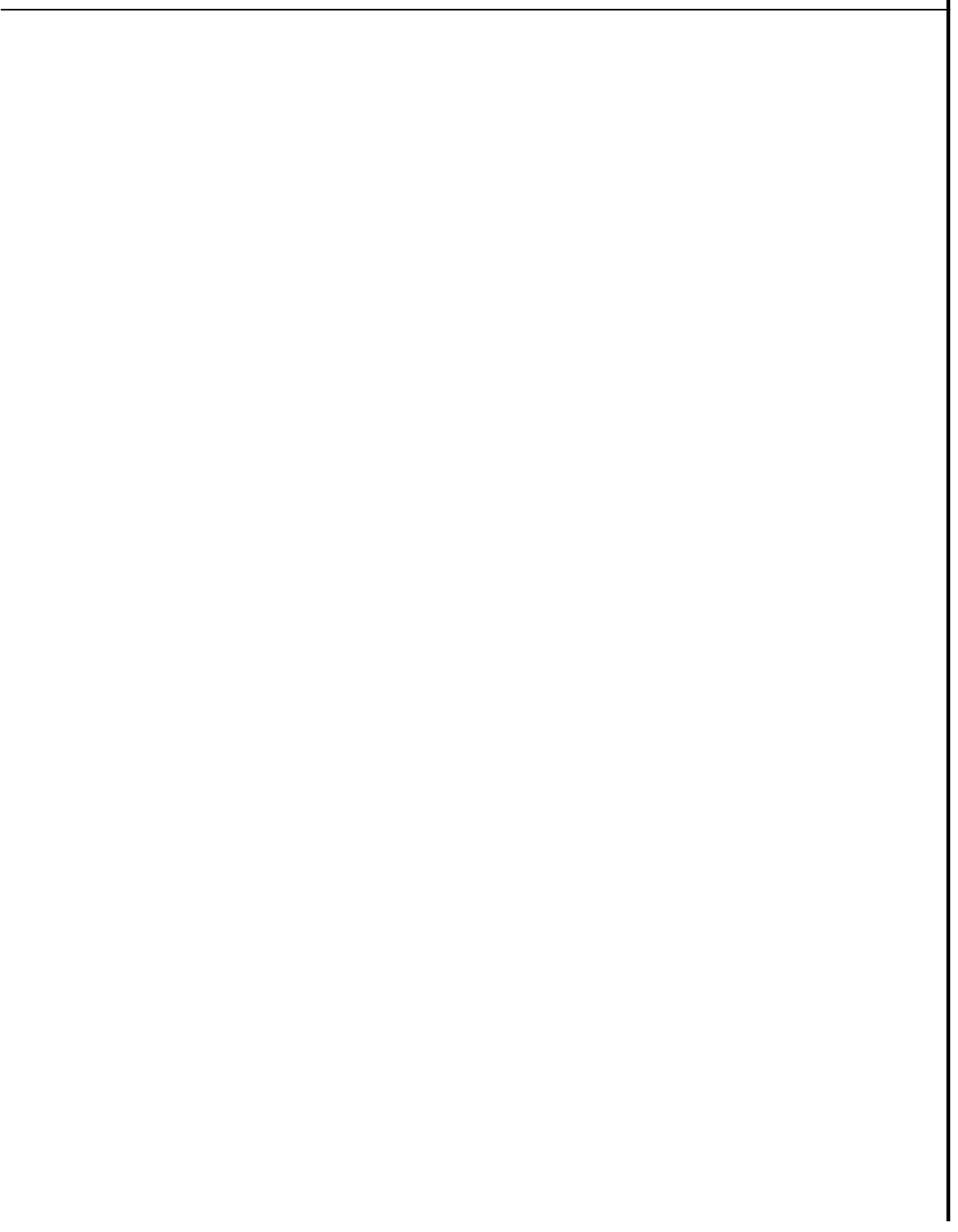
6	Reservoir Characterization Issues	158
6.1	Overview	158
6.2	Effects of Reservoir Heterogeneities	159
6.2.1	Dealing With Heterogeneities	161
6.2.2	Some Historical Approaches	162
6.3	Conditional Simulation	164
6.3.1	Turning Bands Method	165
6.4	Results	166
6.4.1	Methodology	167
6.4.2	Example Realizations	167
6.4.3	Flow Simulation Results	176
6.4.4	Combined Anisotropies	184
6.4.5	Effects of Heterogeneities on Economic Optimization	196
6.5	Interference Testing	198
6.5.1	Finite Conductivity Fractures	199
6.6	Chapter Summary	202
7	Summary and Recommendations	203
7.1	Summary of Results	203
7.2	Conclusions	205
7.2.1	Interference Testing for Finite Conductivity Wells	205
7.2.2	Optimization of Fracture Length and Well Spacing	206
7.2.3	Effects of Reservoir Heterogeneities	207
7.3	Recommendations for Further Study	209
A	Fracture Interaction Issues	210
A.1	Mechanical Interaction of Hydraulic Fractures	210
A.1.1	Earth Stress Effects	211
A.1.2	Predicting Fracture Growth	212
B	Calculation Improvements	213

B.1	Improving Solution Performance	213
B.1.1	Reducing Matrix Order	213
B.1.2	Reducing Matrix Building Requirements	214
B.1.3	Early and Late Time Approximations	215



List of Tables

4.1	Example Design Consideration Data	133
5.1	Input Data For Optimization	146
5.2	Input Data For Optimization	150
6.1	Example Permeability Variations (Log normal pdf)	177



List of Figures

1.1	Illustration of Interference. 0"	6
1.2	Illustration of Interference. 45"	6
2.1	Direction of Maximum Horizontal Compressive Stress in the United States (<i>after Zoback and Zoback</i>)	22
2.2	Histograms of Breakout Azimuths Over a 200 Meter Interval in the Fenton Hill Well (<i>after Barton et al</i>)	23
2.3	Histograms of Breakout Widths Over a 200 Meter Interval in the Fenton Hill Well (<i>after Barton et al</i>)	24
2.4	Stress Distributions Around the Wellbore	25
2.5	Example Televiwer Log	26
2.6	Map Showing Location of Wells and Azimuth of Spalls, <i>after Brown et al</i>	28
2.7	Histogram and Azimuth Frequency Plot for Cotton Valley Study <i>after Brown et al</i>	29
2.8	Comparison of Predicted Orientation of Induced Fractures from Ellipticity and Core Data. <i>after Griffin</i>	35
2.9	Orientation of Vertical Calcite Filled Fractures from Cores (a) and Wellbore Breakouts (b) in the Fluvial Zones of the MWX-1 Well <i>after Teufel et al</i>	37
3.1	Vertical Infinite Slab Source	42
3.2	Horizontal Infinite Plane Source	42
3.3	Combined Sources to Yield Uniform Flux Fracture	43

3.4	Uniform Flux Vertical Fracture in the Center of a Closed Square	49
3.5	Uniform Flux Fracture at 45" and 0" From the x Axis in a Closed Square	50
3.6	Pressure Drop Due to a Uniform Flux Fracture in Closed Rectangles with Aspect Ratios varying from 1:1 to 10:1	51
3.7	Fracture Flow Model for Finite Conductivity Fracture	56
3.8	Reservoir Flow Model for Finite Conductivity Fracture	56
3.9	Comparison of Calculated Wellbore Pressures with Cinco and Samaniego's Data for Finite Conductivity Fractures	63
3.10	Flux Distribution at Various Times Along a Highly Conductive ($F_{cD} =$ 500) Vertical Fracture	64
3.11	Flux Distribution at Various Times Along a Moderate Conductivity ($F_{cD} = 10$) Vertical Fracture	64
3.12	Flux Distribution at Various Times Along a Low Conductivity ($F_{cD} =$ π) Vertical Fracture	65
3.13	Pressure Interference Response at $r_D = 0.2$ from a 'Hydraulically Frac- tured Well with $(k_f b_f)_D = 0.2\pi$	66
3.14	Pressure Interference Response at $r_D = 0.5$ from a Hydraulically Frac- tured Well with $(k_f b_f)_D = 0.2\pi$	67
3.15	Pressure Interference Response at $r_D = 0.8$ from a Hydraulically Frac- tured Well with $(k_f b_f)_D = 0.2\pi$	67
3.16	Dimensionless Pressure Isobars at $t_{Dxf} = 10$ due to a Hydraulically Fractured Well with $(k_f b_f)_D = 0.2\pi, t_{Dxf} = 10$	68
3.17	Dimensionless Pressure Isobars at $t_{Dxf} = 0.1$ due to a Hydraulically Fractured Well with $(k_f b_f)_D = \pi, t_{Dxf} = 0.1$	69
3.18	Dimensionless Pressure Isobars at $t_{Dxf} = 1.0$ due to a Hydraulically Fractured Well with $(k_f b_f)_D = \pi, t_{Dxf} = 1$	70
3.19	Representation of Grid Model for 0" case	72
3.20	Representation of Grid Model for 45" case	73
3.21	Comparison of Uniform Flux Fracture Results for Different Fracture Azimuths	74

3.22	Isopotential Map at Pseudosteady State for the Uniform Flux Fracture	75
3.23	Infinite Conductivity Vertical Fracture, Produced at Constant Pressure, $x_e/x_f = 4/3$, Early Time	77
3.24	Infinite Conductivity Vertical Fracture, Produced at Constant Pressure, $x_e/x_f = 4/3$, Early Time, 45 Degrees	78
3.25	Infinite Conductivity Vertical Fracture, Produced at Constant Pressure, $x_e/x_f = 4/3$, Middle Time, 45 Degrees	79
3.26	Infinite Conductivity Vertical Fracture, Produced at Constant Pressure, $x_e/x_f = 2$, Early Time, 45 Degrees	80
3.27	Infinite Conductivity Vertical Fracture, Produced at Constant Pressure, $x_e/x_f = 2$, Early Time, 45 Degrees	81
3.28	Infinite Conductivity Vertical Fracture, Produced at Constant Pressure, $x_e/x_f = 2$, Middle Time, 45 Degrees.	82
3.29	Low Conductivity Vertical Fracture, Produced at Constant Pressure, $x_e/x_f = 1$, Early Time, 45 Degrees	83
3.30	Low Conductivity Vertical Fracture, Produced at Constant Pressure, $x_e/x_f = 1$, Middle Time, 45 Degrees.	84
3.31	Infinite Conductivity Fracture, $x_e/x_f = 2$, Constant Pressure, (Dashed line is analytic solution, solid is simulation)	85
3.32	Infinite Conductivity Fracture, $x_e/x_f = 2$, Constant, Rate	85
3.33	Infinite Conductivity Fracture, $x_e/x_f = 1$, Constant Pressure, (Solid line is 0", Dashed is 45°)	86
3.34	Infinite Conductivity Fracture, $x_e/x_f = 1$, Constant Pressure, Longer Frac Lengths, (Solid line is 0", Dashed is 45")	87
4.1	Interference With a Hydraulically Fractured Observation Well and a Line Source Active Well	92
4.2	Wellbore Pressure Sensitivity to Number of Fracture Blocks for Infinite Conductivity Fracture, $\theta = 30^\circ$, $r_D = 0.4$	95
4.3	Pressure Response at the Fractured Observation Well with a Line Source Active Well, $r_D = 0.8$.	96

4.4	Pressure Response at the Fractured Observation Well with a Line Source Active Well. $r_D = 2.0$	97
4.5	Pressure Response at the Fractured Observation Well with a Line Source Active Well. $r_D = 4.0$	98
4.6	Pressure Response at the Fractured Observation Well with a Line Source Active Well. $r_D = 0.4$	99
4.7	Fracture Flux Sensitivity in Time. Infinite Conductivity Fractures. $\delta = 30^\circ$, $r_D = 0.4$	100
4.8	Fracture Flux Sensitivity to δ . Infinite Conductivity Fractures. $r_D = 0.4$	100
4.9	Fracture Flux Sensitivity to r_D , fixed t_{Dxf}/r_D^2	101
4.10	Fracture Flux Sensitivity to r_D , fixed t_{Dxf}	101
4.11	Comparison of Interference Responses for a Line Source—Finite Conductivity Fracture Pair. $(k_f b_f)_D = 10\pi$	103
4.12	Nomenclature for Interference with Two Hydraulically Fractured Wells	104
4.13	Active Well Solution for $r_D = 1$. $F_{CD} = \pi$	107
4.14	Observation Well Solution for $r_D = 1$. $F_{CD} = \pi$	108
4.15	Active Well Solution for $r_D = 2$. $F_{CD} = \pi$	108
4.16	Observation Well Solution for $r_D = 2$. $F_{CD} = \pi$	109
4.17	Active Well Solution for $r_D = 4$. $F_{CD} = \pi$	110
4.18	Observation Well Solution for $r_D = 4$. $F_{CD} = \pi$	110
4.19	Active Well Solution for $r_D = 0.5$, $F_{CD} = \pi$	111
4.20	Observation Well Solution for $r_D = 0.5$, $F_{CD} = \pi$	111
4.21	Active Well Solution for $r_D = 1$. $F_{CD} = 100\pi$	112
4.22	Observation Well Solution for $r_D = 1$. $F_{CD} = 100\pi$	113
4.23	Active Well Solution for $r_D = 2$. $F_{CD} = 100\pi$	113
4.24	Observation Well Solution for $r_D = 2$. $F_{CD} = 100\pi$	114
4.25	Active Well Solution for $r_D = 4$. $F_{CD} = 100\pi$	115
4.26	Observation Well Solution for $r_D = 4$. $F_{CD} = 100\pi$	116
4.27	Active Well Solution for $r_D = 0.5$, $F_{CD} = 100\pi$	116
4.28	Observation Well Solution for $r_D = 0.5$, $F_{CD} = 100\pi$	117

4.29	Active Well Solution, $\theta = 15, F_{CD} = a$	117
4.30	Observation Well Solution, $\theta = 15, F_{CD} = \pi$	118
4.31	Active Well Solution, $\theta = 15, F_{CD} = 100\pi$	118
4.32	Observation Well Solution, $\theta = 15, F_{CD} = 100\pi$	119
4.33	Effect of $\Lambda_{[AO]}$ on Observation Well Response, $F_{CD} = \pi, 100\pi, r_D = 0.8$	119
4.34	Effect of $\Lambda_{[AO]}$ on Observation Well Response, $F_{CD} = a, 100\pi, r_D = 3.0$	120
4.35	Active and Observation Well Fluxes at $t_{Dxf} = 0.1, F_{CD} = a, \theta = 15,$ $r_D = 1.0$	121
4.36	Active and Observation Well Fluxes at $t_{Dxf} = 0.1, F_{CD} = \pi, \theta = 45,$ $r_D = 1.0$	121
4.37	Active and Observation Well Fluxes at $t_{Dxf} = 10, F_{CD} = \pi, \theta = 90,$ $r_D = 1.0$	122
4.38	Active and Observation Well Fluxes at $t_{Dxf} = 10, F_{CD} = \kappa, \theta = 15,$ $r_D = 1.0$	122
4.39	Active Well With Both Wells Producing, Low Conductivity Fractures and Line Source Wells, $r_D = 1.0, F_{CD} = \pi, \theta = 15, 90$	123
4.40	Active Well With Both Wells Producing, Low Conductivity Fractures and Line Source Wells, $r_D = 1.0, F_{CD} = \kappa, \theta = 15, 90$	124
4.41	Active Well With Both Wells Producing, High Conductivity Fractures and Line Source Wells, $r_D = 1.0, F_{CD} = 100\pi, \theta = 15, 90$	125
4.42	Active Well With Both Wells Producing, High Conductivity Fractures and Line Source Wells, $r_D = 1.0, F_{CD} = 100\pi, \theta = 15, 90$	126
4.43	Active and Observation Well Fluxes at $t_{Dxf} = 0.1, F_{CD} = 100\pi, \theta = 15,$ $r_D = 1.0$	127
4.44	Active and Observation Well Fluxes at $t_{Dxf} = 0.1, F_{CD} = 100\pi, \theta = 45,$ $r_D = 1.0$	128
4.45	Active and Observation Well Fluxes at $t_{Dxf} = 10, F_{CD} = 100\pi, \theta = 90,$ $r_D = 1.0$	128
4.46	Active and Observation Well Fluxes at $t_{Dxf} = 10, F_{CD} = 100\pi, \theta = 15,$ $r_D = 1.0$	129

4.47	Comparison of Simulated Response With Analytic Results, $F_{CD} = \pi$. .	130
4.48	Analysis of Simulated Interference Test Using Line Source Solution . .	131
4.49	Log-Log Plot of Simulated Interference Test Using Line Source Solution	131
4.50	Analysis of Simulated Interference Test Using Mousli <i>et al.</i> 's Solution .	132
4.51	Analysis of Simulated Interference Test Using Semianalytic Solution . .	133
4.52	Log-Log Plot of Simulated Interference Test Using Semianalytic Solution	134
4.53	Observation Well Response, $r_D = 0.8$	135
4.54	Rescaled Pressure Data (p_D^*) as a Function of t_{Dxf}/d_D^2	136
5.1	NPV10 for Example Economics Case	147
5.2	NPV10/acre for Example Economics Case	147
5.3	NPV10/acre for a Specified Fracture Length	149
5.4	Conventional Well Spacing	149
5.5	Well Spacing Modified Knowing Fracture Azimuth	151
5.6	Economic Optimization for Conventional Well Spacing	151
5.7	Economic Optimization for Modified Well Spacing	152
5.8	Spacing Effects of a 45 ° Error in Fracture Azimuth	153
5.9	Spacing Effects of a 75 ° Error in Fracture Azimuth	154
5.10	Impacts of Errors in Estimated Fracture Azimuth on Net Present Value	154
5.11	Economic Optimization Results With Permeability Anisotropy	155
5.12	Economic Optimization Results With Permeability Anisotropy, Modified Well Spacing	156
6.1	Simulation Grid for Heterogeneous Reservoir with a Hydraulically Fractured Well	168
6.2	Conditional Simulation — Correlation Range= 34, Geometric Anisotropy = 1.0, $\sigma/m = 2.06$	169
6.3	Conditional Simulation — Correlation range= 34. Geometric anisotropy= 4.1. $\sigma/m = 0.87$	170
6.4	Conditional Simulation — Correlation range= 176, Geometric anisotropy = 1.0, $\sigma/m = 0.68$	171

6.5	Conditional Simulation — Correlation range= 17, Geometric anisotropy = 1.0, $a/m = 0.74$	172
6.6	Conditional Simulation — Correlation range= 2, Geometric anisotropy = 1.0, $\sigma/m = 0.98$	173
6.7	Conditional Simulation — Correlation range= 68, Geometric anisotropy = 4.0, $\sigma/m = 0.66$	174
6.8	Conditional Simulation — Correlation range= 68, Geometric anisotropy = 4.0, $\sigma/m = 0.66$	175
6.9	Conditional Simulation Results — White Noise, $\sigma/m = 0.6-1.0$	177
6.10	Three Flow Simulations With Correlation Range= 17, Varying σ/m	178
6.11	Two Flow Simulations With Correlation Range= 176, Varying a/m	179
6.12	Six Flow Simulations With Correlation Range= 68, Varying σ/m	180
6.13	Three Flow Simulations With Correlation Range= 68, Small Geometric Anisotropy..	180
6.14	Five Flow Simulations With Correlation Range= 34, Varying σ/m	181
6.15	Flow Simulations With Correlation Range=34, Geometric Anisotropy=2181	
6.16	Flow Simulations With Correlation Range= 34, Geometric Anisotropy=4182	
6.17	Flow Simulations With Correlation Range= 34, Correlation Range= 10	182
6.18	Flow Simulations With Correlation Range= 34, Correlation Range= 20	183
6.19	Flow Simulations With Correlation Range= 34, Geometric Correction for Correlation Range	183
6.20	Contour Plot of Pressure Distribution for Short Scale Correlation and $\sigma/m = 2$	185
6.21	Contour Plot of Pressure Distribution for Medium Scale Correlation and $\sigma/m = 2$	186
6.22	Perspective Plot of Pressure Distribution for Medium Scale Correlation and $\sigma/m = 2$	187
6.23	Greyscale Plot of Pressure Distribution for Moderate Scale Correlation and $\sigma/m = 1$	188
6.24	Early Time Pressure Distributions for Homogeneous Reservoir, $x_e/x_f =$	2189

6.25	Late Time Pressure Distributions for Homogeneous Reservoir, $x_e/x_f = 2$	190
6.26	Early Time Pressure Distributions for Correlation Length= x_f , $\sigma/m =$ 0.5, $x_e/x_f = 2$	191
6.27	Late Time Pressure Distributions for Correlation Length= x_f , $\sigma/m =$ 0.5, $x_e/x_f = 2$	192
6.28	Conceptual Sketch of Natural Fracturing and Direction of <i>in situ</i> Stresses	195
6.29	Flow Simulations With Correlation Range= 34 , Local Anisotropies of $1 \leq k_x/k_y \leq 100$	196
6.30	Flow Simulations With Correlation Range= 34 , Adjusted for Local Anisotropy.	197
6.31	Interference Match in a Heterogeneous Reservoir, $r_D = 1$, $\delta = 30$, $\sigma/m = 1.0$, Correlation Range= 17, Isotropic	200
6.32	Interference Match in a Heterogeneous Reservoir, $r_D = 1$, $\delta = 30$, $u/m = 1.0$, Correlation Range= 17, Geometric Anisotropy= 10:1	200
6.33	Effects of Finite Conductivity Fractures on Interference Tests in Het- erogeneous Reservoirs	201

Chapter 1

Introduction

The problem of hydraulic fracture interference. A general background for the magnitude and importance of the problem. Impacts of reservoir heterogeneity. The problem statement.

Because the likelihood of further large oil and gas discoveries in the U.S. is low, industry must maximize recovery rates and efficiencies from existing fields. A significant fraction of petroleum engineering research focuses on Enhanced Oil Recovery (EOR), a critical need as oil recoveries are in the 20–40% range in many fields. Much less effort has been concentrated on increasing rates of recovery and recovery efficiencies for low permeability gas reservoirs. Additional infill drilling of low permeability oil and gas reservoirs holds the potential to accelerate (and increase) recoveries from the hundreds of such fields in the country.

As infill drilling continues, **hydraulic fractures** become long compared to inter-well distances, giving rise to potential problems. First, there is a need to determine fracture azimuth (in a compass orientation sense as fractures can generally be assumed vertical at depths of greater than ≈ 1000 m.). Part of this dissertation is a critical survey of techniques available to estimate fracture azimuth. The need to determine azimuth depends strongly on the well spacing and fracture lengths required to recover reserves optimally. *Optimal* must be considered as a Net Present Value (NPV) sense. Therefore, hydrocarbon prices, and well and fracturing costs affect NPV as much as

reservoir factors such as permeability, net thickness, porosity, initial pressure, etc.

The value of knowing fracture azimuth (from the point of view of field development) is a function of how that knowledge actually affects subsequent decisions. Spending money to determine fracture azimuth is useless if that knowledge does not affect subsequent decisions. However, azimuth can be extremely important under certain circumstances and for those cases, must be considered for optimal reservoir management.

1.1 Central Themes

Two central themes motivating this study are:

- o The need to understand hydraulically fractured well behavior in heterogeneous reservoirs and when those fractures might influence the performance of other wells.
- o The importance of a multi-disciplinary approach to optimizing the development of oil and gas fields.
- o The need to understand interactions

Two areas have been inadequately investigated. The first is actual mechanical interaction of a propagating hydraulic fracture in the presence of the pressure draw-down caused by production from another well with a previously created fracture. The second area, the major focus of this research, is pressure transient interference of finite conductivity hydraulically fractured wells. Well performance depends in part on the degree of interference, and the utility of pressure transient tests rests on how sensitive well performance is to fracture azimuth.

Sensitivities to reservoir heterogeneities (permeability anisotropy, varying spatial correlation ranges, geometric anisotropies, etc.) must also be understood to predict well performance and to estimate the economic value of knowing fracture azimuth. Plans for addressing these issues are outlined in a separate section.

- o The need for a multi-disciplinary approach

Optimizing the development of fields with low permeability requires input from geologists and geophysicists beyond the standard historical **structure/isopach** maps. Most methods for determining permeability anisotropy, stress anisotropy, and other reservoir heterogeneities are clearly in the domain of geophysicists and geologists. Unfortunately, few of these techniques are routinely used in low permeability formations. Most reservoir characterization efforts have gone into large oilfields for use in association with EOR projects. Indeed, doing this characterization **has** often been (correctly) assumed, with little quantitative justification, to be economically worthwhile. **A** significant portion of this work is to quantify economic value of reservoir characterization in low permeability field development.

1.2 Background

Low permeability reservoirs, as well as many moderate permeability reservoirs, often require hydraulic fracturing before they are commercially valuable. **A** significant majority ($\approx 75\%$) of wells drilled in the U. S. require such stimulation. Creating extremely long hydraulic fractures for very low permeability wells (less than 0.01 md) has proven to be commercially successful. Massive hydraulic fracture (MHF) treatments can cost over \$ 500,000 and represent more than 30–50% of a well's cost. Optimization of fracture length and well spacing is often critical to the economics of exploiting marginal gas resources.

Determining optimum fracture length and well spacing is both a technical and economic problem. Optimization of ultimate recovery and net present value (NPV) from tight gas fields has historically been approached from the idealization of homogenous, isotropic reservoirs and by neglecting interwell interference. It is possible to model multi-well tight gas reservoir performance using various heterogeneities and taking into account interference between the wells. Most heterogeneities (other than simple permeability anisotropy) require numerical simulation, as do some of the more complex problems of optimization. Using numerical analysis or new semi-analytic solutions, production forecasts can be obtained for various development scenarios; then

economics can be calculated for optimizing well spacing and hydraulic fracture length.

Formation permeability is a key technical criterion because higher permeability wells are able to drain much larger areas. Lower permeability wells require longer hydraulic fractures and closer well spacings. If the fracture length is small compared to well spacings, practically no interference occurs between the wells due to the hydraulic fractures.

Increased well density is typically required when :

- the costs of hydraulic fracture treatments are a significant fraction of well costs;
- fracture length is limited for technical, economic, or regulatory reasons; or,
- well performance indicates substantially smaller fracture lengths than design fracture calculations predict.

In these cases, knowledge of fracture azimuth becomes particularly important for the optimal location of infill wells. The importance of knowing fracture azimuth increases as the well spacing approaches the fracture length. What is the effect of interference? How valuable is it to know fracture azimuth, i.e., what impact does the knowledge of fracture azimuth have on the optimization problem? How sensitive is optimization to the accuracy of the azimuth determination? How do the methods for detecting fracture azimuth work? How do reservoir heterogeneities affect development plans?

These questions are of substantial practical concern to the petroleum industry. Many of the techniques for determining fracture azimuth are geophysical methods that are still being perfected. Other techniques for azimuth detection are derived from well testing, geology, and rock mechanics.

1.2.1 A Quick View

Among the few works to discuss fracture azimuth's effect on tight gas production was that of Smith,²³² for the Wattenberg Gas Field, and that of Lacy,¹⁴¹ who reviewed hydraulic fracture azimuth detection methods. With figures like Figure 1.1,

they argued that as fracture length grew large compared to the interwell distance, the influence of fracture azimuth increased. This had been proven unambiguously for the case of waterflooding and fluid displacement. Smith²³² quantified the effects, based on a descriptive argument he described as 'somewhat qualitative' in nature. This dissertation provides more rigorous solutions to the problem of fracture azimuth interference. For most homogeneous cases of practical interest, the effect of fracture azimuth on production or well tests is easily determined. Earlier approximate solutions, using the uniform flux fracture model, invariably led to the underestimation of interference effects. For the cases of large permeability anisotropies and infill drilling, knowledge of fracture azimuth is quite important.

Drainage patterns for well spacings and fracture orientations, such as in Figure 1.1, are not as simple as indicated. Economic considerations are developed for an example case showing optimum fracture length; well spacing is optimized both for a system that neglects permeability anisotropy and for one accounts for azimuth. The maximum difference in fracture azimuths (corresponding to a 90 degree error) results in a substantial difference in Net Present Value. Knowledge of fracture azimuth for isotropic systems becomes more important as fracture lengths approach interwell distances.

Figures 1.1 and 1.2 illustrate the concepts involved. Transient flow around a hydraulic (vertical) fracture is approximately elliptical at early times. Both figures show eight wells equally spaced on the corners of squares. Fractures are shown that extend to 40% of the distance between wells. For the 0" case (Figure 1.1), considerable overlaps of drainage patterns are obvious. For the 45" case, interference is expected to be negligible. Although this representation is qualitatively useful, actual drainage patterns that result from interference of such wells differ from this simple approximation, thus complicating interpretation.

1.2.2 Reservoir Heterogeneities

Optimal development of heterogeneous oil and gas fields is a major trend in current petroleum engineering research. Such research is primarily concerned with fluid displacement projects, rather than tight gas reservoirs. Low permeability reservoirs

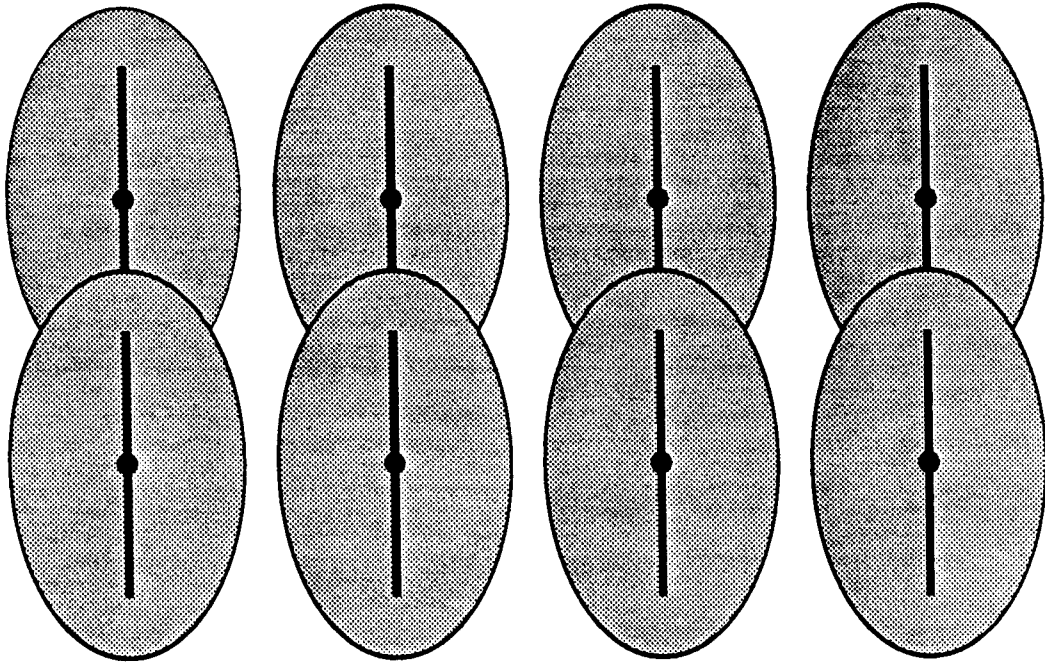


Figure 1.1: Illustration of Interference, 0°

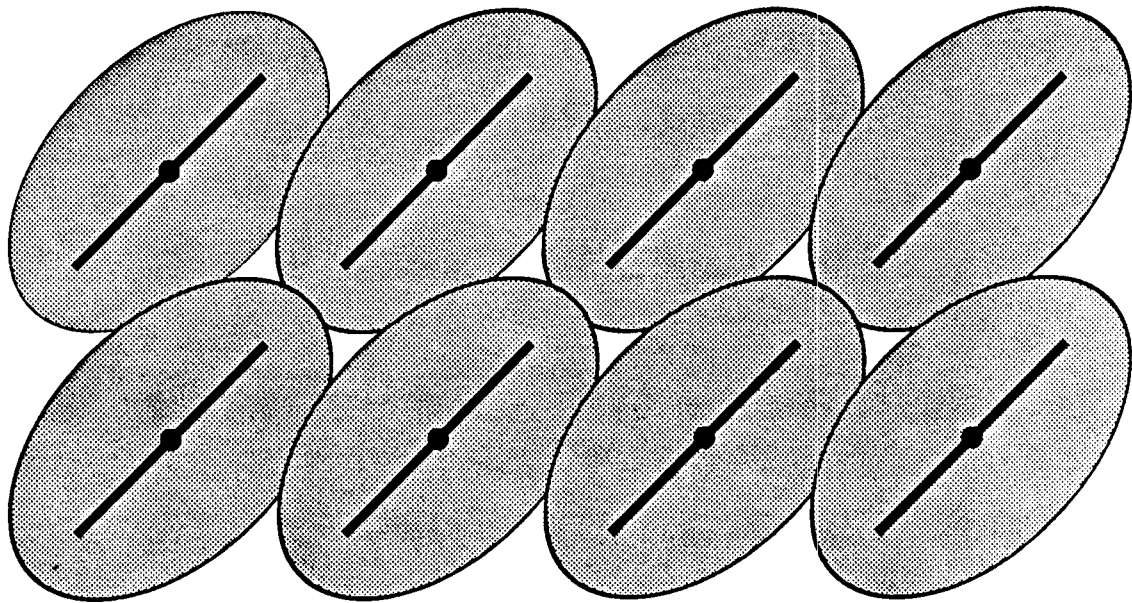


Figure 1.2: Illustration of Interference, 45°

require hydraulic fracturing and are often ‘infill drilled’, with increased well densities to both accelerate and increase ultimate recovery. Increased oil recovery by infill drilling waterflooded reservoirs has been frequently demonstrated; fewer examples of incremental **gas** recovery associated with infill drilling are published¹⁸² .

Incremental **gas** recovery may be obtained by infill drilling when permeability variations are large. Vertical hydraulic fractures intersect producing wells and are aligned according to current stress states in the field. Typically, these stress directions remain fairly constant over distances typical of field sizes. Spatial correlation of permeability and porosity need not be related to hydraulic fracture direction.

1.3 Interference of Hydraulically Fractured Wells in Heterogeneous Formations

Three general areas of concern regarding hydraulically fractured wells are discussed in this dissertation. The first two are the primary subjects of this research, while the third requires further investigation.

- o Effects of fracture azimuth on well performance a; a function of hydraulic fracture length. This includes optimization of fracture length and well spacing, detection of hydraulic fracture azimuth, and prediction of interference behavior of hydraulically fractured wells. This dissertation reviews existing technology, develops improved models of such technology, and develops and implements new analytic solutions and models. Specifically, Laplace space solutions for the interaction of finite conductivity hydraulically fractured wells are developed and used to quantify the effects of fracture azimuth on production and interference testing.
- Effects of reservoir heterogeneities on well performance, and pressure transient interference testing on hydraulically fractured wells. Reservoir heterogeneities included in this dissertation include permeability anisotropy and correlated spatial variations in permeability. Important special cases are used to

show how and when heterogeneities affect performance.

- **Effects of stress variations** caused by pore pressure reduction from an existing hydraulically fractured well on the propagation of a hydraulic fracture from an infill well. Created and propped wing lengths and fracture direction may well be altered for such a case. This topic is discussed generally, identifying additional research needs.

1.4 Problem Statement

This dissertation combines analytic and numerical approaches to solve several closely related problems. The pressure interference problem for arbitrary production conditions at two finite conductivity hydraulically fractured wells was solved. This was done in a general way which allows the incorporation of the results into a range of well testing and reservoir performance techniques. Determining the effects of hydraulic fracture azimuth is the primary objective; however, actual application of this information is academic unless used in reservoir management decisions. Hence, economic impacts of azimuth on well spacing and fracture design is quantified.

Real petroleum reservoirs are very inhomogeneous. Analytic solutions are limited in their ability to handle complex reservoir heterogeneities. Thus, heterogeneity effects are quantified in order to determine whether or not the analytic solutions are useful in real reservoirs.

Chapter 2

Fracturing and Fracture Azimuth

Hydraulic fracturing principles summarized, including reasons for hydraulic fracturing and design principles. Methods to determine hydraulic fracture azimuth including a variety of geophysical and engineering techniques. Field results of published examples.

2.1 Hydraulic Fracturing Mechanics

In their now classic 1957 paper, Hubbert and Willis¹²² discussed the basic principles of hydraulic fracturing. The technique had been observed in petroleum operations in several areas, including pressure parting in water injection/disposal wells; formation breakdown during squeeze cementing; and lost circulation during drilling. J. B. Clark of Stanolind Oil and Gas Company (now AMOCO) formally identified the technique as a stimulation method⁵³. The technique grew rapidly in popularity and has now been used on thousands of wells. In the early days of fracture stimulation, an erroneous model of the process often assumed that hydraulic pressure parted the formation along bedding planes and lifted formation overburden. Although the pressure required to initiate fractures was generally less than the weight of the overburden, other explanations involving 'effective overburdens' were postulated²²³.

Hubbert and Willis¹²² explained the nature of hydraulic fracturing mechanics and

concluded what is taken almost axiomatically today: hydraulically induced fractures propagate approximately normal to the least principal stress. In most areas of the United States, at depths greater than a few thousand feet, this least stress (S_h) will be approximately horizontal and fractures will be vertical to subvertical. At shallow depths, the reverse is true: the least stress will be essentially equal to the overburden pressure and fractures will be horizontal. More sophisticated models of fracture growth have led to the current understanding of how local heterogeneities in rock properties, or stress alterations from other fractured wells, pore pressure, and thermal gradients may affect fracture extension and azimuth 41, 191 .

The pressure required to *initiate* the fracture is a function of existing stresses in the rock, hole geometry, existing natural fissures, and fluid properties. Pressures required to *continue* fracture propagation are essentially determined by rock stresses. Horizontal fractures cannot be created without injection pressures greater than that of the total overburden. In a typical field, vertical fractures should have similar azimuths, or compass orientations. If large variations in effective stress directions are present, pore pressure gradients are large; or if alteration of effective stresses from other wells is significant, this last assumption may not be valid. Small differences between S_H and S_h (the maximum and minimum horizontal compressive stresses) tend to increase the possibilities for altering fracture propagation directions due to interwell interference. In practice, S_h is measured with reasonable accuracy on many wells. Indirect measurements of S_H are less frequently made,

Fundamentals of reservoir engineering show that single phase well flow rates are functions of permeability, thickness, reservoir and wellbore pressures, reservoir geometry, fluid properties, wellbore radius, and skin effect. Most of these properties are solely functions of the reservoir and generally cannot be changed. Only the skin effect can be changed under certain circumstances. Much of the effect of hydraulic fracturing can be understood as decreasing the skin effect, or, alternatively, increasing the effective wellbore radius. Two common methods for reservoir stimulation are hydraulic fracturing and matrix acidization. In addition to increasing the effective wellbore radius, hydraulic fracturing is also used infrequently for novel sand control

and coning problems.

2.1.1 Types of Damage

Both low permeability wells and damaged wells may require hydraulic fracturing to obtain commercial flow rates. High and moderate permeability reservoirs can be damaged (positive skin effect) and suffer reduced flow rates. Mechanical sources of skin effect include 'turbulent' flow; slanted wells or partially penetrating wells ⁴⁵; limited entry to flow ¹⁹⁷; off-centered wells ⁸⁵; low perforation density ¹⁵⁰; short perforations ¹⁵⁵; incorrect phasing of perforations; poor isolation between zones ¹; collapsed or blocked tubulars; scale precipitation in perforations ¹⁸³; drawdowns to pressures below the bubble point for oil reservoirs or the dew point for retrograde gas reservoirs ³⁰. Most of these pseudoskins cannot typically be improved by well stimulation. Sources of formation damage and 'true' skin effect include:

1. Invasion by drilling mud solids ¹⁷ or filtrate ²³⁰, damage by cement slurries ⁶³, washes, or spacers ²⁴.
2. Perforation damage from overbalanced perforations ^{134, 133}, charge debris ²⁴⁰, or insufficient penetration ¹³⁵.
3. Damage from completion and workover fluids ^{76, 202, 218}.
4. Damage to gravel packs ²⁰³ by improper slurry placement, fines migration, plugging by foreign objects, improper design of gravel size or screen size ¹⁰⁰.
5. Damage during production by high flow rates and consequent fines movement ¹⁸⁹, excessive drawdown leading to rock failure or permeability reductions ^{186, 26}, deposition of organic ¹¹³ or inorganic ²⁵³ materials to due pressure reductions.
6. Damage due to well stimulations from wellbore cleanup, acid jobs ⁶², water control treatments, and problems in injection wells ³⁷.

2.1.2 When Hydraulic Fracturing is Applicable

Hydraulic fracturing is a stimulation method for wells with low permeability, e.g. less than 1 md, and occasionally for much higher permeability reservoirs when damage is significant or when heterogeneities actually separate substantial pore volume that could not otherwise be drained⁷⁷. All aspects of well and reservoir must be considered, including type and strength of tubulars, formation fluid sensitivity, mechanical competence and rock properties of adjacent formations, and quality of cement job (for isolation). Very water sensitive formations may still be fracture stimulated with foams that carry sand well, contain less liquid, and are recovered rapidly. Special precautions must be taken if the zone to be stimulated is near a water-bearing or depleted zone.

Fracturing is occasionally undertaken when acidization, or some other stimulation technique, is sufficient. Occasionally, when skin damage due to drilling fluids, completion fluids, acid or other stimulation chemicals is so large as to be irreparable, hydraulic fracture stimulation is the only feasible method of penetrating the damaged region. These types of stimulations give rise to short fractures, usually less than 100–600 feet.

For very low permeability reservoirs, Massive Hydraulic Fractures (MHF) are created by pumping enormous quantities of sand-laden gelled fluids to create hydraulic fractures that may have tip-to-tip lengths in excess of 4000 feet. Costs of such jobs can approach the costs of drilling the well, with millions of pounds of sand displaced into the fracture created. Dimensionless fracture conductivity ratio, F_{CD} is defined as:

$$F_{CD} = \frac{k_f b_f}{x_f k} = (k_f b_f)_D \quad (2.1)$$

where k_f and b_f are the permeability and width of the fracture, x_f is fracture half-length (well axis to fracture tip), and k is formation permeability. This ratio, F_{CD} , must be large to have a substantive, long-term increase in production. For low permeability formations, the denominator becomes small, and efforts to make high conductivity fractures are less important. However, long-term effects of potential proppant crushing, imbedment, fines migration, and other damage to the fracture must be considered. Additionally, long hydraulic fractures have decreased fracture conductivities.

Therefore, a maximum effective fracture length may occur due to diminishing fracture conductivity: The advantage of very high values of F_{CD} diminishes at values above about 50, with significant increases in productivity from 2 to 50.

A value for F_{CD} of 15 is often used for fracture design because higher values improve the productivity of a well marginally under pseudo-steady state flowing conditions. However, many low permeability gas wells require years to reach pseudo-steady state and would benefit from conductivity values higher than 15⁶⁶. In fact, problems associated with closure stress, long-term degradation of proppant conductivity, and fracturing damage may make desired values difficult to obtain^{153, 188, 219, 273}.

2.1.3 Fracture Design

It is not a purpose of this dissertation to give a detailed discussion of fracture design, because this subject is covered extensively in the literature^{7, 53, 154, 252, 254} (especially see Meng and Brown¹⁸⁵). A recent book by Economides and Nolte⁷⁷ covers the entire topic of reservoir stimulation.

Aspects of fracture design include:

- o prediction of well performance for different values of well spacing, fracture length, and fracture conductivity,^{6, 116, 117};
- o prediction of the width, length, etc. for fracture geometry,^{224, 225, 226};
- o selection of propping agents, fluids, chemicals, etc.;
- o optimization of the fracture design based on economics^{12, 185, 250, 251}.

Optimal fracture design requires forecasting of reservoir performance for a given propped fracture geometry, fluid properties, fracture and formation permeability, etc. Very low permeability wells generally require long fractures. Moderate permeability wells rarely benefit from extremely long fractures and require high fracture conductivities to provide a sufficient contrast with the formation. Diminishing returns are expected for excess fracture conductivity or length.

Constraints imposed by limitations on flow rates, frictional drops in tubulars, and operating pressures must also be considered in fracture design. Techniques such as 'NODAL' analysis^{35, 36, 124} can be used to assess these factors. Formation mechanical strength and other rock properties, along with *in situ* stress conditions, are also important. Without sufficient contrast in rock mechanical properties and/or stresses between layers, creation of extremely long propped fractures is impossible due to uncontained vertical growth. This is critical since a major fraction of fracture treatment cost is related to the horsepower required to pump the fluids and proppant. Design improvements using data from 'mini-frac' tests and pressure monitoring during fracturing should improve created and propped length, while avoiding early screenouts (a premature end to the hydraulic fracturing treatment associated with excessive treating pressures) or uncontrolled vertical growth¹⁹⁶.

Other design considerations include fracturing fluid properties such as viscosity as a function of shear, temperature and leakoff characteristics. These factors are important for proppant placement and fracture extension. Pad volume (the quantity of proppant-less fluid pumped initially) is important since it both creates the fracture and cools the formation, enabling the fluid containing the proppant to maintain its viscosity better. Excessive pad volumes result in higher than required fracture costs and inadequate propped fracture lengths. Pumping rates and treating pressures are further design constraints.

2.2 Determining Fracture Azimuth

Although the technology for determining fracture azimuth is far from mature, numerous techniques have been presented. It is important to consider the accuracy and costs of these methods, as well as their reliability. For example, a method that can only be used in open-hole may require a specially drilled well. Several different types of techniques may be required to obtain accurate estimates of fracture azimuth. Economic value of a given level of accuracy is difficult to quantify. After brief discussions

¹ A Mark of Schlumberger

of these methods, some applications are reviewed.

2.2.1 Seismic Methods

The two most common types of seismic body waves are compressional waves and shear waves. Compressional waves, or p-waves, are generally used in surface seismic data. The p-wave motion is in the direction of propagation and, consequently is sensitive to the acoustic impedance of the material through which the waves are propagated. Shear, or s-waves, move perpendicularly to the direction of propagation and are sensitive to the shear strength of the media. The s-wave velocities are approximately one-half the p-wave velocity for the same material.

Velocity anisotropy is the dependency of seismic velocity variations on the direction of measurement. Unequal horizontal stresses should cause azimuthal anisotropy in the shear waves. Shear waves are thus *polarized*, with the fastest component travelling in the direction of the maximum compressive stress. Historically, seismic exploration methods have focused on recording p-waves from explosive or vibrator sources with vertically oriented geophones. Polarization of p-waves is nearly scalar containing only a small fraction of the information carried by the s-waves⁵⁸. Shear wave velocities depend both on measurement location and direction of polarization of the shear wave. The direction of the principal stress axes then determines the (orientation of the velocity with which polarized shear waves will travel.

Shear Wave Splitting

Polarization of three component shear waves can provide information about the stress distributions of the rock through which they propagate. Knowledge of stress anisotropy can lead directly to inference of fracture azimuth. Most discussions of the effects of azimuthal anisotropy appear in the earthquake seismology literature and deal only with the simple case of vertical transverse anisotropy with a horizontal symmetry axis⁵⁹.

A more general case of azimuthal anisotropy is likely to occur in most oilfield

applications⁶⁰. Shear wave splitting (also known as birefringence and double refraction) is routinely observed in shear wave Vertical Seismic Profiles (VSP). Some degree of anisotropy in rock properties is almost universally observed due to some form of oriented structure. Small scale crystal alignment, grain alignment, layering, and aligned cracks or micro-fissures are physical reasons for this anisotropy. Even a perfectly homogenous rock could have different seismic velocities when subjected to stress anisotropies. Small cracks are the most important factor in creating large anisotropies. These cracks are usually oriented parallel to the maximum compressive stress^{20, 194}. Maximum compressive stresses are usually horizontal^{122,121, 272}. Both natural and induced hydraulic fractures should be vertical and aligned with the direction of the compressive stress.

Vertical Seismic Profiles (VSP)

Shear waves at the earth's surface are distorted by phase, amplitude, and mode changes. Surface imposed anomalies complicate analysis of velocity anisotropy interpretation, perhaps beyond hope for the desired application. It is easier to interpret shear waves recorded below the surface. Three-component geophones have been used for this purpose⁹⁰.

Johnston¹²⁶ reported on Exxon's experimental efforts with multiple s-wave polarization surveys in the naturally fractured Austin Chalk formation. Azimuthal anisotropy was confirmed by significant velocity contrasts associated with the preferential orientation of the natural fractures. That orientation was determined by borehole televiewers.

A typical application to measure shear wave propagation directly would use gyroscopically oriented, three-component geophones. One VSP would use a compressional wave vibrator offset between 500-1000 feet from the borehole (for a depth of interest of 10,000 feet) to suppress the tube wave. A pilot signal sweep in the 8-80 hz bandwidth could be used for the compressional wave survey, with a small array of surface geophones to calibrate and orient the geophones. This would allow an accurate velocity tie to surface seismic data and give a measure of Poisson's ratio. The other geophones

would record orthogonally polarized shear waves; location of these monitoring VSPs requires an estimate of *in situ* stress directions.

Hardin and Toksoz¹⁰⁹ discussed a technique designed to utilize the tube waves generated by seismic p-waves incident on a fracture intersecting a borehole. This response is largely due to fluid exchange between the borehole and the fracture with an efficiency theoretically related to fracture permeability. They also determine azimuth by multiple offset VSP surveys.

Tri-Axial Borehole Seismic(TABS)

Dobecki⁷⁰ describes a technique in which a tool like a VSP monitors microfracture events associated with a small hydrofracturing operation. A seismic tool is clamped below the perforations while a fracture treatment is conducted without proppant. The tool contains three orthogonally oriented geophones or accelerometers. Downhole orientation is determined by detonating explosives in shotholes or other wells, or by gyroscopic equipment. Field performance has been successful; however, resolution is complicated by significant natural fracturing¹⁴¹.

The Fenton Hill 'Hot Dry Rock' experiment conducted by Los Alamos National Laboratories⁹ exhibited substantial microseismic activity in the fairly narrow seam of rock enclosing the fracture. Microseismicity continued for several hours after pumping had ceased¹⁹. This permitted mapping fracture azimuth, height and length. Further studies showed potential for mapping the fracture by the TABS technique either in the fractured well²²² or in a nearby observation well. Sorrells and Mulcahy²³⁵ describe further improvements to the TABS technique that incorporate pressure transient data. They reported results of eight successful applications and conclude that the technique is commercially viable.

Wittrisch and Sarda²⁶⁵ describe a similar tool (Simfrac) that has been used in France. Tri-axial accelerometers are incorporated with the horizontal well logging technology developed by IFP. Operation is essentially identical to the TABS method.

2.2.2 Methods Requiring Cores

Core methods have many of the same limitations as the direct observation methods. Although the importance of *in situ* stress measurements for azimuth and magnitude is widely recognized, numerous difficulties remain ⁷¹. Coring methods are generally limited to core lengths of only 30-90 feet. Data scatter, residual stresses, and scale dependency obscure interpretation of core data. Accuracy of orientation is generally limited to the precision of the orienting tool. Difficulties in orientation techniques include core spinning and other translations of the scribe mark, core jamming and breakage; and missing pieces. These difficulties can be overcome by using either high resolution dipmeters or borehole viewers or by improved correlations with CAT scan or NMR methods ¹¹⁸. Core determined orientation of fracture azimuth may be unduly influenced by local heterogeneities, faults, or structural features. On the other hand, multiple tests in a single formation are possible, costs are only marginally higher than for conventional coring, and analysis is straightforward.

Strain Relaxation

Whole cores can be cut at virtually *in situ* strain conditions, depending on the depths, pressures, and rock properties involved. Freshly pulled, cores continue to relax from their initial stresses for several hours following recovery. Blanton and Teufel ^{31, 33, 32, 242, 245} describe a technique for measuring these relative strains. Three or more pairs of sensitive strain gauge transducers are mounted on a solid ring spaced around the oriented core, measuring the strain response. Core dehydration is assumed to be nondirectional; thermal related strains must be considered.

Finley and Lorenz ⁸⁶ discussed the types of core fractures caused by drilling and coring operations. Anelastic strain recovery measurements were used to determine the maximum horizontal stress direction. Petal and petal-centerline fractures are induced ahead of the core bit during drilling and have a strike controlled by a combination of *in situ* stresses and bit torque. The authors suggest that core fracture characteristics can be used to compute whether hydraulically induced fractures will parallel or intersect natural fractures.

Field results for strain relaxation report a variety of results. Teufel's ²⁴⁴ results on a test well near Tulsa, OK gave results agreeing within 10 degrees of values obtained from a downhole television camera and a surface tiltmeter survey. Determination of stress direction is reasonable for vertical holes, flat-lying beds and sedimentary rocks; it is also possible to estimate stress magnitude by this technique ²⁵⁵ . This method can only be performed at the wellsite and has become less applicable as the following techniques have been developed. El Rabaa and Meadows ²⁰⁸ reported on an extension of this technique and observed that cores containing natural fractures may yield strain relaxation stress directions that are in error by 90 degrees!

Differential Strain Analysis

Differential Strain Analysis (DSA) was introduced by Strickland and Ren ²³⁹ and involves repressuring a sample of oriented core above its initial pressure and recording oriented strain data as pressure is reduced. This method has been reported extensively ^{215, 229, 228} and produces results similar to strain relaxation if irreversible changes in the rock have not occurred. Cores recovered from abnormally pressured reservoirs are likely to have such irreversibilities. Field tests of DSA show good agreement for cores up to a few months old. Cores stored longer than a year gave inconsistent results ¹⁴¹ .

Sonic Velocity

Lacy ¹⁴¹ described a method using other azimuth dependent rock properties. If the microcrack model is applicable, sonic waves should be scattered differently depending on the core direction. P-waves should be only marginally attenuated and scattered in a direction parallel to the microcracks, but strongly attenuated and scattered in the direction normal to the microcracks. The phase velocities of p-waves should therefore be a minimum in the maximum stress direction. The extent, of the scattering and attenuation is largely a function of wave frequency and crack width.

Thin sections

Almost all low permeability, productive reservoirs have some degree of natural fracturing. Thin sections may provide direct evidence of the existence of significant anisotropies. Due to the extremely small scale of a core thin section (often smaller than the Representative Elementary Volume ²¹), it would be unwise to determine azimuth solely from thin sections.

2.2.3 Direct Observation Methods

Direct techniques provide virtually indisputable results for determining fracture azimuth when they can be applied. Unfortunately, these methods are often difficult to apply and are unduly influenced by local wellbore conditions. Direct observation generally requires an open-hole section to be tested and hydraulically fractured. A mini-frac in an open hole section may require altering casing setting plans, thus adding substantially to costs. Open hole techniques may not even be feasible for a majority of wells. Local heterogeneities may influence fracture azimuth and make the value ascertained from these techniques unreliable. Some field results show significant influences from nearby faulting and structurally related effects, especially when the difference between the maximum and minimum horizontal stresses is not large.

Borehole Televiewers

Although television type cameras can be used at shallow depths with clear fluids in the hole, most reports of detection of fracture azimuth have been made with the borehole acoustic televiewer ^{25, 114, 206, 201, 241, 264, 268}. This is an ultrasonic tool with a high resolution transducer rotating **360** degrees and generating a map of the borehole surface from the sonic travel time. The acoustic transducer emits a narrow, focused beam with a pulse rate of 1800 times per second. The tool is oriented magnetically with an accuracy similar to that of dipmeter tools. Clear and detailed representations of the borehole walls can be obtained by this technique. Spalling (borehole ellipticity) can be observed and a fairly detailed map of vugs, and natural fractures can be

obtained.

Georgi ⁹² reported degradation of acoustic televiewer images due to low amplitude returns. Transducer energy is strongly collimated requiring the acoustic beam to be nearly normal to the wall. Eccentricity of the tool and borehole ellipticity can produce vertical stripes and loss of information. Stock *et al* ²³⁷ reported representative field application results, and determined the relative magnitudes of S_h and S_v . The presence of vertical fractures at the well was observed and interpreted as drilling induced fractures extending preexisting microcracks.

The mechanism of wellbore stress-induced breakouts was described by Gough and Bell ⁹³, and Zoback ²⁶⁹. Breakouts are the result of localized shear failure around a wellbore due to horizontal compression. The result is spalling on both sides of the hole corresponding to the least horizontal stress. Presuming that this stress is less than the vertical compressive stress, a hydraulically induced fracture will propagate normal to the observed spalls. Zoback and Zoback demonstrated excellent correlation between the stress-induced spalls and independent measures of stress orientation ²⁷¹. Figure 2.1 is an illustration of their studies of the direction of maximum horizontal compressive stress on the coterminous United States based on earthquake focal mechanisms, *in situ* stress measurements, wellbore breakouts, and geological studies.

Barton *et al* ¹⁸ reported the use of a borehole acoustic televiewer for determining *in situ* stress orientation at the Fenton Geothermal Site in New Mexico. The observations of stress-induced breakouts and subsequent analysis yielded a well-resolved orientation of the least principal stress. By analyzing the locations of breakouts along with the lab-measured unconfined rock compressive strength, the authors were able to estimate the magnitude of the principal stresses and explain certain observed geological phenomena. Figures 2.2 and 2.3 illustrate a typical statistical analysis of the televiewer results². The standard deviation of the observed values of breakout azimuths is eleven degrees.

Figures 2.4–2.5 illustrate the rock mechanics concepts associated with wellbore

²Figures 2.2–2.5 are courtesy of C. Barton and M. D. Zoback of Stanford University

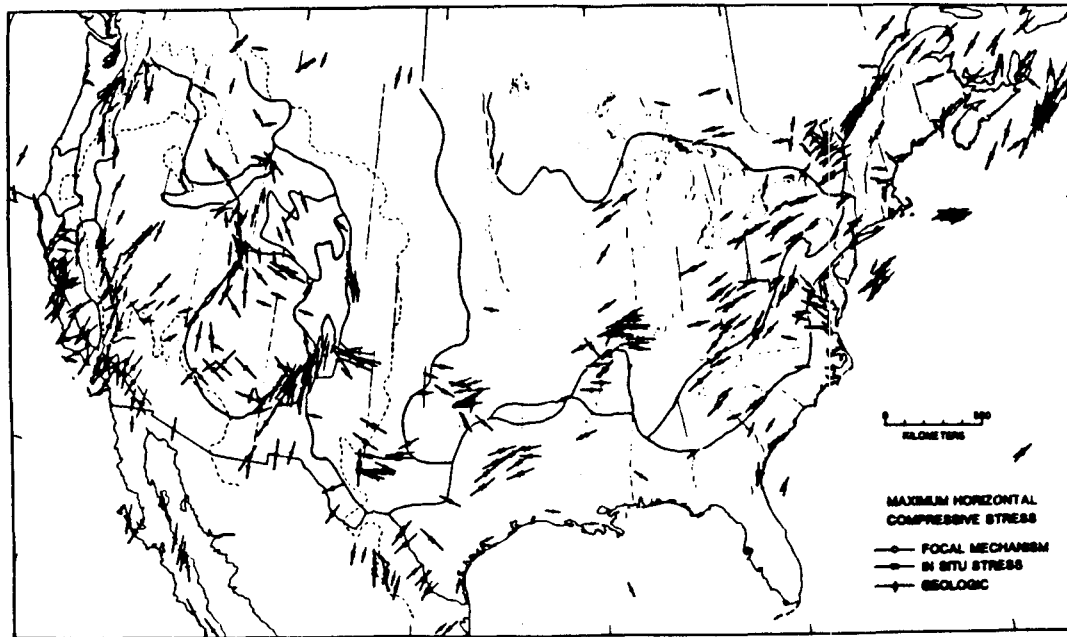


Figure 2.1: Direction of Maximum Horizontal Compressive Stress in the United States (after Zoback and Zoback)

spalling and demonstrate how these are utilized in the borehole televiewer log. Figure 2.4 shows a simple representation of the stress distribution around the wellbore with wellbore spalling (breakouts, ellipticity) in the direction of the minimum horizontal stress. Hydraulic fractures would initiate normal to this direction, in the direction of the maximum horizontal stress. Figure 2.5 shows an actual televiewer log result over a 2 meter interval of open hole that has been hydraulically fractured. Note the occurrence of a breakout, or spall, orthogonal to the vertical fracture.

Olsson *et al* 199 describes an analogous tool developed in France using radar images to detect fracture zones and their images. All previously identified zones and new fractured intervals were determined. Orientation was accomplished using multiple boreholes.

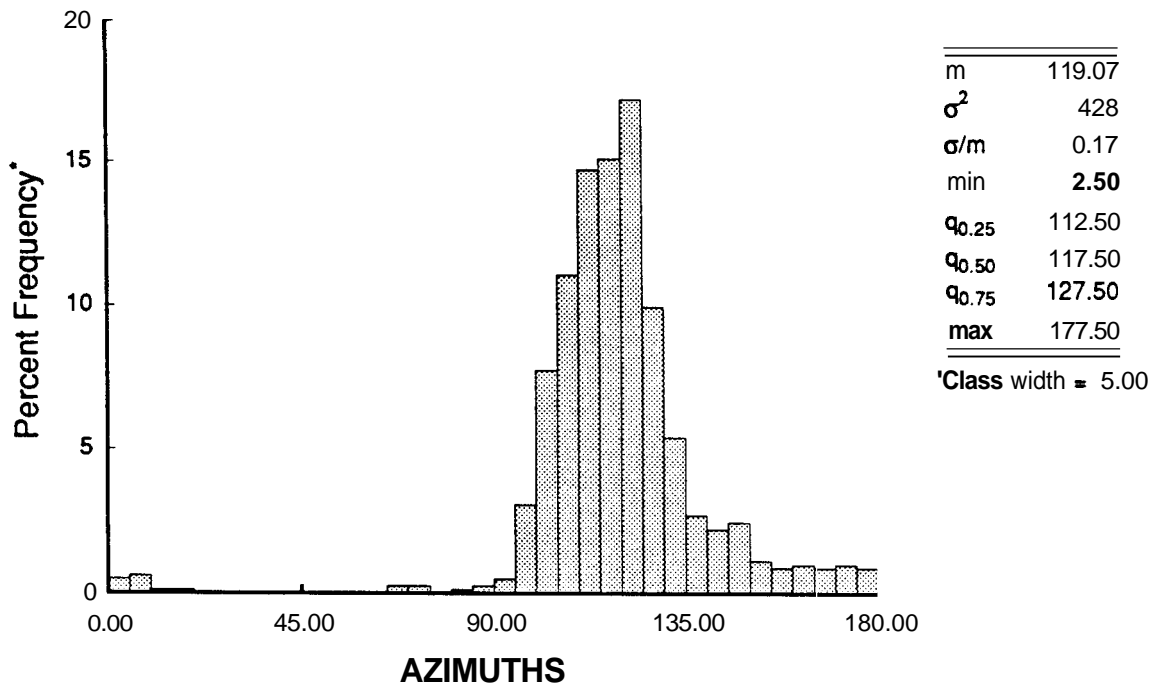


Figure 2.2: Histograms of Breakout Azimuths Over a 200 Meter Interval in the Fenton Hill Well (after Barton *et al*)

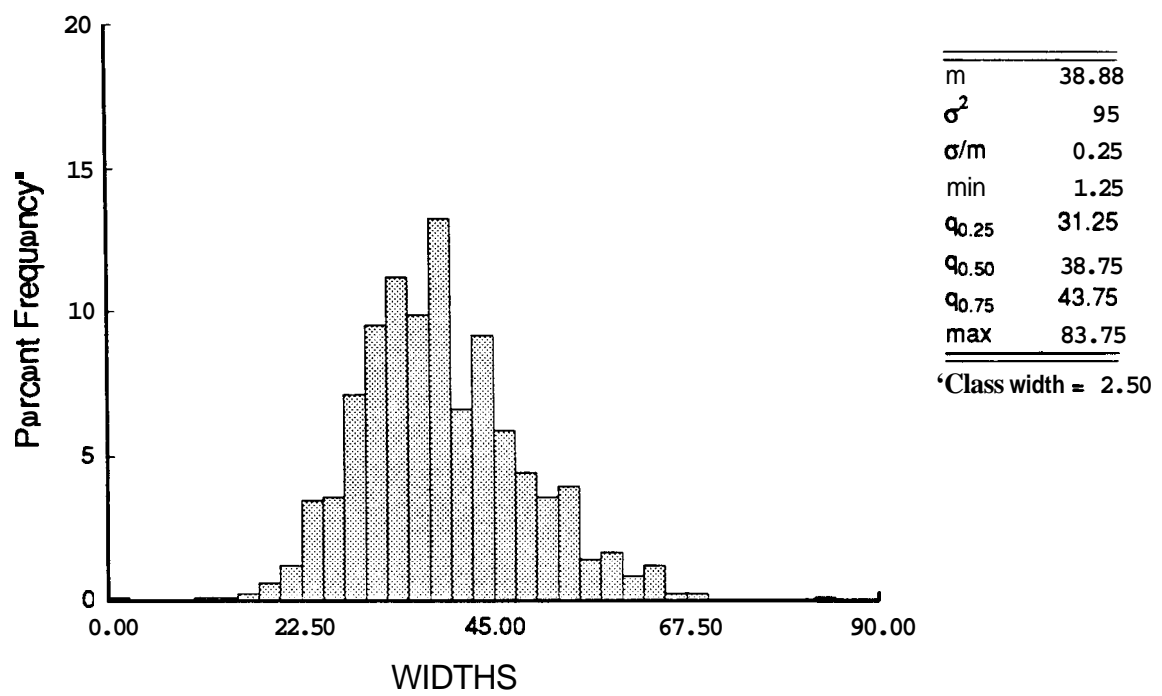


Figure 2.3: Histograms of Breakout Widths Over a 200 Meter Interval in the Fenton Hill Well (after Barton *et al*)

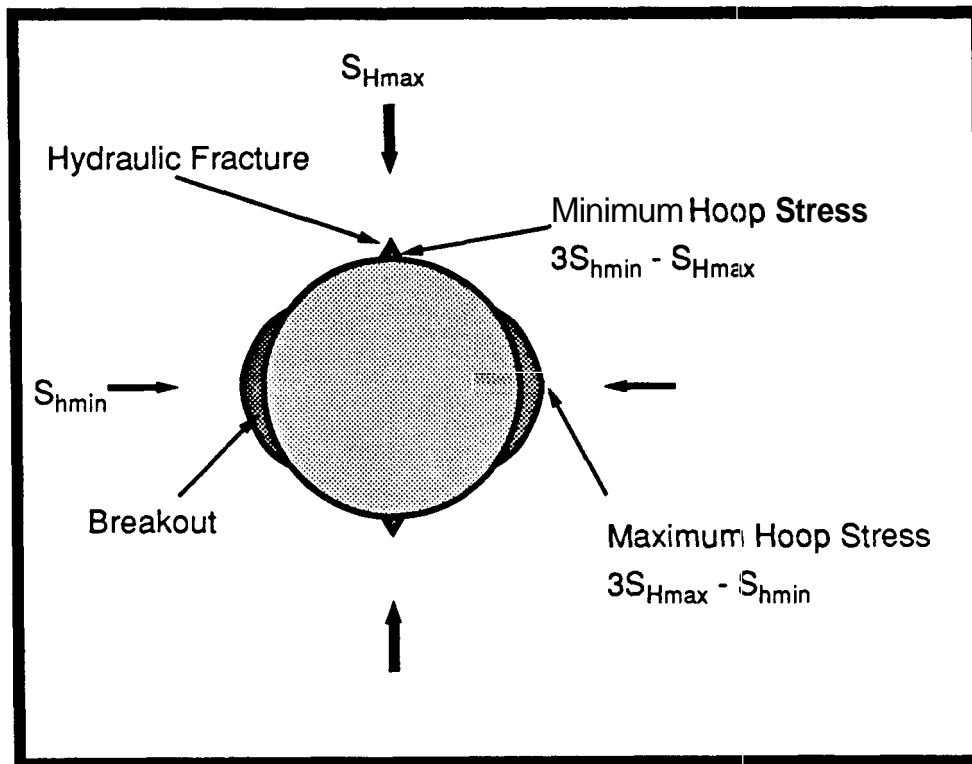


Figure 2.4: Stress Distributions Around the Wellbore

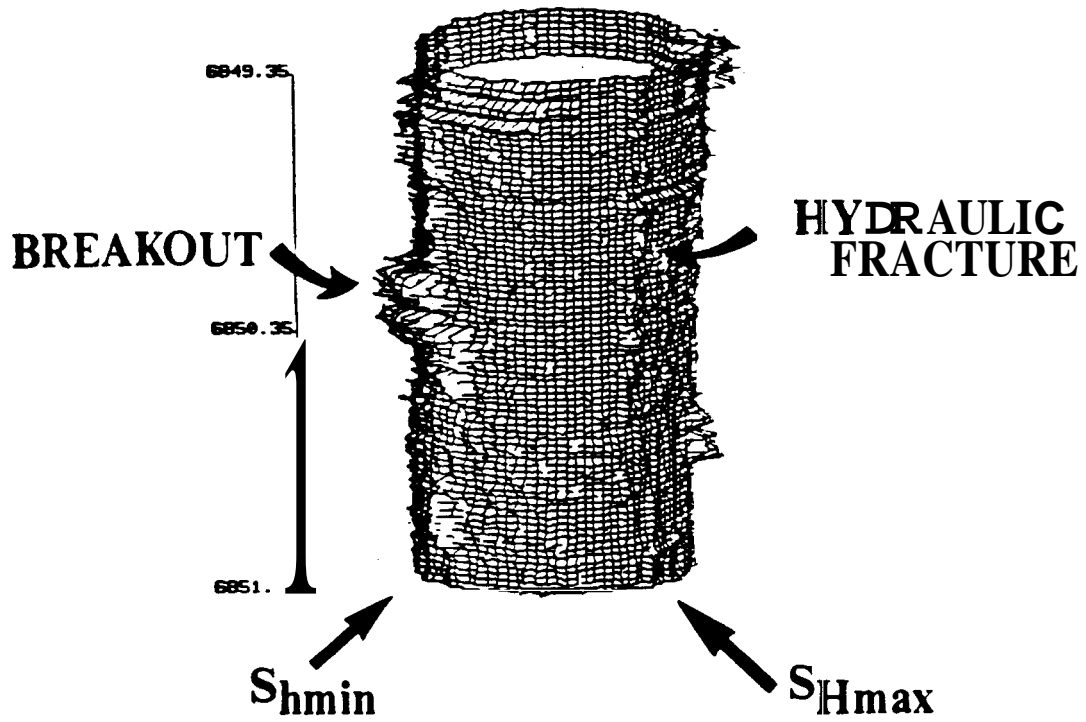


Figure 2.5: Example Televiewer Log

Dipmeters and Other Caliper Logs

Many four-arm dipmeter logs already exist in a wide variety of locations. If spalling is observed continuously over several intervals, dipmeter results may be used to detect stress azimuths as well. Unfortunately, it is not always possible to conclude that borehole ellipticity, as determined by caliper logs such as the (dipmeter, is in fact due to stress-induced wellbore breakouts. Televviewer logs may be analyzed to confirm the nature of the breakouts observed by dipmeters.

Many authors have reported the use of the dipmeter tool either to identify natural fractures or to locate potential breakouts 15, 57, 111, 232 . Brown *et al* 36 presented results from 50 wells in the East Texas Basin's relatively deep Cotton Valley formation. Only 1% of the observed 'washouts' were not in the general direction of the dominant N35W/S35E trend observed in the other wells studied. Although the data presented are excellent, the paper's conclusion that hydraulic fractures will be generated in the same direction as the wellbore breakouts is incorrect. Figure 2.6 is the map presented by Brown *et al.* , showing the remarkable degree of similarity across an area of several hundred kilometers of East Texas. The arrows at each well location are *not* the direction of the fracture azimuth, but rather the direction of spalling. Induced hydraulic fractures will be normal to that direction. Nonetheless, the dipmeter results are remarkably consistent over a wide range.

Figure 2.7 presents a histogram of the borehole elongation azimuths. The distribution of these azimuths is in a narrow range for a group of 50 wells scattered over a large region. The use of borehole televviewers may be required for other areas to clarify which borehole elongations are due to spalling.

Westermarck and Scholes 261 used the cement evaluation tool (CET) for open hole fracture identification for highly acoustically reflective granodiorite. By combining directional survey data, a fracture orientation log was obtained.

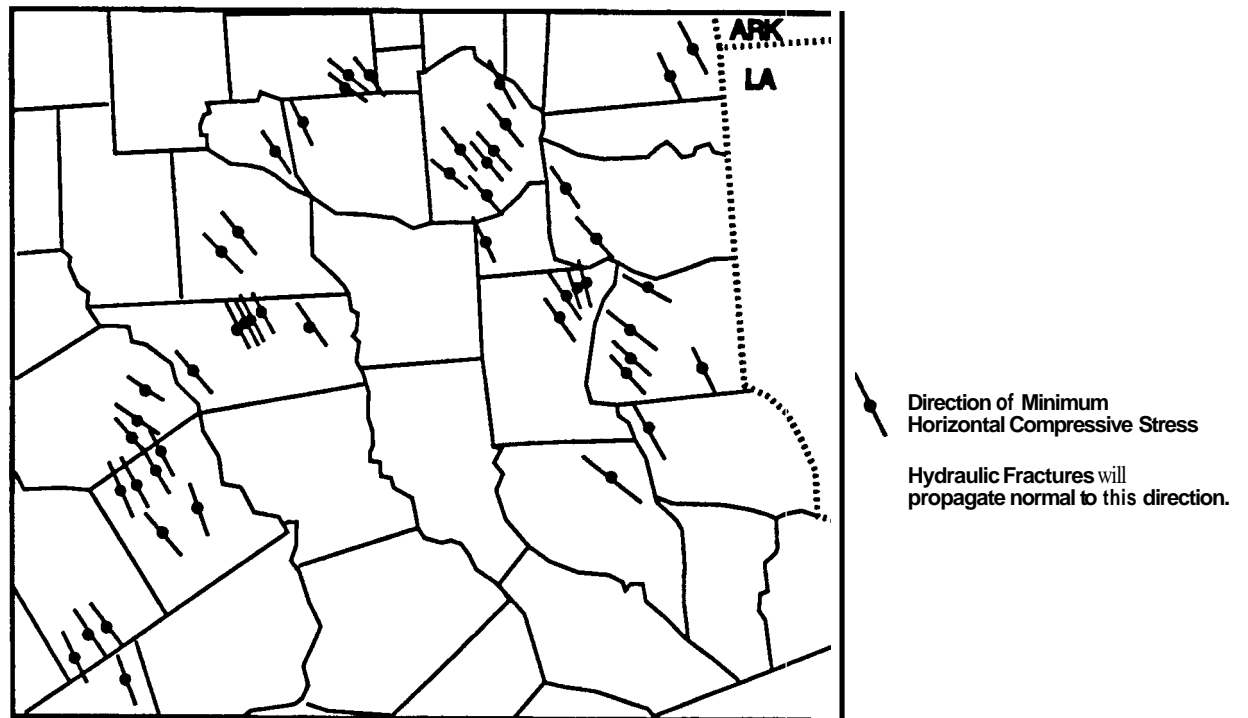


Figure 2.6: Map Showing Location of Wells and Azimuth of Spalls, after *Brown et al.*

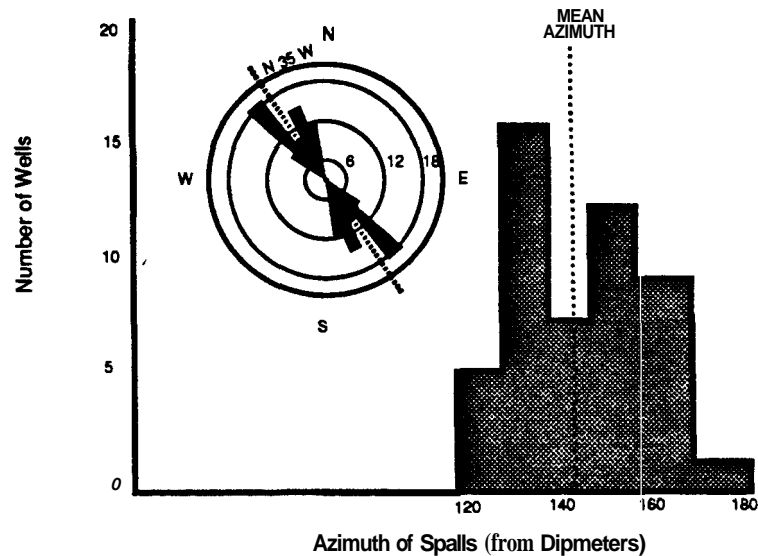


Figure 2.7: Histogram and Azimuth Frequency Plot for Cotton Valley Study *after Brown et al*

Formation MicroScanner

The Formation MicroScanner³ (FMS tool) is an extension of dipmeter technology which substitutes a dense array of microresistivity devices for those on one arm of the dipmeter tool. This array provides a strip image of the wellbore with approximately 14% coverage of the wellbore⁷⁹. This tool provides detailed spatial resolution in addition to conventional dipmeter data. Plumb and Luthi²⁰⁵ contrasted the relative strengths and weaknesses of the FMS and the borehole televiewer. High-resolution FMS images are similar in geological information to a core photograph; natural and drilling induced fractures can also be spotted. Wellbore breakouts are better identified by the televiewer device,

³A Mark of Schlumberger

Impression Packers

Impression packers such as the Lynes inflatable packer have malleable rubber jackets covering metal elements that can be expanded mechanically or hydraulically. Arbitrary lengths can be obtained and run on the end of tubing, but gaps between individual packers can be problematic. This method provides fairly clear estimates of a fracture azimuth, height, and aperture in an open hole section. Mechanical difficulties are common and applications are generally limited. Another factor to be considered for extremely tight reservoirs is that the open hole mini-frac contains no proppant and the induced fracture will close. Sometimes this leaves a mark which is essentially indistinguishable from gouges, cuts, or preexisting hairline fractures. This can be solved by running prefracture packers.

Fraser and Pettit⁸⁷ used impression packers in a well in the Howard Glasscock Field in Texas in 1961 to determine fracture azimuth and improve the waterflood recovery from that field. Anderson and Stahl¹² used impression packers on three fractured wells in the Allegheny Field in New York in the mid-1960's and found that the fracture orientations from well to well did not change very much.

Charlez *et al*⁴⁰ extended the methodology to using straddle inflatable packers surrounding radial displacement transducers. The authors report that a single mini-frac test with this tool can yield azimuth, minimum and maximum stresses, and certain elastic rock constants. Results reported by Hansen and Purcell¹⁰⁴ are discussed in Section 2.3. They reported moderate success due to the shallow depths but, nonetheless had mechanical difficulties and less accuracy than other methods. Similarly, Griffin⁹⁴ reported technical problems and high costs associated with this tool.

Fracture Overcoring

Danésy *et al*⁶⁵ presented a technique included in this section because of its direct nature, even though coring is involved. In this method, a hydraulic fracture is created in the open hole while the well is being drilled. It is assumed that the fracture will extend below the drilled out section, 'ahead of the bit'. An oriented whole core is then

run to recover fractured, but as yet undrilled section of hole. Although the success rate of the method is only about 50 %, the method provides several interesting results.

A summary of pertinent observations follows:

- o The ISIP (Instantaneous Shut In Pressure) obtained when pumping is ceased is a good measure of the least principal stress. Variations of ISIP of 200-300 psi during a test or for different tests within a zone were observed. This led the authors to observe that stress differences less than this amount were insignificant.
- o Essentially no correlation between stress and rock mechanical properties (Young's modulus, Poisson's ratio, or tensile strength) was observed.
- o The orientation of the in *in situ* principal stress remained constant with depth.
- o The recovered fracture surfaces were smooth, vertical, and, when the bottom of the fracture was recovered, there was no mud penetration into the fracture bottom.

This last observation is consistent with the model of Christianovich and Zheltov⁴³

2.2.4 Pressure Analysis Methods

As early as 1960, Elkins and Skov⁸¹ discussed a possible application of pressure transient analysis to determine the azimuth of hydraulic fractures. The method they proposed was a simple one, and assumed the applicability of the line-source solution in an anisotropic reservoir. More sophisticated techniques have been developed; however, their applicability has not been widespread in low permeability reservoirs due to the long test times and high resolution pressure measurement devices required.

Interwell Interference

Pierce *et al.* described a method for determining fracture azimuth and fracture length by pulse testing²⁰⁴; however, the work of Uraiet, *et al*²⁴⁸ provided the most applicable techniques for azimuth determination using pressures recorded at the active

fractured well. Uraiet considered only uniform flux fractures. An extension by Cinco-Ley and Samaniego⁴⁷ considered finite conductivity fractures as well. Unambiguous determination of fracture azimuth will require two observation wells located at other than 90 and 180 degrees from the active well. Other complexities associated with this technique arise from the heterogeneities in the reservoir. For example, the permeability variations in the drainage area of a given well being tested are averaged in a fashion that is not entirely understood. No current model exists to assess the impact of these heterogeneities on interference test determination of fracture azimuth.

Pierce *et al*²⁰⁴ and Abobise and Tiab² also extended the practical applications of this technique. Unfortunately, the extremely low permeabilities of most candidate formations result in the need for both high-resolution (high cost) pressure transducers and very long tests. Reservoir heterogeneities, multiple layers, and surface interference can make azimuth detection by interference testing unacceptable. The resolution with respect to azimuth is also fairly low. Field tests to evaluate fracture azimuth were reported by Frohne and Mercer^{88, 89} and Sarda²²¹.

Offset Monitoring During Fracturing

It is possible that pressure interference methods could be utilized during the actual fracturing of an active well. In such a case, the offset wells would be produced or shut-in continuously during the fracture treatment. Analysis would be by extension of available techniques. Oliver reported on the pressure transients caused by fracturing¹⁹⁸.

2.2.5 Other Methods

Surface Tiltmeters

Sensitive tiltmeters are commercially available for the detection of the orientation of hydraulic fractures^{267, 266}. The sensitivity of the bubble detectors involved is such that tilts in the earth's surface of as little as 10 nanoradians can be detected. The use of tiltmeters rests on the assumption that a significant amount of the total

energy expended in the hydraulic fracturing process deforms the earth's surface. The extremely high sensitivity is required due to the generally small signal-to-noise ratios for deeper fracture treatments. Results of moderate depth tests (4700–5500 feet) in Colorado and Texas yield direction and approximate created lengths for vertical fractures.

Smith *et al*²³⁴ compared tiltmeter and surface electric potential measurements in Wattenburg Field in a comprehensive study of azimuth detection techniques. Riccio²¹⁶ reported on the successful use of tiltmeters for very shallow wells with horizontal fractures. They assumed that the area and shape enclosed by the surface tilt contour corresponded to the area and shape of the fracture. The unknown fracture thickness was a critical missing parameter in fitting observed tilts to calculated fractures. Hanson *et al*¹⁰⁸ studied the theoretical effects of layering on the surface deformation caused by fracturing and compared the results of laboratory tests.

Tidal Strain

The solid earth tidal strain method was discussed by Hanson and Owens¹⁰⁸. It is a passive technique to determine azimuth of natural or hydraulically induced fractures using either static or observation wells. The data acquisition requirements are not excessive and only conventional high resolution pressure monitoring is required. It is also possible to develop estimates for total compressibility and interwell ϕc_t . Pore pressure response to the influence of gravitational forces and barometric pressure loading can be determined in conjunction with well tests. Advanced spectral analysis and correlation analysis are required to extract the tidal response from the pressure record. Hanson^{106, 107} presented field results along with a theoretical review.

Regional Geology/Topography

Regional geology and mapping of faults provides an excellent tool for initial estimation of stress anisotropy. Naturally, this requires geological interpretation of the current state-of-stress being derived from prior events; however, this has proven applicable in numerous comparisons of mapping techniques. When tectonic stresses are large

and active, interpretation is complicated. Heavily faulted areas will also be difficult to interpret. Nonetheless, the local interpretation of the magnitude and azimuth of horizontal stresses must ultimately be resolved to a geologic interpretation.

2.3 Field Results

Many field experiments have been reported in the literature; only the most relevant will be mentioned here. Of greatest interest will be those involving and comparing several methods and emphasizing the determination of fracture azimuth.

Griffin ⁹⁴ reported on an extensive study of the Kuparuk Reservoir in northern Alaska with the objectives of optimizing well spacing and locations for waterflooding. He reported on seven methods used in a single wellbore;

- o ellipticity (spalling) as determined from the calipers of dipmeters,
- o on-site measurement of core relaxation,
- o laboratory core measurements by DSA,
- o laboratory core measurements of sonic velocities,
- o TABS,
- o impression packers, and
- o borehole acoustic televiewer results.

These methods were compared for the individual well and fieldwide DSA data, sonic velocity from geophysical methods, and fault and structure mapping. The borehole televiewer and TABS techniques yielded the most robust results, subject to certain mechanical precautions. All of the core techniques had limitations due to the difficulties in obtaining unbroken, oriented cores. On-site core relaxation method was more erratic than the other two methods. Although impression packers were moderately successful, numerous mechanical problems occurred. Figure 2.8 is a distribution

of the predicted fracture orientation directions as determined from the various tests. Agreement is not as straightforward as in Fig. 2.6, even among identical methods.

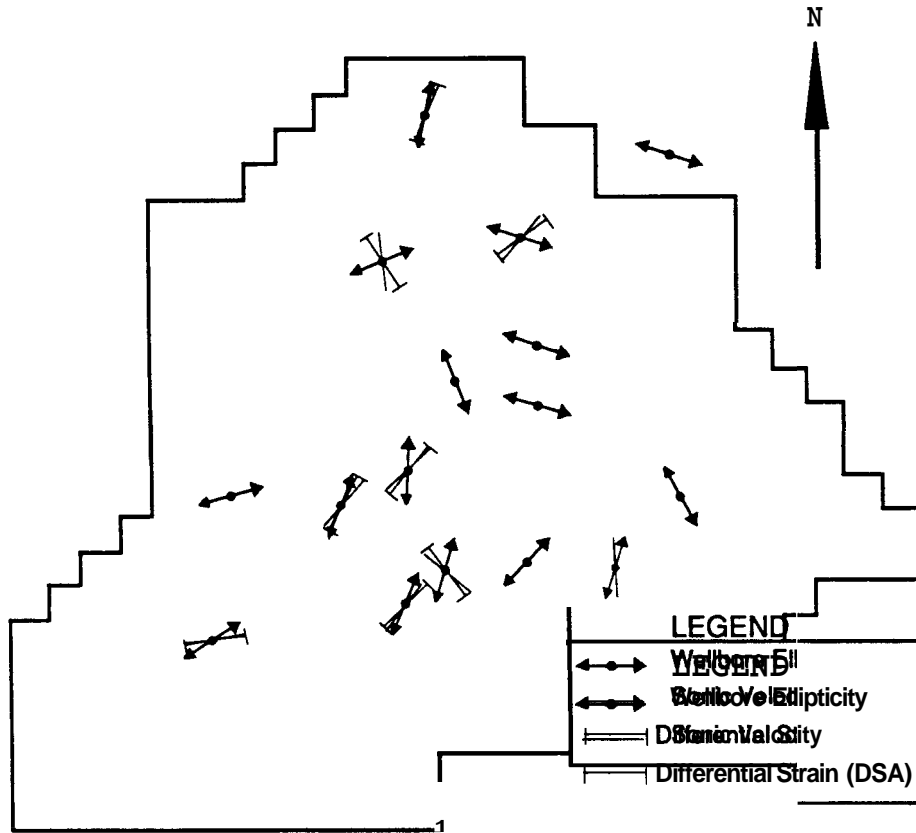


Figure 2.8: Comparison of Predicted Orientation of Induced Fractures from Ellipticity and Core Data, after Griffin

Lacy¹⁴¹ compared five fracture orientation techniques in fields in Alaska and East Texas for wells as deep as 12,000 feet. In addition to TABS and core analysis techniques, Lacy reports fairly extensively on the use of surface tiltmeter arrays including the rather extensive precautions to prevent signal degradation by such influences as trees and surface temperature conditions. Useful resolution of the tiltmeter arrays for deep wells required an increased number of sensors oriented in a fashion requiring *priori* knowledge of the fracture azimuth.

Smith *et al.*²³⁴ compared seven fracture azimuth techniques for a shallow well and reported on significant variations between the techniques. Poor results from

microseismic monitoring suggested the limitations of remote seismic monitoring for sedimentary, hydrocarbon-bearing formations. Hansen and Purcell¹⁰⁴ reported on a detailed study of the giant shallow South Belridge oilfield in Kern County, CA. In addition to the economic interest associated with the steamflood, waterfloods, hydraulic fracturing, and other Enhanced Oil Recovery (EOR) potential of this field, this work has considerable scientific interest in that it parallels and is located less than 20km east of the San Andreas fault. Surface tiltmeters and wellbore breakouts were identified as the most reliable methods for determining stress azimuth. The success of the tiltmeters was largely due to formation depths of only about 500–1000 m. Impression packers and seismic methods had greater scatter.

Smith²³³ reported on the use of surface tiltmeters, surface seismometers, impression packers, borehole viewers, rock strength anisotropy measurements, and surface electric potential surveys in the relatively shallow Wattenburg Gas Field. Although not discussed previously, surface electrical potential has been evaluated by several authors, typically in conjunction with other techniques,^{152, 110}. Interesting conclusions included the observation that unequal fracture lengths in a single well were common; fracture azimuth appeared to vary significantly over a relatively small region; rock anisotropy is important in controlling fracture azimuth; and borehole devices may be misleading in determining fracture azimuth.

Erickson and Waddell compared hydrologic and tracer tests and borehole acoustic televiewer logs to determine stress directions and permeability anisotropy⁸². Evans⁸⁴ discussed geologic analysis of thirteen oriented cores from the Devonian shale. Fractures were correlated with regional stresses and local faulting. Abou-Sayed and Pearson³ reported on four adjacent North Slope oil wells with moderate deviations. Prefracture tests and subsequent fracture treatments were analyzed to provide indications of fracture orientation in deviated wellbores. When the deviated wellbore azimuth was near that of the fracture orientation, the fracture was found to sweep the entire perforated interval.

Clark⁵² compared ten different methods for detecting maximum horizontal stress

direction (and thus fracture azimuth) at the Department of Energy's Multi-Well Experiment (MWX) site in Colorado. Methods ranged from **surface** geological observations, core techniques, and computer simulations of topographic loads. Standard deviation among all methods was surprisingly low.

Recently, Teufel²⁴³ reported on field studies in inclined holes in the North Sea for waterflooding and enhanced oil recovery. Tests for eighteen wells that were deviated approximately 65 degrees from vertical included anelastic strain recovery from cores. Deduced stress azimuths were used to plan the location of injectors and producers to optimize flood recoveries. Zoback *et al*²⁷⁰ compared *in situ* stress and physical property measurements for four shallow core holes and confirmed deeper, regional stresses.

Figure 2.9 compares wellbore breakouts and the orientation of vertical calcite-filled fractures in the MWX well²⁴⁶. It is obvious that current state of stress is nearly the same as that present when the vertical fractures were created and subsequently filled.

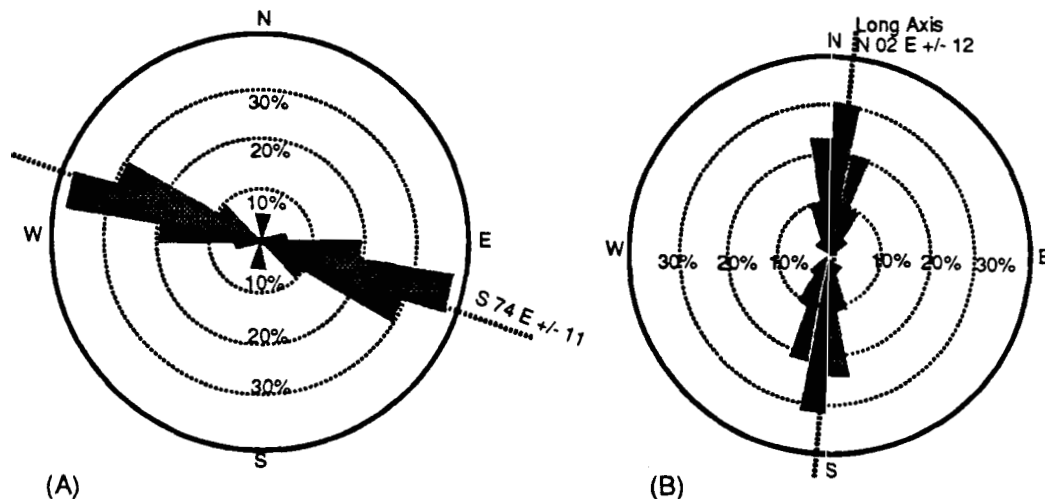


Figure 2.9: Orientation of Vertical Calcite Filled Fractures from Cores (a) and Wellbore Breakouts (b) in the Fluvial Zones of the MWX-1 Well *after Teufel et al.*

Saksa²²⁰ compared radiometric, electrical, dipmeter and acoustic logs to determine geomechanical properties and orientation. They concluded that dipmeter and

acoustic logging do well in detecting fractures and their azimuths, while radiometric methods have inadequate resolution. Sarda²²¹ utilized borehole microseismic events to assist in connecting wells with hydraulic fractures. The most difficult aspect of the operation was determining fracture azimuth.

2.4 Chapter Summary

This chapter has reviewed the fundamentals of hydraulic fracturing including the reasons for stimulation and fracture design principles. A variety of methods to determine hydraulic fracture azimuth were reviewed. These methods range in cost, reliability, and required assumptions. Many of the methods are commercially available and are in routine use. In the next chapter, flow equations and solutions for hydraulically fractured wells will be developed. It will be demonstrated that the uniform flux model is inadequate for interference testing. Finite conductivity fracture models in Laplace space will be developed.

Chapter 3

Flow Equations and Solutions

Performance models for hydraulically fractured wells. Assumptions and derivations for uniform flux and finite conductivity fractures. Laplace transformation of finite conductivity model, advantages of this formulation. Evaluation of resulting integrals, inversion procedure, and verification examples.

3.1 Fundamentals

Fundamental flow equations for Newtonian fluid flow in homogeneous porous media and corresponding assumptions are well known¹⁹⁰. Common assumptions in developing the fundamental diffusivity equation include:

- flow is radial through the porous media with negligible gravity effects (a two-dimensional problem);
- the porous medium is homogeneous and isotropic with constant values for thickness, porosity, and permeability;
- fluid viscosity is constant and the total system compressibility is small and constant; and,
- pressure gradients are small everywhere.

The diffusivity equation is developed by combining Darcy's law with conservation of mass and the constant composition equation of state. The resulting equation is:

$$\nabla^2 p = \frac{k}{\phi \mu c_t} \frac{\partial p}{\partial t} \quad (3.1)$$

in one dimensional radial coordinates, it is:

$$\frac{\partial^2 p}{\partial r^2} + \frac{1}{r} \frac{\partial p}{\partial r} = \frac{k}{\phi \mu c_t} \frac{\partial p}{\partial t} \quad (3.2)$$

Numerous solutions for different boundary conditions have been published. Many of these were direct analogs to solutions of heat conduction problems due to the similarity between the diffusivity equations in temperature and in pressure³⁹. Most solutions involve the Laplace transform or Fourier transform when the radial form of the equation is used. Gringarten popularized the use of Source and Green's functions for solving these problems⁹⁷. Instantaneous Green's functions have these properties:

1. They are solutions to the *adjoint* differential equation, and represent the response to a (fictitious) instantaneous point source of unit strength.
2. They are symmetrical in space with respect to the point at which the fictitious source is introduced and the point at which it is evaluated.
3. They are *delta* functions, vanishing at all points outside the fictitious source boundary and having unit strength at that point.
4. They satisfy the same boundary conditions as the physical problem, except that the Green's functions are *homogeneous*. That is, for cases of specified flux at the outer boundary of the source, the Green's function's normal derivative is zero. For a specified pressure, the function itself vanishes. For infinite systems, the Green's function vanishes at infinity.

3.2 Derivation For the Dimensionless Pressure Drop Due to a Uniform Flux Fracture

Solutions for hydraulically fractured wells using Green's functions can be obtained easily for vertical and horizontal fractures with uniform flux rates per unit area, and approximated very closely for infinite conductivity fractures 44, 95, 96 . The uniform flux fracture solution does not accurately model flow to a fracture *per se*, but has been shown to be a reasonable model for very high flow capacity hydraulic fractures. Most significant differences occur at early times and are more important to well testing problems than to production forecasting.

To solve for the uniform flux fracture, a horizontal plane source and a vertical slab source (both of infinite extent) are combined as in Figures 3.1–3.2. Newman's 195 product method is used to obtain the source function for their product; the uniform flux fracture illustrated in Figure 3.3. The instantaneous source function for the infinite horizontal plane source is:

$$S(y, t) = \exp\left(\frac{-(y - y_w)^2}{4\eta_y t}\right) \cdot \frac{1}{2\sqrt{\eta_y \pi t}} \quad (3.3)$$

For the infinite vertical slab source, the instantaneous source function is:

$$S(x, t) = \frac{1}{2} \left[\operatorname{erf}\left(\frac{x_f + (x - x_w)}{2\sqrt{\eta_x t}}\right) + \operatorname{erf}\left(\frac{x_f - (x - x_w)}{2\sqrt{\eta_x t}}\right) \right] \quad (3.4)$$

The intersection for an isotropic medium, ($\eta_x = \eta_y = \eta$) is:

$$S(x, y, t) = \exp\left(\frac{-(y - y_w)^2}{4\eta t}\right) \cdot \frac{1}{2\sqrt{\eta \pi t}} \cdot \frac{1}{2} \left[\operatorname{erf}\left(\frac{x_f + (x - x_w)}{2\sqrt{\eta t}}\right) + \operatorname{erf}\left(\frac{x_f - (x - x_w)}{2\sqrt{\eta t}}\right) \right] \quad (3.5)$$

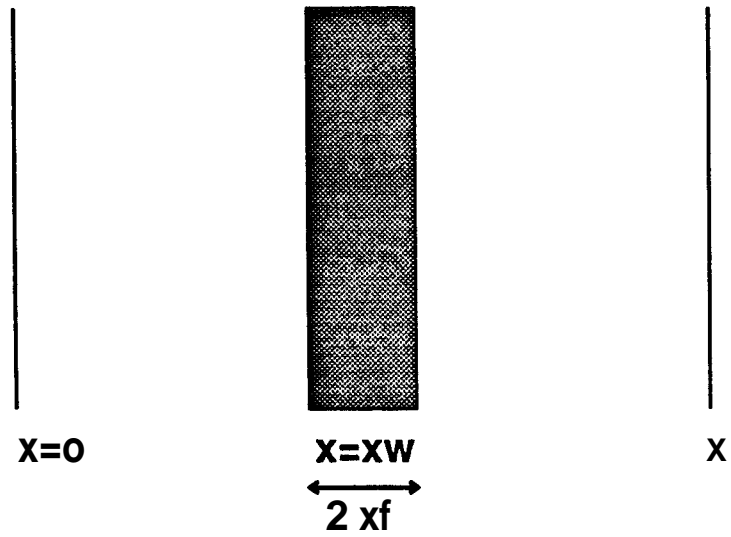


Figure 3.1: Vertical Infinite Slab Source

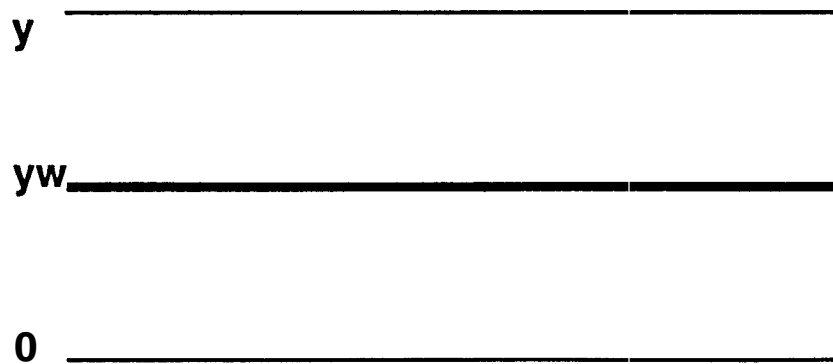


Figure 3.2: Horizontal Infinite Plane Source

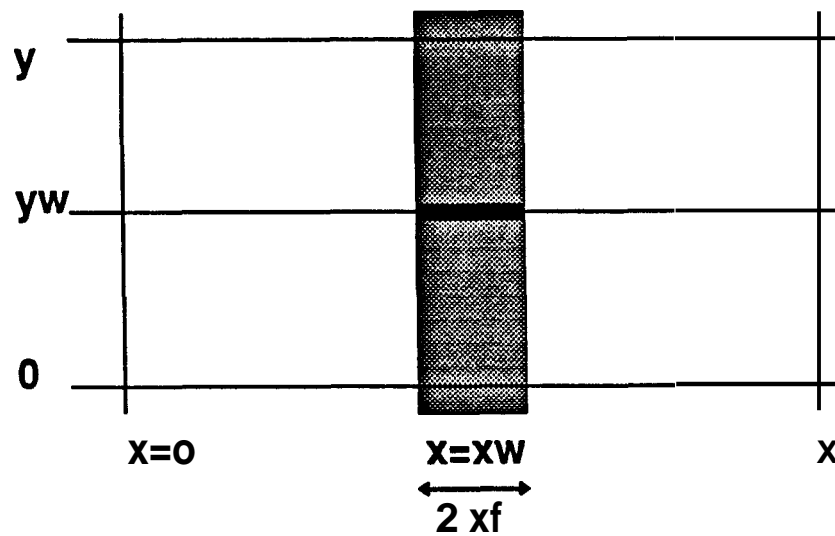


Figure 3.3: Combined Sources to Yield Uniform Flux Fracture

For convenience, dimensionless variables are defined by dividing all of the distances by a characteristic distance, in this case, the fracture half-length, x_f . Gringarten originally used x_f to represent the entire fracture length.

$$y_D = y/x_f \quad (3.6)$$

$$x_D = x/x_f \quad (3.7)$$

$$y_{wD} = y_w/x_f \quad (3.8)$$

$$x_{wD} = x_w/x_f \quad (3.9)$$

Dimensionless time is defined as:

$$t_{D_{x_f}} = t_D \frac{r_w^2}{x_f^2} = \frac{\eta t}{x_f^2} = \frac{kt}{\phi \mu c_i x_f^2} \quad (3.10)$$

The source function can be redefined in terms of the dimensionless time and distance variables:

$$S(x_D, y_D, t_{D_{xf}}) = \exp\left(\frac{-(y_D - y_{wD})^2}{4t_{D_{xf}}}\right) \cdot \frac{1}{2x_f \sqrt{\pi t_{D_{xf}}}}. \quad (3.11)$$

$$\frac{1}{2} \left[\operatorname{erf}\left(\frac{1 + (x_D - x_{wD})}{2\sqrt{t_{D_{xf}}}}\right) + \operatorname{erf}\left(\frac{1 - (x_D - x_{wD})}{2\sqrt{t_{D_{xf}}}}\right) \right] \quad (3.12)$$

In order to obtain the pressure drop at any point \mathbf{M} in space, integrate the source function with respect to time as follows:

$$\Delta P(\mathcal{M}, t) = \frac{1}{\phi c} \int_0^t q(\tau) S(\mathcal{M}, t - \tau) d\tau \quad (3.13)$$

For the constant rate solution, the total flow rate is the product of the instantaneous source rate per unit area and the height and length of the fracture.

$$q = q(\tau) 2x_f h \quad (3.14)$$

Noting that $d\tau = \frac{x_f^2}{\eta} dt_{D_{xf}}$ and $p_D = \frac{2\pi kh}{q\mu} \Delta P$:

$$p_D(x_D, y_D, t_{D_{xf}}) = \frac{\sqrt{\pi}}{4} \int_0^{t_{D_{xf}}} \exp\left(\frac{-(y_D - y_{wD})^2}{4\tau}\right) \cdot \frac{1}{\sqrt{\tau}} \cdot \left[\operatorname{erf}\left(\frac{1 + (x_D - x_{wD})}{2\sqrt{\tau}}\right) + \operatorname{erf}\left(\frac{1 - (x_D - x_{wD})}{2\sqrt{\tau}}\right) \right] d\tau \quad (3.15)$$

where τ is a dummy variable of integration.

3.3 Infinite-Acting Solutions

The integral (Equation 3.15) can be evaluated at $x_D = 0$ and $y_D = 0$ for an infinite reservoir as follows:

$$p_D = \sqrt{\pi t_{D_{xf}}} \operatorname{erf}\left(\frac{1}{2t_{D_{xf}}}\right) - \frac{1}{2} Ei\left(\frac{-1}{4t_{D_{xf}}}\right) \quad (3.16)$$

This solution has linear behavior at early times, such that:

$$p_D = \sqrt{\pi t_{Dxf}} \quad (3.17)$$

Late-time behavior for a uniform flux fracture in an infinite system becomes identical to the solution for constant rate radial flow using an effective well radius.

$$p_D = \frac{1}{2} [\ln t_{Dxf} + 2.809071] \quad (3.18)$$

3.3.1 Analytic Solution

The integral of Equation 3.15 can be evaluated for the pressure drop at any point in an infinite reservoir due to a single uniform flux fracture²⁴⁸. The derivation is summarized here, starting with Equation 3.15. Substituting in the relation $\operatorname{erfc}(u) = 1 - \operatorname{erf}(u)$ and rearranging, :

$$\begin{aligned} p_D(x_D, y_D, t_{Dxf}) = & \quad (3.19) \\ & \frac{\sqrt{\pi}}{4} \int_0^{t_{Dxf}} \frac{\exp(-y_D^2/4\tau_D)}{\sqrt{\tau_D}} \cdot \operatorname{erfc}\left(\frac{x_D - 1}{2\sqrt{\tau_D}}\right) d\tau_D \\ & - \frac{\sqrt{\pi}}{4} \int_0^{t_{Dxf}} \frac{\exp(-y_D^2/4\tau_D)}{\sqrt{\tau_D}} \cdot \operatorname{erfc}\left(\frac{x_D + 1}{2\sqrt{\tau_D}}\right) d\tau_D \end{aligned}$$

These two integrals are identical except for the argument of the complementary error function. Therefore, it is only necessary to consider:

$$I = \frac{\sqrt{\pi}}{4} \int_0^{t_{Dxf}} \frac{\exp(-y_D^2/4\tau_D)}{\sqrt{\tau_D}} \cdot \operatorname{erfc}\left(\frac{a}{2\sqrt{\tau_D}}\right) d\tau_D \quad (3.20)$$

where either:

$$a = \frac{x_D - 1}{2} \quad (3.21)$$

or:

$$a = \frac{x_D + 1}{2} \quad (3.22)$$

Since the pressure distribution in the reservoir is symmetric with respect to both x and y axes, the integral need only be evaluated for a portion of the region. Two specific solutions result for cases with $x_D > 1$ and $x_D < 1$ ($a \neq 0$).

Case A $|x_D| > 1$

In this case, the appropriate integral for evaluation is:

$$I = 1/2 \int_0^{t_{Dxf}} \frac{1}{\sqrt{\tau_D}} \exp\left(\frac{-y_D^2}{4\tau_D}\right) \int_\alpha^\infty \exp(-\lambda^2) d\lambda d\tau_D \quad (3.23)$$

where:

$$\alpha = a/\sqrt{\tau_D} \quad (3.24)$$

By interchanging the order of integration and simplifying, we have:

$$I = \int_\alpha^\infty \exp(-\lambda^2) \sqrt{\tau_D} d\lambda - a \int_\alpha^\infty \exp(-\lambda^2 y_D^2 / (4a)^2) \exp(-\lambda^2) \frac{d\lambda}{\lambda} + y_D \left[\int_\alpha^\infty \exp(-\lambda^2) \int_0^{\beta\lambda} \exp(-u^2) du d\lambda - \int_\alpha^\infty \exp(-\lambda^2) \int_0^{\beta\lambda} \exp(-u^2) du d\lambda \right] \quad (3.25)$$

where:

$$\beta = \frac{y_D}{2a} \quad (3.26)$$

Using the results outlined by Uraiet et al. 248, the integral may be expressed as:

$$I = \left[\frac{\sqrt{\pi t_{Dxf}}}{2} \exp(-y_D^2 / 4t_{Dxf}) + \pi y_D / 4 \operatorname{erf}(y_D / 2\sqrt{t_{Dxf}}) \right] \cdot \operatorname{erfc}(a/\sqrt{t_{Dxf}}) + \frac{a}{2} Ei \left[- \left(\frac{4a^2 + y_D^2}{4t_{Dxf}} \right) \right] - y_D / 2 \cdot \exp\left(\frac{-a^2}{t_{Dxf}}\right) \int_0^\beta \exp(-a^2 u^2 / t_{Dxf} u^2 + 1) du \quad (3.27)$$

Case A $|x_D| < 1$

For this case, the argument a can be either positive or negative. For positive values of a , the results of the previous section can be used. A separate solution for negative values of a can also be obtained. Final expressions for this region are:

$$p_D(x_D, y_D, t_{Dxf}) = \left[\frac{\sqrt{\pi t_{Dxf}}}{2} \exp(-y_D^2 / 4t_{Dxf}) + \frac{\pi y_D}{4} \operatorname{erf}\left(\frac{y_D}{2t_{Dxf}}\right) \right]$$

$$\begin{aligned} & \cdot \left[\operatorname{erf}\left(\frac{1-x_D}{2\sqrt{t_{Dxf}}}\right) + \operatorname{erf}\left(\frac{1+x_D}{2\sqrt{t_{Dxf}}}\right) \right] \\ & - \left(\frac{1-x_D}{4}\right) \operatorname{Ei} \left[-\frac{(1-x_D)^2 + y_D^2}{4t_{Dxf}} \right] \\ & - \left(\frac{1+x_D}{4}\right) \operatorname{Ei} \left[-\frac{(1+x_D)^2 + y_D^2}{4t_{Dxf}} \right] \\ & + C(x_D, y_D) + I_1 + I_2 \end{aligned} \quad (3.28)$$

where

$$C(x_D, y_D) = 0 \text{ for } x_D > 1 \quad (3.29)$$

$$C(x_D, y_D) = -\frac{\pi y_D}{2} \text{ for } x_D < 1 \quad (3.30)$$

and:

$$C(x_D, y_D) = -\frac{1}{4} \text{ for } x_D = 1 \quad (3.31)$$

$$\begin{aligned} I_1 = & \quad \frac{y_D}{2} \exp \left[-\frac{(1-x_D)^2}{4t_{Dxf}} \right] \\ & \int_0^{\alpha_1} \exp \left[-\frac{(1-x_D)^2}{4t_{Dxf}} u^2 \right] \frac{du}{u^2+1} \end{aligned} \quad (3.32)$$

$$\begin{aligned} I_2 = & \quad \frac{y_D}{2} \exp \left[-\frac{(1+x_D)^2}{4t_{Dxf}} \right] \\ & \int_0^{\alpha_2} \exp \left[-\frac{(1+x_D)^2}{4t_{Dxf}} u^2 \right] \frac{du}{u^2+1} \end{aligned} \quad (3.33)$$

and:

$$\alpha_1 = y_D / (1 - x_D)$$

$$\alpha_2 = y_D / (1 + x_D)$$

Integrals 3.32–3.33 may be evaluated numerically or through a recursion relationship. In this study, the IMSL routine DQDAGS was used. Alternative evaluation techniques would be to evaluate both dimensionless real space integrals or to use a Laplace space solution.

3.3.2 Closed Boundary Solutions

No-flow or constant pressure boundaries can be obtained by superposition of the pressure drops from more than one well. A simple case has been presented by Gringarten⁹⁵ and requires the summation of the responses of a double infinite array of wells. Simply put, the no-flow boundaries are created by generating the pressure drops due to an infinite array of wells on a square grid with the fractures oriented parallel to the grid axis. In this arrangement, no-flow boundaries are generated equidistant between wells. In a practical sense, the actual number of wells required for the superposition is a function of producing time. At very early times, the well is infinite acting and is independent of the other wells in the system. As time increases, the other wells have increasing effects.

To evaluate the integral for the case of equally spaced wells numerically, simply evaluate the pressure drop at (0,0) due to the well and add increasing numbers of offset wells until the incremental pressure drop resulting from distant wells is a negligible fraction of the total pressure drop. In practice, symmetry considerations substantially reduce the number of calculations required. Application of Poisson's formulation will transform this solution from a double infinite sum to the product of two infinite sums obtained by Gringarten. Consider a well located at the origin, and let the indices n and m count the number of x and y units which separate the wells. The integral to be evaluated is:

$$p_D(t_{D_{z'}}) = \sum_{n=-\infty}^{\infty} \sum_{m=-\infty}^{\infty} \frac{\sqrt{\pi}}{4} \int_0^{t_{D_{z'}}} \exp\left(\frac{-(my_D)^2}{4\tau}\right) \cdot \frac{1}{\sqrt{\pi\tau}} \cdot \left[\operatorname{erf}\left(\frac{1+(nx_D)}{2\sqrt{\tau}}\right) + \operatorname{erf}\left(\frac{1-(nx_D)}{2\sqrt{\tau}}\right) \right] d\tau \quad (3.34)$$

If the wells are equally spaced but the fractures are oriented at an angle, the rotation matrix can be used to recast the wells in a revised; coordinate system with all of the fractures parallel with the x-axis. New well locations are as follows:

$$\begin{pmatrix} x' \\ y' \end{pmatrix} = \begin{pmatrix} \sin(\theta) & -\cos(\theta) \\ \cos(\theta) & +\sin(\theta) \end{pmatrix} \begin{pmatrix} x \\ y \end{pmatrix} \quad (3.35)$$

These values can be substituted into Equation 3.34 to find the pressure drops as a function of θ and dimensionless time (Equation 3.36).

$$p_D(\theta, t_{Dxf}) = \sum_{n=-\infty}^{\infty} \sum_{m=-\infty}^{\infty} \frac{\sqrt{\pi}}{4} \int_0^{t_{Dxf}} \exp\left(\frac{-(my'_D)^2}{4\tau}\right) \cdot \frac{1}{\sqrt{\pi\tau}} \cdot \left[\operatorname{erf}\left(\frac{1+(nx'_D)}{2\sqrt{\tau}}\right) + \operatorname{erf}\left(\frac{1-(nx'_D)}{2\sqrt{\tau}}\right) \right] d\tau \quad (3.36)$$

3.3.3 Some Results

Figure 3.4 gives results for various values of x_e/x_f ranging from 1.0 to infinity. Results obtained here match those presented by Gringarten *et al.* 95 . Figure 3.5 gives the results for fractures oriented at 45 degrees. Only values of x_e/x_f of one and two are included in this figure since at larger values, the results are nearly the same.

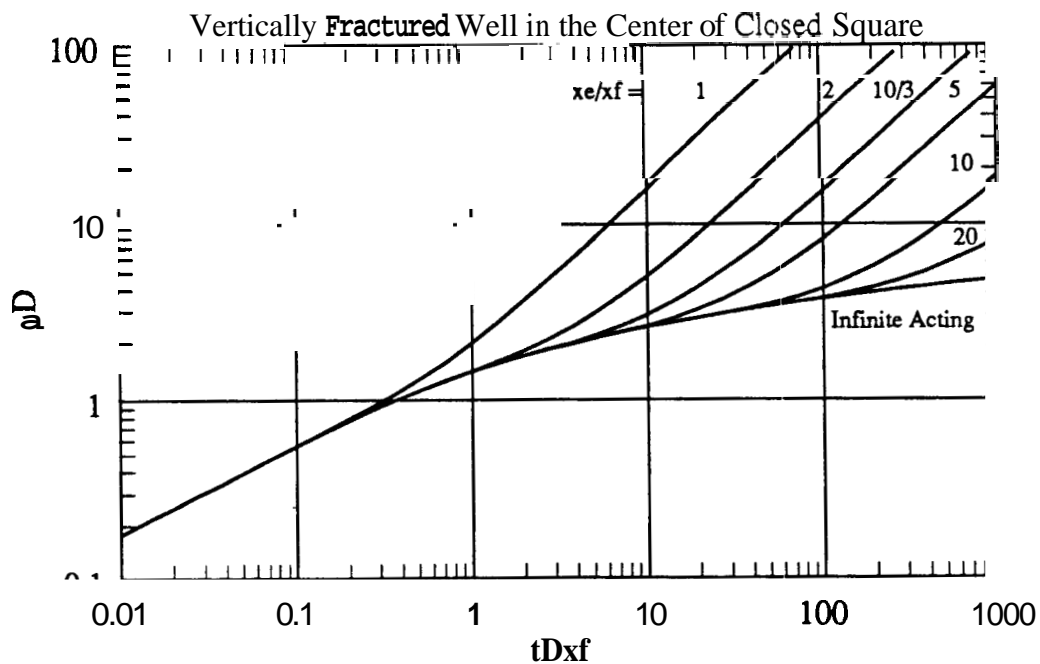


Figure 3.4: Uniform Flux Vertical Fracture in the Center of a Closed Square

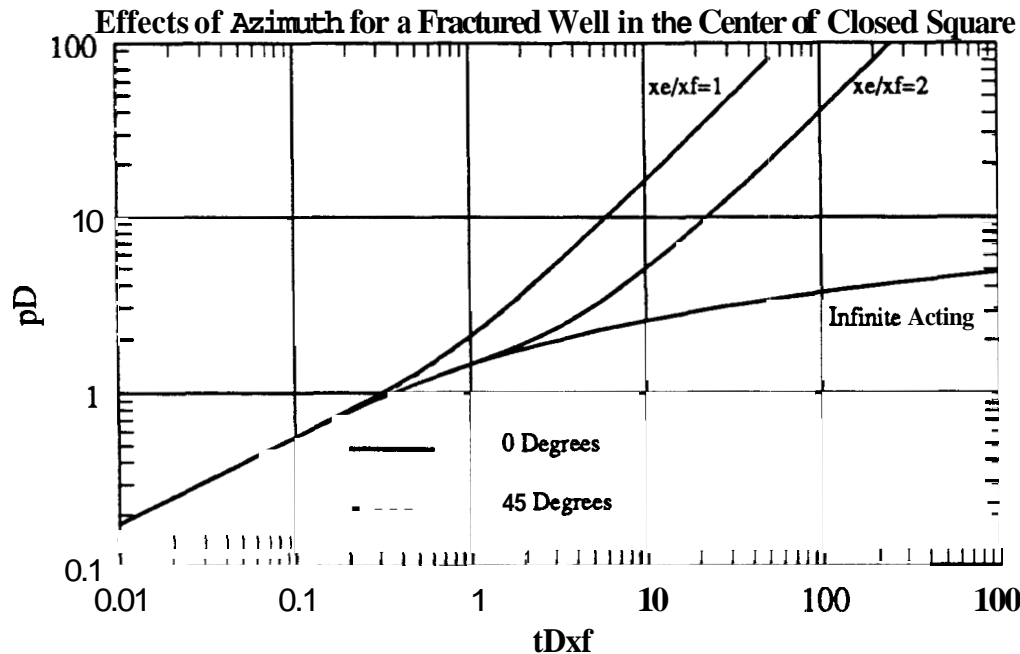


Figure 3.5: Uniform Flux Fracture at 45° and 0° From the x Axis in a Closed Square

3.3.4 Rectangular Boundaries

Figure 3.6 shows the dimensionless pressure drop due to a uniform flux fracture in a square, and rectangles of size 2:1, 4:1 and 10:1. Increasing pressure drops occur with the increasing aspect ratio of the rectangle. Since all have the same fracture lengths, the early time behaviors are identical, i.e., infinite acting. However, additional pressure drop occurs early for the high aspect ratio situations and in fact exceeds the linear flow pressure drop for the 4:1 case. Since all wells have the same drainage area, they must ultimately reach the same value of dP/dt . Time to reach pseudosteady state is increased for the longer rectangles.

3.4' Anisotropic Case

A prior assumption was that the hydraulic diffusivity is equal in all directions, i.e., permeability isotropy. For the case of simple permeability anisotropy, the ratio of

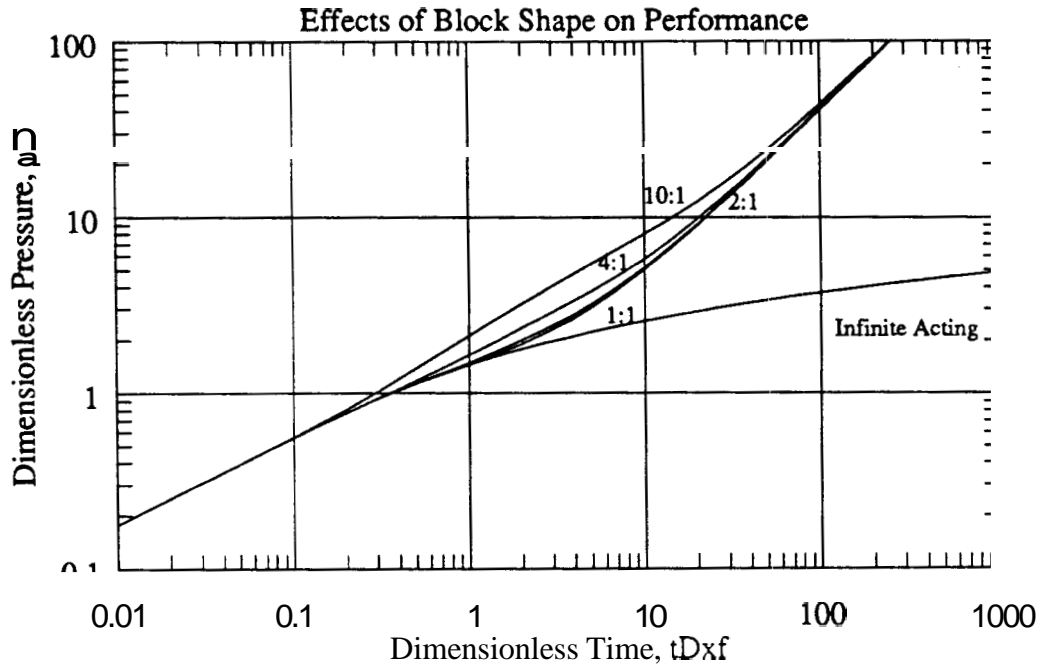


Figure 3.6: Pressure Drop Due to a Uniform Flux Fracture in Closed Rectangles with Aspect Ratios varying from 1:1 to 10:1

principle permeabilities is defined as:

$$\lambda = \frac{\eta_x}{\eta_y} \quad (3.37)$$

This ratio is unity for the isotropic case. Large permeability anisotropies are generally aligned with the direction of S_H . With no loss of generality, the principle axes of permeability and fracture orientation are assumed to be aligned with the coordinate system. Permeability anisotropy ratio (λ) values greater than 1.0 are generally anticipated if the stresses which affect the permeability contrast are identical to the current stresses controlling fracture azimuth. Values of λ greater than 1.0 are generally unfavorable. The resultant equation is:

$$p_D(\theta, t_{D_{xf}}) = \sum_{n=-\infty}^{\infty} \sum_{m=\infty}^{\infty} \frac{\sqrt{\pi\lambda}}{4} \int_0^{t_{D_{xf}}} \exp\left(\frac{-\lambda(my'_D)^2}{4\tau}\right) \cdot \frac{1}{\sqrt{\pi\tau}} \cdot \left[\operatorname{erf}\left(\frac{1+(nx'_D)}{2\sqrt{\tau}}\right) + \operatorname{erf}\left(\frac{1-(nx'_D)}{2\sqrt{\tau}}\right) \right] d\tau \quad (3.38)$$

3.5 Infinite Conductivity Fractures

Of the common models of hydraulic fracture performance, a simple model of infinite fracture conductivity might intuitively appear best. Conductivity of a propped hydraulic fracture is ordinarily so much greater than that of the formation, that the pressure drawdown in the fracture **seems** negligible compared to the large formation pressure drawdown. Effects of finite fracture conductivity are important at early times. At late times, these effects should be essentially a skin effect. However, reaching *pseudosteady state* may take many years for low permeability reservoirs.

Mathematical solutions for the single infinite-acting infinite conductivity fracture can be obtained approximately at the well by using the pressure of a uniform flux fracture at a certain location along the well ⁹⁵ . However, to solve for a pressure at a location other than the well for an infinite conductivity fracture is difficult. Kuchuk ¹³⁹ , Kuchuk and Brigham ¹⁴⁰ , and Papatzacos ²⁰⁰ presented solutions using elliptical flow.

Kuchuk's solution for the constant pressure fracture in Laplace space is:

$$\bar{p}_D = \sum_{n=0}^{\infty} (-1)^n \frac{1}{2\varpi} \frac{A_0^{2n} \text{Fek}_{2n}(\psi, -\varpi)}{\text{Fek}_{2n}(\psi_w, -\varpi)} \text{ce}_{2n}(\eta, -\varpi) \quad (3.39)$$

where: $\mathbf{a} = s/4$, s being the time variable in Laplace space, A_0^{2n} are Fourier coefficients and functions of q , $n = 0, 1, \dots$, ψ, η are the space coordinates in the elliptical coordinate system, and $\text{Fek}_{2n}(\psi, -\varpi), \text{ce}_{2n}(\eta, -\varpi)$ are Mathieu functions. From this pressure, the changing flow rates and cumulative production corresponding to production at constant flowing pressure may be obtained. Kuchuk also presents the inversion of this solution into real space and provides a method of obtaining the pressure drop at any point in space due to a constant well flow rate from an infinite conductivity fracture. This requires the continuous convolution integral to calculate changing flowing pressures due to a constant rate.

Several problems make it difficult to apply these solutions to the interference problem:

1. The solutions are complicated to evaluate. Evaluation of certain untabulated

Mathieu functions is notoriously complex. Some Mathieu functions are poorly convergent; others are infinite series of Bessel functions.

2. The solutions do not necessarily work for superposition solutions. Uniform flux fracture solutions require only Neumann boundary conditions. Superimposing another constant flux fracture fracture at another point in space does not necessarily violate this boundary condition. However, prescribing a constant pressure (Dirichlet) inner boundary condition for the infinite conductivity fracture removes the ability to superimpose other wells rigorously and respect the inner boundary conditions. This becomes acute when interference is significant—which is exactly the case of interest.
3. Infinite conductivity models will generally be poor for the long hydraulic fracture lengths associated with low permeability gas reservoirs;. Due to these problems, a finite difference simulator **was** used for the heterogeneous reservoir simulations.

To approximate infinite conductivity fracture behavior in finite difference simulations, an extremely large fracture permeability **was** used. It can be demonstrated that dimensionless fracture conductivities greater than about 200 are essentially equivalent to infinite conductivity.

3.6 Extension to Finite Conductivity Wells

This section presents the finite conductivity fracture pressure and flux calculations and the technique used to evaluate the modified Bessel function integrals (3.6.3). Laplace space formulations for equations are used, simplifying the problem and increasing flexibility of the solution.

3.6.1 Derivation of Laplace Transformation Model for Finite Conductivity Fractures

Cinco and Samaniego⁴⁸ presented a mathematical model that has become standard for evaluating finite conductivity hydraulic models. The basic procedure is a 'semianalytic' one in which the hydraulic fracture is modeled with a large number of elements (usually 20 to 40 per wing). Each element is modeled as having uniform flux; however, flux distribution is not known *a priori*. Reservoir and fracture flow equations are equated along the fracture and the discretized system is solved for wellbore pressure and flux distribution. Numerous extensions of the technique have been published.

Cinco and Meng⁵⁰ and van Kruijsdijk²⁴⁹ recently presented formulations in Laplace space for finite conductivity fractures. Solving the equations in Laplace space has several advantages; *viz.*,

1. This method is fast using the Stehfest algorithm²³⁶ for rapid inversion to real space. Previous techniques required discretization in both time *and* space.
2. Addition of wellbore skin effect and wellbore storage are easily obtained. Inclusion of wellbore storage will typically be important for real well testing problems. Sandface dimensionless pressure (p_{sD}) is simply conventional dimensionless pressure plus skin damage effect (S),

$$p_{sD} = p_D + S \quad (3.40)$$

Wellbore storage solutions are obtained by a simple manipulation of the constant rate Laplace solution with skin ($\bar{p}_{sD}(s)$):

$$\bar{p}_{wD}(s) = \frac{\bar{p}_{sD}(s)}{1 + C_D s^2 \bar{p}_{sD}(s)} \quad (3.41)$$

3. By solving in Laplace space, constant pressure solutions for q_D and Q_D are easily obtained.

$$\bar{q}_{wD}(s) = \frac{1}{s [1 + C_D s^2 \bar{p}_{sD}(s)]} \quad (3.42)$$

Cumulative production for constant pressure production is simply 'dimensionless flow rate divided by the Laplace space variable (s), as integrating with respect to time is synonymous to division by s .

4. The pressure derivative group p'_d term is obtained analytically.
5. Convolution to obtain variable rate solutions is sufficiently rapid that computerized automatic type-curve regression is possible.
6. The Laplace space formulation allows immediate solution of transient pressure response for naturally fractured cases by substituting the term $sf(s)$ for s in the wellbore pressure solution terms that result from the reservoir flow model. Here, $f(s)$ will be one of the dual porosity models, typically either:

- o For **transient matrix flow**,

$$f(s) = \omega + (1 - \omega)A_{fD}\sqrt{\frac{\eta_{maD}}{s}}\tanh\left(\sqrt{\frac{s}{4\eta_{maD}}}\right) \quad (3.43)$$

- A_{fD} is dimensionless fracture area .
- η_{maD} is dimensionless matrix hydraulic diffusivity.
- w is the familiar dimensionless fracture storativity.

- o For **pseudosteadystate matrix flow**,

$$f(s) = \omega + \frac{(1 - \omega)\lambda_f}{(1 - w)s + \lambda_f} \quad (3.44)$$

- λ_f is the interporosity flow coefficient.

- o For **homogeneous reservoirs**, $f(s) = 1$. This is retained in successive derivations unless otherwise specified.

Cinco and Meng presented a formulation that neglected compressible flow in the fracture (fracture linear flow). Cinco⁵⁰ demonstrated the accuracy of this approximation. The van Kruijsdijk model included fracture compressible flow. In the following derivation, Cinco and Meng's assumption will be incorporated.

Fracture flow equations

Consider a fracture to be a homogeneous slab of uniform porous media with height h , width b_f and half length x_f . Since fracture length is much longer than fracture width, fluid influx at the fracture ends (Figure 3.7) may be neglected. Fluid enters the fracture faces at a rate $q(x, t)$ per unit of fracture length (Figure 3.8). Unsteady-state

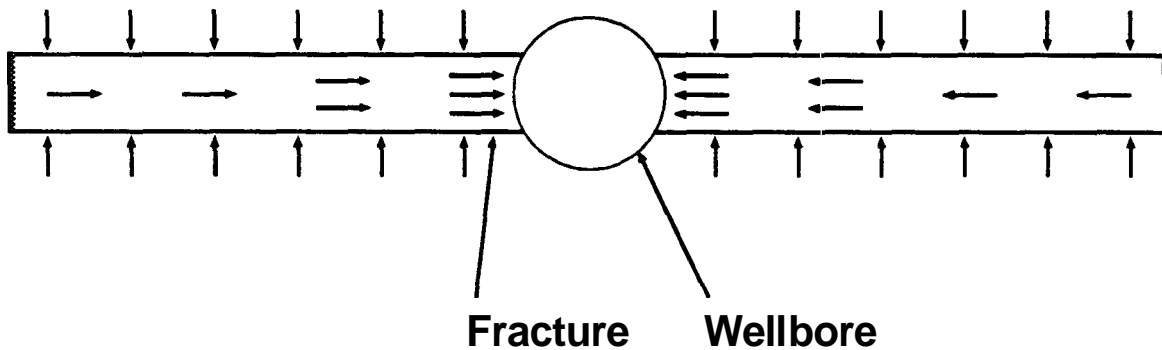


Figure 3.7: Fracture Flow Model for Finite Conductivity Fracture

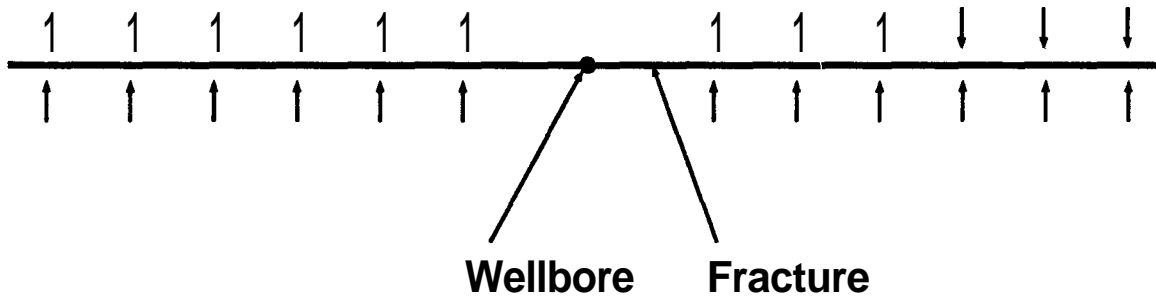


Figure 3.8: Reservoir Flow Model for Finite Conductivity Fracture

flow in the fracture can be described as:

$$\frac{\partial^2 p_f}{\partial x^2} + \frac{\mu q_f(x', t_{Dxf})}{k_f b_f h} = \frac{\phi_f \mu c_{ft}}{k_f} \frac{\partial p_f}{\partial t} \tag{3.45}$$

with the following initial and boundary conditions:

$$\left. \frac{\partial p_f}{\partial x} \right|_{x=0} = -\frac{q_w \mu}{2b_f k_f h} \tag{3.46}$$

$$\left. \frac{\partial p_f}{\partial x} \right|_{x=x_f} = 0 \quad (3.47)$$

and

$$p_f(x, t = 0) = p_i, \quad 0 \leq x \leq x_f \quad (3.48)$$

By neglecting the fracture compressibility term:

$$\frac{\partial^2 p_f}{\partial x^2} = -\frac{\mu}{k_f} \frac{q_f(x', t_{Dx_f})}{b_f h} \quad (3.49)$$

Now, defining dimensionless variable as follows,

$$x_D = \frac{x}{x_f} \quad (3.50)$$

$$q_{fD}(x', \tau) = \frac{2q_f(x', t_{Dx_f})x_f}{q_w} \quad (3.51)$$

$$p_{fD}(x_D, t_{Dx_f}) = \frac{kh(p_i - p_f(x, t))}{2\pi q_w} \quad (3.52)$$

noting that

$$p_{fD}(x, t) = -\frac{2\pi q_w \mu}{kh} p_{fD} \quad (3.53)$$

and

$$x = x_f^2 x_D \quad (3.54)$$

Substitution and cancellation leads to,

$$\frac{\partial^2 p_{fD}(x_D, t_{Dx_f})}{\partial x_D^2} = \frac{\pi}{(k_f b_f)_D} q_{fD}(x', \tau) \quad (3.55)$$

where

$$(k_f b_f)_D = \frac{k_f b_f}{k x_f} = F_{CD} \quad (3.56)$$

This equation can be integrated twice to yield the pressure drop between the wellbore and any point in the fracture:

$$p_w(t_{Dx_f}) - p_{fD}(x_D, t_{Dx_f}) = \frac{\pi}{(k_f b_f)_D} \left\{ x_D - \int_0^{x_D} \int_0^{x'} q_{fD}(x'', t_{Dx_f}) dx'' dx' \right\} \quad (3.57)$$

This integration uses the no **flux** boundary condition at the tips, the known value of dimensionless pressure at the origin, and the total flux condition to evaluate the constants of integration.

Reservoir flow equations

Dimensionless pressure drop at any point in space due to a plane source of height h , length $2x_5$ with flux density $q_f(x', t_{Dxf})$ is:

$$p_D(x_D, y_D, t_{Dxf}) = \frac{1}{4} \int_0^{t_{Dxf}} \int_{-1}^1 q_D(x', \tau) \frac{\exp \left\{ - \left[\frac{(x_D - x')^2 + y_D^2}{4(t_{Dxf} - \tau)} \right] \right\}}{t_{Dxf} - \tau} dx' d\tau \quad (3.58)$$

Equating Equations 3.58 and 3.59 for $y_D = 0$ and $-1 \leq x_D \leq 1$ and taking the Laplace transform yields:

$$\begin{aligned} \bar{p}_{wD}(s) - \frac{1}{2} \int_{-1}^1 \bar{q}_{fD}(x', s) K_0(|x_D - x'| \sqrt{s}) dx' \\ + \frac{\pi}{(k_f b_f)_D} \int_0^{x_D} \int_0^{x'} \bar{q}_{fD}(x'', s) dx'' dx' = \frac{\pi x_D}{s(k_f b_f)_D} \end{aligned} \quad (3.59)$$

For the Laplace transformation, the following properties are used (reference equation numbers from Reference 4 are shown in bold face).

29.2.1

$$f_i(s) = \mathcal{L}(F_i(t)) = \int_0^\infty e^{-st} F_i(t) dt = \bar{F}_i \quad (3.60)$$

29.2.8

$$\mathcal{L}\left(\int_0^t F_1(t - \tau) \cdot F_2(\tau) d\tau\right) = f_1(s) f_2(s) \quad (3.61)$$

29.3.120

$$\mathcal{L}\left(\frac{1}{2t} \exp \frac{-k^2}{4t}\right) = K_0(k\sqrt{s}) \quad (3.62)$$

As the fracture is symmetric for the simplest cases, $\bar{q}_{fD}(x_D, s) = \bar{q}_{fD}(-x_D, s)$, and;

$$\begin{aligned} \bar{p}_{wD}(s) - \frac{1}{2} \int_0^1 \bar{q}_{fD}(x', s) \left[(K_0 |x_D - x'| \sqrt{s}) + (K_0 |x_D + x'| \sqrt{s}) \right] dx' \\ + \frac{\pi}{(k_f b_f)_D} \int_0^{x_D} \int_0^{x'} \bar{q}_{fD}(x'', s) dx'' dx' = \frac{\pi x_D}{s(k_f b_f)_D} \end{aligned} \quad (3.63)$$

3.6.2 Discretization and matrix formulation

The integral involving the K_0 terms can be integrated for the discretized fluxes as described in Section 3.6.3. Discretization into n equal length fracture segments (on each fracture half-length) and the approximation of uniform flux over each section reduces the double integral of the fluxes to:

$$\int_0^{x_D} \int_0^{x'} \bar{q}_{fD}(x'', s) dx'' dx' = \sum_{i=1}^{j-1} \bar{q}_{fDi}(s) \left\{ \frac{(\Delta x)^2}{2} + \Delta x(x_{Dj} - i\Delta x) \right\} + \frac{(\Delta x)^2}{8} \bar{q}_{fDj}(s) \quad (3.64)$$

Subscripts for x_D imply that locations x_{Dj} are midpoints of the j th segment. Values for x_{Di} and x_{Di+1} are at the beginning and end of the i th segment, respectively. The combined equation then becomes:

$$\begin{aligned} \bar{p}_{wD}(s) - \frac{1}{2} \sum_{i=1}^n \bar{q}_{fDi}(s) \int_{x_{Di}}^{x_{Di+1}} [K_0(|x_{Dj} - x'| \sqrt{s}) + K_0(|x_{Dj} + x'| \sqrt{s})] dx' \\ + \frac{\pi}{(k_f b_f)_D} \sum_{i=1}^{j-1} \bar{q}_{fDi}(s) \left\{ \frac{(\Delta x)^2}{2} + \Delta x(x_{Dj} - i\Delta x) \right\} + \frac{(\Delta x)^2}{8} \bar{q}_{fDj}(s) \\ = \frac{\pi x_{Dj}}{s (k_f b_f)_D} \end{aligned} \quad (3.65)$$

This constitutes n equations for each fracture segment. Unknowns are n fluxes and the wellbore pressure. The remaining equation states that the sum of the fluxes from each fracture segment is equal to the well flow rate. Discretized in Laplace space, this is:

$$\Delta x \cdot \sum_{i=1}^n \bar{q}_{fDi}(s) = \frac{1}{s} \quad (3.66)$$

This system of equations can be written as:

$$\begin{pmatrix} A_{11} & A_{12} & \dots & A_{1n} & 1 \\ A_{21} & A_{22} & \dots & A_{2n} & 1 \\ \vdots & \vdots & \vdots & \vdots & \vdots \\ \vdots & \vdots & \vdots & \vdots & \vdots \\ A_{n1} & A_{n2} & \dots & A_{nn} & 1 \\ \Delta x & \Delta x & \Delta x & \Delta x & 0 \end{pmatrix} \begin{pmatrix} \bar{q}_{fD1} \\ \bar{q}_{fD2} \\ \vdots \\ \bar{q}_{fDn} \\ \bar{p}_{wD}(s) \end{pmatrix} = \frac{\pi}{s (k_f b_f)_D} \begin{pmatrix} x_{D1} \\ x_{D2} \\ \vdots \\ x_{Dn} \\ 1 \end{pmatrix} \quad (3.67)$$

A_{ij} terms consist of the following:

for all i, j

$$-\frac{1}{2} \int_{x_{D_i}}^{x_{D_{i+1}}} [K_0(|x_{D_j} - x'| \sqrt{s}) + K_0(|x_{D_j} + x'| \sqrt{s})] dx' \quad (3.68)$$

for $i = j$

$$+ \frac{(\Delta x)^2}{8} \quad (3.69)$$

and, for $i > j$

$$+ \frac{(\Delta x)^2}{2} + \Delta x(x_{D_j} - i\Delta x) \quad (3.70)$$

3.6.3 Integrating the Modified Bessel Function

Equation 3.65 requires evaluating the integral of $\sqrt{s} |x_{D_j} - x'|$ and $\sqrt{s} |x_{D_j} + x'|$ from x_{D_i} to $x_{D_{i+1}}$ with respect to x' . Abramowitz and Stegun ⁴ provide a closed form infinite series for a similar integral as follows:

11.1.9

$$\begin{aligned} \int_0^\zeta K_0(t) dt = & -(\gamma + \ln(\zeta/2))\zeta \sum_{k=0}^{\infty} \frac{(\zeta/2)^{2k}}{(k!)^2(2k+1)} \\ & + \zeta \sum_{k=0}^{\infty} \frac{(\zeta/2)^{2k}}{(k!)^2(2k+1)^2} \\ & + \zeta \sum_{k=1}^{\infty} \frac{(\zeta/2)^{2k}}{(k!)^2(2k+1)} \left(1 + \frac{1}{2} + \dots + \frac{1}{k}\right) \end{aligned} \quad (3.71)$$

However, the first equation to be integrated is of the form:

$$\int_{x_{D_i}}^{x_{D_{i+1}}} K_0(\sqrt{s} |x_{D_j} - x'|) dx' \quad (3.72)$$

which can be separated into two integrals and expressed as $\int_0^{x_{D_{i+1}}} - \int_0^{x_{D_i}}$ of the same function. Substituting for the argument of the integral:

$$u = \sqrt{s} |x_{D_j} - x'| \quad (3.73)$$

and noting:

$$dx' = -\frac{du}{\sqrt{s}} \quad (3.74)$$

the integration limits can be altered accordingly. Regardless of relative magnitudes of x_{Dj} and x_{Di} , the resultant integral can be expressed as follows:

$$\int_0^{x_{Di}} K_0(\sqrt{s} |x_{Dj} - x'|) dx' = \int_{\sqrt{s}x_{Dj}}^{\sqrt{s}|x_{Dj}-x_{Di}|} \frac{K_0(u)}{\sqrt{s}} du \quad (3.75)$$

This integral may be combined for both upper and lower values (x_{Di} and x_{Di+1}), the following expression is obtained, after some algebra:

$$\begin{aligned} \int_{x_{Di}}^{x_{Di+1}} K_0(|x_{Dj} - x'| \sqrt{s}) dx' = & \left[\frac{x_{Di+1} - x_{Dj}}{|x_{Di+1} - x_{Dj}|} \right] \cdot \int_0^{|x_{Dj} - x_{Di+1}| \sqrt{s}} \frac{K_0(u)}{\sqrt{s}} du \\ & - \left[\frac{x_{Di} - x_{Dj}}{|x_{Di} - x_{Dj}|} \right] \cdot \int_0^{|x_{Dj} - x_{Di}| \sqrt{s}} \frac{K_0(u)}{\sqrt{s}} du \end{aligned} \quad (3.76)$$

The second integral is simpler as the term to be integrated is $|x_{Dj} + x'| \sqrt{s}$ and the relative positions of the x_{Dj} and x_{Di} are not critical to the formulation. So, the final expression is:

$$\int_{x_{Di}}^{x_{Di+1}} K_0(|x_{Dj} + x'| \sqrt{s}) dx' = \int_0^{|x_{Dj} + x_{Di+1}| \sqrt{s}} \frac{K_0(u)}{\sqrt{s}} du - \int_0^{|x_{Dj} + x_{Di}| \sqrt{s}} \frac{K_0(u)}{\sqrt{s}} du \quad (3.77)$$

Handling cases for the relative positions of x_{Di} and x_{Dj} was simplified as more general expressions were introduced.

3.6.4 Inversion Procedure

Unknowns are solved by inverting the left hand side matrix (Equation 3.67). This matrix is represented as $A \cdot x = b$ where A is the known $(n+1)$ by $(n+1)$ coefficient matrix, x is the unknown flux distribution vector, and b is the right-hand side vector. Matrix inversion is accomplished by computing the LU factorization of the coefficient matrix. Factorization fails if the upper triangular part of the factorization has a zero diagonal element. Iterative refinement is performed on the solution vector to improve accuracy. The iterative refinement routine is as follows:

- $x_0 = A^{-1}b$
- If $(|x_0|_0 \leq \epsilon)$ exit

- **Fori = 1, 50**
 - $r_i = Ax_{i-1} - b$ computed in higher precision
 - $p_i = A^{-1}r_i$
 - $x_i = x_{i-1} + p_i$
 - if ($\|p_i\|_\infty \leq \epsilon \|x_i\|_\infty$) Exit

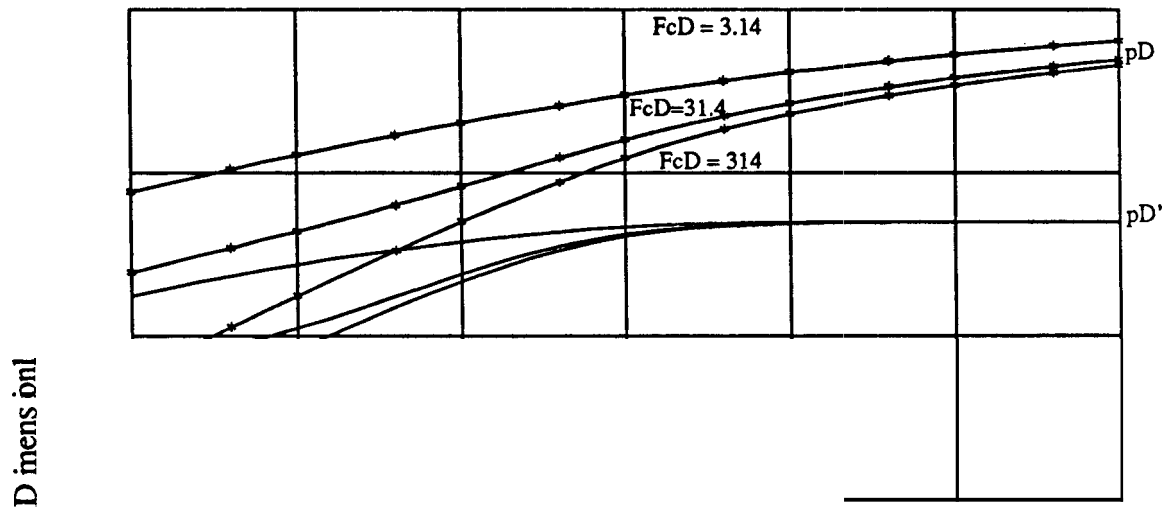
As matrix A is double precision, special quadruple precision routines are used for calculating values of r_i . Machine precision is used for ϵ . For estimated condition numbers greater than $1/\epsilon$, a warning is given which indicates near singularity. The IMSL subroutine **DSLARG** was used for matrix solution. The Stehfest algorithm is used to invert Laplace transformed variables into real space.

3.6.5 Verification and Example Results

So far, this formulation parallels that of Cinco and Meng⁵⁰, except for treatment of naturally fissured systems. Tables presented in Cinco and Sarnanigo⁴⁸ were matched very well, as shown in Figure 3.9 comparing reported values of p_wD as a function of t_{Dxf} for $(k_f b_f)_D = \pi - 100\pi$. Pressure derivatives are also plotted for this figure.

Flux distributions calculated also match data presented by Cinco and Samanigo⁴⁸. For example, their Figure 5 shows flux distribution at various times along a highly conductive vertical fracture ($(k_f b_f)_D = 10^4\pi$). In Figure 3.10, the same concept is illustrated for $(k_f b_f)_D = 500$. Pressures discussed in this section are wellbore pressures. At early times, most of the production is from the part of the fracture nearest the wellbore, while for values of $t_{Dxf} \approx 10^{-4} - 10^{-3}$, flux distribution is essentially uniform. At one point in the fracture, the dimensionless flux remains fairly constant. For low fracture conductivities, a different series of flux distributions results. Figures 3.11 and 3.12 illustrate similar flux distributions for values of $(k_f b_f)_D$ of 10π and π respectively. Stabilized flux distributions have almost all of their influx near the center of the fracture at early times, and for $(k_f b_f)_D = \pi$, this continues through late times.

In fact, effective limits to fracture length may be estimated with known values of formation permeability and fracture permeability width product. Although arbitrarily



long fractures may be created, when $(k_f b_f)_D < 0.1$, incremental length provides negligible additional flux. Given the potential for excessive vertical height growth, overly optimistic fracture design models, and permeability anisotropy, actual hydraulic fractures obtained in practice frequently indicate much shorter effective lengths than design lengths.

The pressure derivative plotting function is defined as:

$$p'_D = \frac{dp_D}{d \ln t_D} = t_D \cdot \frac{dp_D}{dt_D} \quad (3.78)$$

In Laplace space formulation:

$$\mathcal{L}\left(\frac{dp_D}{dt_D}\right) = s \cdot \bar{p}_D + p_D(0) \quad (3.79)$$

and $p_D(0) = 0$.

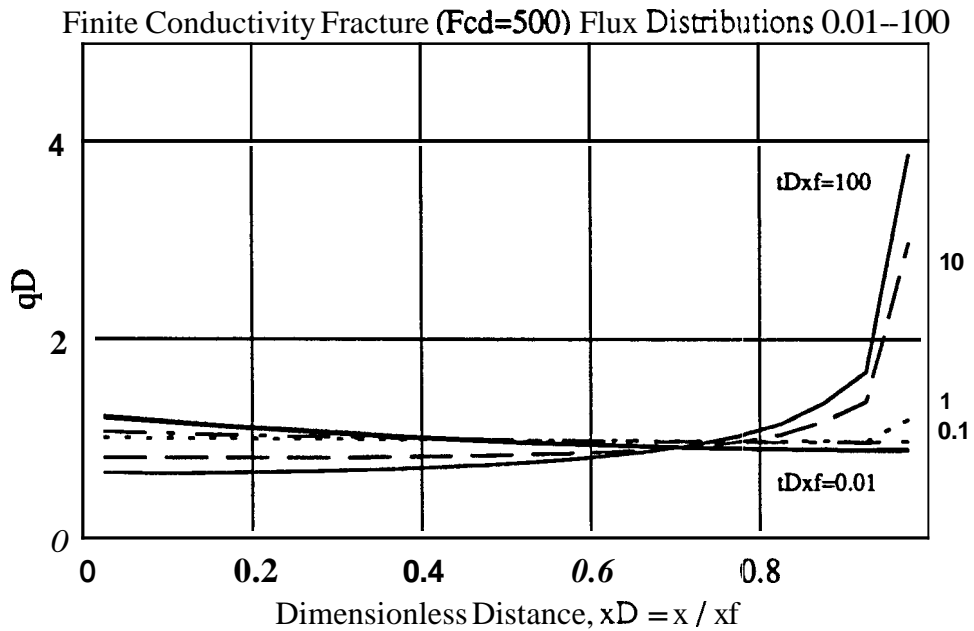


Figure 3.10: Flux Distribution at Various Times Along a Highly Conductive ($F_{cD} = 500$) Vertical Fracture

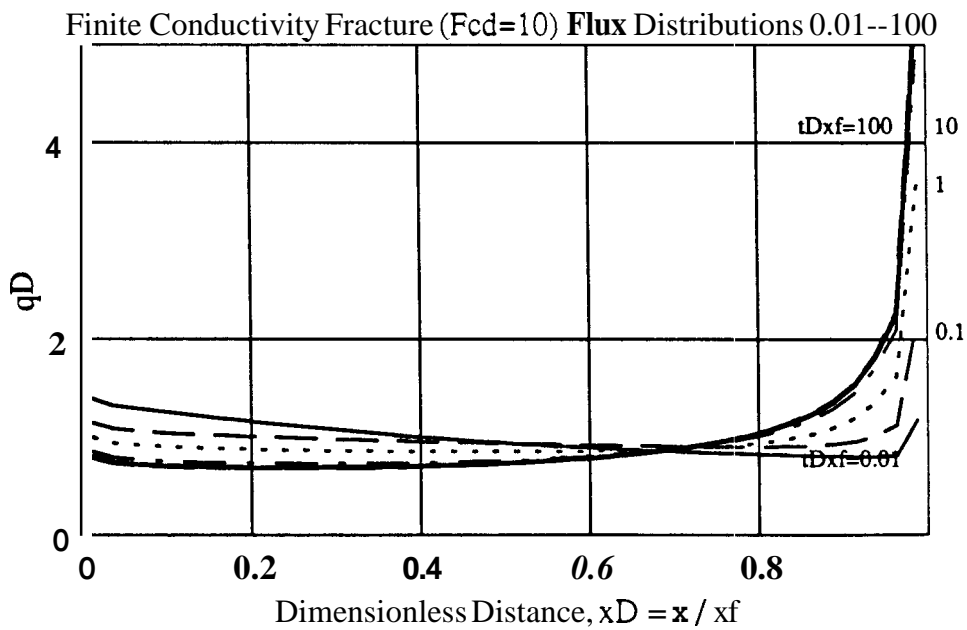


Figure 3.11: Flux Distribution at Various Times Along a Moderate Conductivity ($F_{cD} = 10$) Vertical Fracture

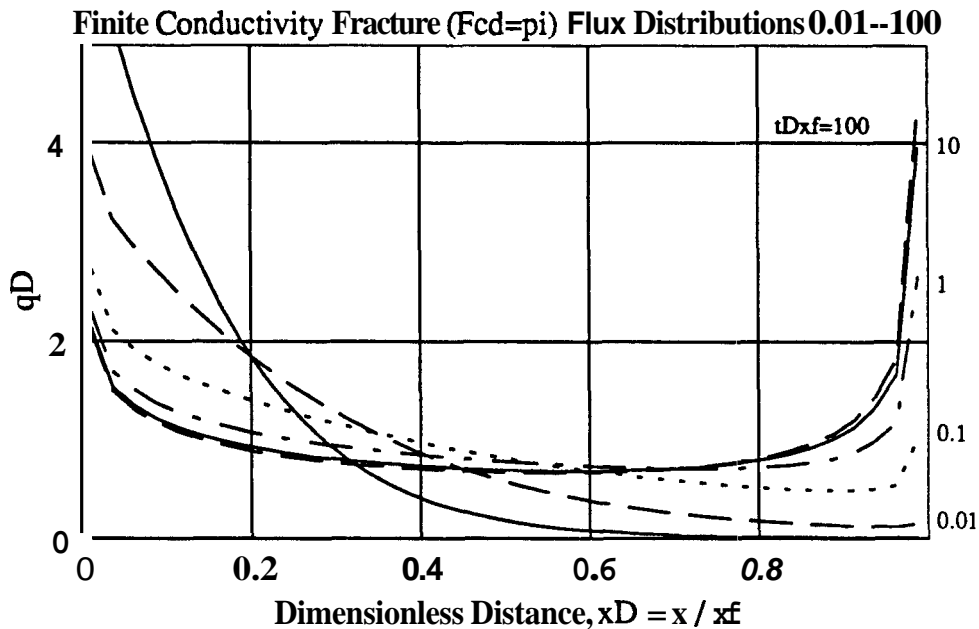


Figure 3.12: Flux Distribution at Various Times Along a Low Conductivity ($F_{cD} = \pi$) Vertical Fracture

3.7 Interference results

Cinco and Samaniego⁴⁷ presented an extension of Uraiet *et al.*'s²⁴⁸ calculation of interference response at a line source well due to production/injection from a hydraulically fractured well. The Cinco and Samaniego paper solved the problem for a finite conductivity well, and demonstrated errors that could result from using the uniform flux type curve for low conductivity fractures at the active well. There is negligible information at the observation well about fracture conductivity, so the active well's fracture length and finite conductivity must be determined *a priori*, or at least simultaneously with an interference test.

Laplace space formulation leads to interference pressures more straightforwardly than is possible with the original work⁴⁷. When a fracture flux distribution is determined for any given value of t_{Dxf} (i.e., a given number of passes through the Stehfest algorithm) and $(k_f b_f)_D$, the Laplace transform of the pressures at any value of r_D and δ can be determined. Figures 3.13-3.15 are a series of type curves that give

pressure response at r_D values of **0.2**, **0.5**, and **0.8** for a finite conductivity fracture with $(k_f b_f)_D = 0.2\pi$ and $\delta = 0, 15, \dots, 90$. Most sensitivity is present for smaller values of δ . For $r_D > 2.0$, virtually no sensitivity is present. Response for wells with high fracture conductivity approaches infinite conductivity response.

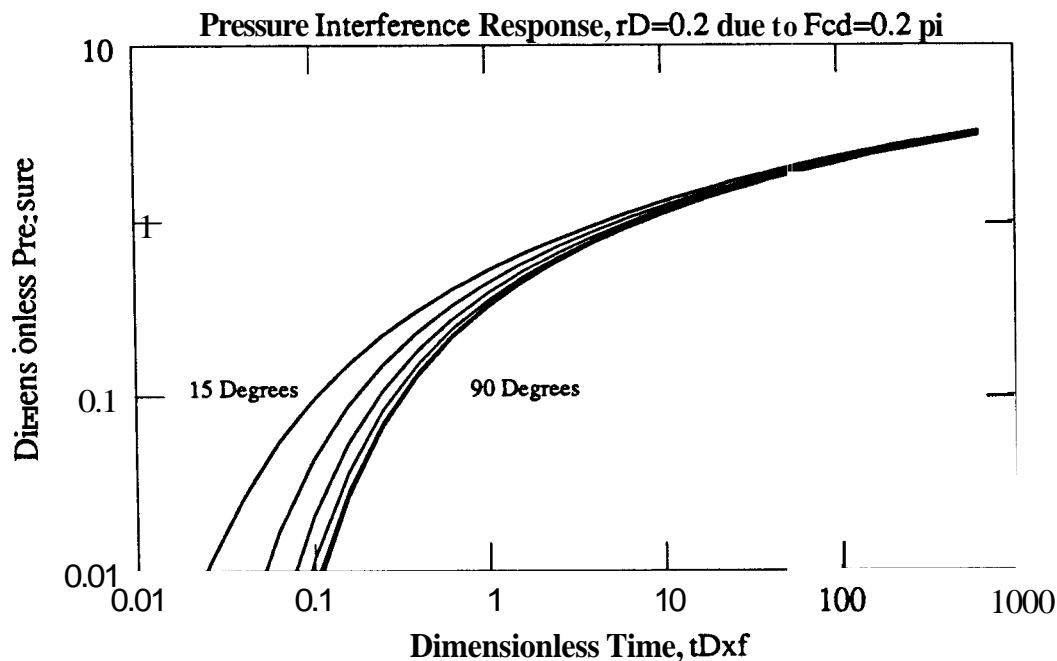


Figure 3.13: Pressure Interference Response at $r_D = 0.2$ from a Hydraulically Fractured Well with $(k_f b_f)_D = 0.2\pi$

For a fractured well with $(k_f b_f)_D = 0.2\pi$, pseudoradial flow is present by $t_{Dxf}/r_D^2 \approx 10$ as is illustrated in Figure 3.16. In this figure, the isobars are nearly circular. For $(k_f b_f)_D = \pi$ and values of $t_{Dxf} = 0.1, 1.0$, a pressure distribution in space is more elliptical as shown in Figures 3.17–3.18.

3.8 Numerical Simulation

Numerical simulation is used in this analysis for several reasons, including:

1. It is desirable to evaluate infinite conductivity fracture and finite flow capacity fracture cases for feasibility of detecting effects of azimuth. These techniques can

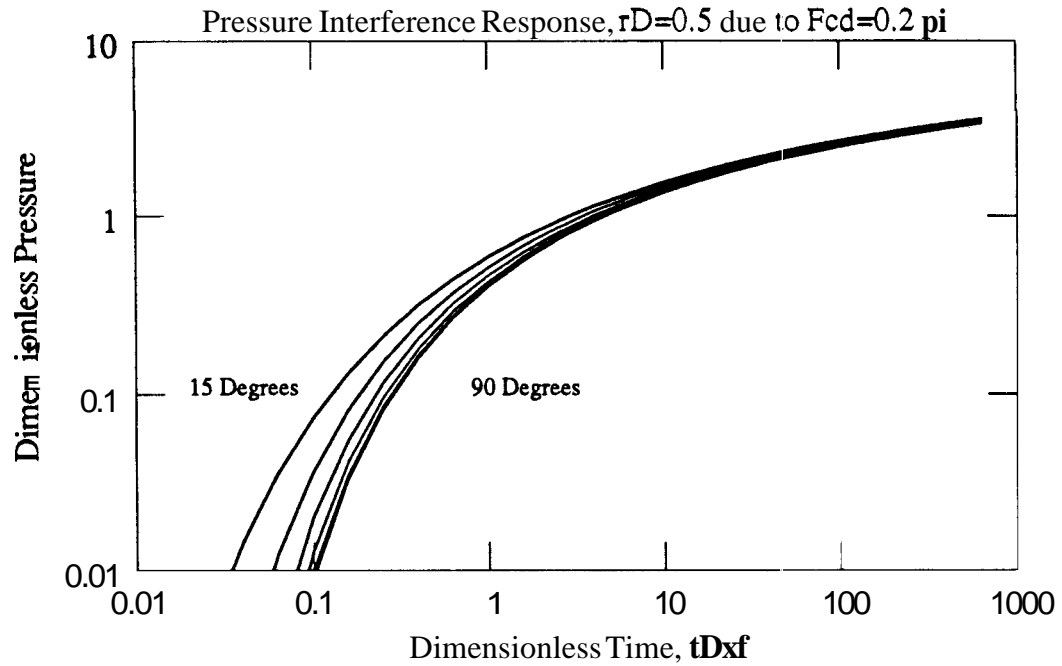


Figure 3.14: Pressure Interference Response at $r_D = 0.5$ from a Hydraulically Fractured Well with $(k_f b_f)_D = 0.2\pi$

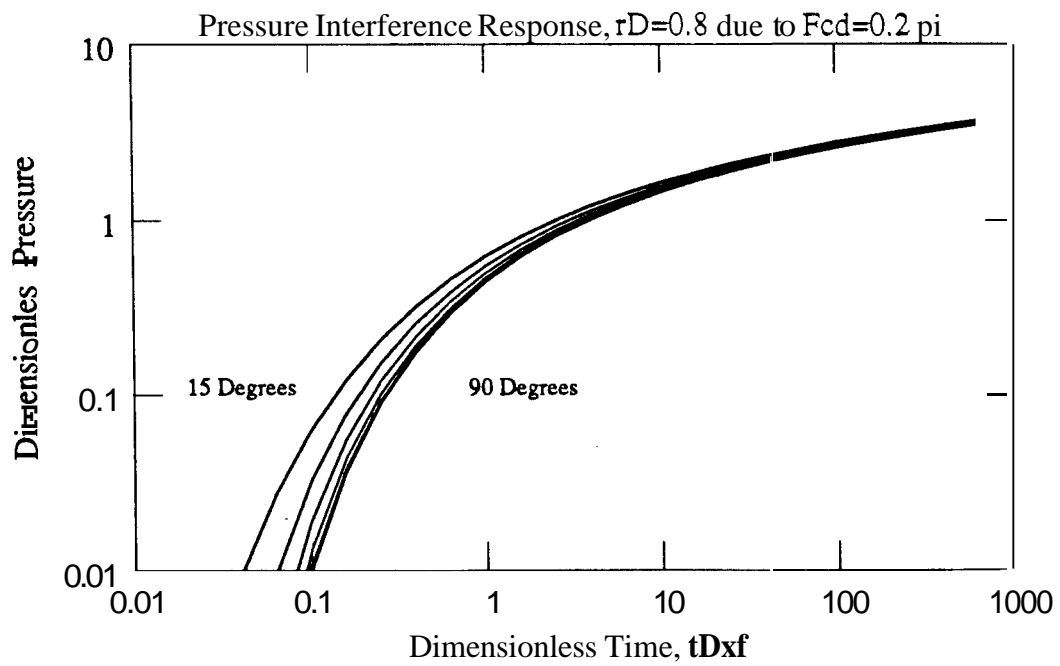


Figure 3.15: Pressure Interference Response at $r_D = 0.8$ from a Hydraulically Fractured Well with $(k_f b_f)_D = 0.2\pi$

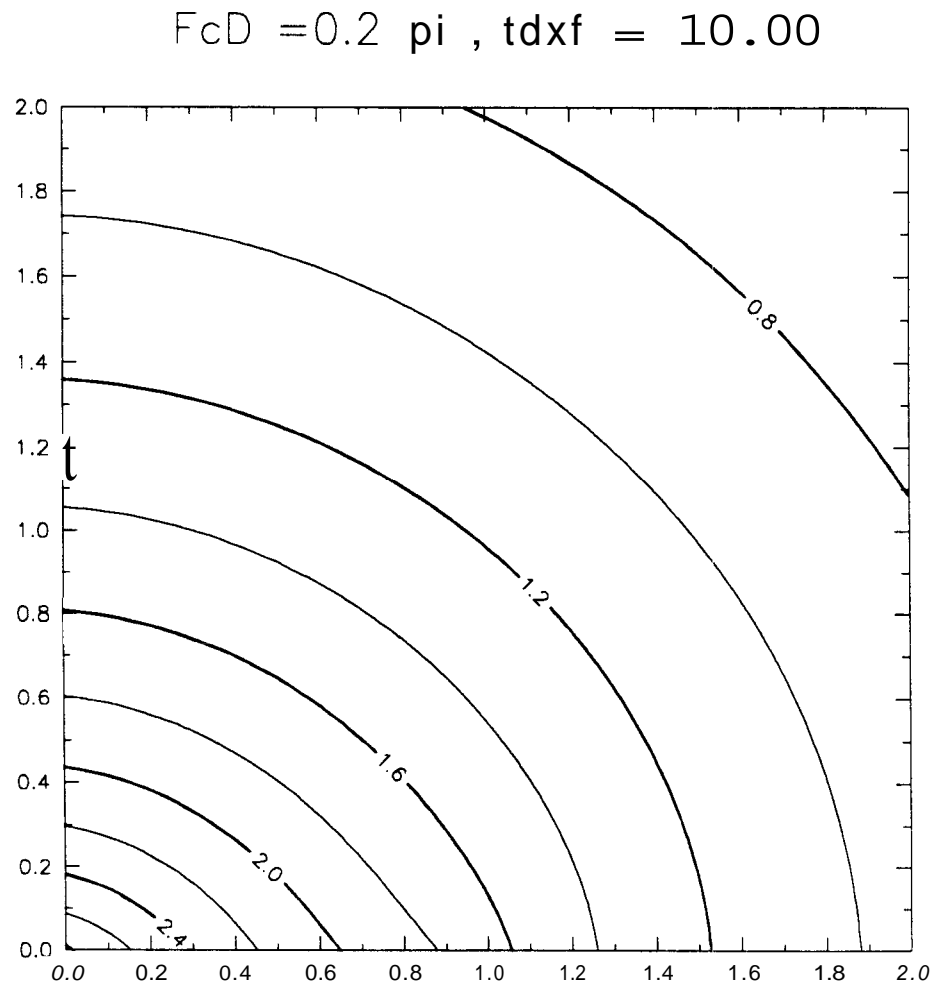


Figure 3.16: Dimensionless Pressure Isobars at $t_{Dxf} = 10$ due to a Hydraulically Fractured Well with $(k_f b_f)_D = 0.2\pi, t_{Dxf} = 10$

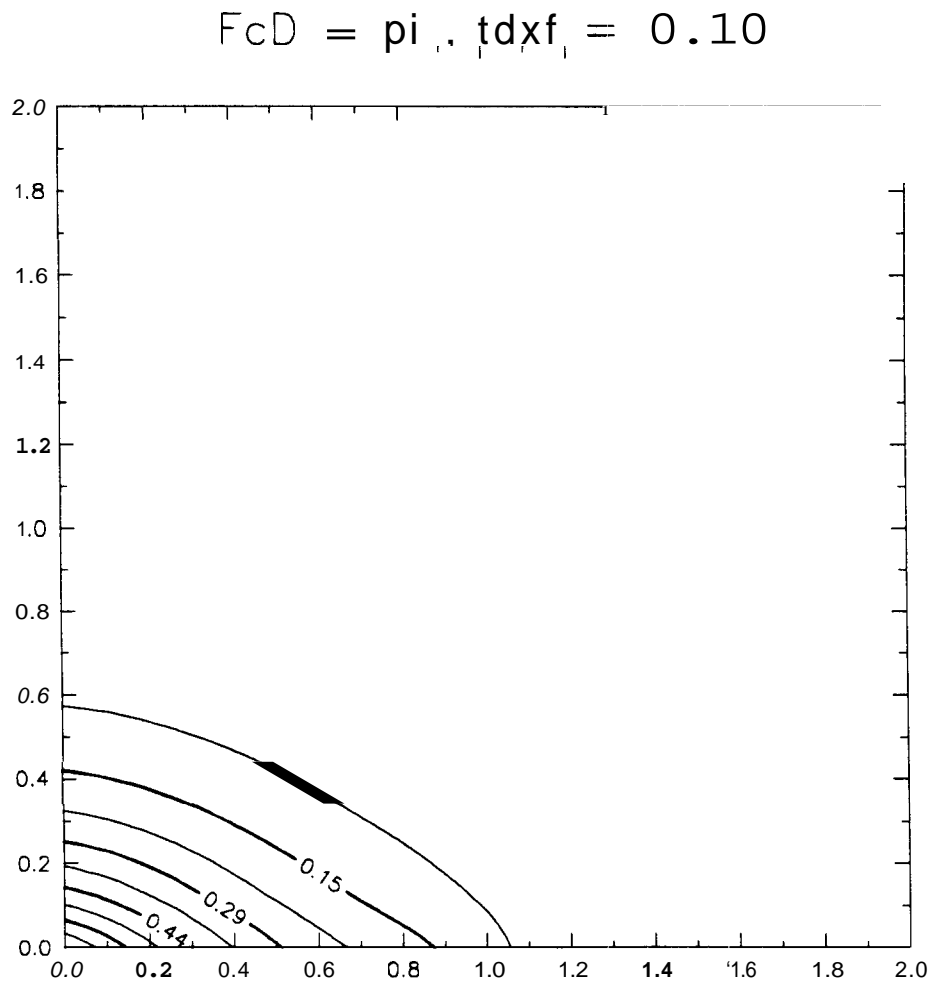


Figure 3.17: Dimensionless Pressure Isobars at $t_{Dxf} = 0.1$ due to a Hydraulically Fractured Well with $(k_f b_f)_D = \pi$, $t_{Dxf} = 0.1$

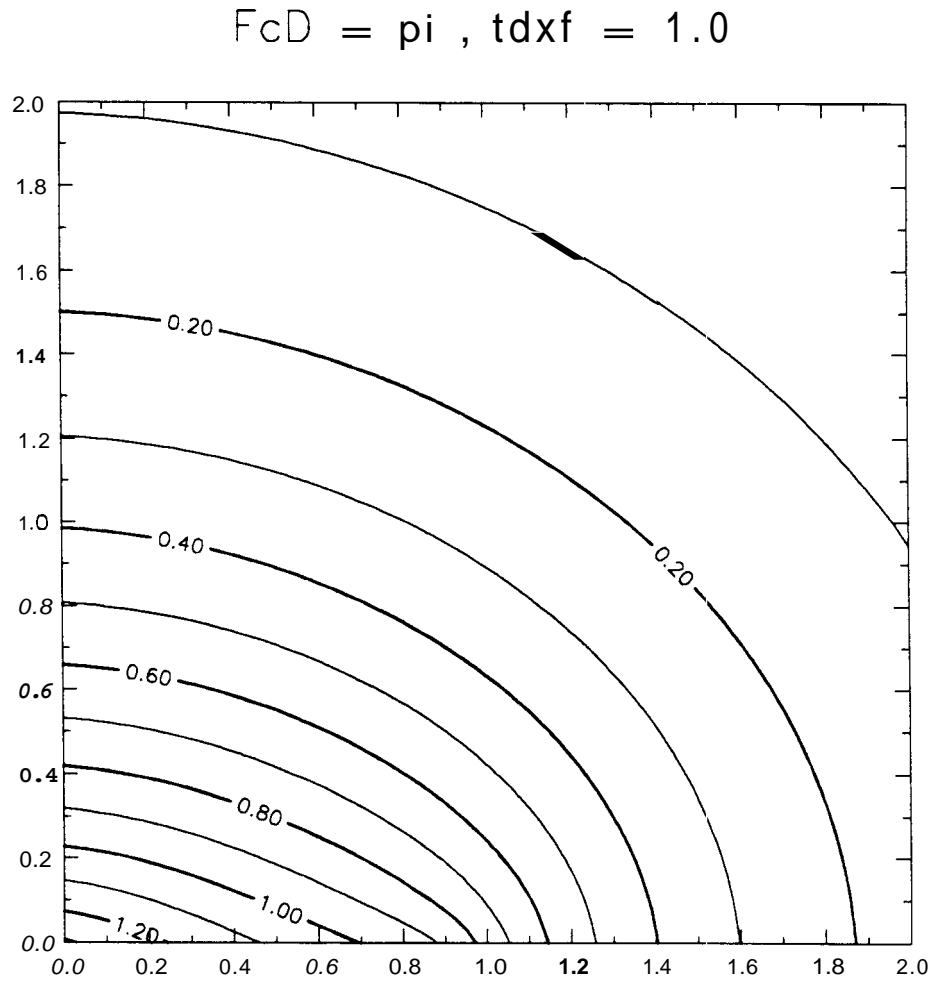


Figure 3.18: Dimensionless Pressure Isobars at $t_{Dxf} = 1.0$ due to a Hydraulically Fractured Well with $(k_f b_f)_D = \pi$, $t_{Dxf} = 1$

confirm solutions obtained analytically and handle cases for which either there is no analytic solution, or solution is so difficult to evaluate that simulation is computationally more efficient.

2. Effects of formation heterogeneities can be evaluated by flow simulation. It will be demonstrated that anisotropies are important in evaluation of well performance. Geostatistical models will be implemented to provide complex distributions of permeability that are both heterogeneous and anisotropic.
3. Analytic solutions for superposition in time can model infill drilling; however, variability in rate constraints and a possible need to include two phase flow favors finite difference methods.
4. Gas flow calculations are simplified, and turbulence may be easily handled.

The Calgary Modelling Group's (CMG) IMEX simulator was used for this problem. In the mode utilized (single-phase, slightly coincompressible fluid), results compare favorably with analytic solutions. In fact, resultant output will generally be presented as dimensionless pressures and flow rates for comparison with analytic results. The two azimuth representations used were 0° and 45° with both infinite conductivity and uniform flux fractures modeled. Figures 3.19–3.20 are schematic representations of grids used for these two cases. For the 0° case, the smallest rectangular symmetry case which can be easily modeled is the 1/4 square that is x_e on a side with a $x_e/2$ fracture. For the 45° case, the corresponding unit is a square $\sqrt{2}x_e$ on a side with two $x_e/2$ fractures at opposite sides of the square.

3.8.1 Uniform Flux Fractures

Uniform flux cases were modeled by placing wells in the center of each of the many very narrow grid blocks representing the fracture. Flow rate for the constant rate cases was allocated uniformly based on block length. Cases in which x_e/x_f was either 1 or 2 were evaluated for both angles. Just as in the analytic solutions, virtually no difference in wellbore flowing pressures could be noticed for the 0–45° cases.

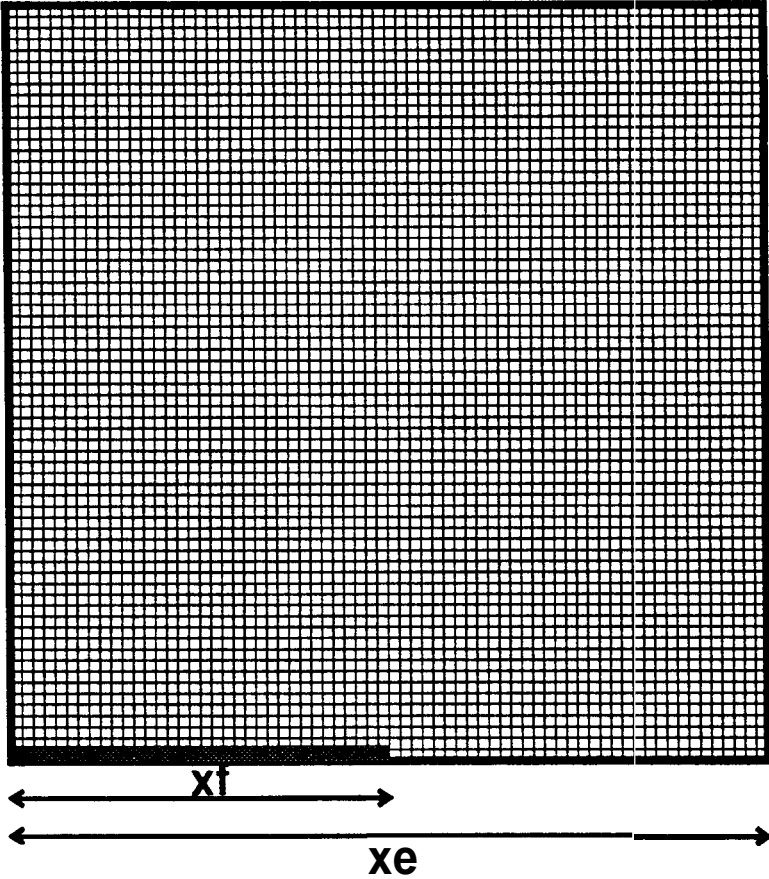


Figure 3.19: Representation of Grid Model for 0" case

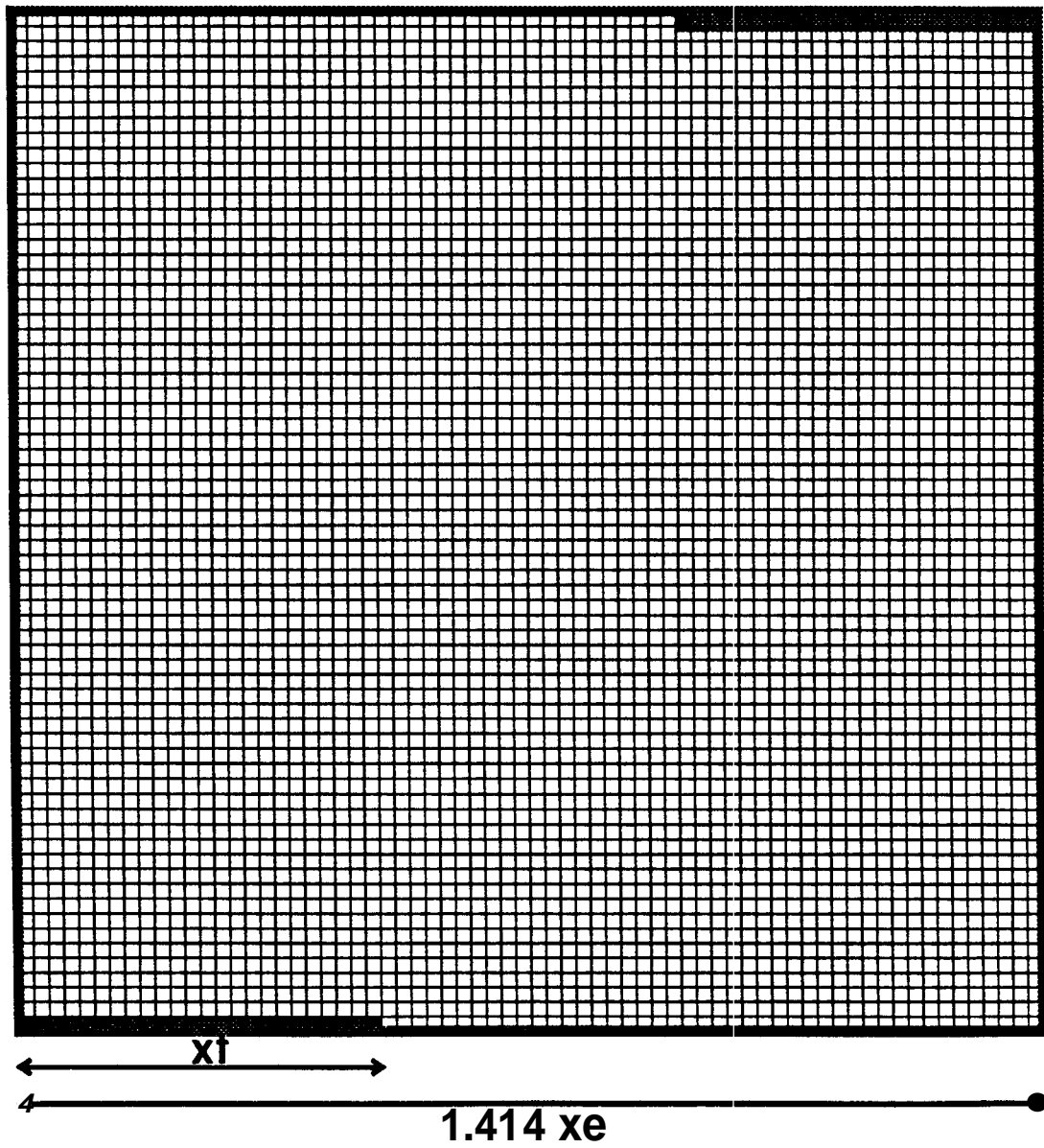


Figure 3.20: Representation of Grid Model for 45° case

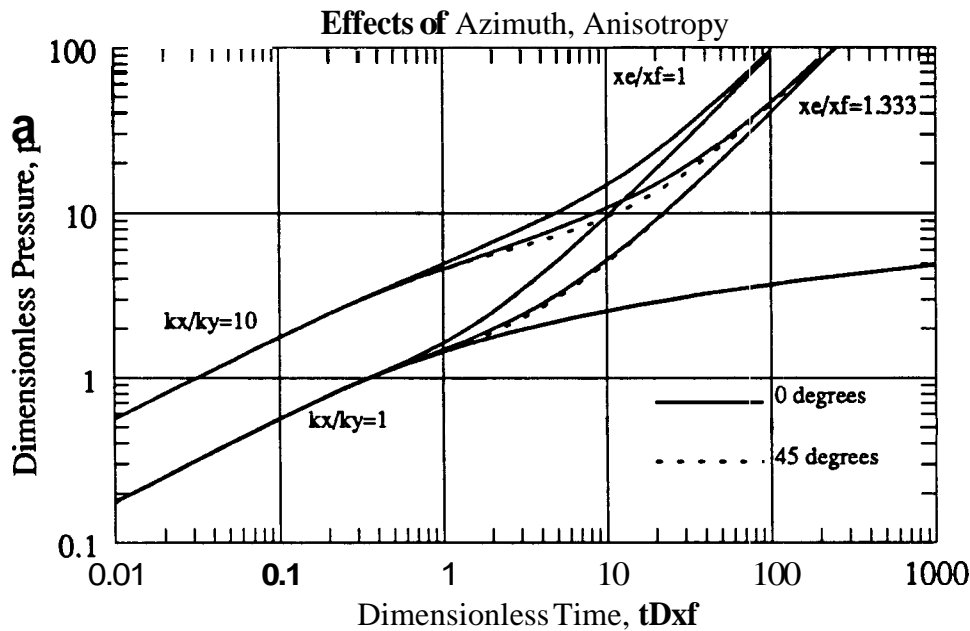


Figure 3.21: Comparison of Uniform Flux Fracture Results for Different Fracture Azimuths

Figure 3.21 compares two extreme cases of $0\text{--}45^\circ$ fracture azimuths for wellbore pressure versus time, giving the same degree of agreement as in the analytic solution. Figure 3.22 is a map of isopotentials at pseudosteady state for the uniform flux fracture and $\theta = 0$.

3.8.2 Infinite Conductivity Fractures

In order to have truly infinite conductivity, there must be zero pressure drop along the fracture. In practice, dimensionless conductivity ratios of well over **10000** resulted in maximum pressure drops of less than **2** psi in all cases. For infinite conductivity fractures, both constant well rate and constant well flowing pressures are easily represented by simulation. Two cases of 0 and 45 degrees were simulated by the symmetric methods previously discussed. For graphical representations of pressure distributions, the 0° case will show the entire well and its full drainage volume. The 45° case will show the well and will be bounded on four corners by one quarter of the diagonal

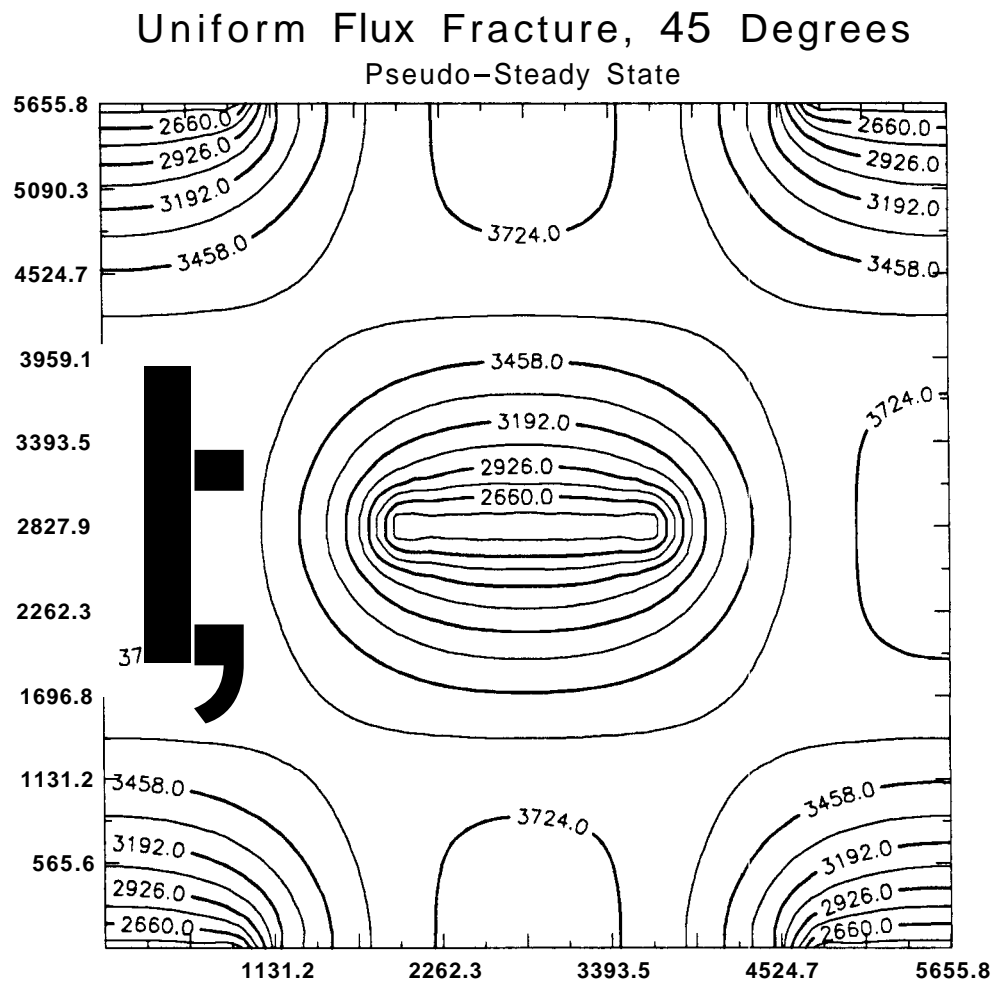


Figure 3.22: Isopotential Map at Pseudosteady State for the Uniform Flux Fracture

offsets. Drainage boundaries in this case are not rectangular and are curved.

3.8.3 Drainage Patterns

At early times, well performance for all cases is independent of fracture azimuth. At later times, interference between wells increases and differences, if any, will become apparent. Figures 3.23-3.25 are a series of pressure distributions for $x_e/x_f = 4/3$, for a well produced at constant pressure. Initial reservoir pressure was 5000 psi, and initial flowing pressure was 2000 psi. At $t_{D_{xf}} = 0.079$, flow is elliptical, with large pressure gradients around each well, corresponding to high flow rates.

At $t_{D_{xf}} = 1.228$, effects of interference have become noticeable at the boundaries nearest the fracture tips, but the majority of isobars are still closely spaced near the well, with steepest gradients near the fracture tips. At $t_{D_{xf}} = 2.67$ effects of interference are significant, and are felt at all of the boundaries. At $t_{D_{xf}} = 4.363$ reservoir depletion has reached an advanced stage, with much of the reservoir feeling boundary effects. Isobars are still more elliptical than circular.

Drainage patterns for constant rate depletion look different in that the early time patterns do not have steep pressure gradients; the near well gradients are constant, corresponding to the constant flow rate. However, the basic pattern of increasing interference is the same as in the constant pressure case. For the 45" case, the same qualitative behavior can be seen. Figures 3.26-3.30 show early and late time pressure distributions about fractures corresponding to x_e/x_f values of 1.0 and 2.0 respectively. Figures 3.26 and 3.27 illustrate results for the early time case. Drainage areas associated with nonzero angles are not, in general, rectangular or square in shape.

3.8.4 Performance Results

For a well spacing of 2000 feet, the 0 and 45" cases from simulation resulted in virtually indistinguishable results (Fig. 3.31), just as in the analytic solution for the uniform flux, constant rate case. A constant rate infinite conductivity case also showed little difference (Fig. 3.32). As x_e/x_f decreases to unity for the 0° case, the separation in

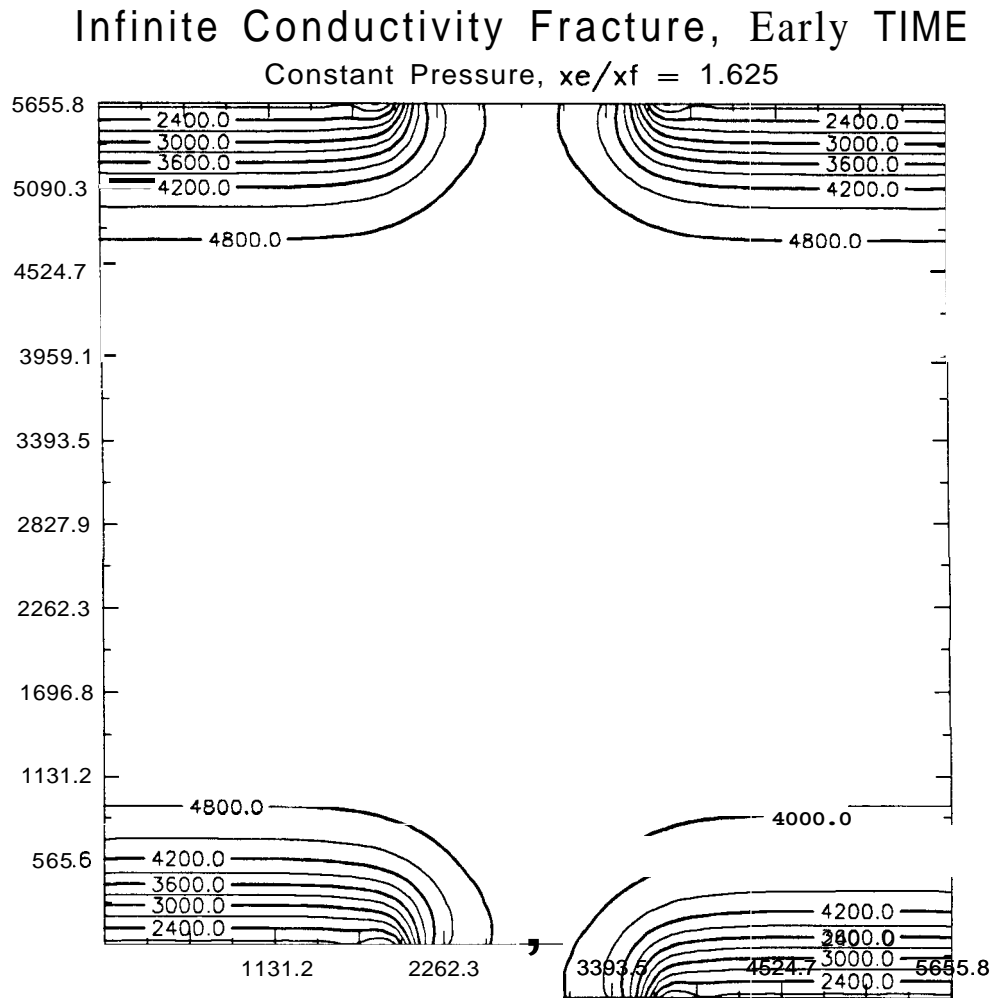


Figure 3.23: Infinite Conductivity Vertical Fracture, Produced at Constant Pressure, $x_e/x_f = 4/3$, Early Time

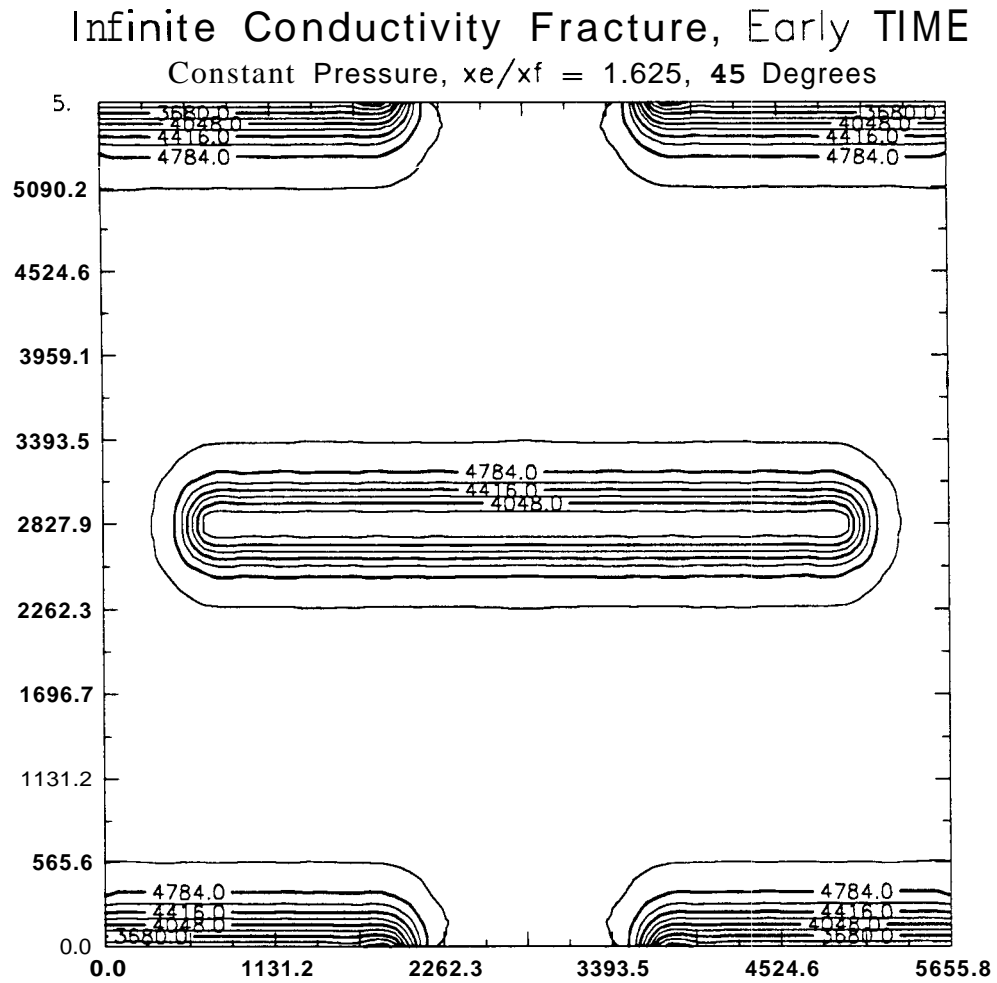


Figure 3.24: Infinite Conductivity Vertical Fracture, Produced at Constant Pressure, $x_e/x_f = 4/3$, Early Time, 45 Degrees

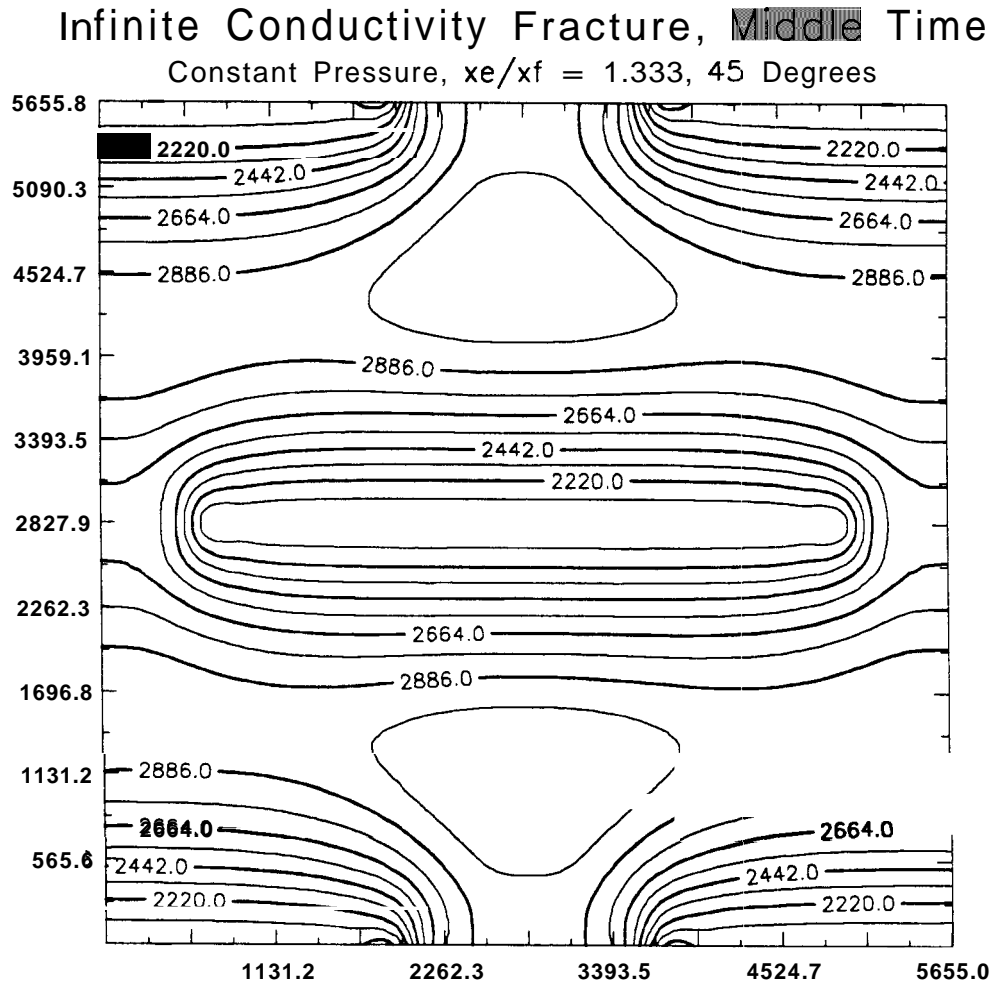


Figure 3.25: Infinite Conductivity Vertical Fracture, Produced at Constant Pressure, $x_e/x_f = 4/3$, Middle Time, 45 Degrees

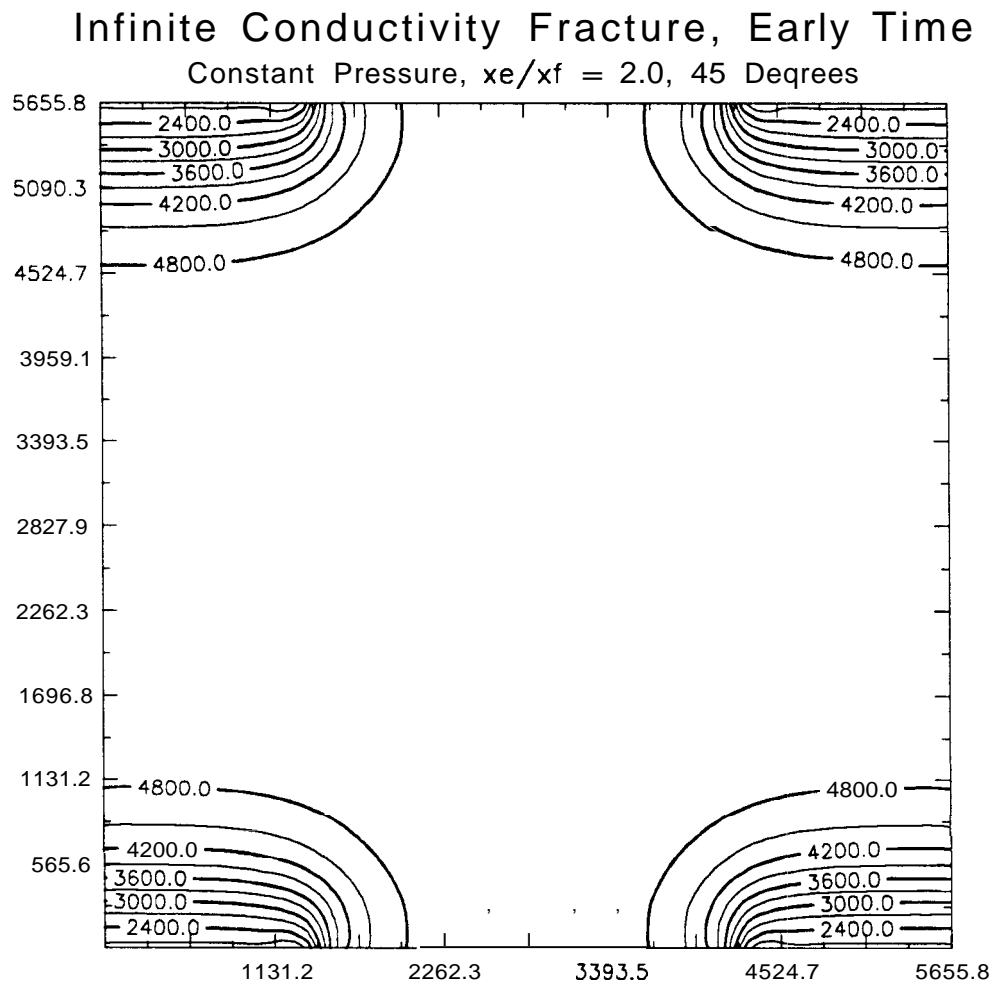


Figure 3.26: Infinite Conductivity Vertical Fracture, Produced at Constant Pressure, $x_e/x_f = 2$, Early Time, 45 Degrees

Infinite Conductivity Fracture, Early Time

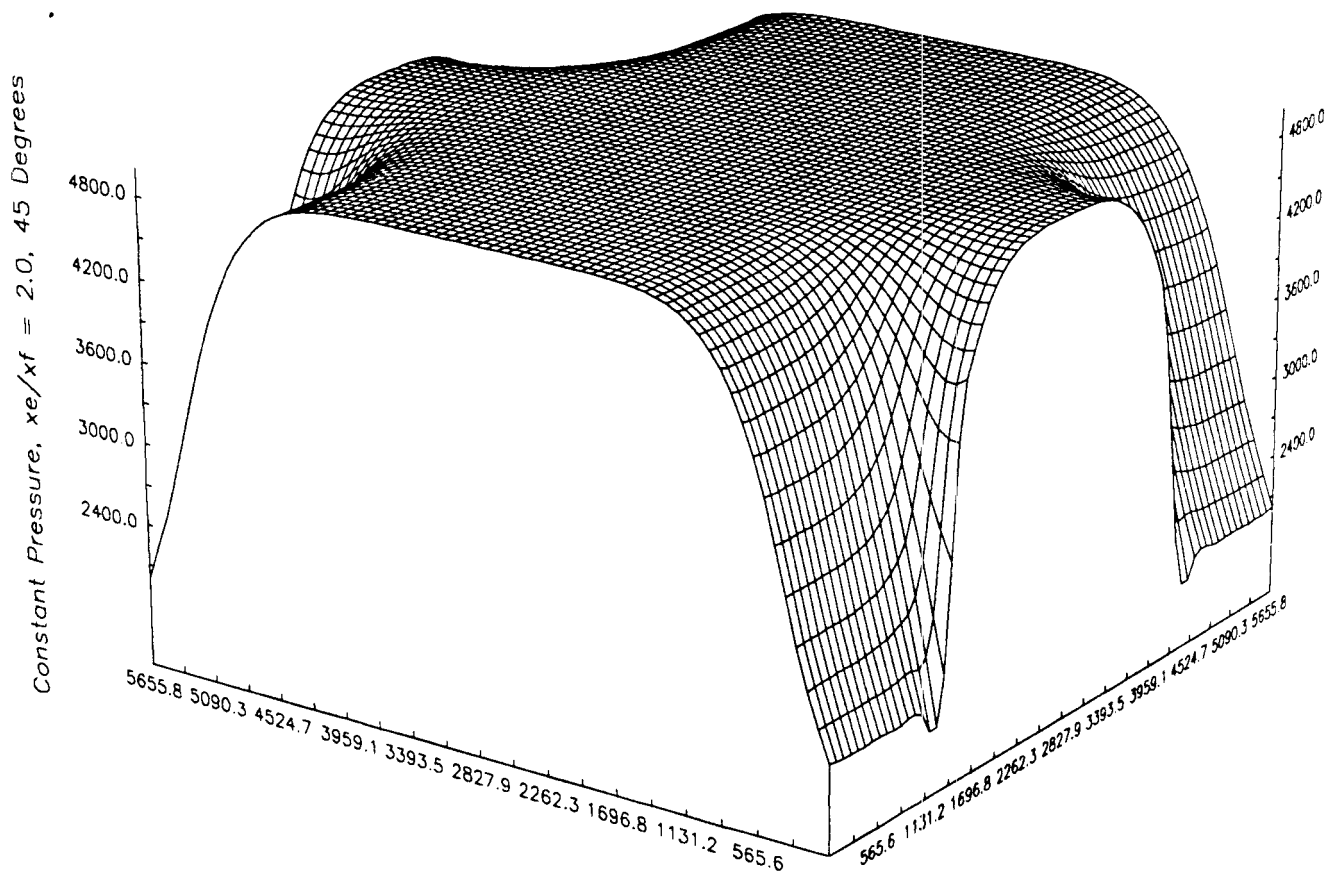


Figure 3.27: Infinite Conductivity Vertical Fracture, Produced at Constant Pressure, $x_e/x_f = 2$, Early Time, 45 Degrees

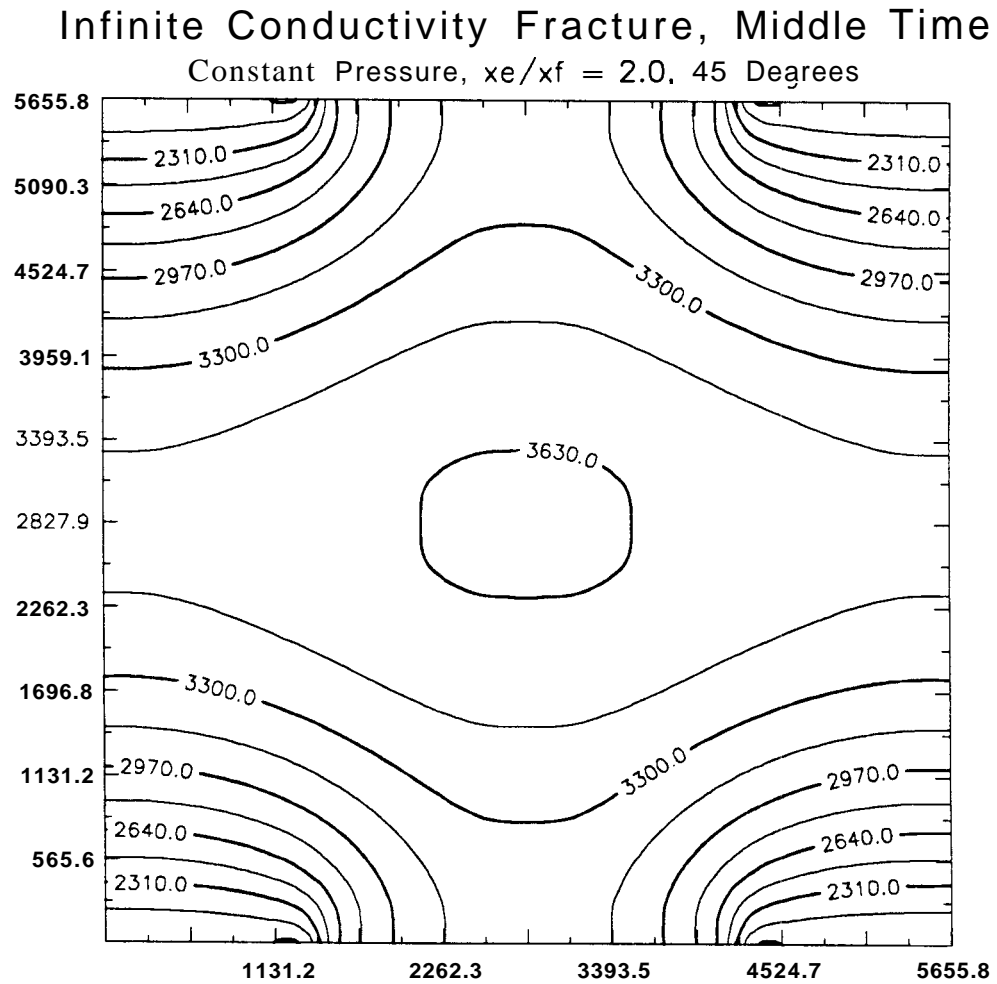


Figure 3.28: Infinite Conductivity Vertical Fracture, Produced at Constant Pressure, $x_e/x_f = 2$, Middle Time, 45 Degrees

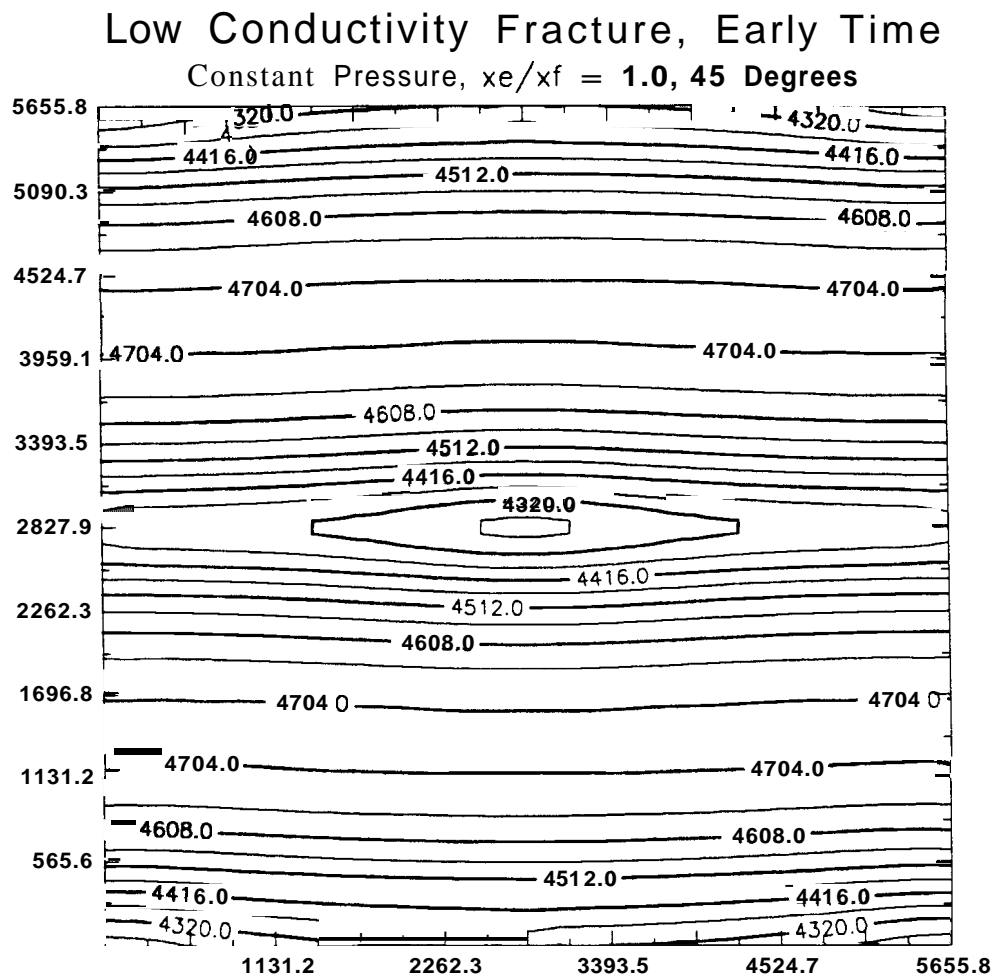


Figure 3.29: Low Conductivity Vertical Fracture, Produced at Constant Pressure, $x_e/x_f = 1$, Early Time, 45 Degrees

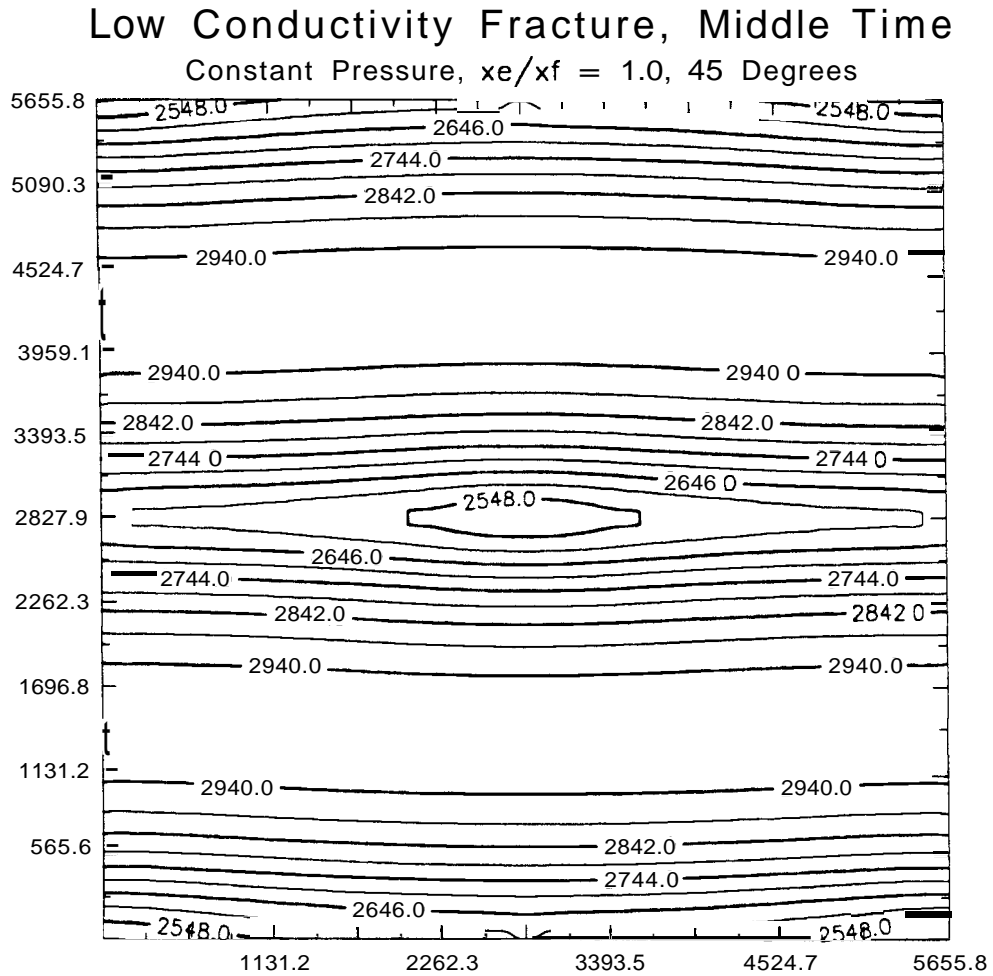


Figure 3.30: Low Conductivity Vertical Fracture, Produced at Constant Pressure, $x_e/x_f = 1$, Middle Time, 45 Degrees

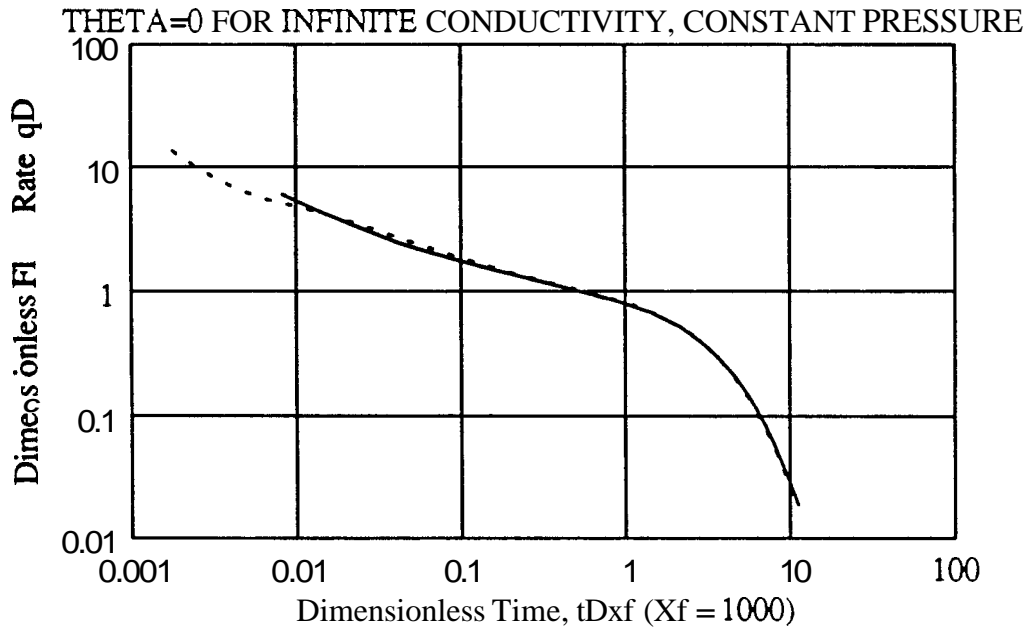


Figure 3.31: Infinite Conductivity Fracture, $x_e/x_f = 2$, Constant Pressure, (Dashed line is analytic solution, solid is simulation)

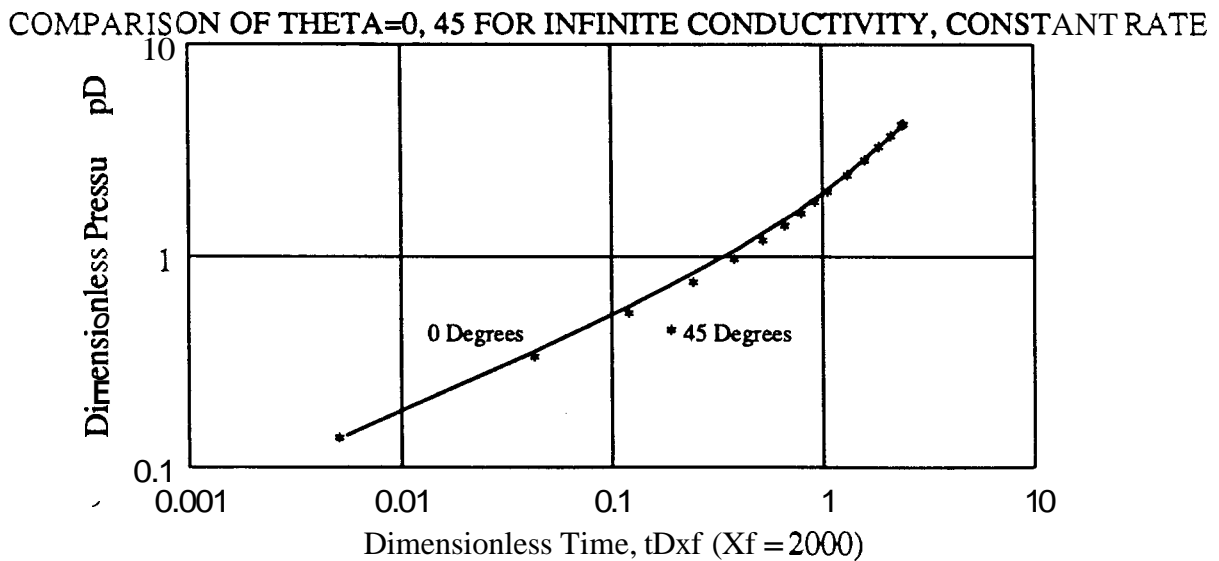


Figure 3.32: Infinite Conductivity Fracture, $x_e/x_f = 2$, Constant Rate

the two curves becomes more noticeable for the infinite conductivity case than in the uniform flux case. Figures 3.33 and 3.34 compare the $x_e/x_f = 1$ cases for 0 and 45°.

Initial flow rates for dimensionless times less than about 1.0 for these cases are approximately equal to infinite-acting values. For many low permeability wells with short fractures, this period could extend for weeks to years. Subsequently, we see a range of dimensionless times for which flow rates are as much as 20% greater for the 45° case than the 0° case. Longer fractures which are only possible when azimuth is known can also improve flow rates; however, economic analysis is required to determine the extent to which this is valuable. As a practical matter, it is not technically possible to achieve exactly these results, due to the excess unpropped fracture length (created length) that could physically interfere with another productive well.

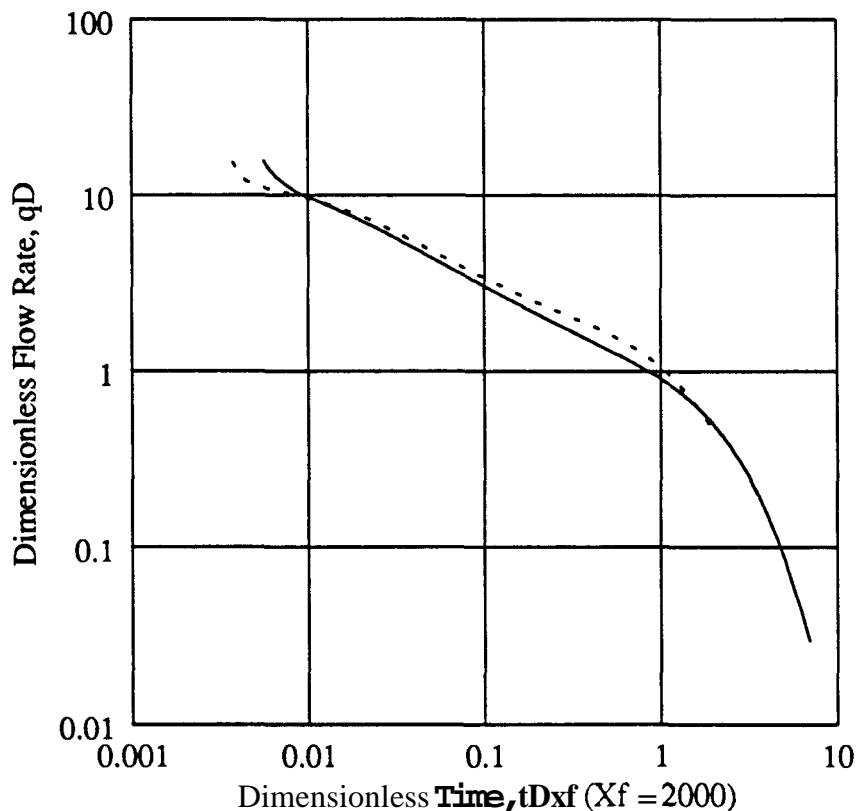


Figure 3.33: Infinite Conductivity Fracture, $x_e/x_f = 1$, Constant Pressure, (Solid line is 0°, Dashed is 45°)

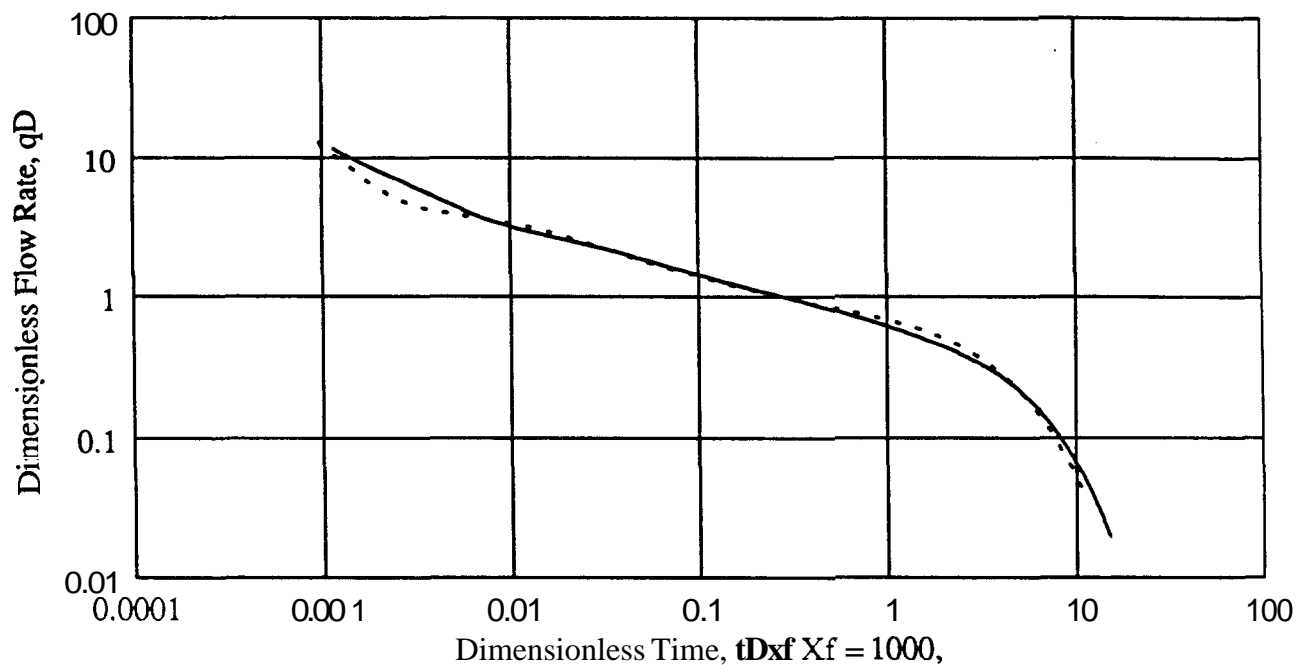


Figure 3.34: Infinite Conductivity Fracture, $x_e/x_f = 1$, Constant Pressure, (Solid line is 0", Dashed is 45")

3.9 Chapter Summary

Mathematical solutions for uniform flux and finite conductivity fracture flow have been developed. An analytic solution to the real space uniform flux model is presented, and extended to closed rectangular systems, anisotropic system, and systems with varying fracture azimuths. When two hydraulically fractured wells are close to each other ($x_e/x_f \leq 4$), or when fracture dimensionless conductivity is low, the uniform flux model is inaccurate. Finite conductivity fracture flow models are developed in Laplace space. Solution methods are detailed. Both solutions are used to analyze areal distributions of pressure in closed systems. The finite conductivity model is extended to a Laplace space solution for interference from a finite conductivity hydraulically fractured well with a line source observation well. Simulation models were described which verified the semianalytic solutions.

The next chapter discusses the interference problem with two hydraulically fractured wells and develops new Laplace space solutions for several combinations of line

source wells, infinite conductivity hydraulically fractured wells, **and** finite conductivity hydraulically fractured wells. Numerous sensitivities for the general problem of interference between two finite conductivity hydraulically fractured wells will be presented.

Chapter 4

Interference and Interaction

Historical approaches summarized. Laplace space formulations for various combinations of fracture models. A general solution for two finite conductivity wells. Comparisons with prior solutions. Stability and block size requirements. Effects of varying interference test parameters. Permeability anisotropy. Constant pressure production at the active well.

4.1 Historical Approach

A major application of interference tests is determination of fracture orientation in hydraulically fractured wells (i.e., wells intersecting a vertical fracture). Pierce *et al.* ²⁰⁴ described a method for determining fracture azimuth and fracture length using pulse testing. This method requires pulse tests before and after the fracture, and is not applicable for very low permeability systems or finite conductivity fractures. Uraiet *et al.* ²⁴⁸ developed a technique for azimuth determination using pressures recorded at an unfractured observation well. This work considered only uniform flux fractures; an extension by Cinco-Ley and Samaniego ⁴⁷ considered finite conductivity fractures. Neither method works for hydraulically fractured observation wells. Abobise and Tiab ² and Ekie *et al.* ⁷⁸ also used uniform flux models for interference work. Unambiguous determination of fracture azimuth requires two observation wells

located at orientations other than 90 and 180 degrees from the active well. Reservoir heterogeneities complicate determination of fracture azimuth from interference tests. Permeability variations in the drainage area of a well are averaged in a manner that is not understood. No current model exists (to our knowledge) to assess the impact of heterogeneities on interference test determination of fracture azimuth.

Unfortunately, both high-resolution (high cost) pressure transducers and very long tests are required for these interference tests because of the extremely low permeability of most candidate formations. Reservoir heterogeneities, multiple layers, and surface interference can render azimuth detection by interference testing infeasible. Resolution with respect to azimuth is also fairly low at angles greater than 45°. Field tests used to evaluate fracture azimuth were reported by Frohne and Mercer ^{88, 89} and Sarda ²²¹. Elkins and Skov ⁸¹, Komar *et al.* ^{137,136}, Komar and Shuck ¹³⁸, and Locke and Sawyer ¹⁵⁰ described field experiments that involved contouring pressures at offset wells during drawdowns, fracturing operations, and injection.

Historically, most work **has** used the 'line source' approximation at the observation well. This is not without reason, as numerous interference tests in fields with known heterogeneities have resulted in tests that match the classical exponential integral solution. The uniform flux model is only reasonable for fairly short fractures, and in these cases, the observation well must be *very* close to the active well to differentiate between various fracture azimuths. Extensions to infinite conductivity fracture models are unrealistic for low permeability fields of interest, where very long fractures are created in order to flow commercial rates.

4.2 Interference With Two Fractures

Mousli *et al.* ¹⁸⁷ first addressed the problem of two hydraulically fractured wells. This paper extended an important paper by Cinco *et al.* ⁴⁹. Cinco's paper solved the problem of transient pressure behavior of a well near an incompressible, infinite conductivity natural fracture. Wells completed in reservoirs with widely spaced natural fractures may not actually intercept an individual fracture; however, Cinco's model

illustrated how such a well might show naturally fissured behavior or, in some cases, behavior like a hydraulically fractured well. This solution also has applications in well control operations where a hydraulic fracture from a relief well might pass near a blowout.

Mousli *et al.* rearranged this solution to determine pressure at an infinite conductivity well with either a line source well or uniform flux fractured well, as the active well. The general procedure for this solution is as follows:

- Start with the equation for dimensionless pressure drop (along the fracture due to a line source well at the origin and a hydraulic fracture: whose center is located at a dimensionless horizontal distance x_{mD} , and whose dimensionless vertical distance is d_D (Figure 4.1):

$$\begin{aligned}
 p_{fD}(x_D, y_D, d_D, x_{mD}, t_{Dxf}) & \quad (4.1) \\
 &= -1/2 E_i \left[-\frac{(x_D^2 + y_D^2)}{4t_{Dxf}} \right] + 1/2 \int_0^{t_{Dxf}} \int_{x_{mD}-1}^{x_{mD}+1} \\
 & \cdot \frac{q_D \exp \left\{ -\left[(x_D - x'_D)^2 + (y_D - d_D)^2 \right] / \left[4(t_{Dxf} - \tau_D) \right] \right\}}{t_{Dxf} - \tau_D} dx'_D \cdot d\tau_D
 \end{aligned}$$

- o The condition of uniform pressure over the fracture [(infinite conductivity) is satisfied by dividing the plane source into a number of segments and writing a system of equations which discretizes the time and space integrals. System unknowns are the n block flow rates at a given time level. To solve the problem, the sum of the fluxes (q_{fD}) is equal to zero and all of the fracture block pressures are identical.
- o The resultant ($n \cdot n$) matrix is solved for fluxes that are in turn used to calculate observation well pressures. Mousli *et al.* determined that as many as 90 fracture blocks would be required to determine fluxes to the desired accuracy. This limitation was overcome by using Richardson's extrapolation technique 217 . .

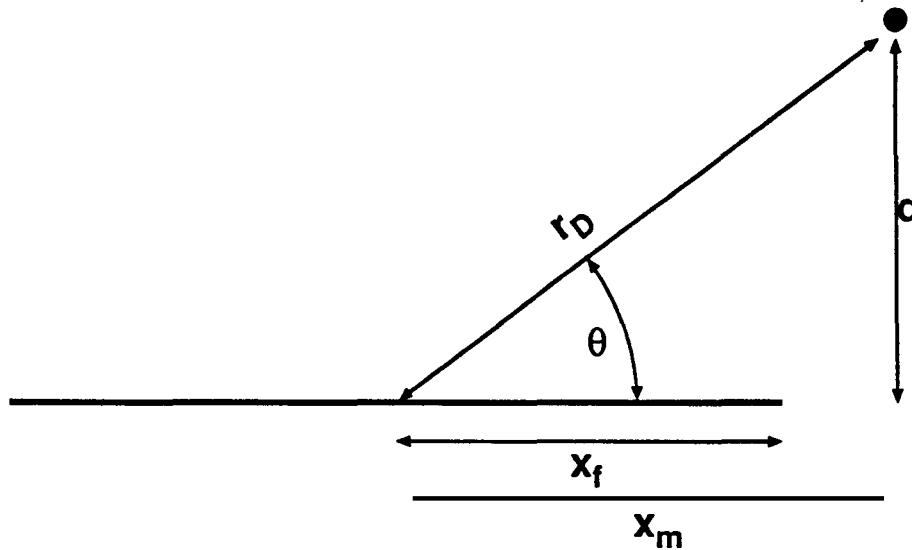


Figure 4.1: Interference With a Hydraulically Fractured Observation Well and a Line Source Active Well

4.3 Extension to Finite Conductivity Wells

This section derives equations for finite conductivity fracture pressure and flux calculations. Laplace space formulations of these equations are **used** to simplify the problem and increase solution flexibility.

4.3.1 Derivation of Laplace Transformation Model for Interference Testing with Infinite Conductivity Fractures

Mousli *et al.* ¹⁸⁷ solved an interference testing problem with an infinite conductivity fracture intersecting the observation well, and either a line source or uniform flux fracture at the active well. Their method was an extension of previous work by Cinco *et al.* ⁴⁹. In this subsection, a different approach is taken to solve the problem in Laplace space. This approach makes it possible to solve the problem of interference testing with an infinite conductivity fracture intersecting the observation well and constant pressure production from the active well(s). This method is extended to interference testing with a finite conductivity hydraulic fracture at the active well.

For the fracture flow equation, the assumption of steady state flow in the fracture is retained.

$$\frac{\partial^2 p_f}{\partial x^2} + \frac{\mu}{k_f} \frac{q_f(x', t_{Dxf})}{b_f h} = 0 \quad (4.2)$$

This can also be expressed as a constant pressure condition over the length of the fracture, when combined with the infinite conductivity assumption.

$$p_{wD}(t_{Dxf}) - p_{fD}(x_D, t_{Dxf}) = 0 \quad (4.3)$$

There are two wells in the system under consideration: a line source well located at a vertical distance d_D , and a horizontal distance x_{mD} from the center of the observation (infinite conductivity fracture) well. Horizontal distance is considered parallel to the hydraulic fracture. Dimensionless pressure drop at any point in space as a result of the combined wells is:

$$\begin{aligned} p_D(x_D, y_D, t_{Dxf}) = & \\ & \frac{1}{4} \int_0^{t_{Dxf}} \int_{-1}^1 q_D(x', \tau) \frac{\exp\left\{-\left[\frac{(x_D - x')^2 + y_D^2}{4(t_{Dxf} - \tau)}\right]\right\}}{t_{Dxf} - \tau} dx' d\tau \\ & - 1/2E_i \left[-\frac{(x_D - x_{mD})^2 + d_D^2}{4t_{Dxf}} \right] \end{aligned} \quad (4.4)$$

The first term on the right hand side is the pressure drop due to the fracture fluxes, while the second term is the line source response. Note the change of origin to the center of the fractured well from Mousliet *al.*'s¹⁸⁷ formulation. There is no longer (necessarily) any symmetry which reduces matrix size. Combining Equations 4.3 and 4.4 for $y_D = 0$ and $-1 \leq x_D \leq 1$ and taking the Laplace transform results in:

$$\bar{p}_{wD}(s) - \frac{1}{2} \int_{-1}^1 \bar{q}_{fD}(x', s) K_0 \left[(|x_D - x'| \sqrt{s}) \right] dx' = \frac{K_0 \left[\sqrt{s} \cdot ((x_D - x_{mD})^2 + d_D^2) \right]}{s} \quad (4.5)$$

This requires knowledge of the following Laplace transformation⁴ :

29.3.120

$$\mathcal{L}\left(-1/2E_i \frac{-k^2}{4t}\right) = \frac{K_0(k\sqrt{s})}{s} \quad (4.6)$$

The discretized form of the equation is much simpler than for the finite conductivity case:

$$\bar{p}_{wD}(s) - \frac{1}{2} \sum_{i=1}^n \bar{q}_{fD_i}(s) \int_{x_{D_i}}^{x_{D_{i+1}}} [K_0 [|x_{D_j} - x'| \sqrt{s}]] dx' = \frac{K_0(\sqrt{s}r_{D_j})}{s} \quad (4.7)$$

This constitutes n equations for each of the fracture segments. Unknowns are the n fluxes and the wellbore pressure. One remaining equation states that the sum of the fluxes from each fracture segment is equal to zero. Discretized in Laplace space, this is:

$$\sum_{i=1}^n \bar{q}_{fD_i}(s) = 0 \quad (4.8)$$

This system of equations can be written as:

$$\begin{pmatrix} A_{11} & A_{12} & \dots & A_{1n} & 1 \\ A_{21} & A_{22} & \dots & A_{2n} & 1 \\ \vdots & \vdots & \vdots & \vdots & \vdots \\ \vdots & \vdots & \vdots & \vdots & \vdots \\ A_{n1} & A_{n2} & \dots & A_{nn} & 1 \\ 1 & 1 & 1 & 1 & 0 \end{pmatrix} \begin{pmatrix} \bar{q}_{fD1} \\ \bar{q}_{fD2} \\ \vdots \\ \vdots \\ \bar{q}_{fDn} \\ \bar{p}_{wD}(s) \end{pmatrix} = \frac{1}{s} \begin{pmatrix} K_0(r_{D1}\sqrt{s}) \\ K_0(r_{D2}\sqrt{s}) \\ \vdots \\ \vdots \\ K_0(r_{Dn}\sqrt{s}) \\ 0 \end{pmatrix} \quad (4.9)$$

where r_{Dj} is the dimensionless distance between the active well and the center of the j th fracture segment. A_{ij} terms consist of the following:

for all i, j

$$-\frac{1}{2} \int_{x_{D_i}}^{x_{D_{i+1}}} K_0 [|x_{D_j} - x'| \sqrt{s}] dx' \quad (4.10)$$

Unknowns are solved by inverting the matrix on the left hand side of the equation. The Stehfest algorithm is used to invert the transformed variables back into real space. The matrix Equation 4.9 may be reduced from its current size of $(n + 1) \cdot (n + 1)$ to $(n \cdot n)$ by the techniques described in Appendix B.1.1.

4.3.2 Some Results

Mousliet *al.* 187 reported a sensitivity analysis in order to determine the optimum number of fracture blocks. A similar study was conducted for this analysis requiring an

additional sensitivity to the number of passes through the Stehfest algorithm $n_{Stehfest}$. Figure 4.2 is a plot of the calculated value of p_{wD} as a function of $n_{FractureBlocks}$ for $\theta = 30^\circ$ and $r_D = 4$ and t_{Dxf}/r_D^2 . The optimum number of blocks is specified as when the change in the estimated value of p_{wD} is less than 0.5%; for this example, the optimum occurs at 80 blocks. A sensitivity over a wide number of values of t_{Dxf} and r_D indicated a maximum of 90–100 for $n_{FractureBlocks}$. The flux distributions become stable for $n_{FractureBlocks} > 40$.

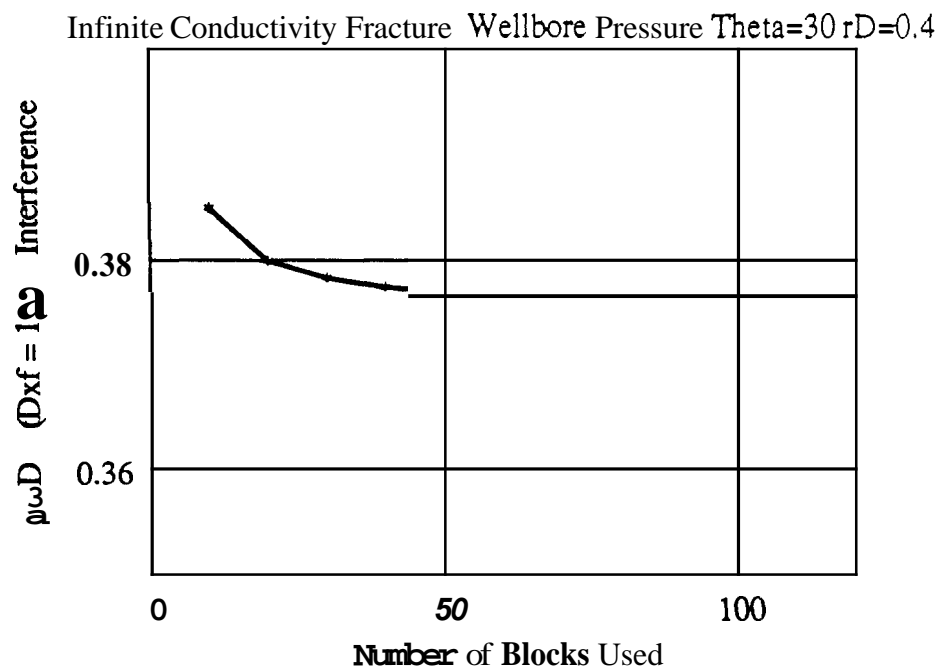


Figure 4.2: Wellbore Pressure Sensitivity to Number of Fracture Blocks for Infinite Conductivity Fracture, $\theta = 30^\circ$, $r_D = 0.4$

Results were compared with the published results of Mousli *et al.* 187 . Mousli *et al.*'s Figures 2-4 illustrate results for values of r_D of 0.4, 1.0, and 2.0, with r_D defined on the basis of the total fracture length L_f , rather than x_f as here defined. Figures 4.3-4.5 are corresponding figures for values of r_D equal to 0.8, 2.0, and 4.0 using the Laplace formulation. Agreement is good over all ranges. The exponential integral solution is also plotted on these figures, illustrating that for tests of less than $r_D = 2.0$, hydraulic fracture effects are substantial. Figure 4.6 shows an even closer

result for $r_D = 0.4$.

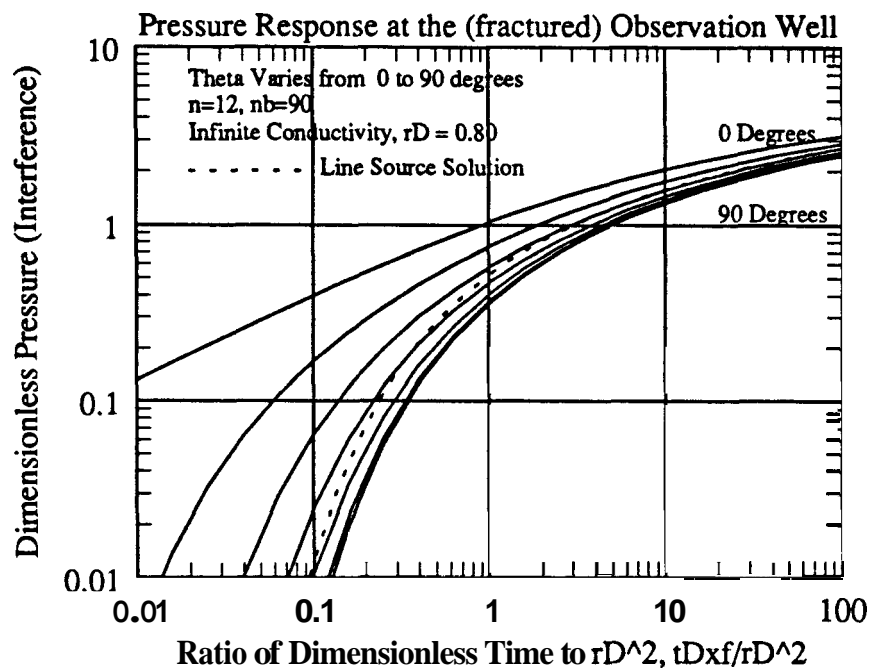


Figure 4.3: Pressure Response at the Fractured Observation Well with a Line Source Active Well, $r_D = 0.8$

The next series of figures presents computed flux distributions. These distributions are useful in visualizing the interference with the infinite conductivity fracture; flux distributions will also be compared to finite conductivity results. Figure 4.7 shows the fracture flux distributions for various values of t_{Dxf}/r_D^2 ranging from 0.01 to 100. At low values of t_{Dxf} , the calculated value of p_{wD} is negligible; however, the flux distribution is already taking shape. Flux distributions appear to stabilize for values of $t_{Dxf}/r_D^2 > 10$. Figure 4.8 shows flux distributions for a fracture with the line source active well located at $r_D = 0.4$ and $0^\circ \leq \theta \leq 90^\circ$. A sharp decrease in the flux at $x_D = 0.4$ for the 0° case is slightly anomalous, as it corresponds with the line source well intersecting the fracture at that location. Figures 4.9–4.10 represent the sensitivities of flux distribution to different values of r_D . The value of r_D directly affects the dimensionless time scale being used; therefore, both fixed values of t_{Dxf}/r_D^2 and t_{Dxf} are presented.

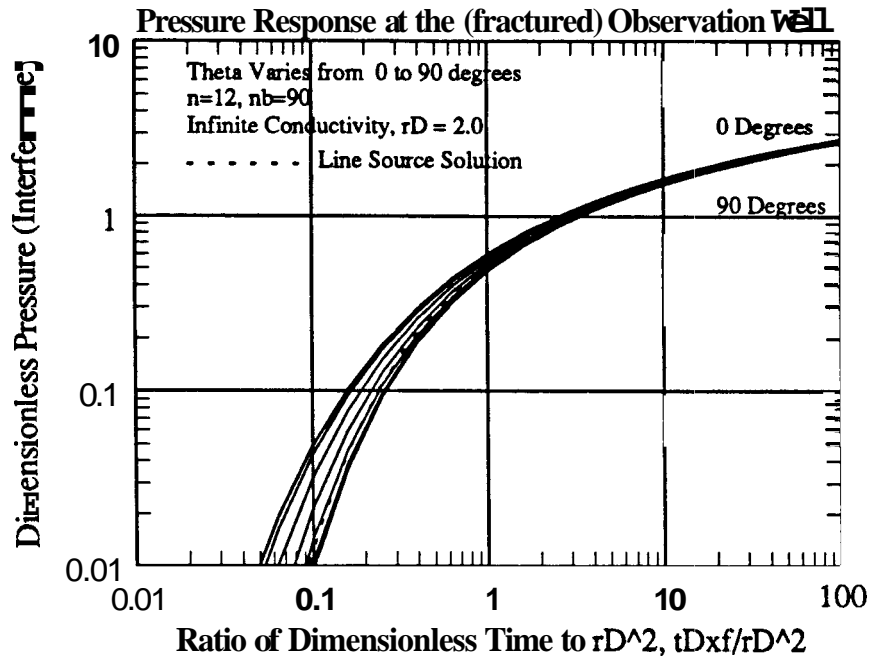


Figure 4.4: Pressure Response at the Fractured Observation Well with a Line Source Active Well, $rD = 2.0$

4.3.3 Interference Between a Finite Conductivity Fracture Intersecting the Observation Well and a Line Source Active Well

The Laplace space solution to this previously unsolved problem follows from the combination of the two previous problems. Interference of the line source well with an infinite conductivity fracture had been solved in dimensionless space by Mousli *et al.* 187 . By solving the coupled problem in Laplace space, several new solutions are possible.

First, the pressure drop in space due to the line source active well and the finite conductivity observation well:

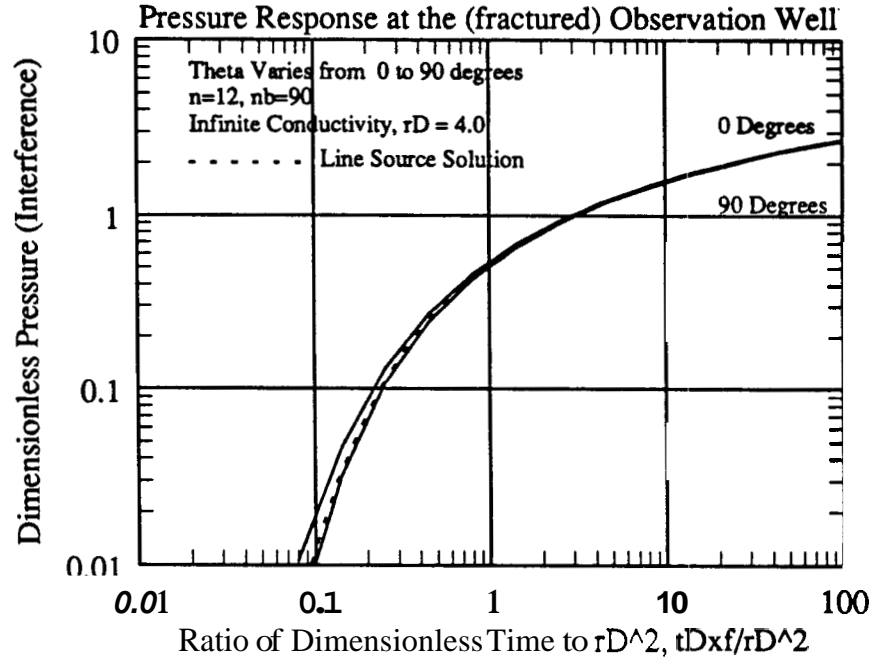


Figure 4.5: Pressure Response at the Fractured Observation Well with a Line Source Active Well, $rD = 4.0$

$$\begin{aligned}
 p_D(x_D, y_D, t_{Dxf}) = & \\
 & \frac{1}{4} \int_0^{t_{Dxf}} \int_{-1}^1 q_D(x', \tau) \frac{\exp \left\{ - \left[\frac{(x_D - x')^2 + y_D^2}{4(t_{Dxf} - \tau)} \right] \right\}}{t_{Dxf} - \tau} dx' d\tau \\
 & - 1/2 E_i \left[- \frac{(x_D - x_{mD})^2 + d_D^2}{4t_{Dxf}} \right] \quad (4.11)
 \end{aligned}$$

This is combined with the fracture **flow** equation for the finite conductivity well.

$$p_{wD}(t_{Dxf}) - p_{fD}(x_D, t_{Dxf}) = \frac{\pi}{(k_f b_f)_D} \left\{ x_D - \int_0^{x_D} \int_0^{x'} q_{fD}(x'', t_{Dxf}) dx'' dx' \right\} \quad (4.12)$$

Equating the fracture and reservoir equations for $y_D = 0$ and $-1 \leq x_D \leq 1$ and taking the Laplace transform results in:

$$\bar{p}_{wD}(s) - \frac{1}{2} \int_{-1}^1 \bar{q}_{fD}(x', s) K_0 \left[(|x_D - x'| \sqrt{s}) \right] dx' \quad (4.13)$$

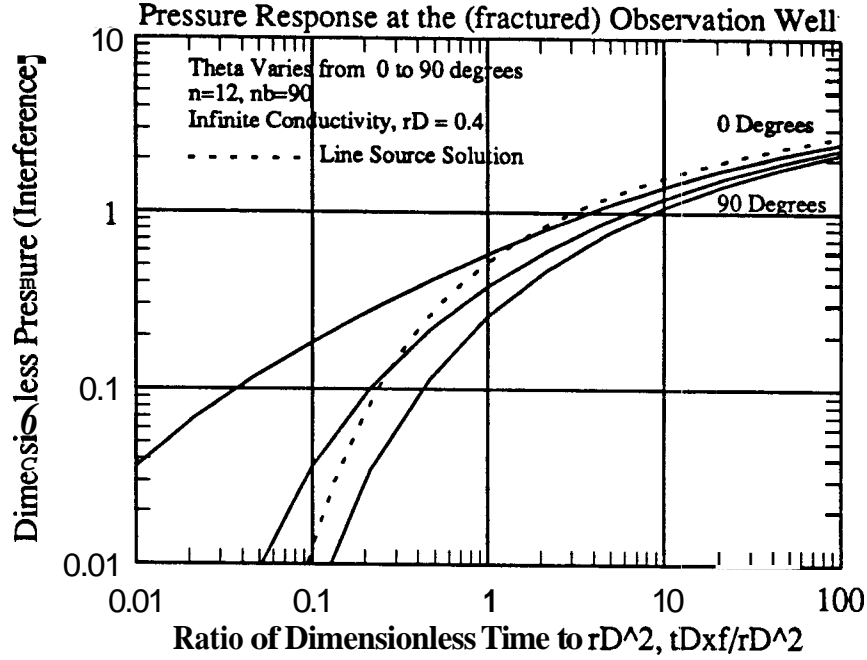


Figure 4.6: Pressure Response at the Fractured Observation. Well with a Line Source Active Well, $rD = 0.4$

$$+ \frac{\pi}{(k_f b_f)_D} \int_0^{x_D} \int_0^{x'} \bar{q}_{fD}(x'', s) dx'' dx' = \frac{\pi x_D}{(k_f b_f)_D s} + \frac{K_0(r_D \sqrt{s})}{s}$$

The discretized combined equation is:

$$\begin{aligned} \bar{p}_{wD}(s) - \frac{1}{2} \sum_{i=1}^n \bar{q}_{fDi}(s) \int_{x_{Di}}^{x_{D,i+1}} K_0[|\ x_{Dj} - x' \ | \ \sqrt{s}] dx' \\ + \frac{\pi}{(k_f b_f)_D} \sum_{i=1}^{j-1} \bar{q}_{fDi}(s) \left\{ \frac{(\Delta x)^2}{2} + \Delta x(x_{Dj} - i\Delta x) \right\} + \frac{(\Delta x)^2}{8} \bar{q}_{fDj}(s) \\ = \frac{\pi x_{Dj}}{(k_f b_f)_D s} + \frac{K_0(r_{Dj} \sqrt{s})}{s} \end{aligned} \quad (4.14)$$

This constitutes n equations for each of the fracture segments. Unknowns are the n fluxes and the wellbore pressures. The remaining equation states that the sum of the fluxes from each fracture segment is equal to the well flow rate. Discretized in Laplace space, this is:

$$\Delta x \cdot \sum_{i=1}^n \bar{q}_{fDi}(s) = \frac{1}{s} \quad (4.15)$$

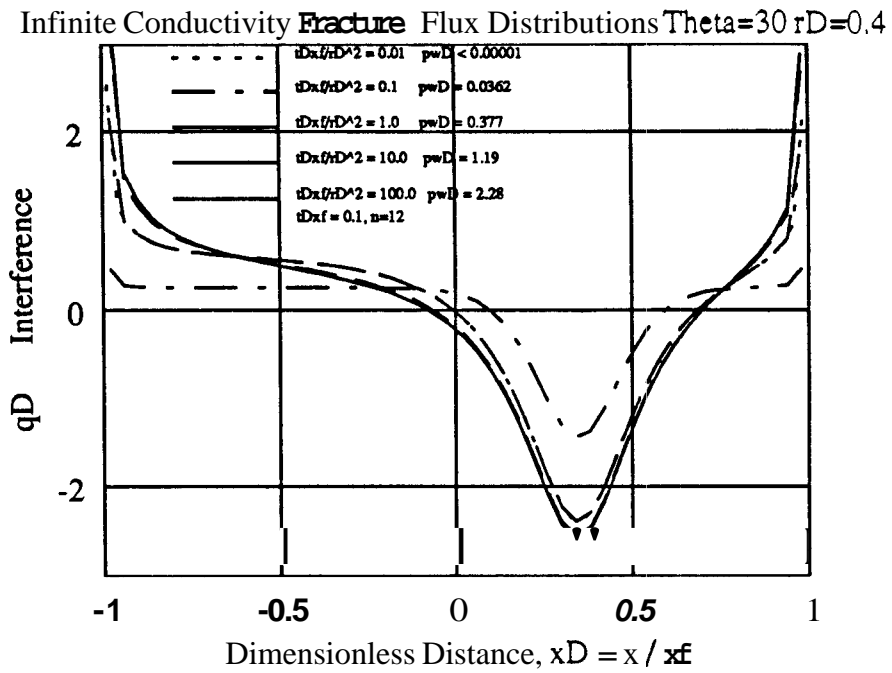


Figure 4.7: Fracture Flux Sensitivity in Time, Infinite Conductivity Fractures, $\Theta = 30^\circ$, $r_D = 0.4$

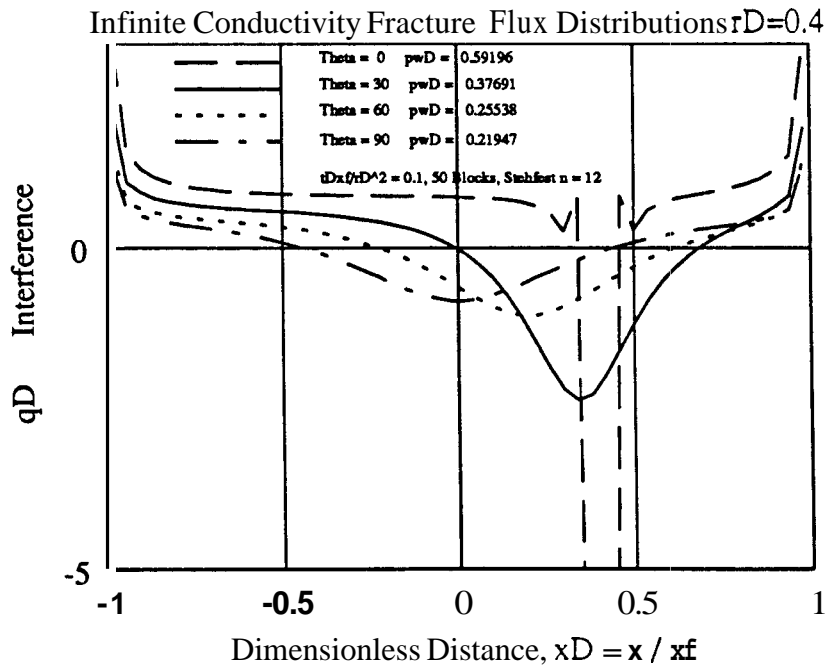


Figure 4.8: Fracture Flux Sensitivity to Θ , Infinite Conductivity Fractures, $r_D = 0.4$

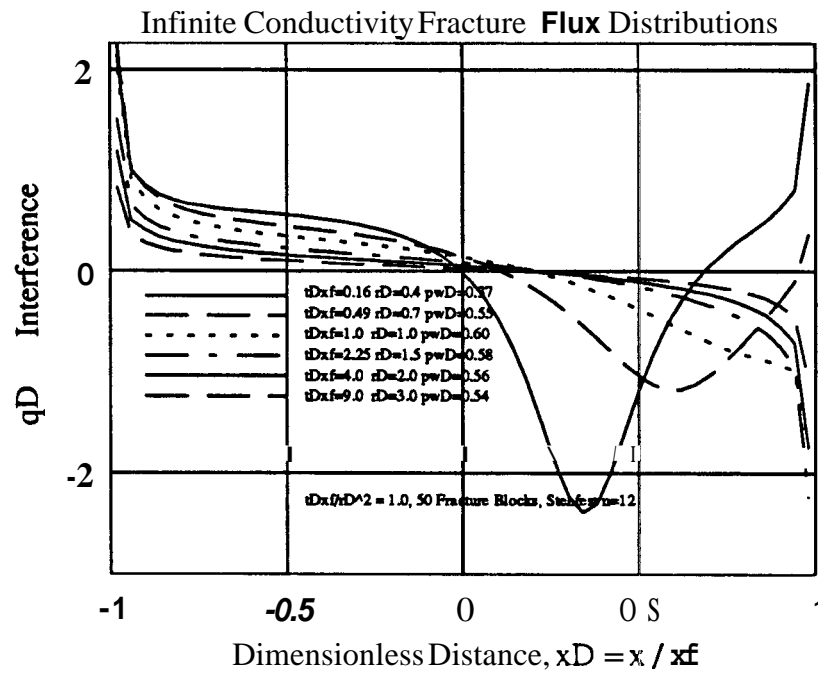


Figure 4.9: Fracture Flux Sensitivity to r_D , fixed t_{Dxf}/r_D^2

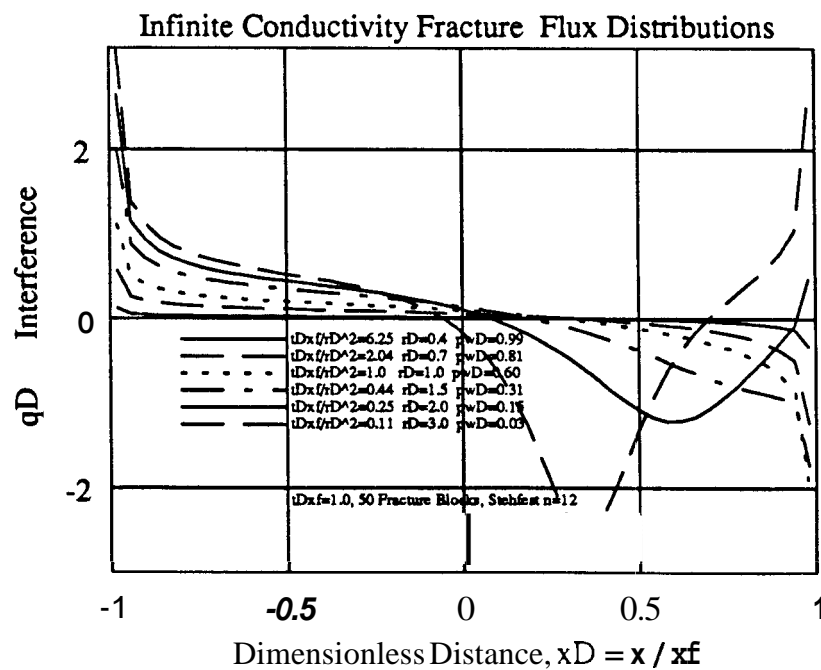


Figure 4.10: Fracture Flux Sensitivity to r_D , fixed t_{Dxf}

The system of equations can be written as:

$$\begin{vmatrix} A_{11} & A_{12} & \dots & A_{1n} & 1 \\ A_{21} & A_{22} & \dots & A_{2n} & 1 \\ & & & \vdots & \vdots \\ & & & \vdots & \vdots \\ A_{n1} & A_{n2} & \dots & A_{nn} & 1 \\ A_x & A_x & A_x & \Delta x & 0 \end{vmatrix} \begin{vmatrix} \bar{q}_{fD1} \\ \bar{q}_{fD2} \\ \vdots \\ \vdots \\ \bar{q}_{fDn} \\ \bar{p}_{wD}(s) \end{vmatrix} = \begin{vmatrix} \frac{\pi}{(k_f b_f)_D s} x_{D1} + \frac{K_0(\tau_{Dj}\sqrt{s})}{s} \\ \frac{\pi}{(k_f b_f)_D s} x_{D2} + \frac{K_0(\tau_{Dj}\sqrt{s})}{s} \\ \vdots \\ \vdots \\ \frac{\pi}{(k_f b_f)_D s} x_{Dn} + \frac{K_0(\tau_{Dj}\sqrt{s})}{s} \\ \frac{\pi}{(k_f b_f)_D s} + \frac{K_0(\tau_{Dj}\sqrt{s})}{s} \end{vmatrix} \quad (4.16)$$

$A_{,,}$ terms are identical to those outlined in Section 3.6.2. Matrix solution and numerical inversion were obtained as described in Section 3.6.4. Some difficulties were encountered in the detailed numerical analysis, especially for low fracture conductivities and very early times. However, this solution procedure is a more difficult method than required to solve the problem, as the reciprocity principle can be invoked to obtain these solutions. Pressure drops at a fractured observation well due to an active well are interchangeable when observation and active wells are reversed. Figure 4.11 shows the pressure response at any point located at a distance r_D from a finite conductivity well with $(k_f b_f)_D = 10\pi$. Individual solid lines are for values of theta ranging from 0-90 degrees. Superimposed asterisks are the calculated well pressures at a hydraulically fractured observation well due to production from a line source well at $r_D = 0.6$. The exponential integral solution is also shown as a dashed line. Results for a low conductivity fracture are compared in Figure 4.11.

4.4 Interference Between Two Finite Conductivity Hydraulically Fractured Wells

In this section, a solution is generated for the combined interference problem of finite conductivity fractures intersecting both active and observation wells. Formulation is for different length fractures with different values of $(k_f b_f)_D$.

This solution can evaluate behavior of either a line source well or finite conductivity hydraulically fractured well located near a natural fracture or another hydraulically

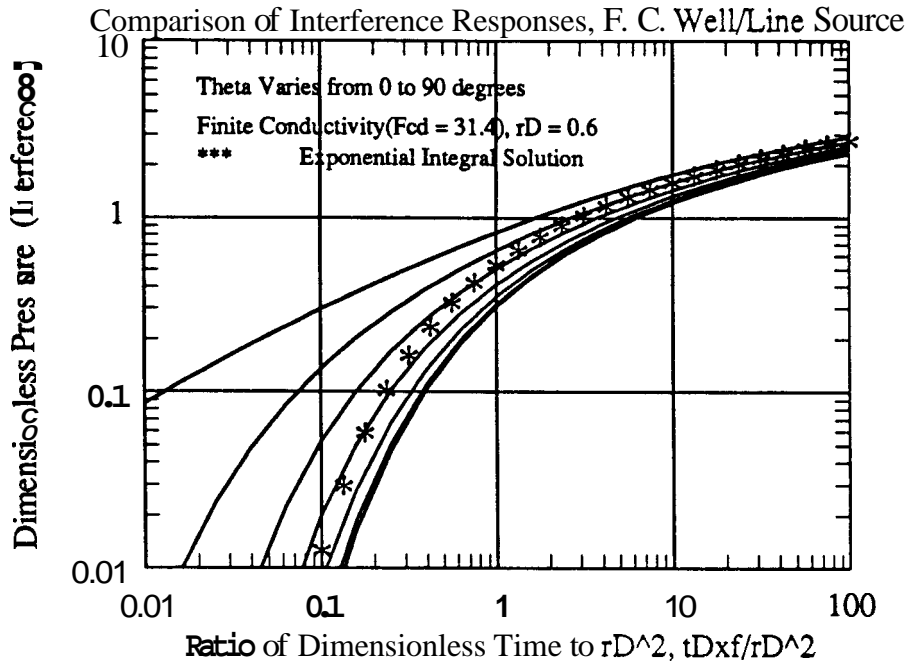


Figure 4.1: Comparison of Interference Responses for a Line Source—Finite Conductivity Fracture Pair, $(k_f b_f)_D = 10\pi$

fractured well. This method quantifies such impacts and predicts the behavior of a hydraulically fractured well in a naturally fractured system with large, widely spaced fractures. Primary use of the solution is for the well testing interference problem. Appropriate nomenclature is illustrated in Figure 4.12.

4.4.1 Semianalytic Solution

Fracture flow equations and reservoir equations are written and coupled for each well as in previous derivations. However, in this solution, fluxes from both fractures must be specified. In Laplace space, the dimensionless pressure drop at the active well is:

$$\begin{aligned}
 \bar{p}_{wD}(s) - \frac{1}{2} \int_{-1}^1 \bar{q}_{fDA}(x', s) K_0[|x_D - x'| \sqrt{s}] dx' \\
 + \frac{\pi}{(k_f b_f)_D} \int_0^{x_D} \int_0^{x'} \bar{q}_{fD}(x'', s) dx'' dx' = \frac{\pi x_D}{(k_f b_f)_D s} + \\
 \frac{1}{2} \int_{x_{mD}-1/\Lambda_{[AO]}}^{x_{mD}+1/\Lambda_{[AO]}} \bar{q}_{fDO}(x', s) K_0(\sqrt{s} \sqrt{(x_D - x')^2 + d_D^2}) dx' \quad (4.17)
 \end{aligned}$$

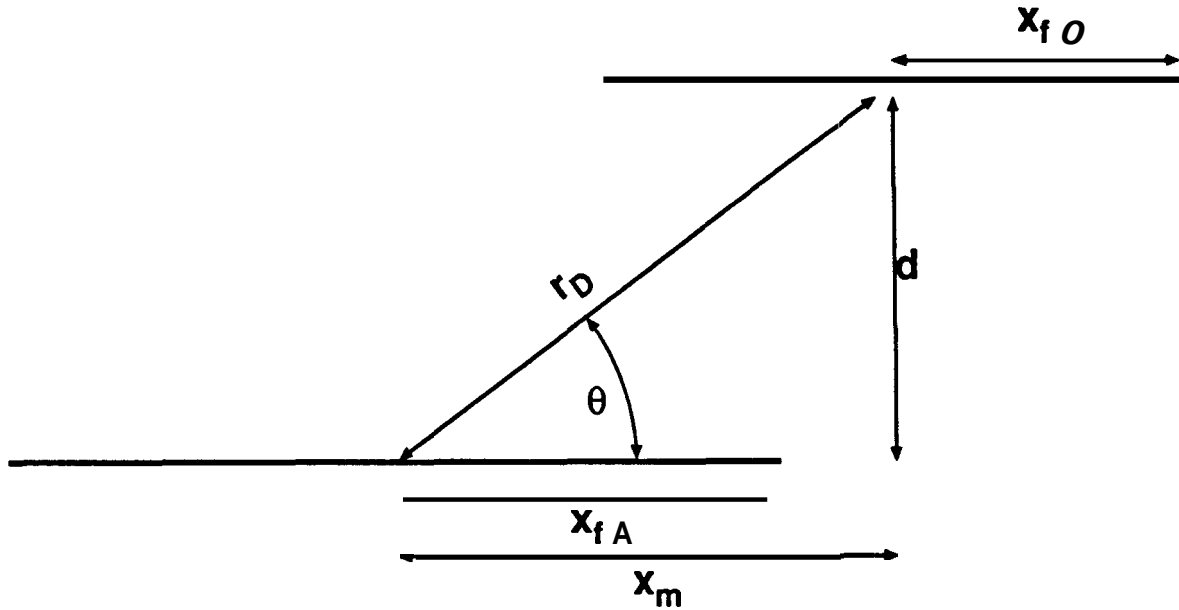


Figure 4.12: Nomenclature for Interference with Two Hydraulically Fractured Wells

Similarly, for the observation well,

$$\begin{aligned} \bar{p}_{wD}(s) - \frac{1}{2} \int_{x_{mD}-1/\Lambda_{[AO]}}^{x_{mD}+1/\Lambda_{[AO]}} \bar{q}_{fDO}(x', s) K_0 [|x_D - x'| \sqrt{s}] dx' \\ + \frac{\pi}{(k_f b_f)_D} \int_0^{x_D} \int_0^{x'} \bar{q}_{fD}(x'', s) dx'' dx' = \\ \frac{1}{2} \int_{-1}^1 \bar{q}_{fDA}(x', s) K_0(\sqrt{s} \sqrt{(x_D - x')^2 + d_D^2}) dx' \end{aligned} \quad (4.18)$$

The equation for the observation well only holds for equal fracture conductivities. Modifications for different conductivities and permeability anisotropy will be given in Sections 4.4.2 and 4.4.3. If n matrix blocks are used for each fracture half length, the above equations constitute $4n$ equations for $4n + 2$ unknowns. For the remaining two equations, the flux conditions at each well are incorporated.

Letting $m = 2n$ for the total number of fracture blocks,

for the active well:

$$\Delta x \cdot \sum_{i=1}^m \bar{q}_{fDA} = \frac{2}{s} \quad (4.19)$$

for the observation well

$$\sum_{i=1}^m \bar{q}_{fDO} = 0 \tag{4.20}$$

For the simplified case of equal fracture lengths and equal fracture conductivities, the matrix formulation becomes:

$$\begin{vmatrix} A_{11} & A_{12} & \dots & A_{1,m} & 1 & B_{11} & B_{12} & \dots & B_{1,m} & 0 \\ A_{21} & A_{22} & \dots & A_{2,m} & 1 & B_{21} & B_{22} & \dots & B_{2,m} & 0 \\ \vdots & \vdots & \vdots & \vdots & \vdots & \vdots & \vdots & \vdots & \vdots & \vdots \\ \vdots & \vdots & \vdots & \vdots & \vdots & \vdots & \vdots & \vdots & \vdots & \vdots \\ A_{m,1} & A_{m,2} & \dots & A_{m,m} & 1 & B_{m,1} & B_{m,2} & \dots & B_{m,m} & 0 \\ \Delta x & \Delta x & \Delta x & \Delta x & 0 & 0 & 0 & 0 & 0 & 0 \\ C_{11} & C_{12} & \dots & C_{1,m} & 0 & D_{11} & D_{12} & \dots & D_{1,m} & 1 \\ C_{21} & C_{22} & \dots & C_{2,m} & 0 & D_{21} & D_{22} & \dots & D_{2,m} & 1 \\ \vdots & \vdots & \vdots & \vdots & \vdots & \vdots & \vdots & \vdots & \vdots & \vdots \\ \vdots & \vdots & \vdots & \vdots & \vdots & \vdots & \vdots & \vdots & \vdots & \vdots \\ C_{m,1} & C_{m,2} & \dots & C_{m,m} & 1 & D_{m,1} & D_{m,2} & \dots & D_{m,m} & 1 \\ 0 & 0 & 0 & 0 & 0 & 1 & 1 & 1 & 1 & 0 \end{vmatrix} \begin{vmatrix} \bar{q}_{fDA1} \\ \bar{q}_{fDA2} \\ \vdots \\ \vdots \\ \bar{q}_{fDAm} \\ \bar{p}_{wDA}(s) \\ \bar{q}_{fDO1} \\ \bar{q}_{fDO2} \\ \vdots \\ \vdots \\ \bar{q}_{fDOm} \\ \bar{p}_{wDO}(s) \end{vmatrix} = \frac{\pi}{(k_f b_f)_D s} \begin{vmatrix} x_{D1} \\ x_{D2} \\ \vdots \\ x_{Dn} \\ 1 \\ 0 \\ 0 \\ \vdots \\ 0 \\ 0 \end{vmatrix} \tag{4.21}$$

A_{ij} terms and D_{ij} terms arise from the pressure drops at the fractured active and observation wells due to the fluxes at each of those wells respectively. For the special case of $x_{fA} = x_{fO}$ and $(k_f b_f)_A = (k_f b_f)_O$, these two terms will be identical. The B_{ij} and C_{ij} terms are the *cross terms*, which contribute to the effects of the active well fluxes on the wellbore pressure at the observation well, and vice versa.

Although the basic nature of the discretizations are similar to those given in Section 3.6.2, numerous changes are required. A first series of modifications is due to the inclusion of the entire fracture length in the solution. This alters the discretization of the fracture pressure drop terms as in Equation 3.65–3.67. Both the A and D matrices must be subdivided into quarters. The $i = j$ terms again require an additional $(\Delta x)^2/8$. In each submatrix, the upper left and lower right submatrices have additional terms consisting of $(\Delta x)^2/2 + \Delta x(x_{Dj} - i\Delta x)$. The counters for the ij terms

must be kept consistent with the direction of discretization.

4.4.2 Modifications for Different Fracture Lengths, Conductivities

Distances require scaling when fracture lengths or conductivities are not equal. The ratio of the active well's hydraulic fracture length to that of the observation well is given as:

$$\Lambda_{[AO]} = \frac{x_{fA}}{x_{fO}} \quad (4.22)$$

and the relative fracture permeability width product as:

$$[k_f b_f]_{AO} = \frac{(k_f b_f)_A}{(k_f b_f)_O} \quad (4.23)$$

The ratio of the values of $(k_f b_f)_D$ for the two wells is then:

$$(k_f b_f)_D \left[\frac{A}{B} \right] = \frac{[k_f b_f]_{AO}}{\Lambda_{[AO]}} \quad (4.24)$$

Because the origin of the observation well is displaced x_{mD} along the x-direction and d_D in the y-direction, additional changes to the formulation are also required. Solution consistency requires the active and observation wells to be formulated in their specific coordinate systems. For example, the integration limits for the A_{ij} terms are $[-1;1]$. Corresponding limits for the D_{ij} terms are $[x_{mD} - 1/\Lambda_{[AO]}; x_{mD} + 1/\Lambda_{[AO]}]$.

At early times (large values of s), the cross terms (BC) are negligible. The result is infinite acting behavior at the active well and zero pressure drop at the observation well. At late times, the magnitude of the cross terms approaches that of the main diagonal. As in all of the previous matrix representations, the illustrated solution is representative in nature. In practice, the order of the matrix can be reduced, in this case from $(rn+2) \cdot (rn+2)$ to $m \cdot m$. This reduction speeds the matrix inversion and reduces storage. Matrix inversion is typically repeated eight times in each time step in the Stehfest algorithm numerical Laplace transform inversion. Details of this reduction are presented in Appendix B.1.1. Other methods for accelerating the solution, both for filling the matrix and inversions, are discussed in Appendix B.1.2–B.1.3.

4.4.3 Effects of Azimuth and Spacing

In this section, a series of figures are used to summarize solution results. A series of figures will give the dimensionless pressure (p_D) and dimensionless pressure derivatives (p'_D) at the active and observation wells. Dimensionless pressure derivative groups are useful for evaluating more subtle characteristics and as a diagnostic tool. These derivatives are calculated from the Laplace space solutions directly and do not require numerical differentiation.

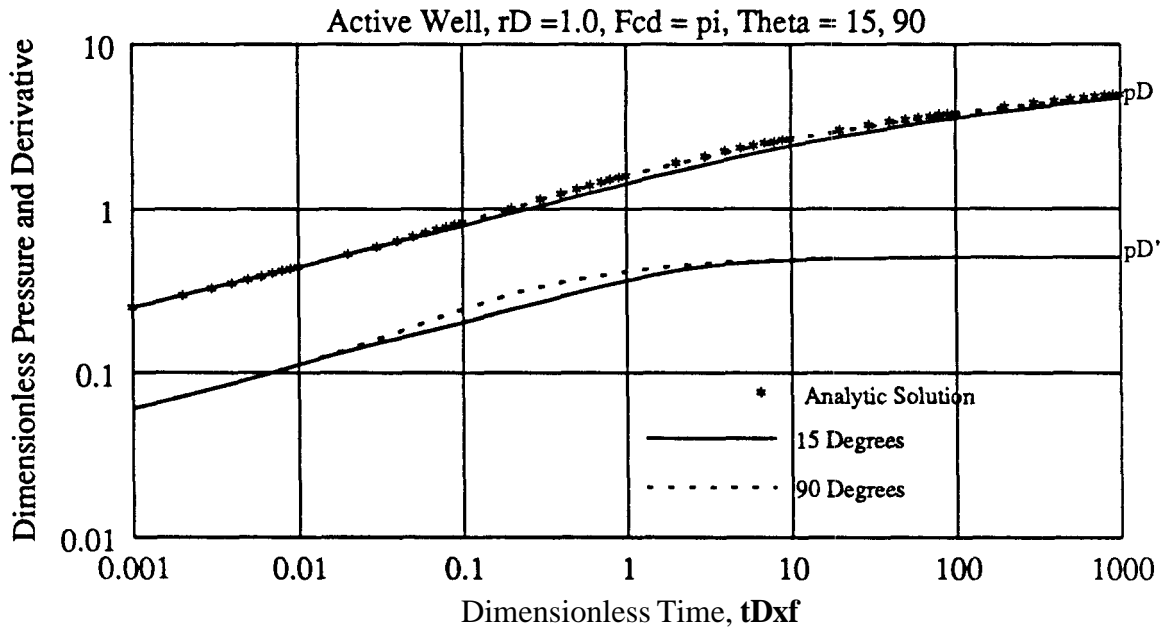


Figure 4.13: Active Well Solution for $r_D = 1$, $F_{CD} = \pi$

Typically, a group of curves is displayed showing varying fracture azimuths which range from 15–90°. As active well responses show small variations due to fracture azimuth, only the 15 and 90 degree cases are displayed. Observation well figures show responses for each 15 degree increment, except for cases when all of the responses are spaced very close together. For the graphs of p_D at the active well, the infinite acting solution is also displayed. Active well solutions are plotted as a function of t_{Dxf} . Invariably, the infinite acting solution overlays the data at early times. At late times, the active well interference solutions show varying levels of negative skin. During a

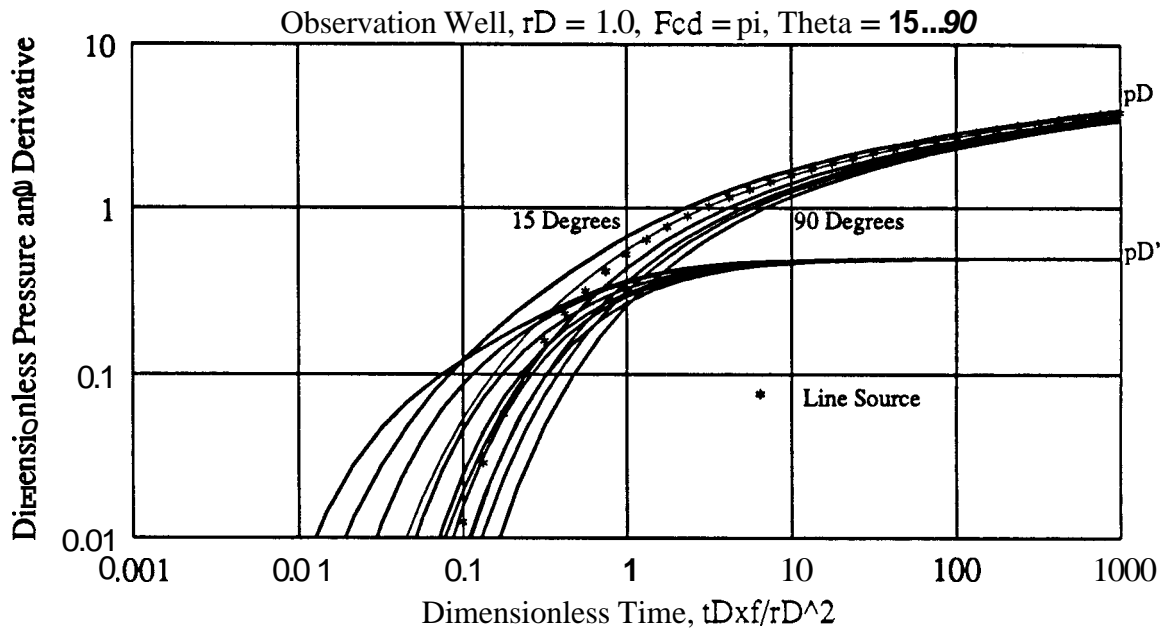


Figure 4.14: Observation Well Solution for $r_D = 1$, $F_{CD} = \pi$

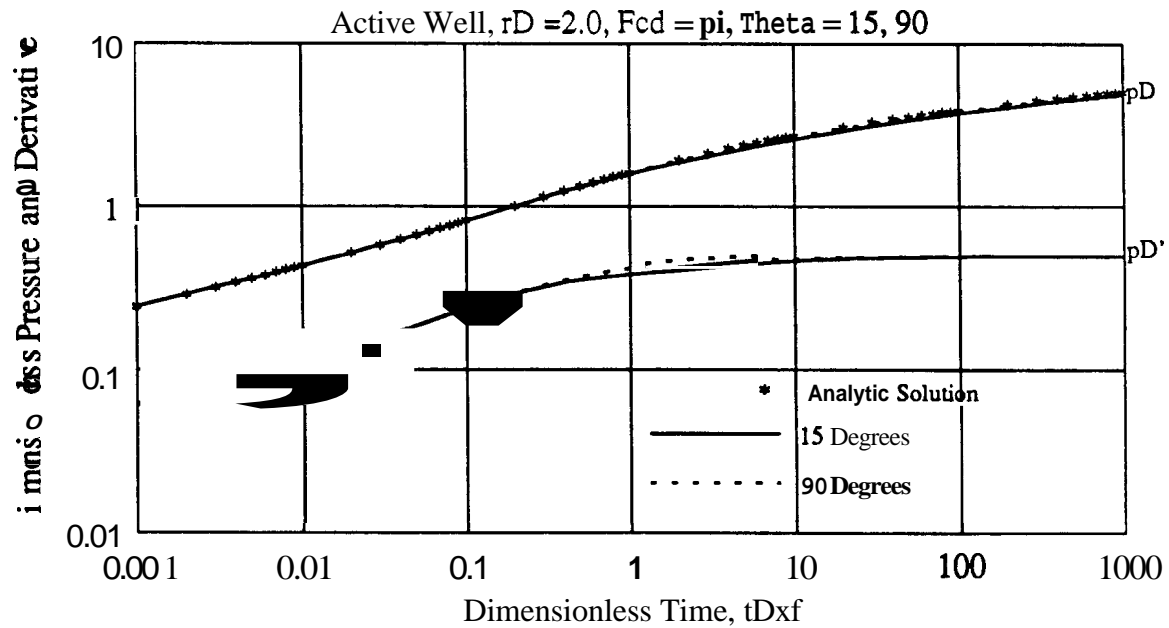


Figure 4.15: Active Well Solution for $r_D = 2$, $F_{CD} = \pi$

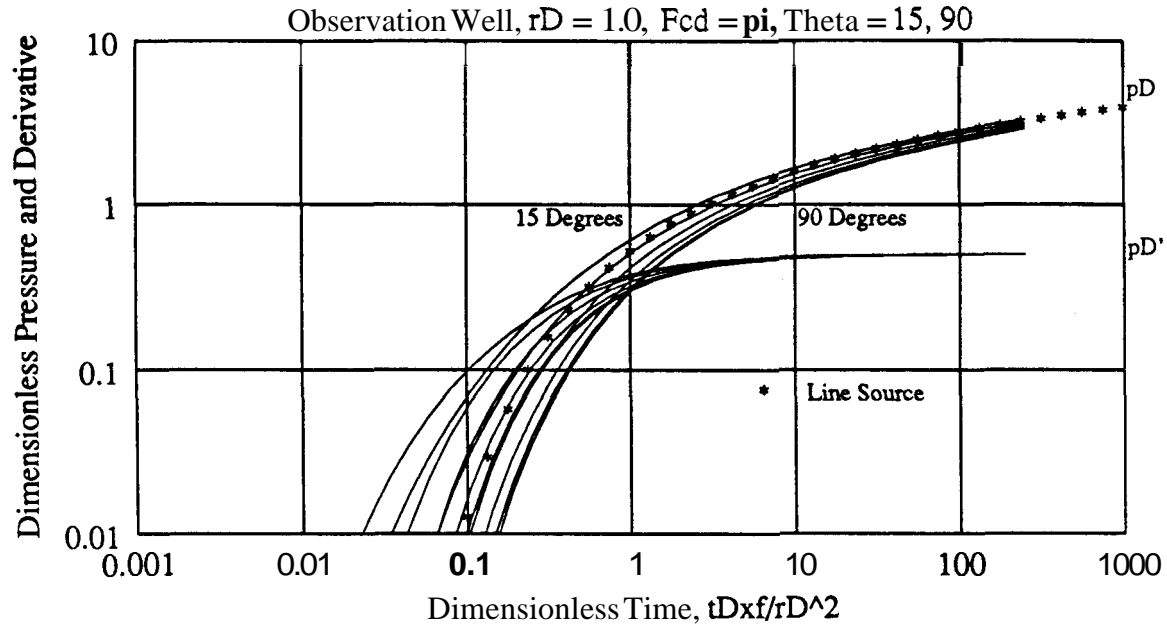


Figure 4.16: Observation Well Solution for $r_D = 2$, $F_{CD} = \pi$

transition period of varying length, active well pressures and the pressure derivative groups fall below the corresponding values for the infinite acting well. During this time, interference is most pronounced.

For the interference wells, the exponential integral is plotted, along with p_D and p'_D . Observation well solutions are plotted as a function of t_{Dxf}/r_D^2 . For relatively small values of r_D , and for low values of azimuth, it is clear that the line source solution is a poor approximation. As r_D increases to values of four and above, all of the azimuth solutions collapse to the line source solution. Figures 4.13–4.20 present type curves for $(k_f b_f)_D = \pi$ for values of r_D varying from 0.5–4.0. Figures 4.21–4.28 present type curves for $(k_f b_f)_D = 100\pi$ for values of r_D varying from 0.5–4.0. Figures 4.29–4.32 illustrate results for fixed values of the angle θ and values of r_D ranging from 0.5–4.0. Attempts to collapse these curves further by use of various correlating parameters were unsuccessful. However, either early or late time behaviors can be correlated for the interference case by use of correlating parameters (Section 4.6).

Fracture fluxes at active and observation wells were different for both high and low

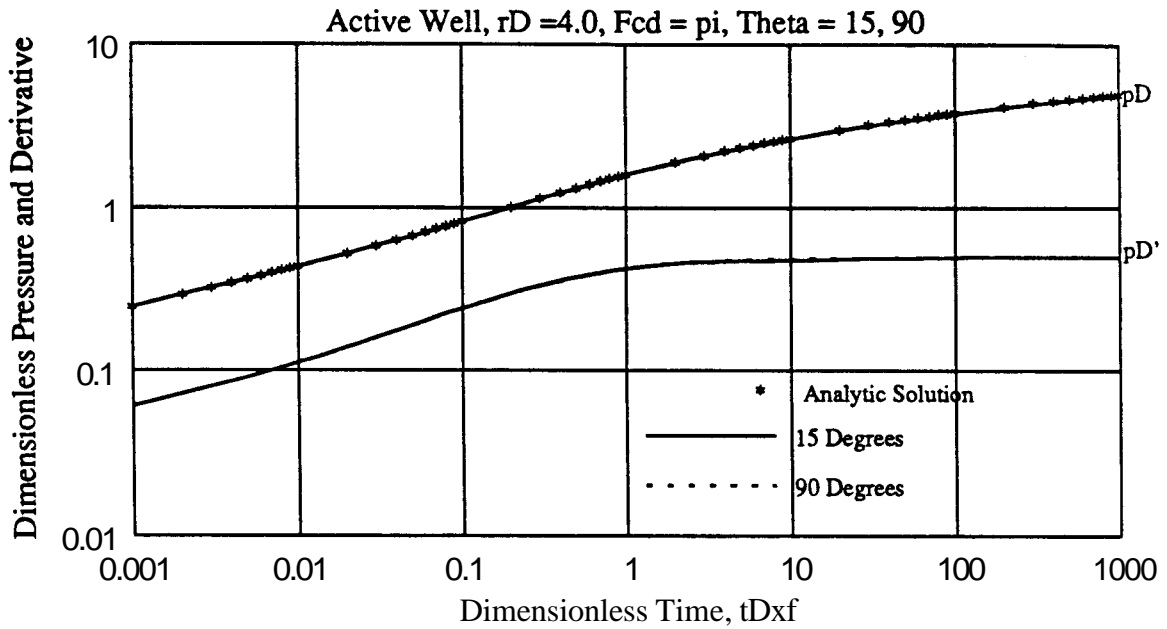


Figure 4.17: Active Well Solution for $r_D = 4$, $F_{CD} = \pi$

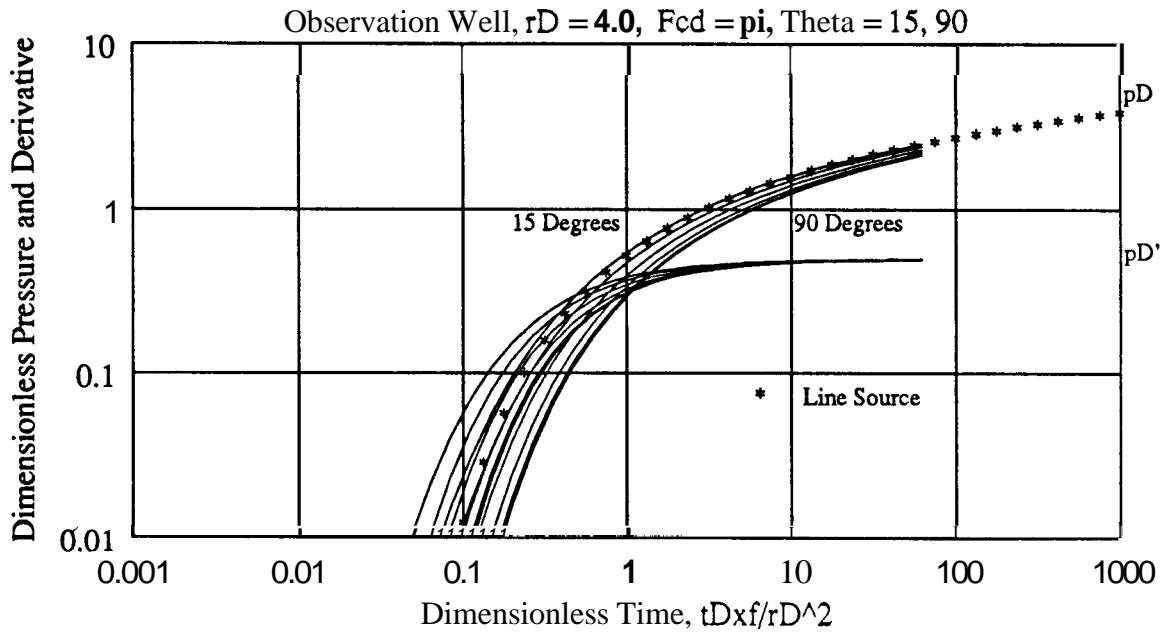


Figure 4.18: Observation Well Solution for $r_D = 4$, $F_{CD} = \pi$

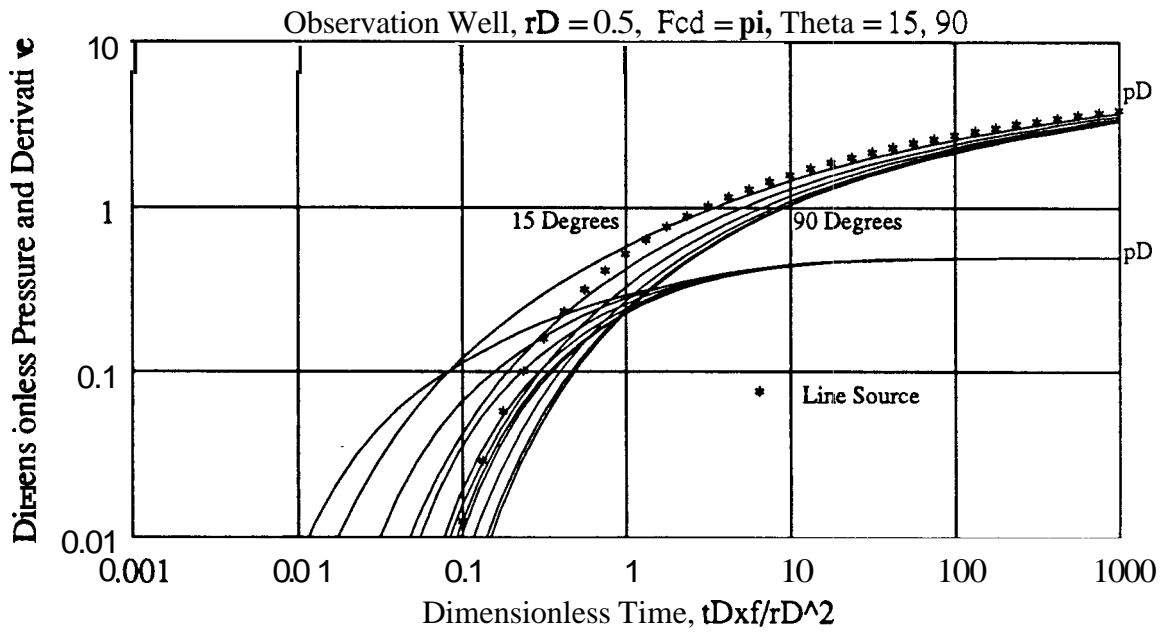
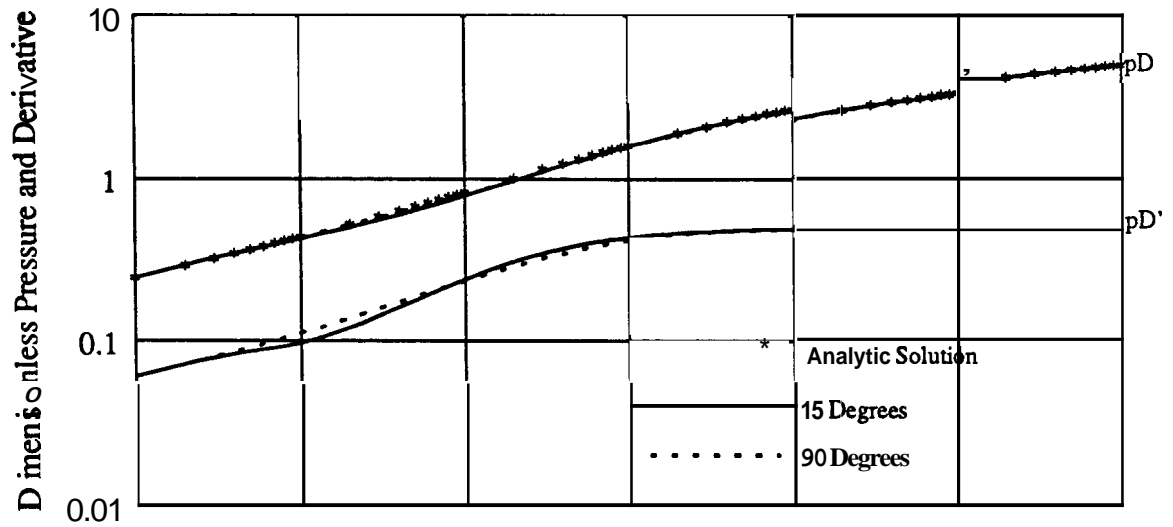


Figure 4.20: Observation Well Solution for $r_D = 0.5$, $F_{CD} = \pi$

conductivity cases. Figures 4.35-4.46 illustrate early and late time fluxes at the active and observation wells for both high and low fracture conductivity cases and fracture azimuths varying from 15–90°.

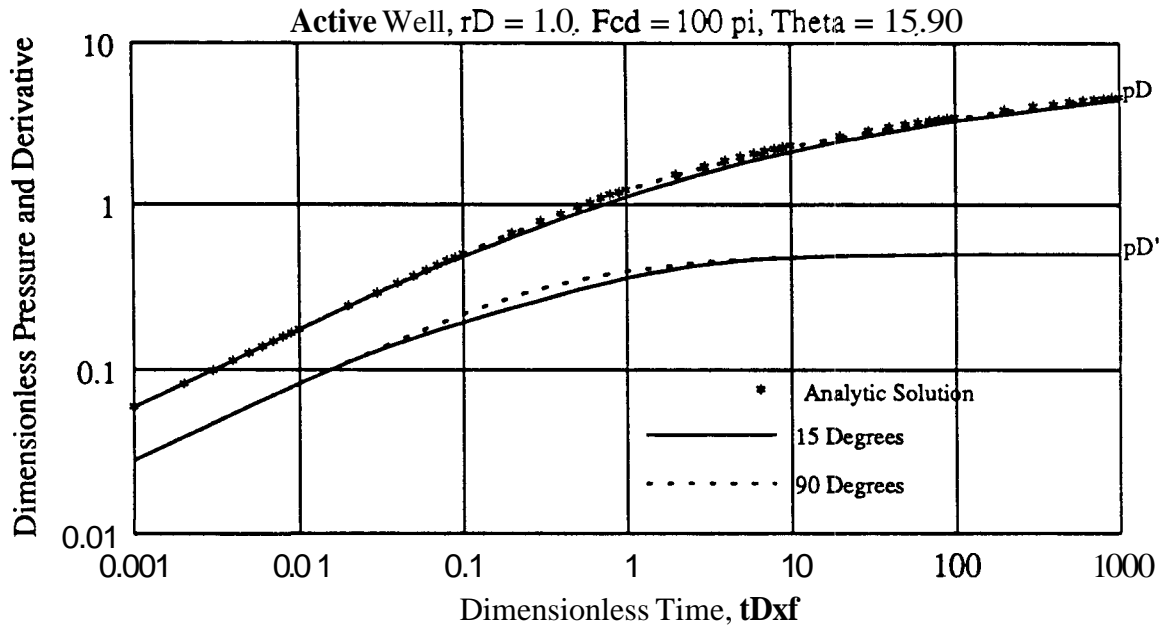


Figure 4.21: Active Well Solution for $r_D = 1$, $F_{CD} = 100\pi$

Permeability Anisotropy

Permeability anisotropy can be handled in the semianalytic solution by substitution of the series of geometric substitutions found in Section 6.4.4. Approximations for the dimensionless fracture conductivity are poor for very low values of conductivity and very early times. However, substitutions of the values of \bar{k} and x'_j into the definitions of p_D and t_{Dxf} are, for practical purposes, exact. Solutions for closed boundaries and interference tests require only the adjusted geometries. By rescaling axes for \bar{k} and x'_j , identical wellbore dimensionless pressures are obtained.

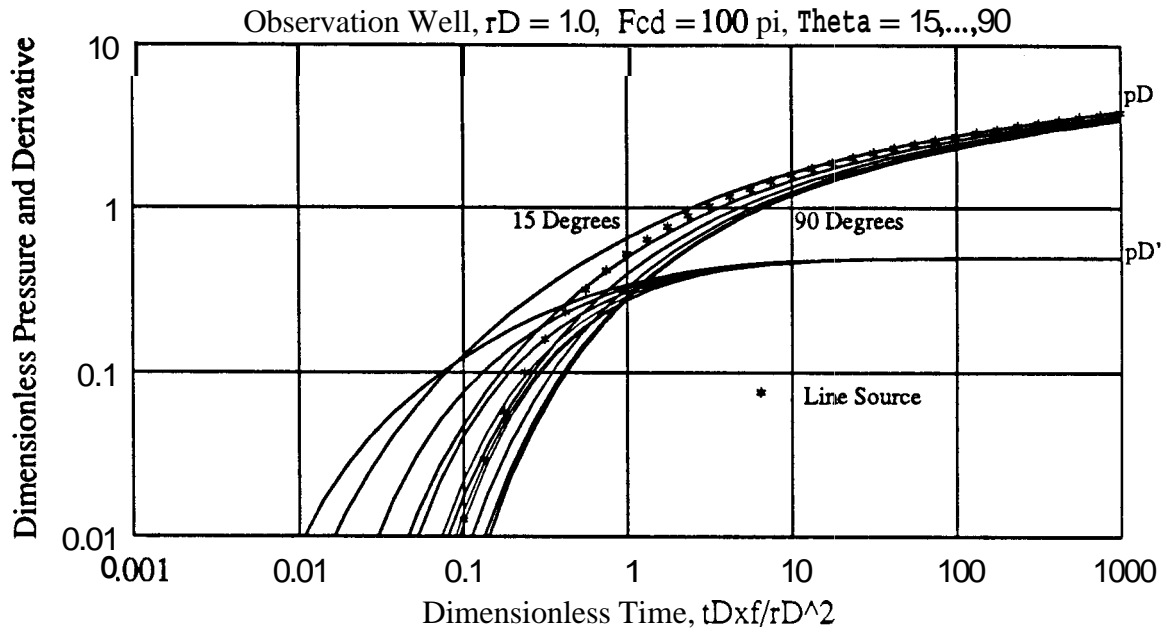


Figure 4.22: Observation Well Solution for $r_D = 1$, $F_{CD} = 100\pi$

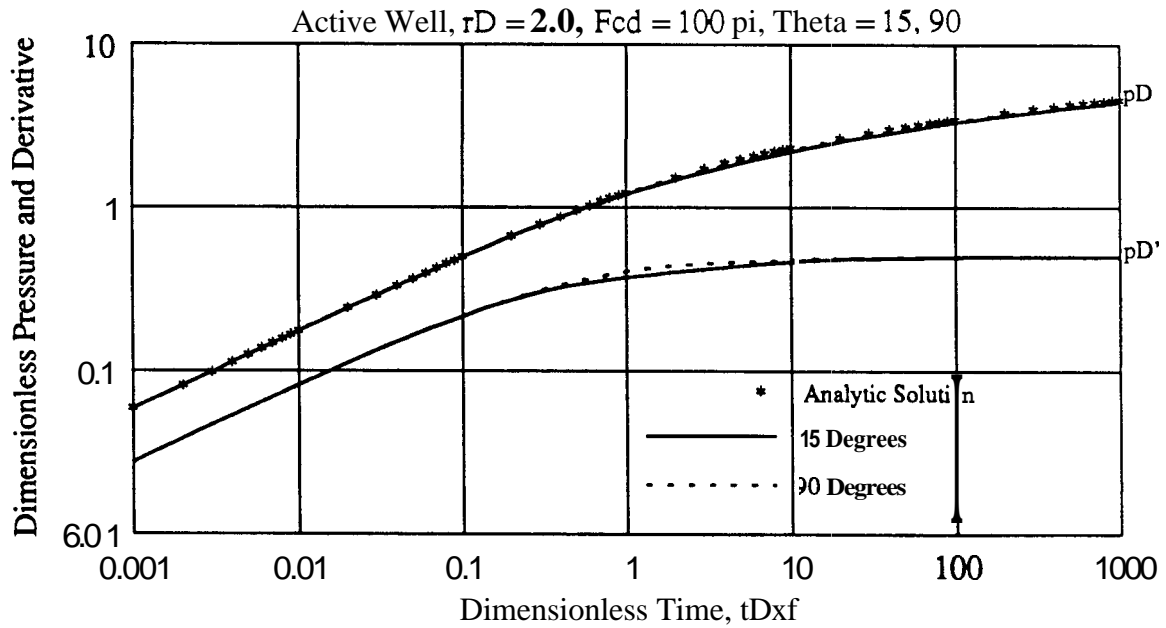


Figure 4.23: Active Well Solution for $r_D = 2$, $F_{CD} = 100\pi$

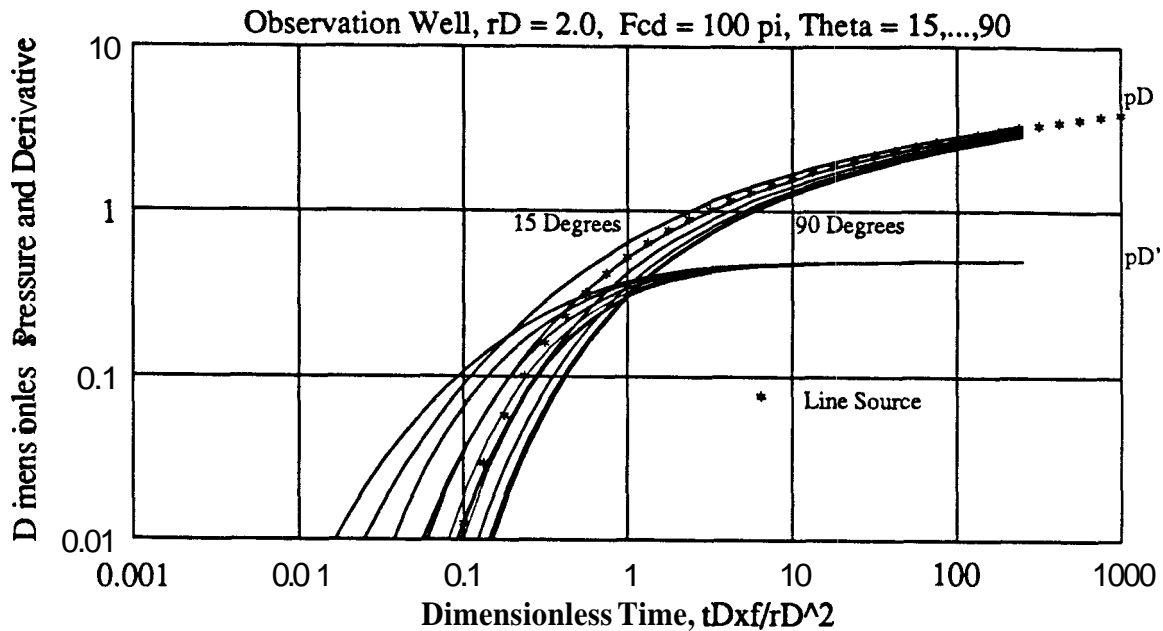


Figure 4.24: Observation Well Solution for $r_D = 2$, $F_{CD} = 100\pi$

4.4.4 Effects of Different Fracture Lengths and Conductivities

The effect of the fracture length ratio $\Lambda_{[AO]}$ is investigated by keeping the active well at unit length and varying the length of the observation well. Predicted responses for

- $\Lambda_{[AO]}$ ranging from 0.5–2.0,
- azimuth angles of 15° and 90°, and
- dimensionless conductivities of π and 100π

are shown in Figures 4.33 and 4.34. For each of these examples, the relative fracture conductivities $[k_f b_f]_{AO}$ are held constant; this implies changing values for the fracture permeability width product. However, this makes no practical difference over the range of interest because sensitivity to $[k_f b_f]_{AO}$ is negligible. Values of $\Lambda_{[AO]}$ for $\theta = 0$ and $r_D \leq 1 + \Lambda_{[AO]}$ were not considered because the two fractures would physically overlay each other. Low fracture angles in which the two fractures were in close

proximity often required increased numbers of fracture blocks for stability. Uniform flux over a given fracture block is assumed; fracture blocks were given a *maximum* size equal to one tenth the distance to the other well, d_D .

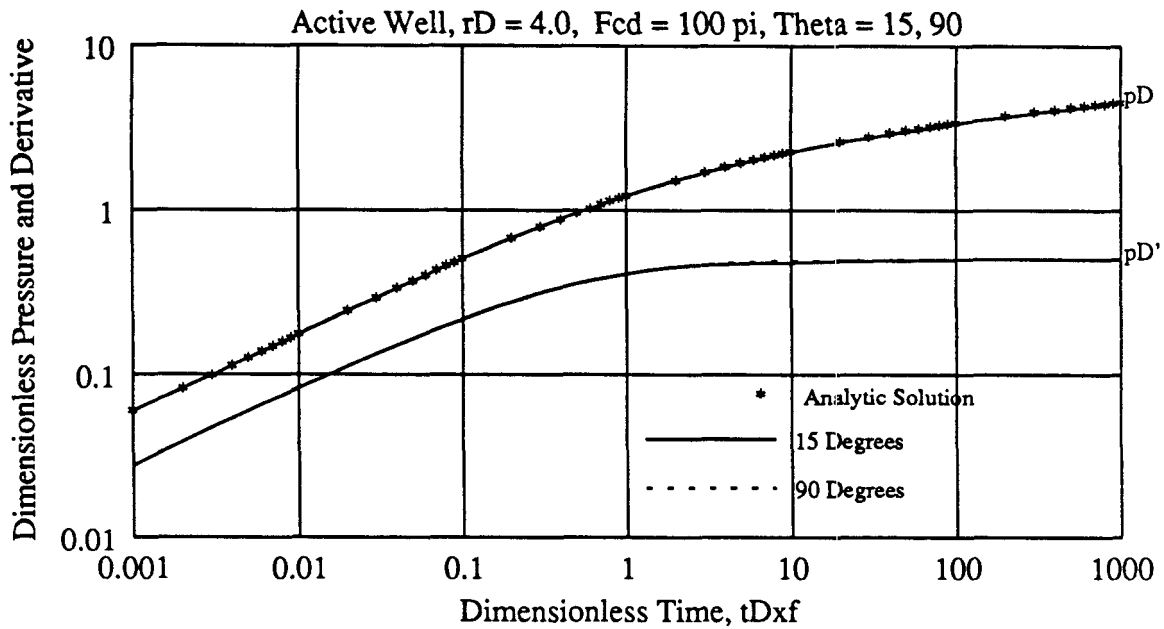


Figure 4.25: Active Well Solution for $r_D = 4$, $F_{CD} = 100\pi$

Similarities in these curves make it clear that fracture lengths and conductivities for the two wells cannot be determined by a single interference test, and should be determined independently for the two wells. This requires tests of sufficiently short duration to avoid interference. However, the effect of interference at the active well is not generally large except for small values of θ and r_D . Comparing the curves for varying values of $\Lambda_{[AO]}$ shows minimal sensitivity for angles greater than 45° . Caution should be exercised in analyzing tests with large values of θ due to the difficulty in differentiating between these angles. Initial estimates of fracture azimuth (from other techniques) should be used to avoid attempting tests large angles.

At late times, the influence of θ on observation well response decreases and becomes negligible for most cases at about $t_{Dxf}/r_D^2 > 10$. Values of $r_D > 4.0$ also show minimal response to θ at all times. The effect of finite conductivity in the observation well is

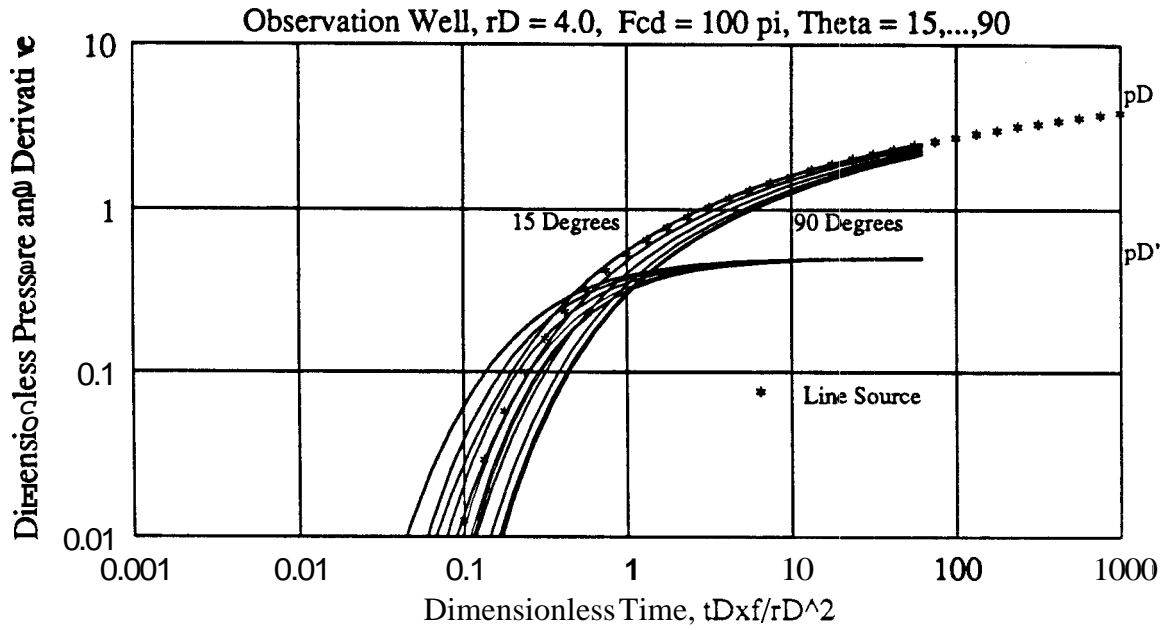


Figure 4.26: Observation Well Solution for $r_D = 4$, $F_{CD} = 100\pi$

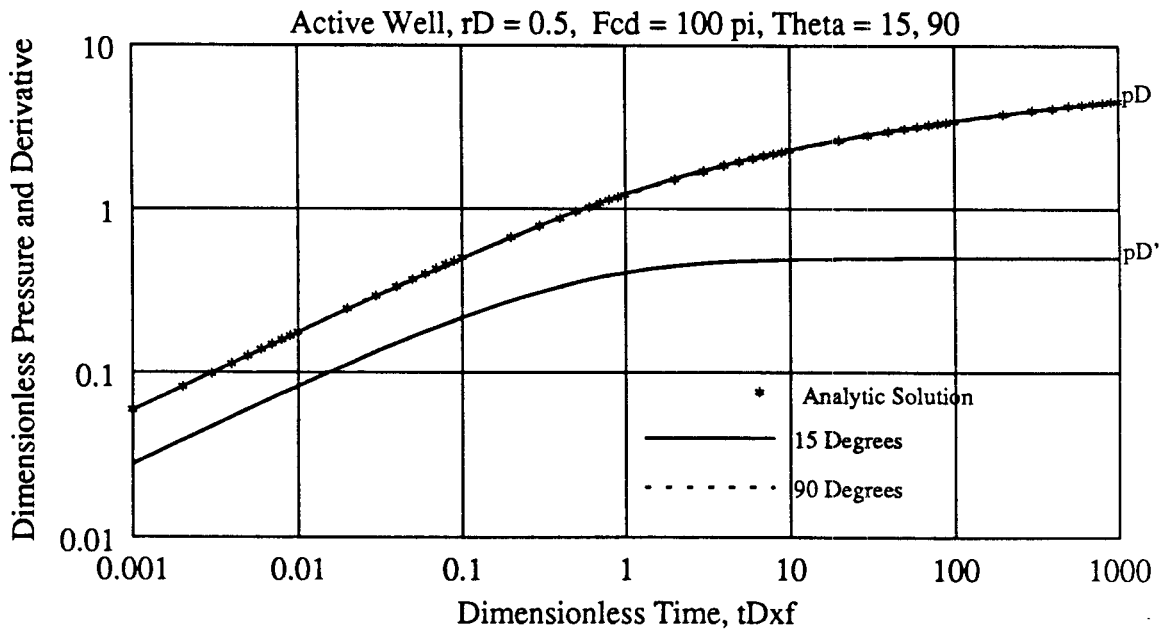


Figure 4.27: Active Well Solution for $r_D = 0.5$, $F_{CD} = 100\pi$

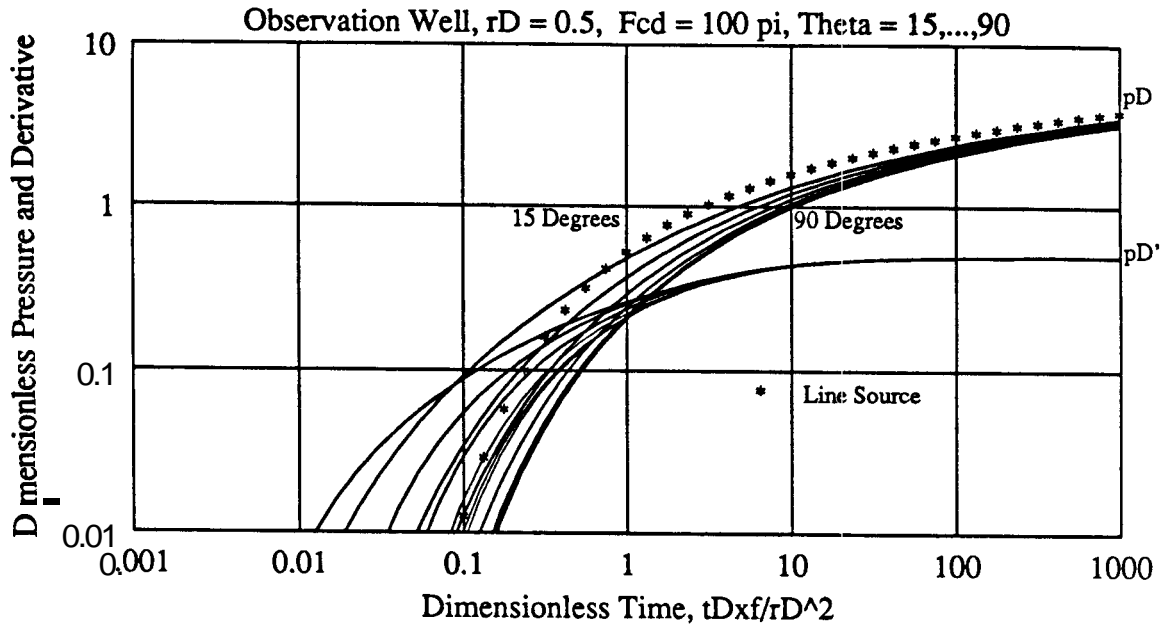


Figure 4.28: Observation Well Solution for $r_D = 0.5$, $F_{CD} = 100\pi$

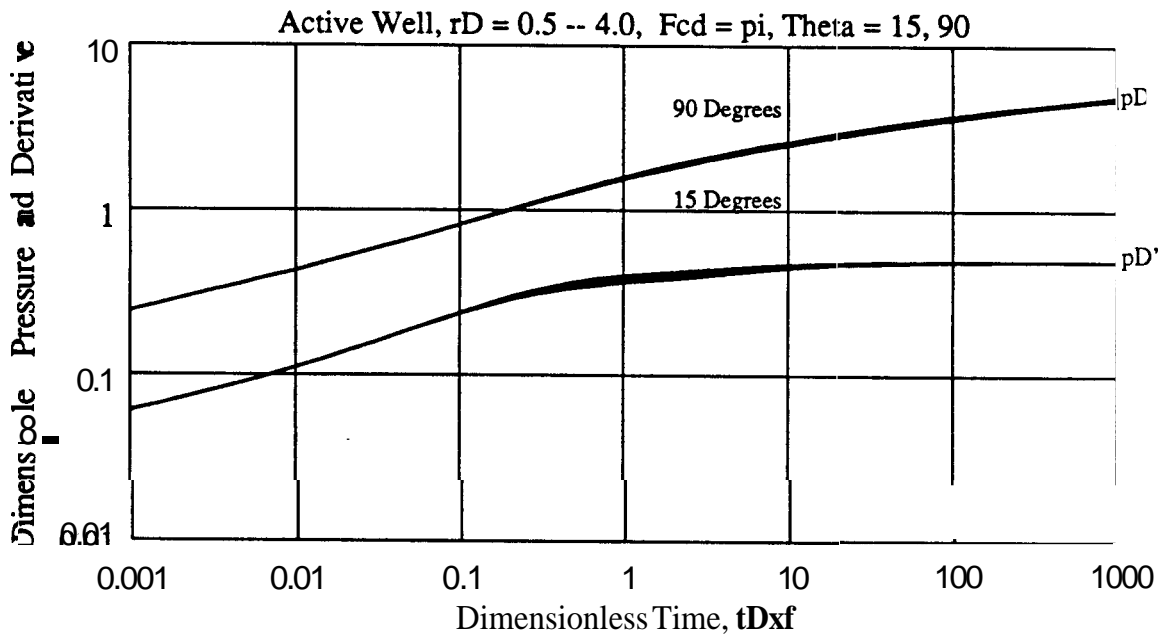


Figure 4.29: Active Well Solution, $\theta = 15$, $F_{CD} = \pi$

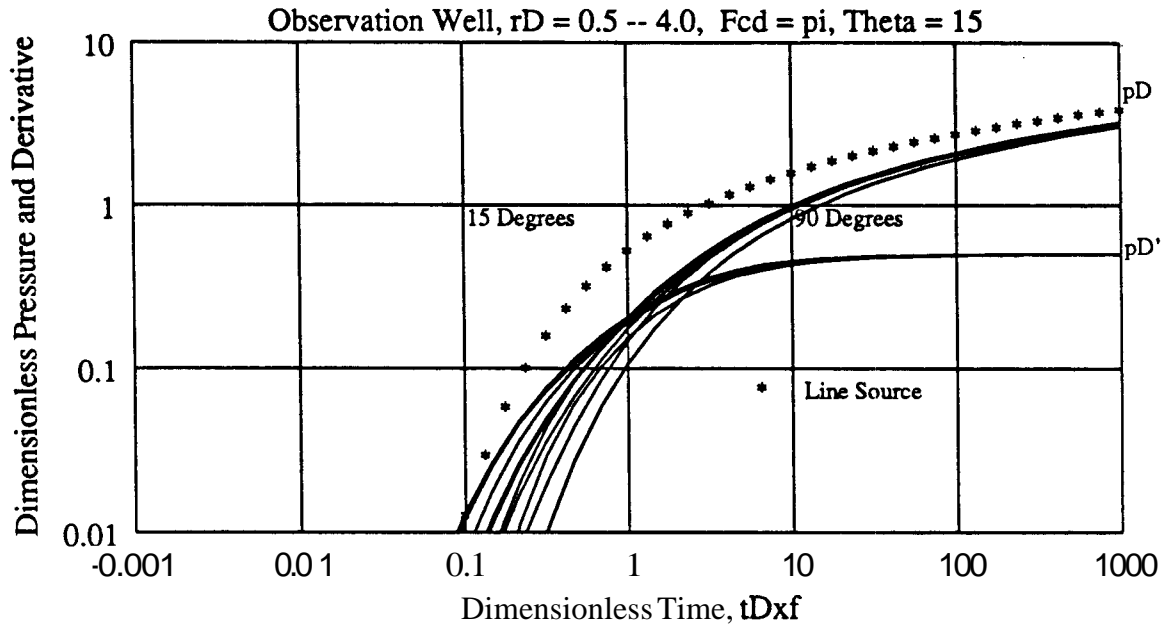


Figure 4.30: Observation Well Solution, $\theta = 15$, $F_{CD} = a$

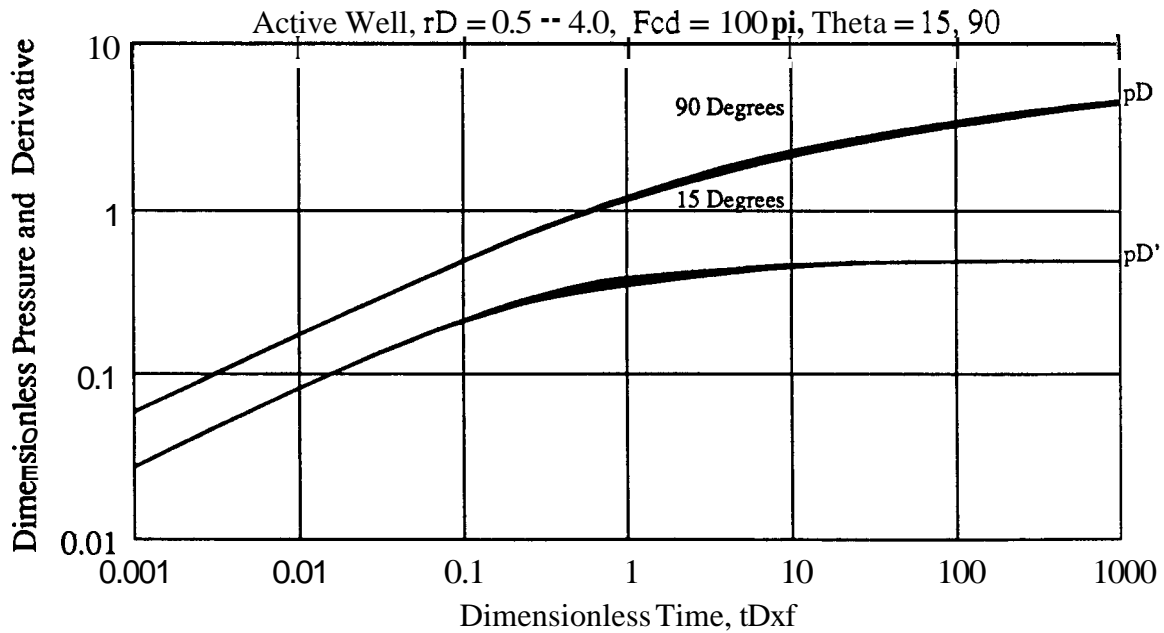


Figure 4.31: Active Well Solution, $\theta = 15$, $F_{CD} = 100\pi$

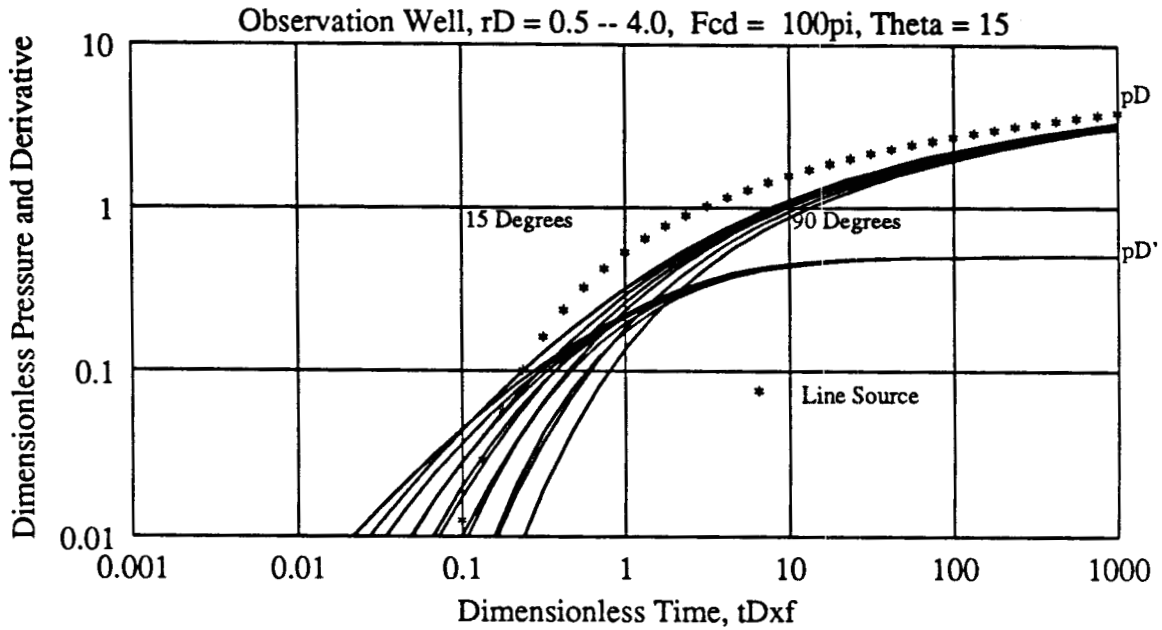


Figure 4.32: Observation Well Solution, $\theta = 15$, $F_{CD} = 100\pi$

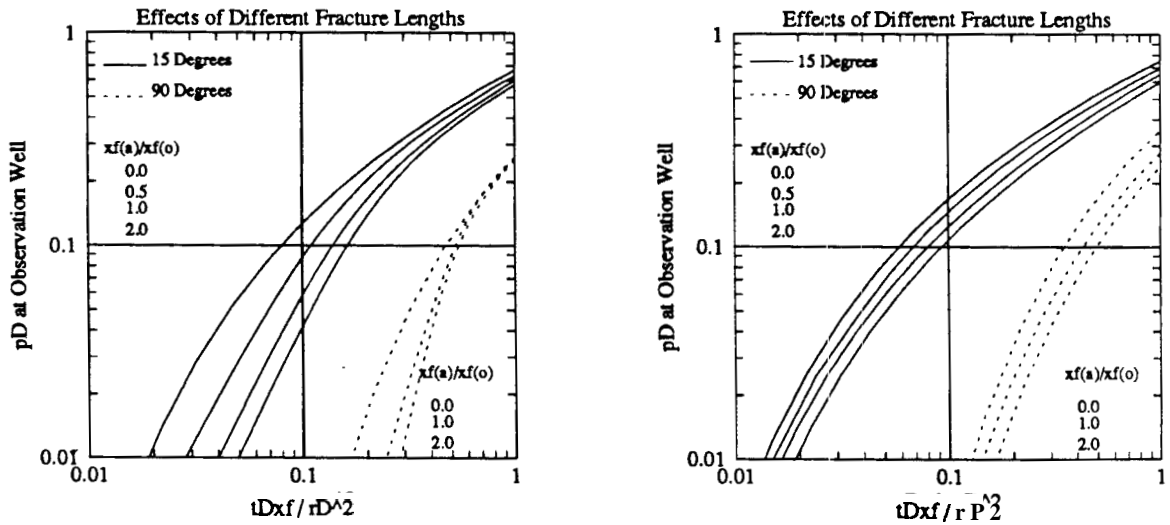


Figure 4.33: Effect of $\Lambda_{[AO]}$ on Observation Well Response, $F_{CD} = \pi, 100\pi$, $r_D = 0.8$

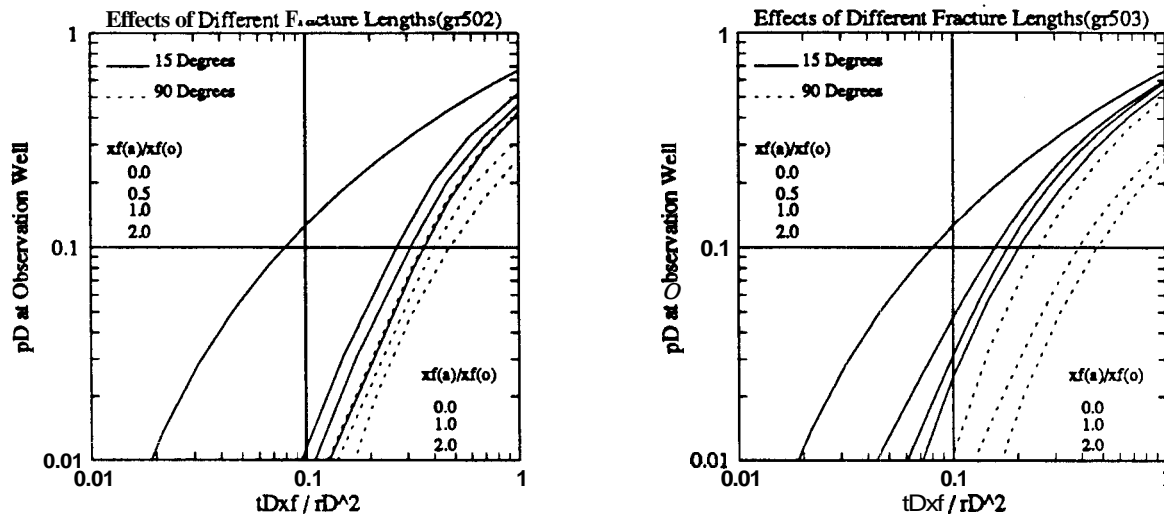


Figure 4.34: Effect of $\Lambda_{[AO]}$ on Observation Well Response, $F_{CD} = \pi, 100\pi, r_D = 3.0$

minimal, except at extremely early times. Observation well responses show negligible differences for varying values of $[k_f b_f]_{AO}$. It is therefore impossible to determine the value of F_{CD} for either well from interference testing. The active and observation wells value of F_{CD} and x_f must be determined by independent, active tests.

4.4.5 Interference With Two Active Wells

By altering the previous matrix formulation, the effects of both wells producing can be demonstrated. Of interest here is delineating when the fracture interference between the wells is of importance. Figures 4.39 and 4.40 compare the performance of two wells ($\theta = 15, 90$, and $r_D = 1$) with low dimensionless fracture conductivity with that of two line source wells. By using the effective wellbore radius of the pseudosteady state behavior at the line source well, similar results are obtained. Therefore, solutions for the finite conductivity hydraulically fractured well in a closed rectangular reservoir require only superposition of modified line source image wells.

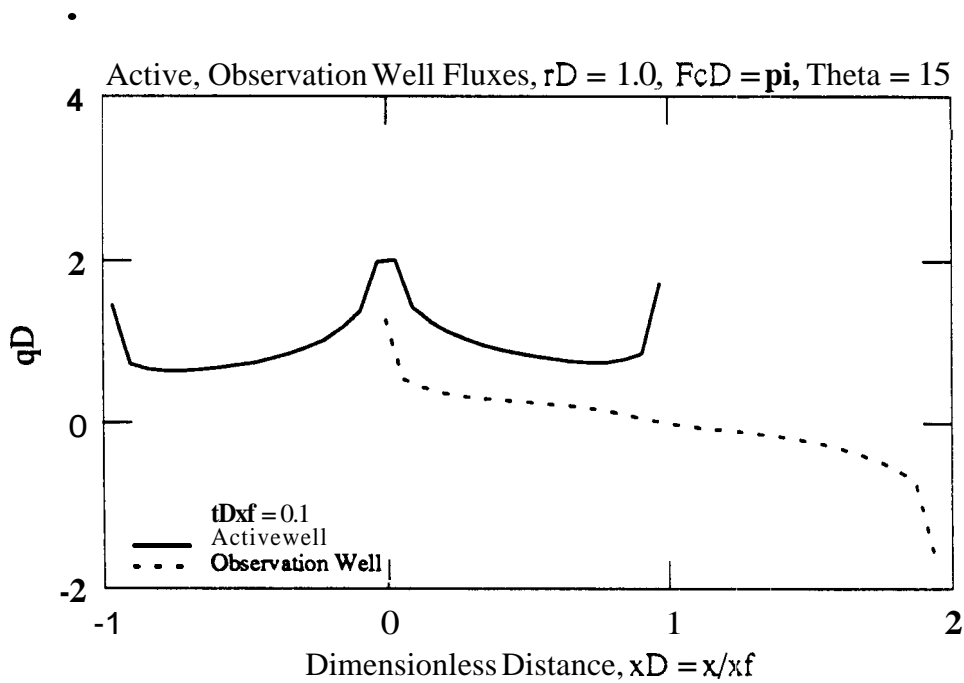


Figure 4.35: Active and Observation Well Fluxes at $t_{Dxf} = 0.1$, $F_{CD} = \pi$, $\theta = 15$, $r_D = 1.0$

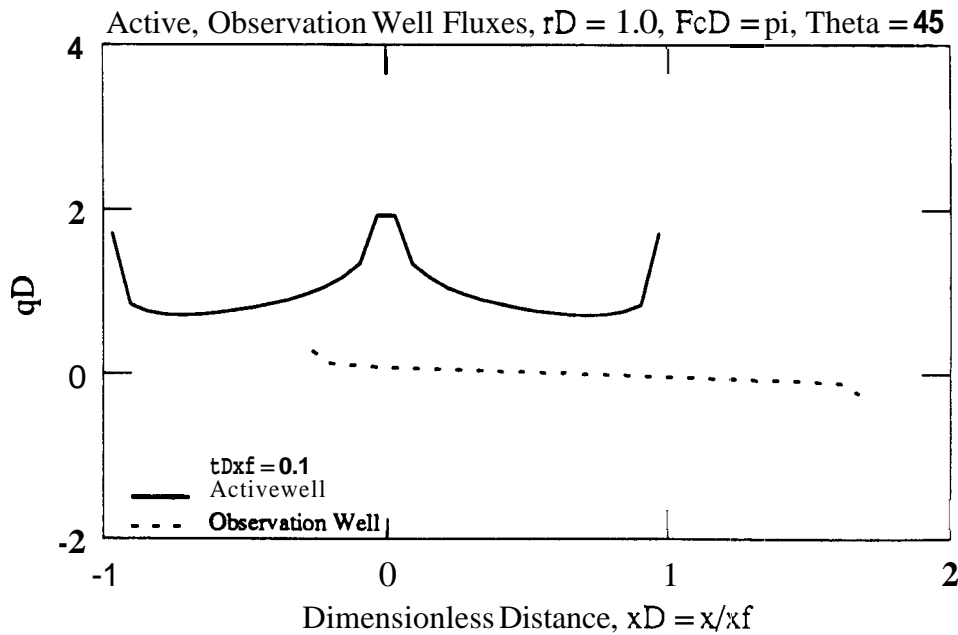


Figure 4.36: Active and Observation Well Fluxes at $t_{Dxf} = 0.1$, $F_{CD} = \pi$, $\theta = 45$, $r_D = 1.0$

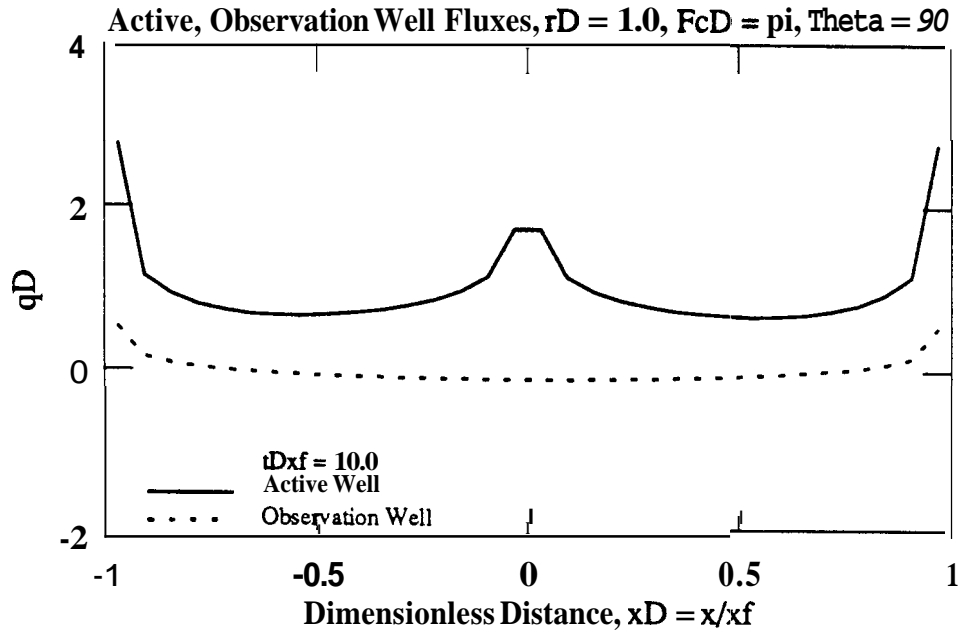


Figure 4.37: Active and Observation Well Fluxes at $t_{Dxf} = 10$, $F_{CD} = \pi$, $\theta = 90$, $r_D = 1.0$

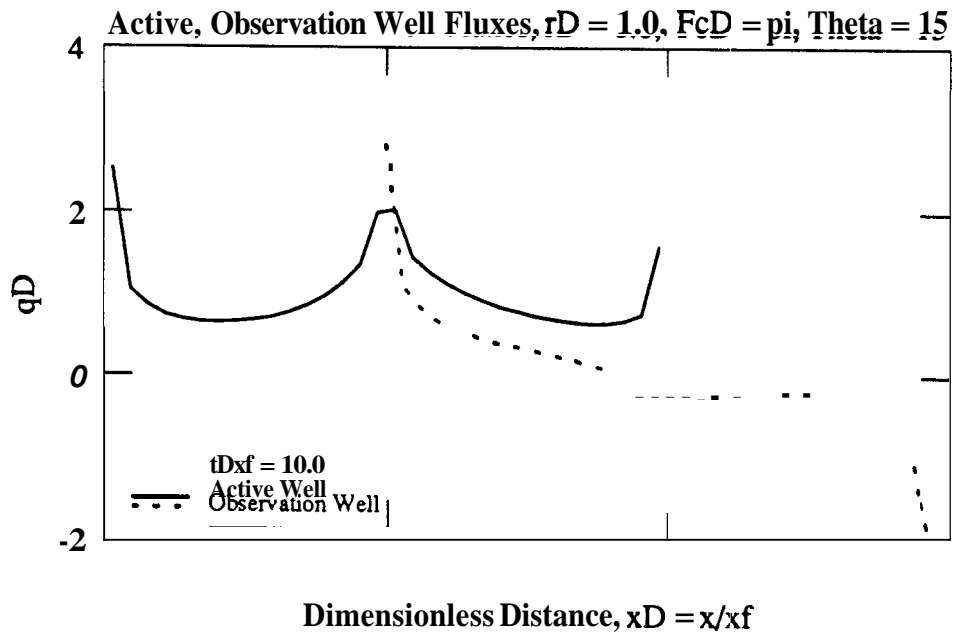


Figure 4.38: Active and Observation Well Fluxes at $t_{Dxf} = 10$, $F_{CD} = \pi$, $\theta = 15$, $r_D = 1.0$

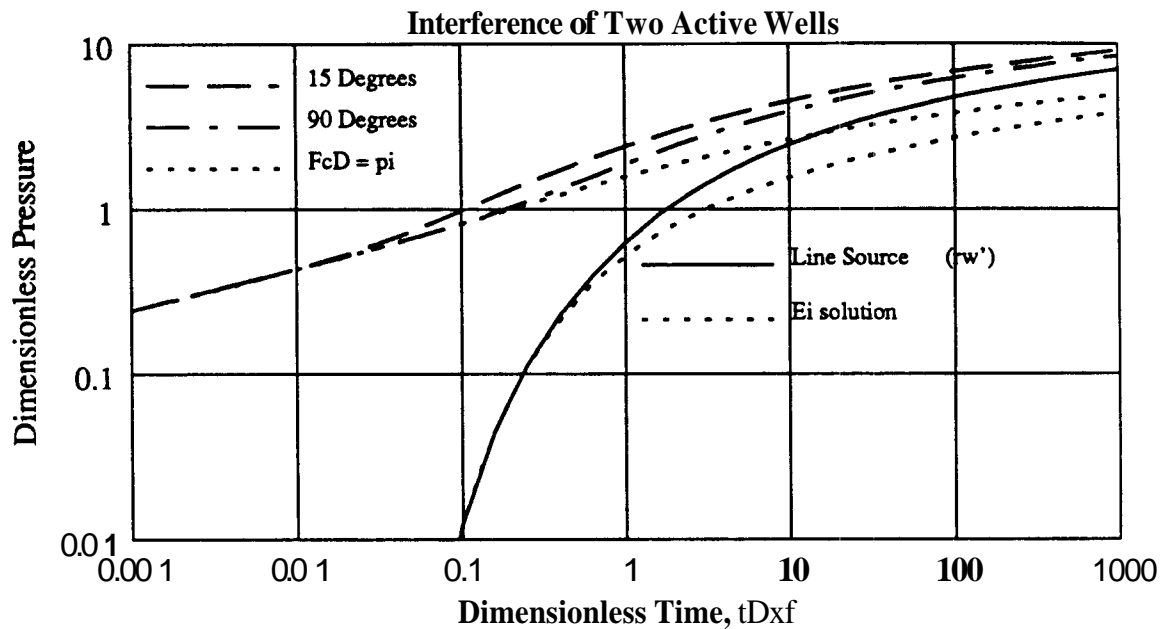


Figure 4.39: Active Well With Both Wells Producing, Low Conductivity Fractures and Line Source Wells, $r_D = 1.0$, $F_{CD} = \pi$, $\theta = 15, 90$

4.4.6 Interference With a Constant Pressure Active Well

Most interference tests are designed for constant rate behavior at the active well. Low permeability reservoirs may require weeks or months to obtain the desired reservoir information. In practice, maintaining constant flow rates for low permeability wells during that length of time is difficult. It is much easier to maintain constant surface flowing pressure. If pressure drops are large (as is the case for many low permeability wells), bottomhole pressure drops may vary slightly in time for constant values of surface flowing pressures. These variations are typically small for moderate flow rates.

4.5 Verification Comparisons, Example Problem

A series of validation runs were used to ensure the applicability of these new solutions over a wide range of values. Comparisons with published results for simpler cases and with simulation responses have been used. Results were good in all cases. Numerical simulation resulted in predicted behavior matching the semianalytical solution for a

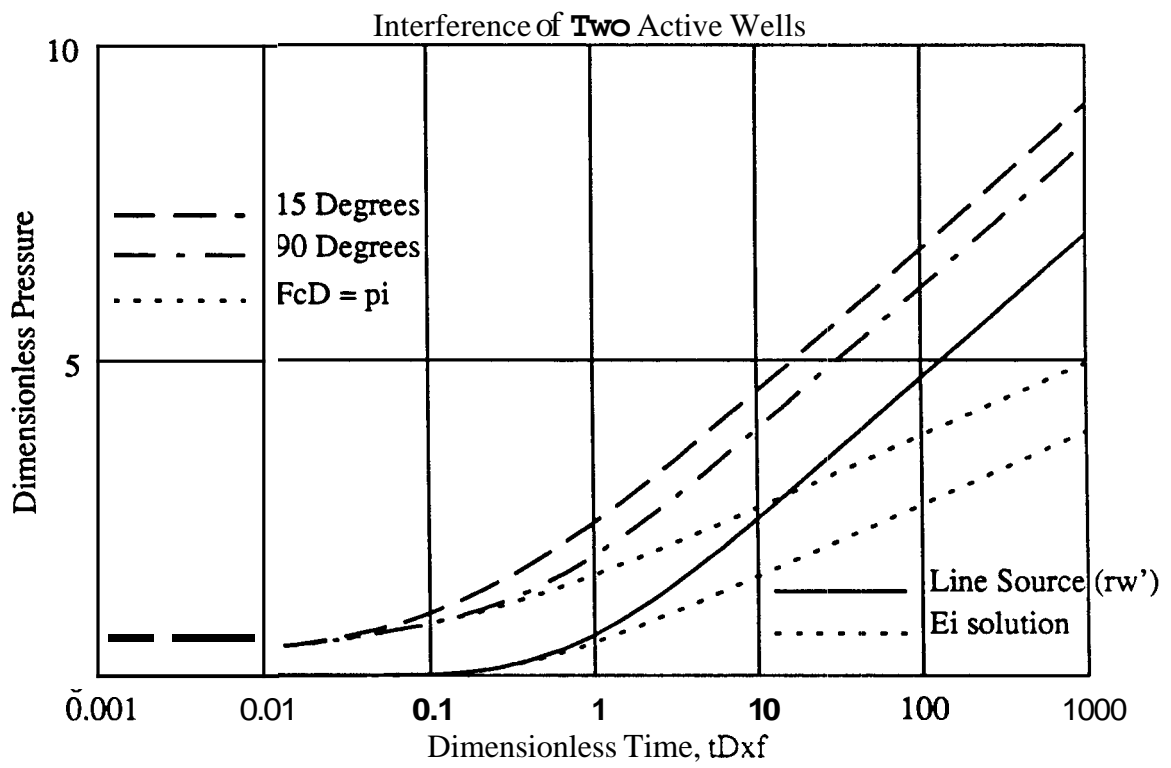


Figure 4.40: Active Well With Both Wells Producing, Low Conductivity Fractures and Line Source Wells, $r_D = 1.0$, $F_{cD} = \pi$, $\theta = 15, 90$

wide range of cases. In Figure 4.47, a low conductivity fracture in a bounded reservoir is placed on the type curve solution using the input values of permeability, fracture length, x_e/x_f , etc. The upward bend at late time is due to the closed boundaries; however, the agreement is good at early times.

The next series of figure illustrate the automated solutions using nonlinear regression from the commercial software package, **AUTOMATE 11**. The custom type curve feature of this package was used to find a ‘best fit’ to the models provided. The input data was simulated using $F_{CD} = \pi$, $\theta = 45$, and $r_D = 1$. Figures 4.48 and 4.49 are the results of matching the simulated interference data to the line source solution. This is the typical method of analyzing interference well tests. The data match reasonably well at late times, but do not match well at early times. Estimated reservoir parameters are in error by 10% for permeability and 18% for the $\phi c_i h$ product. No information is obtained about fracture azimuth from this type of analysis.

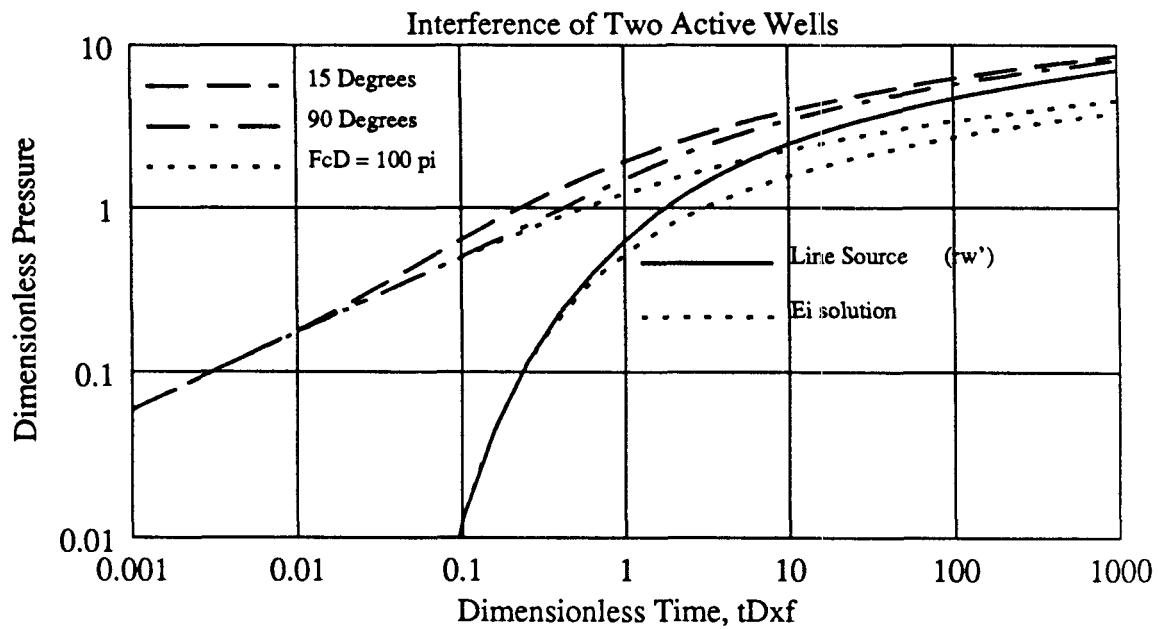


Figure 4.41: Active Well With Both Wells Producing, High Conductivity Fractures and Line Source Wells, $r_D = 1.0$, $F_{CD} = 100\pi$, $\theta = 15, 90$

Figure 4.50 shows Mousli *et al.*'s ¹⁸⁷ solution for $r_D = 1$ and $15 \leq \theta \leq 90$. In this solution, the active well is a uniform flux fracture, while the observation well has an

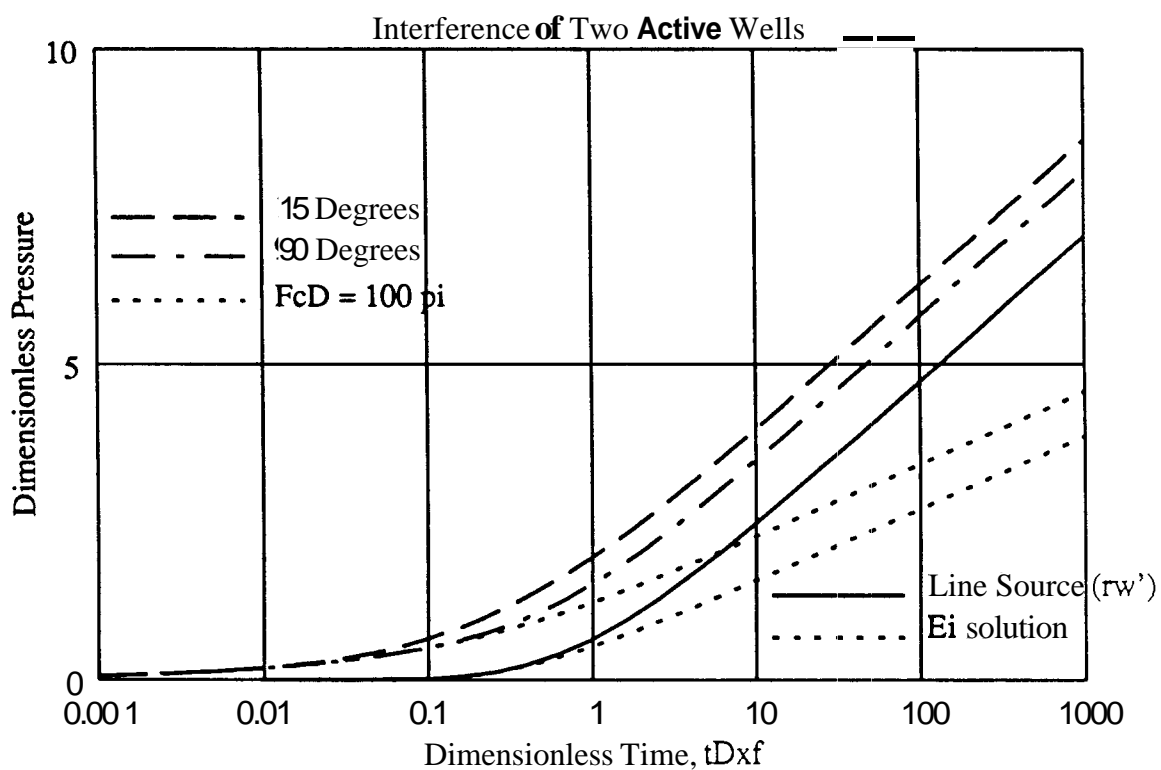


Figure 4.42: Active Well With Both Wells Producing, High Conductivity Fractures and Line Source Wells, $r_D = 1.0$, $F_{CD} = 100\pi$, $\theta = 15, 90$

infinite conductivity hydraulic fracture. The estimated error associated with the nonlinear regression is small ($\leq 5\%$ for k, θ , and $\phi c_i h$); however, these parameters are in error by 4%, 9%, and 21% respectively. The estimates for permeability and $\phi c_i h$ are fairly good. The fracture azimuth estimate by this technique is poor. Varying the initial estimated fracture azimuth did not alter the nonlinear regression estimate. Figure 4.51 and 4.52 illustrate the results for the model developed in this dissertation. Agreement is good, with the estimated values of k , $\phi c_i h$, and θ in error by $\leq 1\%$ for all three cases. Estimated fracture azimuth was 44.6° and was independent of the initial parameter estimates. An additional simulation model with $\theta = 15$ resulted in an estimated fracture azimuth of 18° .

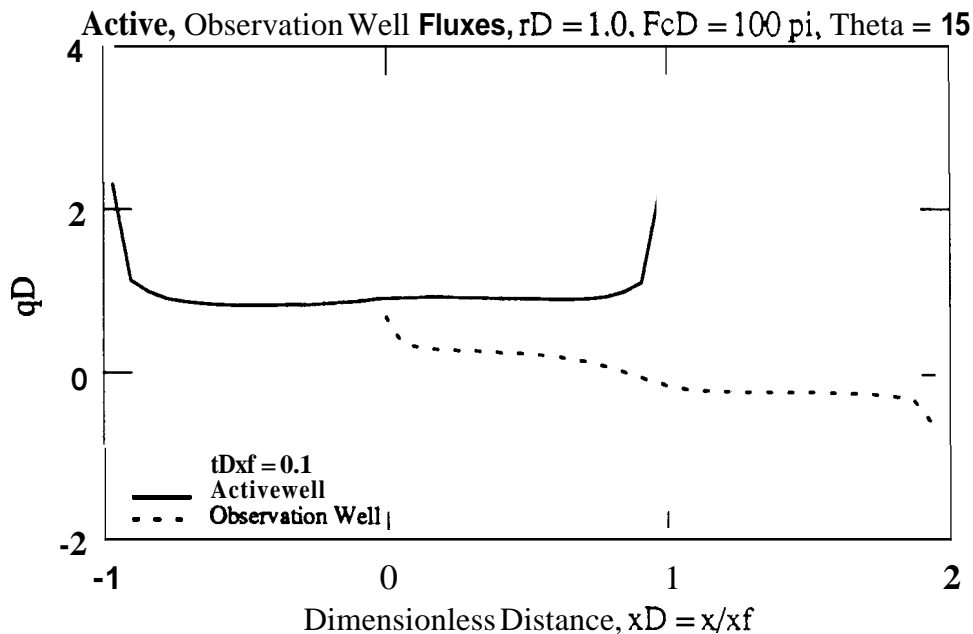


Figure 4.43: Active and Observation Well Fluxes at $t_{Dxf} = 0.1$, $F_{CD} = 100\pi$, $\theta = 15$, $r_D = 1.0$

4.6 Early Behavior

Observation well responses have been plotted as a function of t_{Dxf}/r_D^2 where r_D is the distance between the wellbores of the active and observation well scaled by the

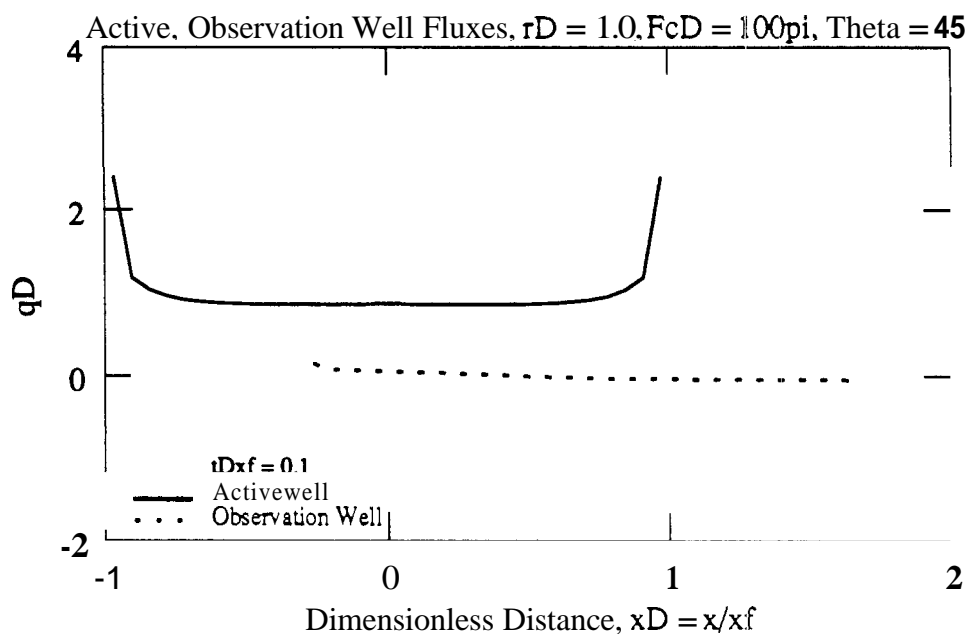


Figure 4.44: Active and Observation Well Fluxes at $t_{Dxf} = 0.1, F_{CD} = 100\pi, \theta = 45, r_D = 1.0$

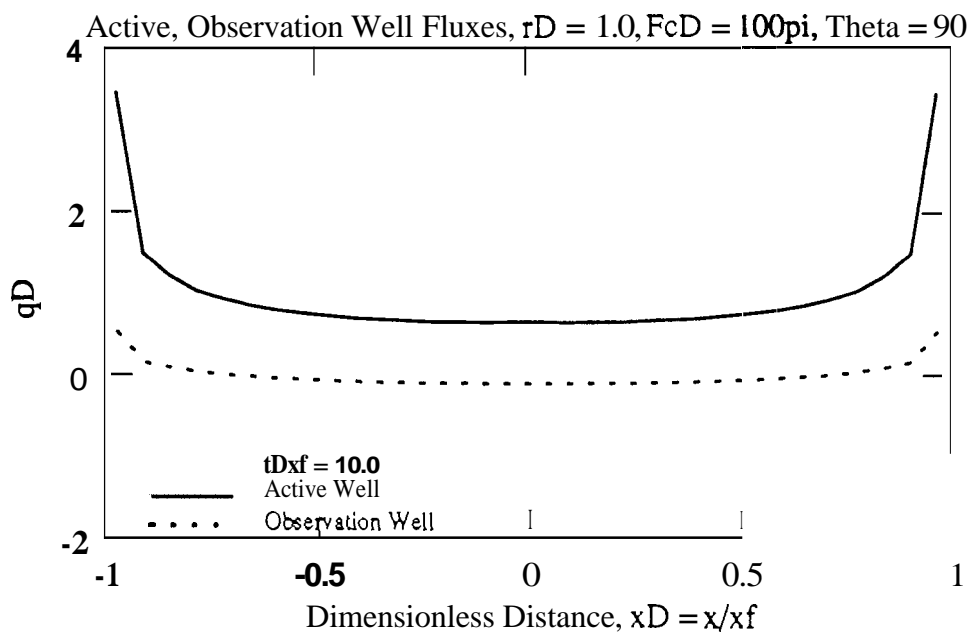


Figure 4.45: Active and Observation Well Fluxes at $t_{Dxf} = 10, F_{CD} = 100\pi, \theta = 90, r_D = 1.0$

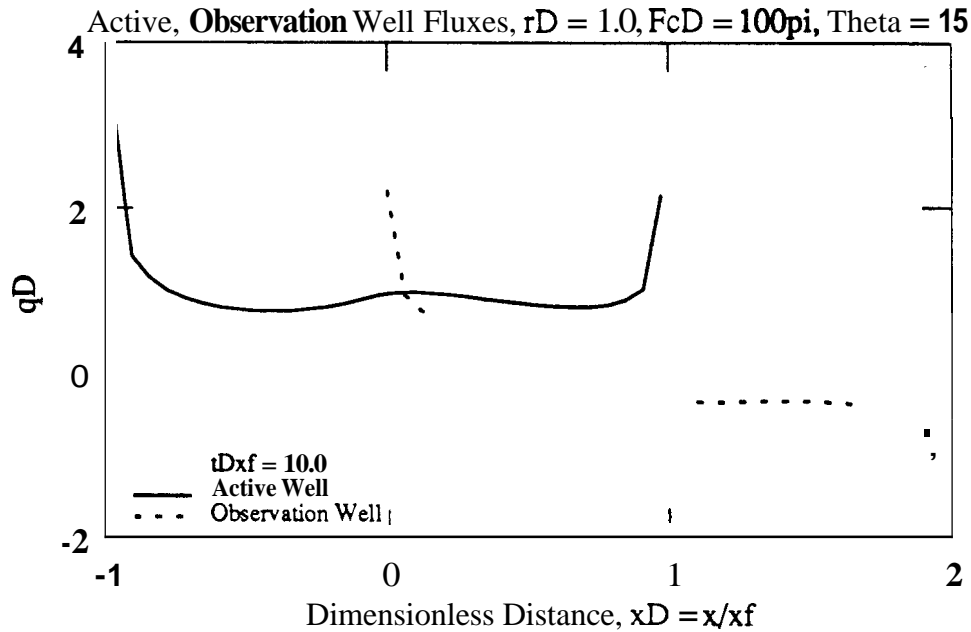


Figure 4.46: Active and Observation Well Fluxes at $t_{Dxf} = 10, F_{CD} = 100\pi, \theta = 15, r_D = 1.0$

active well fracture length. Other plotting functions were investigated for the time and pressure axes. None of them were completely successful in collapsing all of the responses. Approximate reductions are obtained for either early or late times.

Figure 4.53 is the observation well response for $r_D = 0.8$ for $15 \leq \theta \leq 90$ with the dimensionless pressure (p_D) and dimensionless pressure derivative group (p'_D) plotted as a function of t_{Dxf}/r_D^2 . The curves tend to collapse at late times; none of the curves matches the E_s solution exactly. All derivatives reach a value of 0.5 (corresponding with pseudo radial flow) at approximately the same value of t_{Dxf}/r_D^2 . Figure 4.54 shows shifted and scaled pressure and time data. Dimensionless pressure is rescaled as:

$$p_D^* = p_D \frac{r_D}{d_D} \tag{4.25}$$

where d_D is the vertical distance (normal to the fracture direction) as defined in Figure 4.12. Dimensionless time t_{Dxf} is divided by d_D rather than by r_D .

This rescaling and reshifting also works for different values of $(k_f b_f)_D$ and $\Lambda_{[AO]}$. Unfortunately, it is impractical for test analysis since the desired parameter, fracture

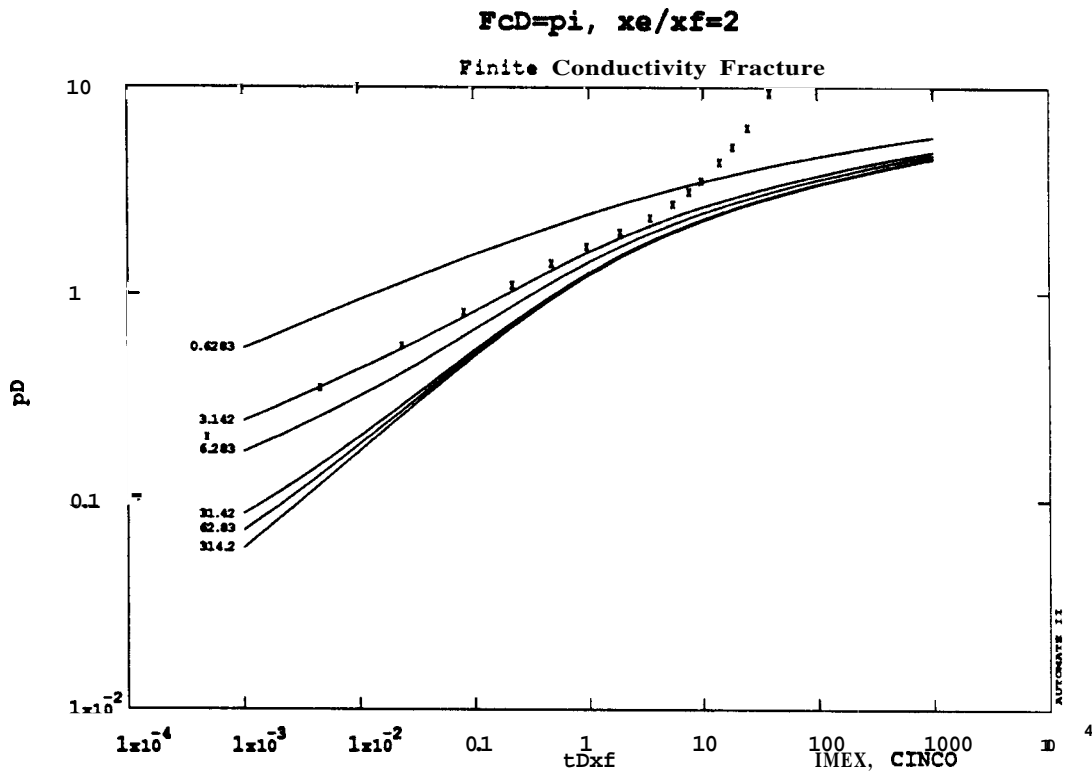


Figure 4.47: Comparison of Simulated Response With Analytic Results, $F_{CD} = \pi$

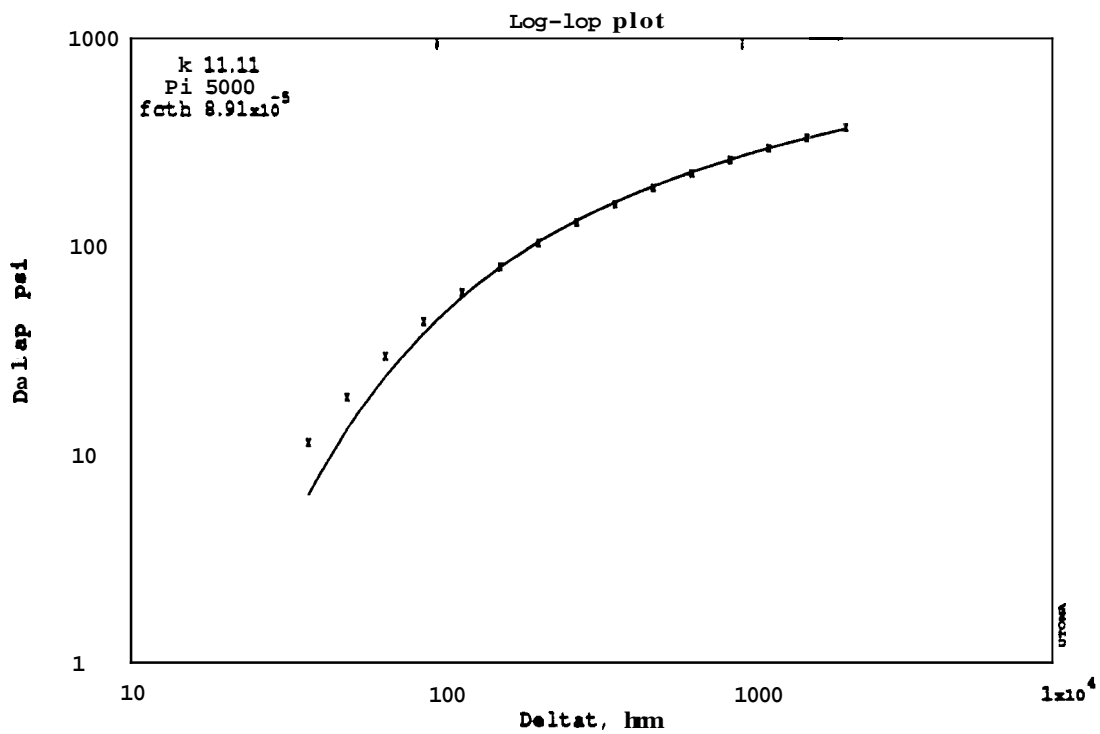


Figure 4.48: Analysis of Simulated Interference Test Using Line Source Solution

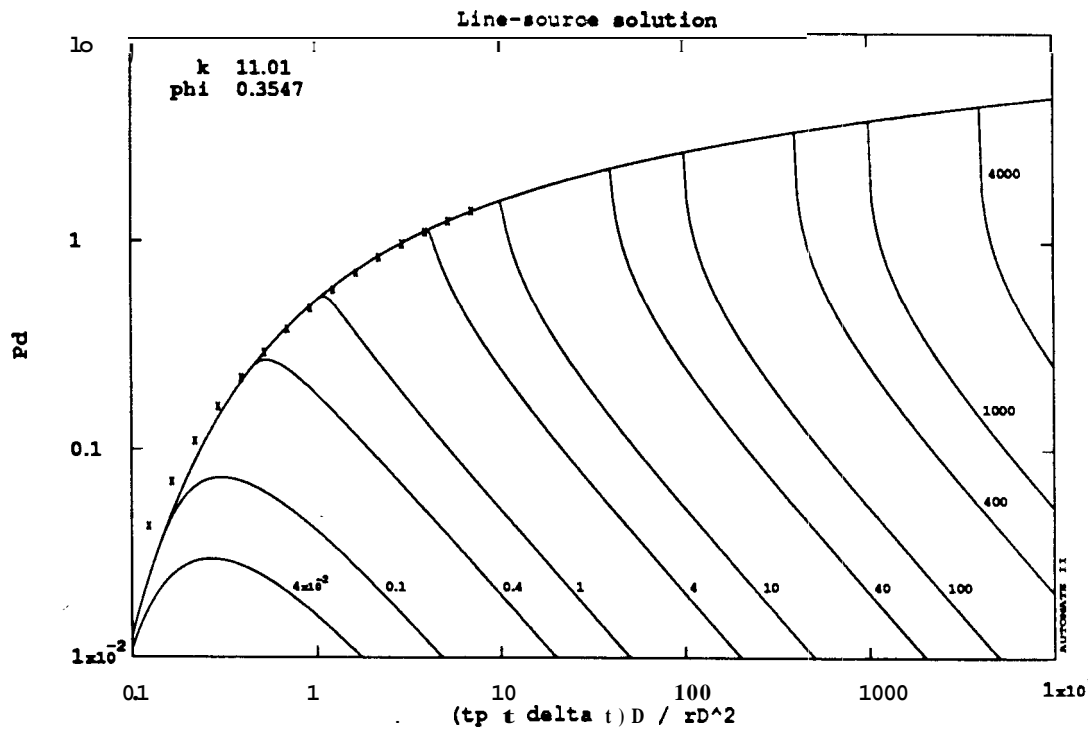


Figure 4.49: Log-Log Plot of Simulated Interference Test Using Line Source Solution

azimuth (θ) appears in both axes. However, Figure 4.54 and this shift is relevant for test design and understanding. If an estimated azimuth can be obtained *a priori* by another method, the type of plot given as Figure 4.54 indicates a minimum test design to differentiate fracture behavior. As an example, for the parameters given in Table 4.1, an unacceptably long test may be required.

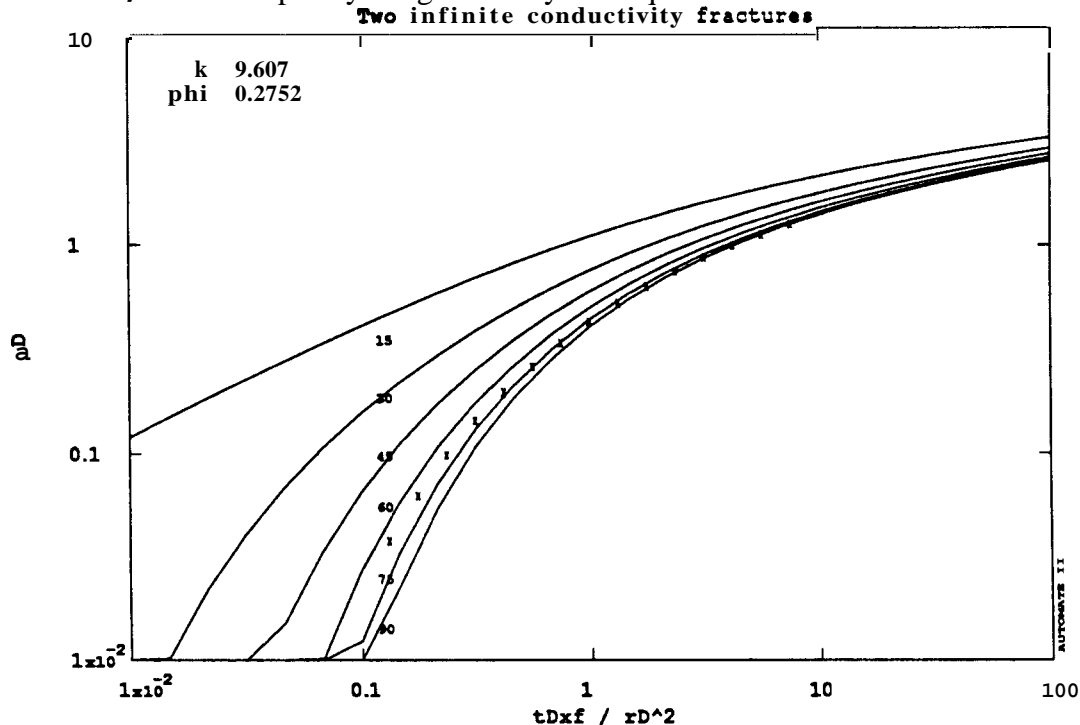


Figure 4.50: Analysis of Simulated Interference Test Using Mousli *et al.*'s Solution

Other typical PVT properties were used to calculate dimensionless parameters, resulting in an estimated test duration of 350 days to differentiate to within 10% of the values of the curves shown for 15 and 45°. Considering the effects of reservoir heterogeneities, it is unlikely that such tests will be practical for very low permeability reservoirs.

4.7 Chapter Summary

In this chapter, the topic of pressure interference between two hydraulically fractured wells has been discussed. Laplace space models were developed for two problems that

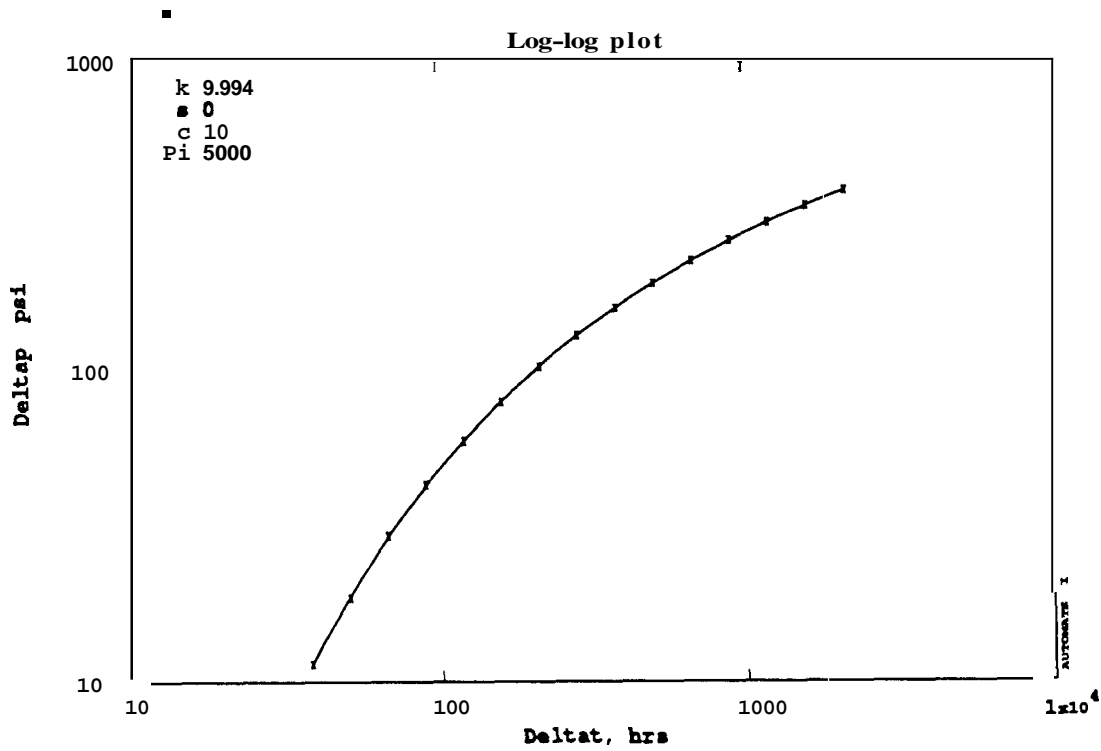


Figure 4.51: Analysis of Simulated Interference Test Using Semianalytic Solution

Table 4.1: Example Design Data

Permeability	0.01	md
Thickness	40	feet
Gas Gravity	0.60	
Porosity	15	%
Flow Rate	1000	Mcf/Day
Fracture length	1000	feet (both wells)
Fracture Conductivity	2000	Dimensionless
Fracture Azimuth	30	Degrees
Interwell distance	800	feet

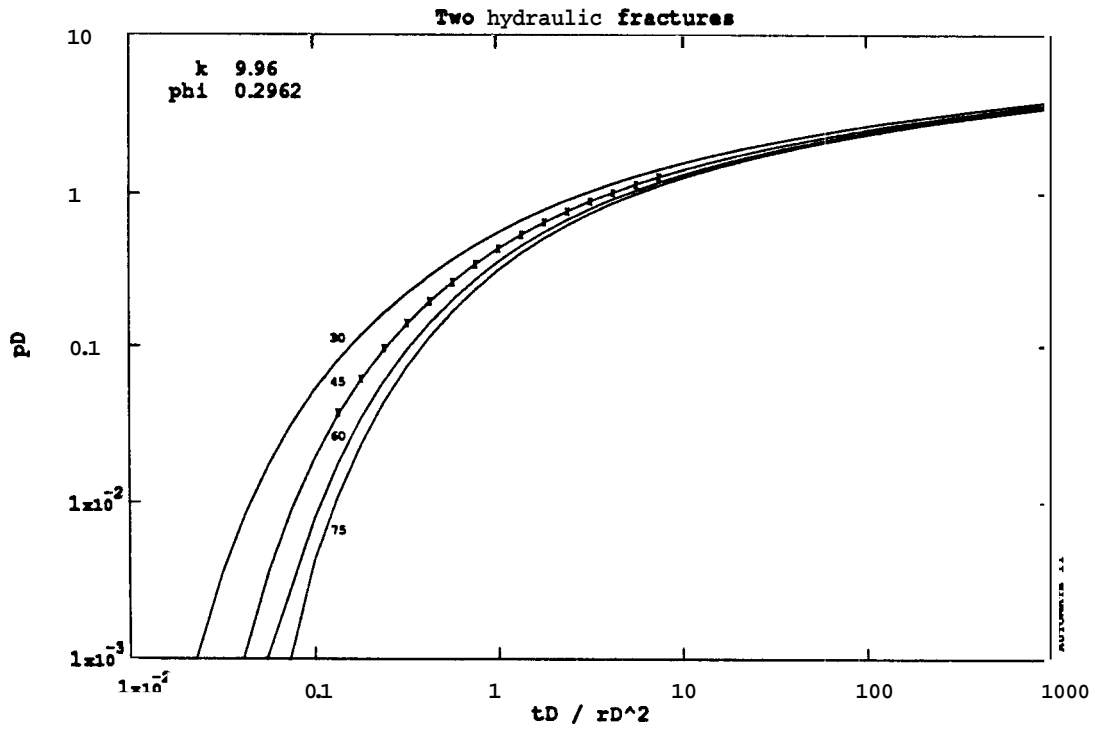


Figure 4.52: Log-Log Plot of Simulated Interference Test Using Semianalytic Solution

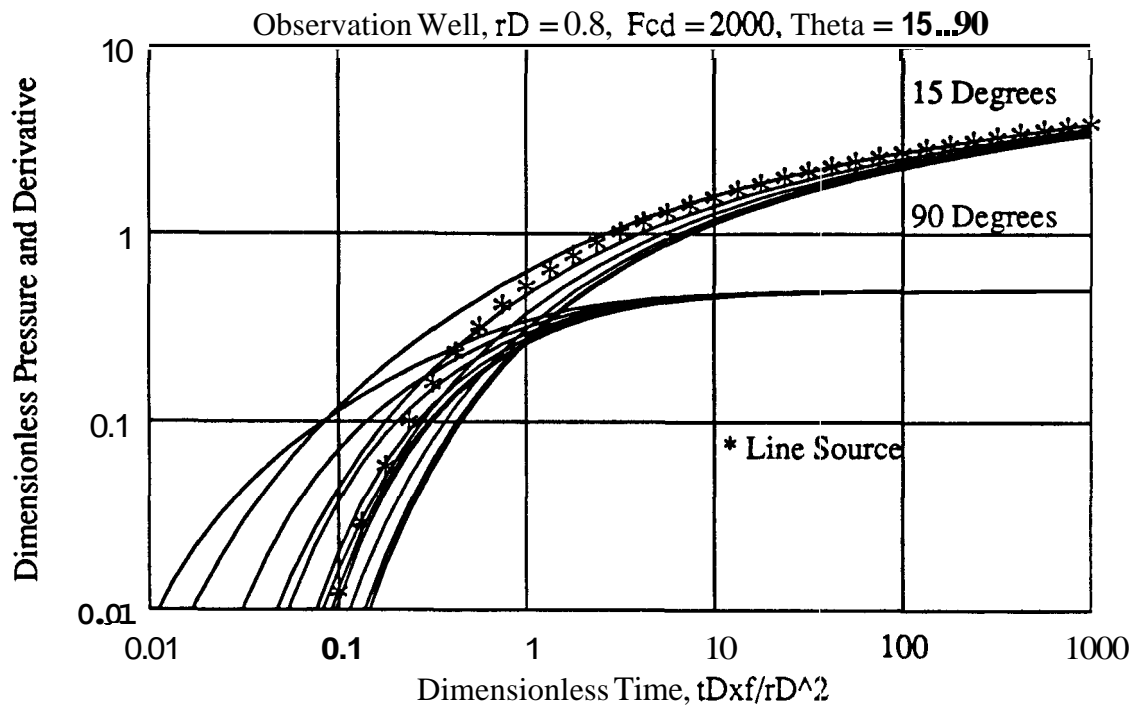


Figure 4.53: Observation Well Response, $r_D = 0.8$

had been previously solved in real space; these are:

1. interference at an unfractured well **near** an infinite conductivity fracture, such as a nearby joint, and
2. observation response at an infinite conductivity hydraulically fractured well due to either an active line source well or a well with a uniform flux fracture.

Both of these models were extended to finite conductivity fractures. None of these models required flux distributions to be calculated at more than one well. An additional new Laplace space solution was developed for the interaction of two finite conductivity hydraulically fractured wells, requiring simultaneous solution of the fluxes at both wells. The sensitivity to changing interwell distance and different fracture lengths and conductivities was demonstrated. Characteristic behavior of the solution was discussed and correlating parameters for early time were introduced.

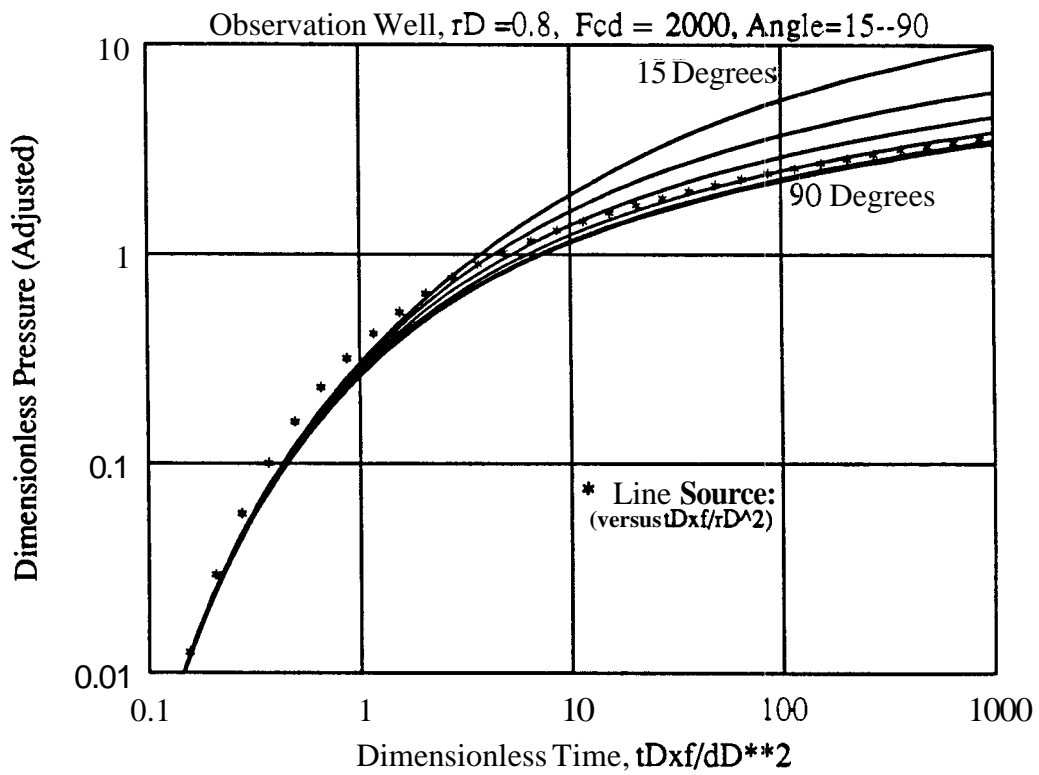


Figure 4.54: Rescaled Pressure Data (p_D^*) as a Function of t_{Dxf}/d_D^2

These solutions will be used in Chapter 5 for evaluating the effects of variations in fracture azimuth on economic results. They will also be used in Chapter 6 to compare interference response in heterogeneous reservoirs to the behavior of the idealized homogeneous case.

Chapter 5

Economic Optimization

Historical methodology and its pitfalls. Use of Net Present Value criteria for parametric studies. Typical approximations and economic assumptions. Development of a fracture model for a hydraulically fractured well in an anisotropic closed system. Drainage boundaries are not restricted to rectangles. An example case.

Optimization of reservoir development has long been documented as an activity of monetary worth, but fraught with **risks**. When a field is discovered, development proceeds at a pace dictated by the relative economic attractiveness of development wells, the extent of field delineation, anticipated prices, market for hydrocarbons (especially for gas production), competitive force, and regulatory requirements. For gas fields, the basic principles of optimizing development were laid down by van Dam ⁶⁴ in his 1968 paper. Reserve estimation, reservoir performance, extent of aquifer support, inflow performance, well spacing, tubing performance, and economic calculations remain the fundamentals.

When low permeability gas reservoirs are involved, many of these items are less critical, i.e. early drainage by offset wells and strong water drives are not common. Initial well spacing is often set by regulatory bodies at fairly wide spacings; however, most of these fields will ultimately require closer well spacing by future drilling.

5.1 Historical Methodology

Well spacing, hydraulic fracture lengths and conductivities are the chief parameters over which an operator has *some* control. Fracture lengths and conductivities are also large costs with respect to well drilling costs. Results from extremely large hydraulic fracture treatments have encouraged operators to attempt even greater fracture lengths. Holditch *et al*¹¹⁵ presented an early paper addressing overt optimization of fracture length and well spacing. Holditch *et al.* combined a fracture simulation program with a simple uniform flux solution, linking the two with an economics model. This study did not actually optimize results *per se*, but restrained well spacings to those typically used in fields of interest, e.g. 160, 320, and 640-acres/well. In all of these cases, 160-acre fracture lengths extend only to 1320 feet, the maximum obtainable for $\theta = 0$ in a well in the center of a closed square. Similarly, the 320-acre case is limited to $x_f = 1867$. In several of their curves, net present value (NPV) continues to increase *as* a function of increasing x_f . Knowledge of fracture azimuth and larger fracture lengths could enable increased NPV.

Holditch *et al.* estimated job costs *as* nearly linear with volume of fracturing fluid pumped. While it is true that materials costs increase linearly with volume, costs increase at a higher *rate as* a function of fracture length. The simplified model used by Holditch *et al.* did not directly include sand transport, fracturing out of zone, etc. More sophisticated models represent costs with a power model relating to fracture length⁷⁷, (Equation 5.2).

Holditch *et al.* concludes that formation permeability and gas-in-place per acre were the most significant factors determining optimum fracture length, and that longer fractures and shorter well spacings were dictated by decreasing permeabilities. Unfortunately, simple transient *flow* models completely neglect fracture azimuth. Additionally, optimization results often indicate optimal well spacings either smaller or larger than physically reasonable ranges.

Lemon *et al*¹⁴⁷ used numerical simulation to determine the effects of fracture length and azimuth on production. They conclude that fracture azimuth was 'critical' for spacings below 320-acre; however, they made fairly arbitrary assignments of

drainage shapes to determine the effects of fracture azimuth. Their 2:1 rectangles with a fracture centered in the block parallel to one of the major or **minor** axes can alternatively be interpreted representing the effects of permeability anisotropy. They conclude that fracturing normal to the direction of maximum permeability was far superior to the other case that is, in fact, the most likely.

Tison *et al* ²⁴⁷ presented results of a study in the East Texas Cotton Valley play in which simulation was used to estimate the performance of infill drilling locations. Their study neglected fracture azimuth, basically assuming that it was known; however, they approximated results for the best and worst fracture azimuth cases with their simulations. They modeled the infill well by arbitrarily imposing a no-flow boundary parallel with the fractures and half-way between the wells. One questionable conclusion was the importance they attach to static pressure measurements for the initial infill wells. It is particularly difficult to measure the initial pressure for such wells in low permeability reservoirs ¹⁸² and most errors will be in the direction of underestimating the initial pressure. For multiple layer reservoirs like the Cotton Valley which have different initial pressures and permeabilities by layer, the results can be even more difficult to obtain.

5.1.1 Waterflooding and EOR; Historical Efforts

Early researchers realized that hydraulic fractures alter flowlines, pressure drops, and sweep efficiency in waterfloods. Crawford and Collins ⁶¹ studied line drive patterns with a potentiometric model showing effects of both azimuth and fracture length. Unfavorable azimuths were found to do more harm to recovery than favorable ones improve recovery. Dyes *et al* ⁷³ used X-ray shadowgraphs for five-spot patterns with fractures oriented in the best and worst possible directions at either the injectors or the producers. Hartsock ¹³¹ used a similar model to investigate the developed five-spot; Hansford ¹⁰⁵ and Donohue *et al* ⁷² investigated the cases where all wells were fractured in a five-spot pattern. This latter work combined potentiometric models with numerical simulation and investigated varying angles for fracture azimuth. Potentiometric models essentially 'solve' the steady-state unit mobility case (where $\frac{dP}{dt}$

is zero). For low-permeability cases, the transient flow period may be a substantial fraction of the well's life and dominating economic results. A further limitation of these analog studies is their emphasis on sweep efficiency at breakthrough.

Donohue *et al* reported equipotential distributions and **isopotentials** which are directly comparable to their pseudosteady state counterparts calculated analytically in this study. Their conclusion was that for values of x_e/x_f greater than about 4.0, fracture azimuth is relatively unimportant. Their results for calculated and experimental isopotentials demonstrate the areal efficiency at breakthrough as a function of the angle of orientation and fracture length. These results show a more dramatic impact of fracture azimuth than those obtained for single phase depletion in this study.

5.2 Value of Knowing Fracture Azimuth

Sensitivity to errors in fracture azimuth is substantial for certain applications. For uniform flux fractures with fracture lengths less than the well spacings, azimuth appears to be virtually irrelevant. For finite conductivity wells, interference can be more pronounced; however, errors in estimating fracture azimuth of less than 15° have minimal impact, except for interference tests. The economic value of knowing fracture azimuth is most pronounced when fracture azimuth is used to select well locations in very low permeability or highly anisotropic reservoirs.

Benefits from large expenditures to determine fracture azimuth for tight gas reservoirs appear to be unjustified. Relatively simple techniques based on borehole eccentricity measurements from conventional dipmeter logs or acoustic borehole viewers can provide answers to the desired degree of accuracy when stable hole conditions prevail. All near well methods and many indirect methods fail, for extremely rugose, or washed out holes. Large scale geophysical techniques such as TABS, interwell VSP, and cross hole tomography may provide valuable reservoir characterization information, or improve fracture mapping capability. However, marginal improvement in azimuth resolution does not necessarily improve reservoir management decisions. Some of these efforts are aimed towards finding fracture length and height; these are likely

to yield only the created and not the propped, or effective lengths.

The value of knowing fracture length increases when considerable flexibility in well spacing is available. It is possible to place increased numbers of wells in the direction normal to the direction of propagation for the fractures. Numerical examples of this value are given in Section 5.4.2. Elbel⁸⁰ discussed this approach and provided an analytic approximation that depends critically on knowing fracture azimuth. It also neglects the relationship of fracture costs to increased lengths, permeability anisotropy, and fracture conductivity. The economic procedure developed here includes fracture azimuth, permeability anisotropy, and can be coupled to pertinent cost models.

5.3 Economics

Forecasts of p_D as a function of $t_{D,f}$ immediately translate into pressure responses versus time when the appropriate reservoir parameters (permeability, viscosity, porosity, thickness, fracture length, etc.) are specified. For gas wells, the nonlinear behavior of the fluid properties requires the introduction of the real gas pseudopressure, $\Psi(p)$ ⁵, also known as the real gas potential. It is defined as:

$$\Psi(p) = \int_{p_b}^p \frac{2p}{\mu z} dp \quad (5.1)$$

Dimensionless variables can be readily redefined to reflect the use of pseudopressure.

Similarly, constant pressure performance can be obtained by calculating a continuously varying rate which maintains a constant pressure at the well. This can be done either by use of the convolution integral or by taking the Laplace transform of the constant rate solution and converting it to a constant pressure solution (Section 3.6.1).

For a set of reservoir parameters, well spacing, fracture azimuths, permeability anisotropies, etc., one can generate a forecast of rate and cumulative production given arbitrary sets of production constraints. Two of the simplest are:

1. Constant pressure production—Produce whatever the well will make, subject only to a specified flowing bottom hole pressure. This approximates uncurtailed field practices with constant surface pressures.

2. Curtailed production— Production rates are restricted to a given maximum value until the well is no longer able to produce that rate given the well's flowing pressure. Subsequently, the well will change to constant pressure production.

Both production constraints terminate when a minimum flow rate at the final flowing surface pressure is obtained. The minimum flowing pressure is determined by line pressure and the economic attractiveness of compression. The minimum rate (economic limit) is a function of marginal well operating costs. Field wide minimum rates exceed the sum of individual well economic limits.

Reasons for rate constraints include regulatory requirements such as allowables, lack of market, prevention of coning of water, and the presence of moveable fines. Mechanical effects which may serve as rate constraints include limited production facilities, tubing friction, or critical (sonic) pressure drops in the flow system.

A flow rate forecast can be translated to net cash flows (NCF) by convolving the rates with (escalating) prices, subtracting operating expenses, and discounting. After subtracting total initial well costs, a Net Present Value (NPV) of cash flows is determined for a specific fracture length and drainage area.

The NPV per acre and Q_f (ultimate recovery) can be determined for any specific set of economic and technical parameters. These can be optimized and the optimum values correlated. Several economic and timing assumptions are utilized for these examples, including:

- Cash flows and NPV calculations are done on a before Federal Income Tax (BFIT) basis. Operating expenses are presumed to be separable into two types, a variable (\$/Mcf or \$/BOE) and a fixed (\$/Month) component.
- Well costs are approximated as

$$\$COST = A + Bx_f^n \quad (5.2)$$

The value of A is the well cost plus any fixed costs associated with the fracturing of the well. B and n are a coefficient and exponent used to estimate fracture costs as a function of fracture length, x_f and must be estimated over the range

of fracture length in the specific application. The exponent n has a minimum value of 1.0 for the case in which fracture length is directly proportional to fluid volume. For almost all cases, an increase in total job size does not give a proportionate increase in propped fracture length. Additionally, larger jobs generally require increased pump horsepower. Maximum pump horsepower required is a large part of the fracturing cost. In general, values of n will be greater than unity. The procedure described by Meng and Brown¹⁸⁵ and in Chapter 8 of Economides and Nolte⁷⁷ provides details of cost/length/conductivity calculations. More complex cost models may be used in practice.

- o Constant wellbore pressure is used as a first approximation for operating conditions with additional consideration of the sensitivities to critical flow constraints, periods of constant production prior to constant pressure rate decline, and constant surface pressure. Effects of ‘turbulence’ and two-phase flow are not included in this work.
- o Effects of permeability anisotropies are investigated both in the analytic solutions and on optimal well spacing and fracture length. Economic value of ascertaining the magnitude of permeability anisotropy is shown to be significant.
- o Similarly, sensitivities for irregular lengths of boundaries can be obtained.
- o Economic optimization is also used later in Section 6.4.5 to show the effects on optimum well spacing and fracture length for heterogeneous reservoirs.

5.4 Example Economics

This subsection is devoted to example calculations which illustrate the process of optimization of fracture length as well as well spacing. One example will include the effects of knowing fracture azimuth on the optimum NPV. The effects of permeability anisotropy are included in the third example.

5.4.1 Optimizing Spacing and Fracture Length

For this example case, the parameters from Table 5.1 are inputs for the optimization process. Spacing limitation requirements exist in most states; these rules limit the number of wells and allowable production rates as well as the locations. Economic optimization will generally result in locations and spacing which is different than a *priori* state regulations. Many of these regulations can be revised; alternatively, economic optimization can be performed subject to additional constraints. This example optimizes both fracture length and well spacing subject to constraints typical for U.S. well spacing, i.e. 80, 160, 320, and 640-acre alternatives. No rate constraints are used. It is assumed that all wells are drilled at the same time and that the reservoir is very large and homogeneous.

The procedure is to select a well spacing and fracture length, determine the costs, make the production forecast based on constant pressure production, calculate the economics and NPV for the case, and then change the fracture length. Starting with small fracture lengths, the NPV will increase to a maximum and decrease as diminishing returns are obtained for more costly (per foot) fractures. The next spacing is then selected. Comparisons are made on the NPV per acre. All negative NPV values indicate uneconomic values. The optimum spacing and fracture length are determined from the results of these studies.

Figures 5.1–5.3 show both the total NPV and NPV per acre for Case 1. For Figures 5.1 and 5.2, a range of well spacings starting at 40 acres and increasing by 80 acre increments was used. A range of fracture lengths of 100–900 feet was selected for the ‘first pass’ using technical data as shown in Table 5.1. Figure 5.1 is the absolute NPV at 10% for each case, while Fig. 5.2 is the NPVIO per acre. The highest NPV for this case was for the 200-acre case at a fracture length of approximately 300 feet. The graph of NPV obviously increases for larger drainage areas, representing the NPV of a single well. Maximizing economic value for an entire field requires optimizing NPV per acre.

Further refinements using 10 acre increments result in an optimum value of x_f of 300 feet and well spacing of 160 acres. It is possible to optimize NPVIO with respect

Table 5.1: Input Data For Optimization

<i>TECHNICAL DATA</i>	<i>Initial Value</i>	<i>Units</i>
Permeability	0.1	md
Porosity	10	%
Thickness	30	feet
Water Saturation	30	%
Initial Pressure	5000	psi
Flowing Bottom Hole Pressure	800	psi
Reservoir Temperature	200	°F
Viscosity	0.02	cp
Total Compressibility	0.00014	<i>psi⁻¹</i>
Ratio of k_x to k_{r1}	1.0	
<i>ECONOMIC DATA</i>		
Discount Rate	10	%
Well Costs (without frac)	500,000	\$
Frac Costs	$0.8 \cdot x_f^2$	\$
Annual Operating Expenses	2.5	% of capital costs
Escalation Rates	5	% per year
Initial Net Gas Price	1.50	\$ /Mcf

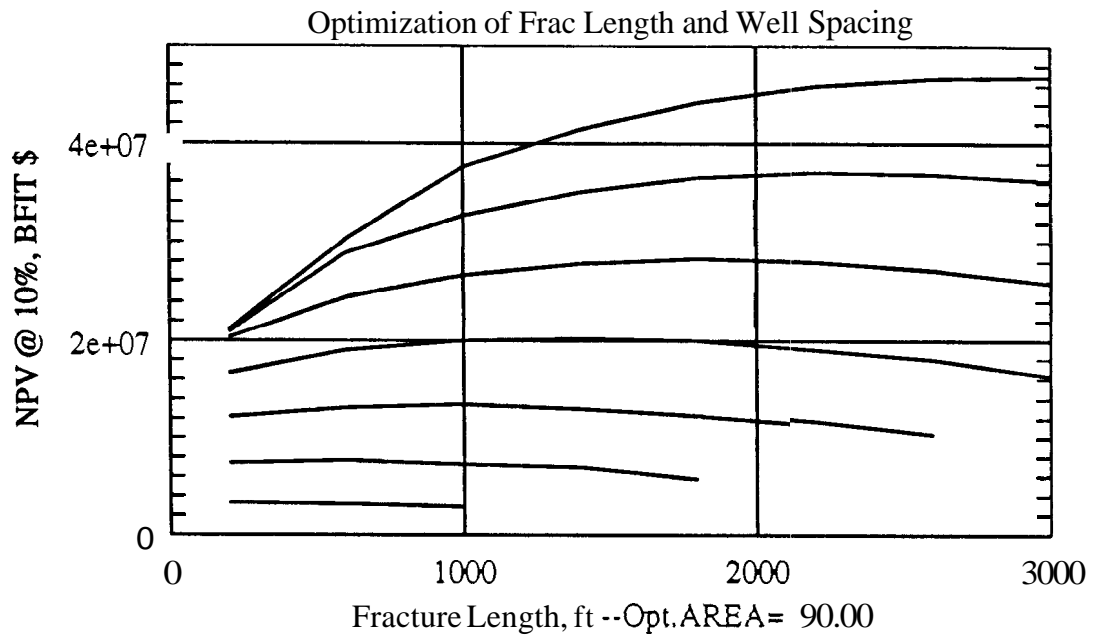


Figure 5.1: NPVIO for Example Economics Case

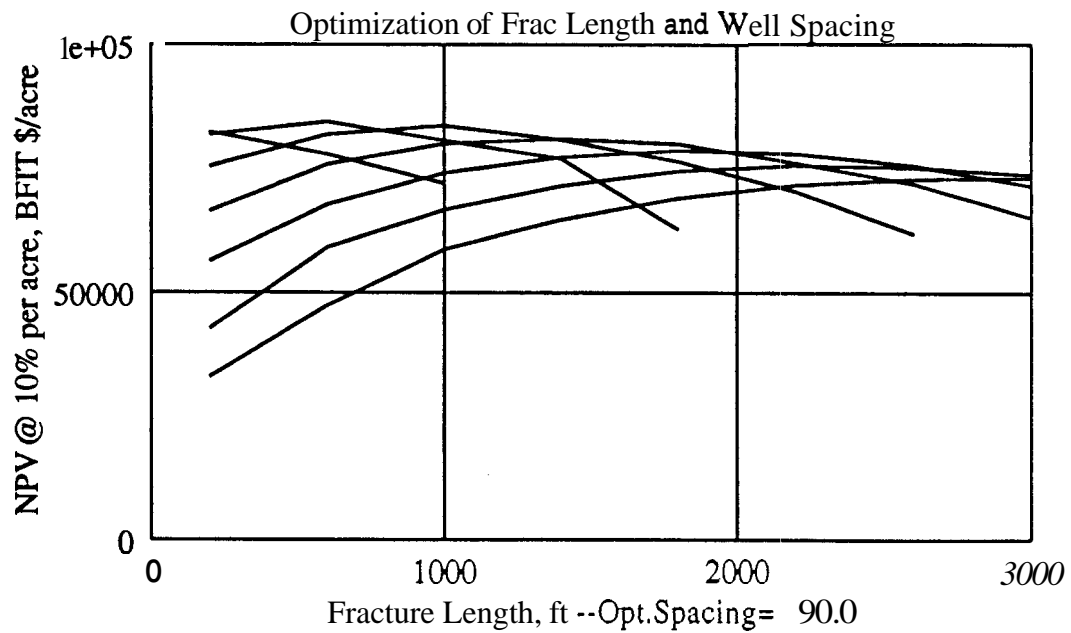


Figure 5.2: NPV10/acre for Example Economics Case

to well spacing and fracture length to greater detail than in this illustration. However, in practice this is generally futile, because:

1. It is not practical to require well spacings without a tolerance to locations of at least 2–5%. In practice, spacing tolerances of 5–10% are the rule.
2. Estimates of k , ϕ , x_f , price escalators, etc. are not sufficiently accurate to justify finer optimization.
3. As the NPV per acre reaches a maximum, effects of reservoir heterogeneities, constant pressure production and equal start date assumptions, and other economic approximations result in errors which are large compared to the changes in NPV/acre over a few acres.
4. It is not technically feasible to control fracture length to within several tens of feet, so optimization with variations smaller than plus or minus fifty feet is unnecessary.
5. Figure 5.3 shows the sensitivity of NPVIO per acre to well spacing for a fixed value of fracture length, pointing out how flat the curve is near the maximum.

5.4.2 Economic Examples — Effect of Azimuth

The effects of fracture azimuth are essentially negligible for the previous case, because the optimum value was at $x_e/x_f > 4$. For this case, the assumptions of Table 5.2 are used. The permeability has been decreased, while the fracture exponent has been lowered, Therefore larger economic values of fracture length are possible.

Optimization graphs for NPV per acre for two sets of well patterns are given. Conventional well spacing is shown in Figure 5.4, while Figure 5.5 illustrates a different set of well spacings. The corresponding economic optimizations are given in Figures 5.6 and 5.7. The optimum fracture length and well spacing have fairly significant differences. Optimal fracture length for the 4:1 rectangle requires a 65% longer fracture and increases NPVIO by 10%. Achieving well spacings for 4:1 rectangles as

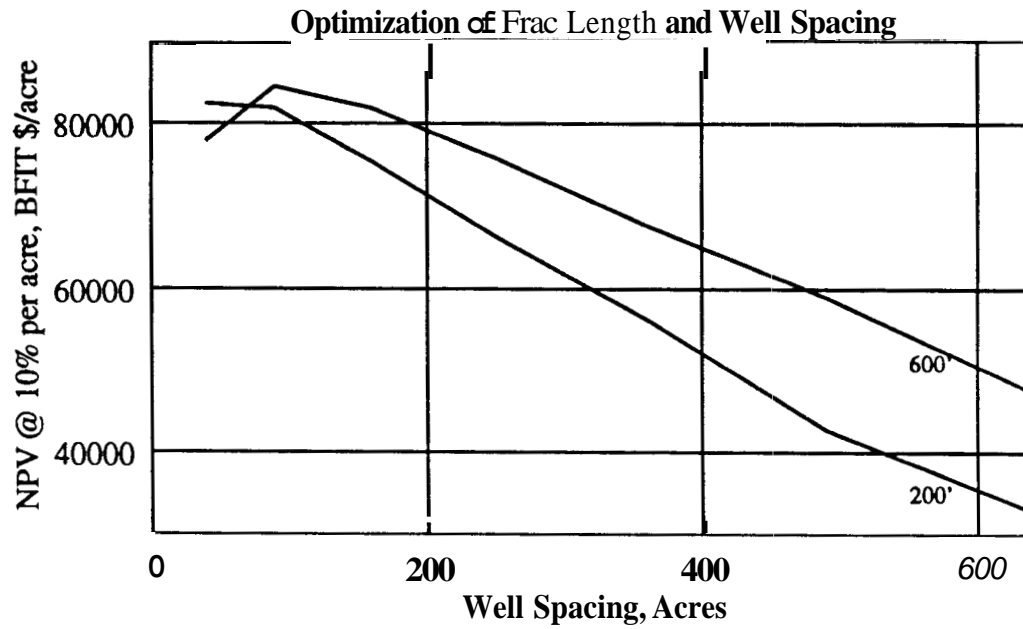


Figure 5.3: NPV10/acre for a Specified Fracture Length

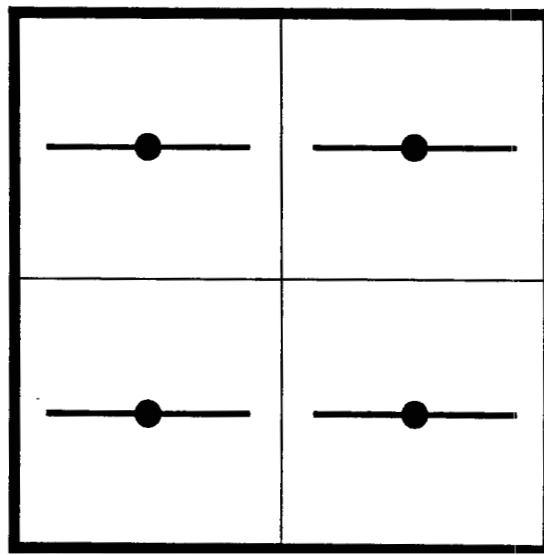


Figure 5.4: Conventional Well Spacing

Table 5.2: Input Data For Optimization

<i>TECHNICAL DATA</i>	<i>Initial Value</i>	<i>Units</i>
Permeability	0.02	md
Hydrocarbon Porosity	15	%
Thickness	60	feet
Water Saturation	30	%
Initial Pressure	5000	psi
Flowing Bottom Hole Pressure	800	psi
Reservoir Temperature	200	°F
Viscosity	0.02	cp
Total Compressibility	0.00014	psi ⁻¹
Ratio of k_x to k_y	1.0	
<i>ECONOMIC DATA</i>		
Discount Rate	10	%
Well Costs (without frac)	400,000	\$
Frac Costs	$9 \cdot x_f^{1.7}$	\$
Monthly Operating Expenses	1700	\$
Escalation Rates	5	% per year
Initial Net Gas Price	1.80	\$/Mcf

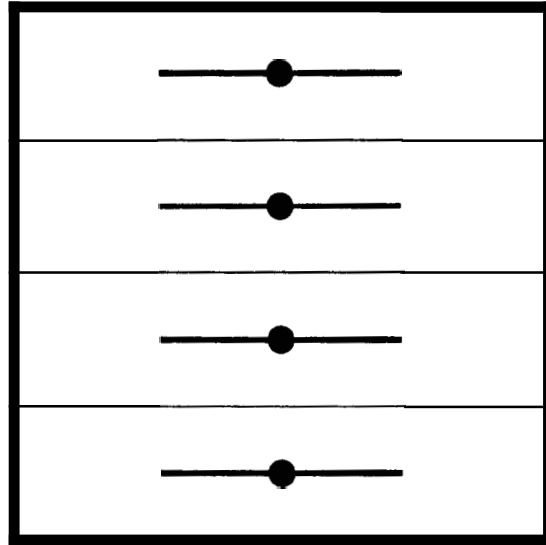


Figure 5.5: Well Spacing Modified Knowing Fracture Azimuth

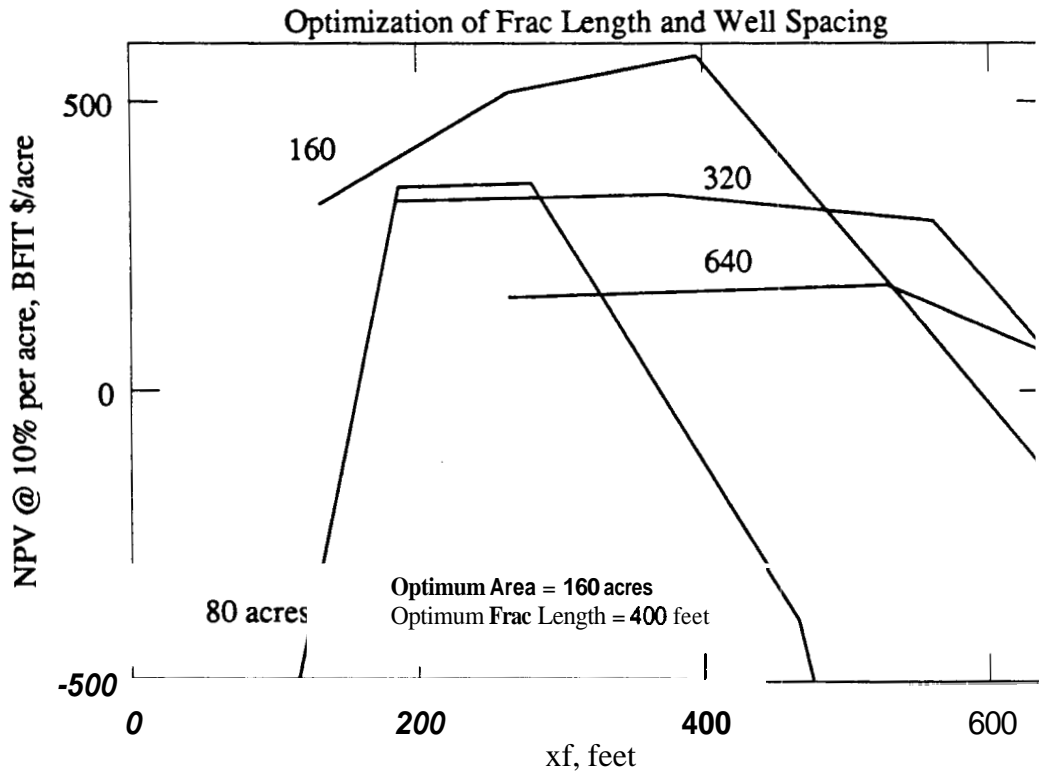


Figure 5.6: Economic Optimization for Conventional Well Spacing

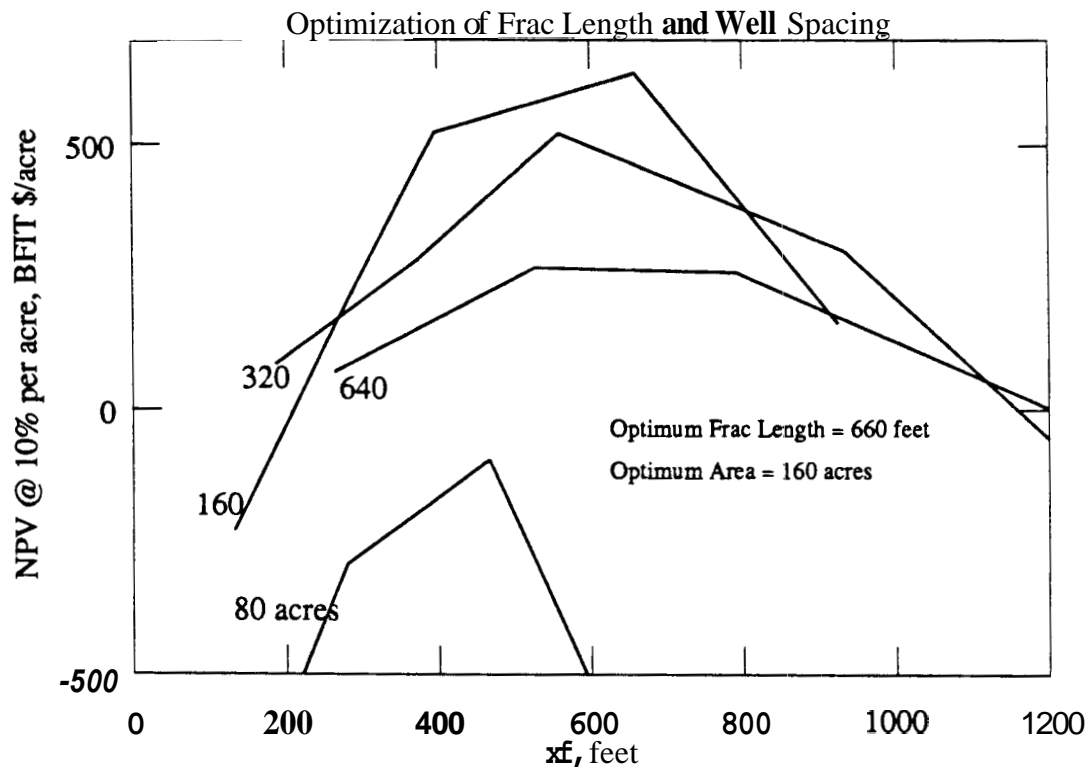


Figure 5.7: Economic Optimization for Modified Well Spacing

shown in Figure 5.5 requires knowing fracture azimuth with a reasonable degree of accuracy. For the indicated optimum propped fracture lengths, longer created lengths are required. Small errors in estimated lengths will not alter the results significantly, since all of the wells should have essentially parallel fractures. Large errors will result in much poorer performance. Figure 5.8 and 5.9 show two possible effects of errors in fracture azimuth on the modified well spacing. For an error of 45° , it is intuitive that well performance will be affected; the effect of a 75° error appears disastrous! Figure 5.10 summarizes the impact of an error in knowing fracture azimuth on NPV for this example. The design fracture length and well spacing for these cases are those derived from Figure 5.7, that is, when azimuth is known. In this case, it can be inferred that azimuth should be determined to within a range of $\pm 20\text{--}30^\circ$. This level of accuracy can be obtained by commercially available technology.

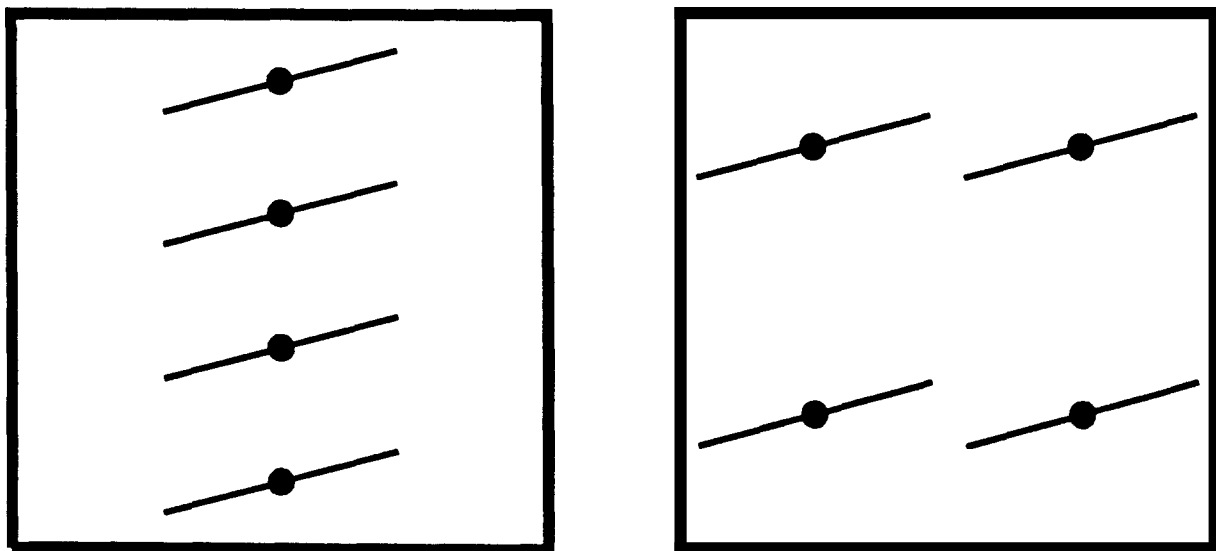


Figure 5.8: Spacing Effects of a 45° Error in Fracture Azimuth

5.4.3 Economic Sensitivity to Permeability Anisotropy

The information from Table 5.2 is again used; however, a moderate permeability anisotropy ($k_x/k_y = 20$) is used. For the first case, conventional well spacing is again used, with a small change in indicated optimum (Figure 5.11). If azimuth is known

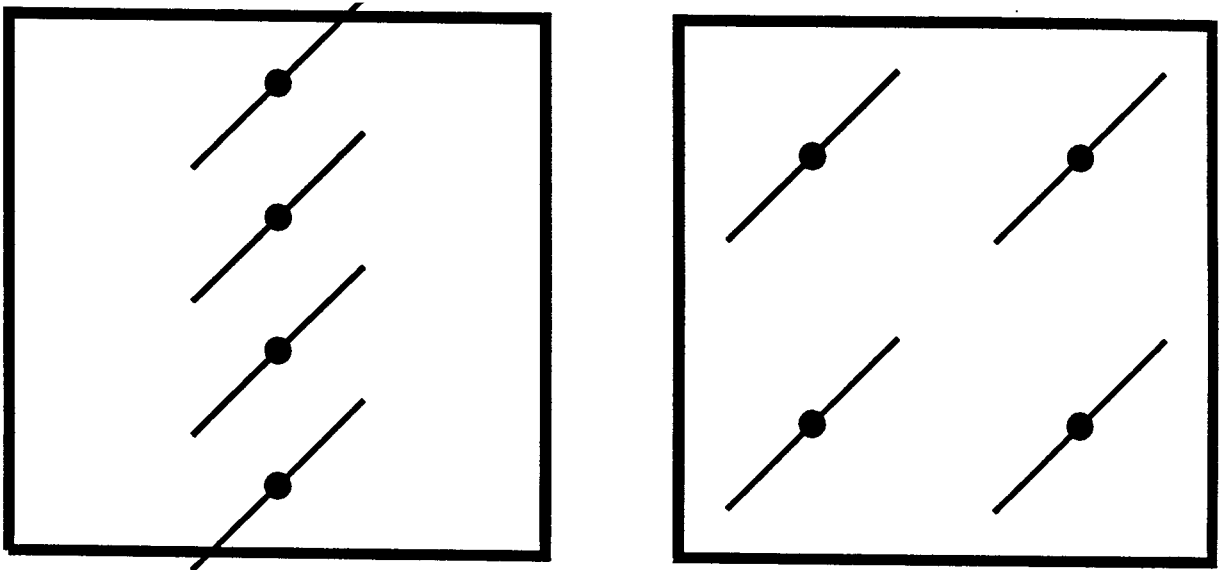


Figure 5.9: Spacing Effects of a 75° Error in Fracture Azimuth

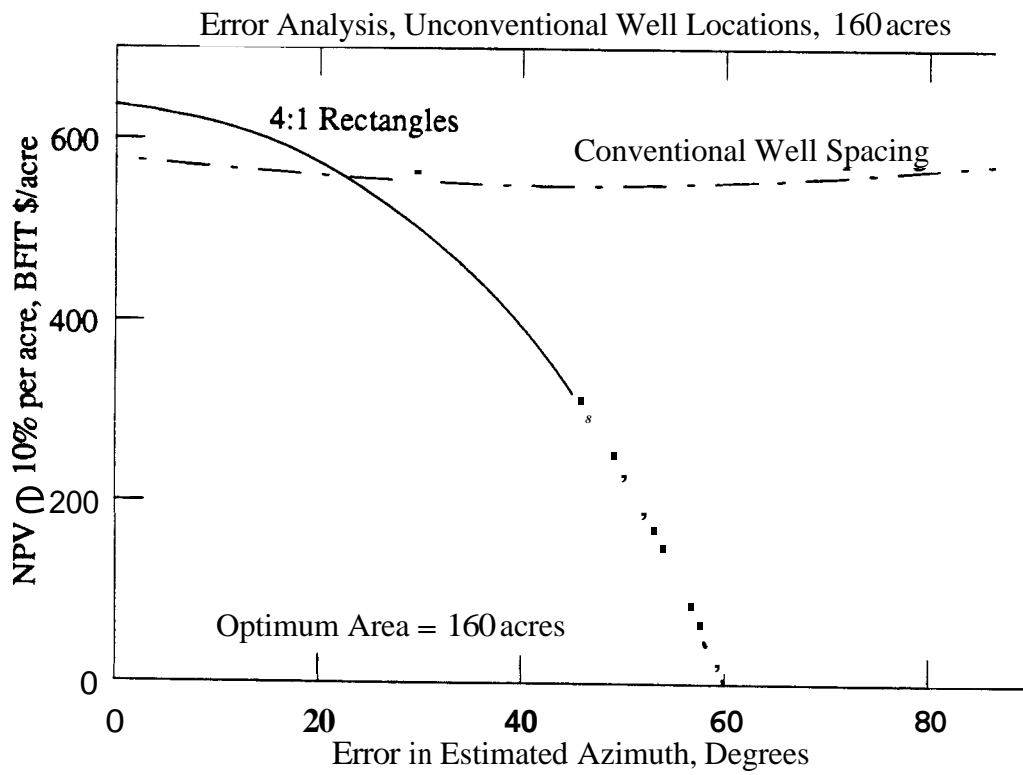


Figure 5.10: Impacts of Errors in Estimated Fracture Azimuth on Net Present Value

with accuracy, larger fracture lengths and further modifications of well spacing are possible. When k_x/k_y is large, the effective fracture length is decreased. Overall economic profitability is decreased. It is not known *a priori* whether more or fewer wells will be the indicated economic optimum. If azimuth and anisotropy are known, various well spacings may be investigated. For this particular set of economic parameters, consider a 10:1 rectangle for well spacing. The economic results for this case (Figure 5.12) are significantly improved, as the previous case was nearly uneconomic.

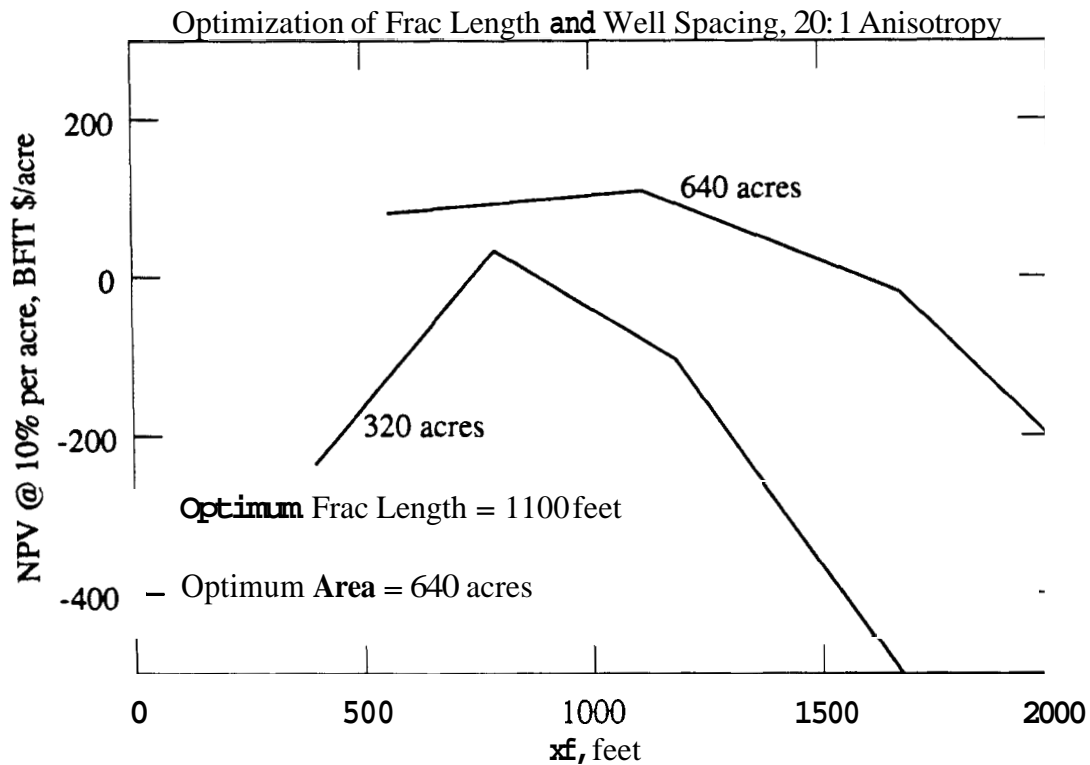


Figure 5.11: Economic Optimization Results With Permeability Anisotropy

5.5 Chapter Summary

A general and flexible economics model was developed in this chapter to calculate the net present values of cash flows associated with production from a hydraulically

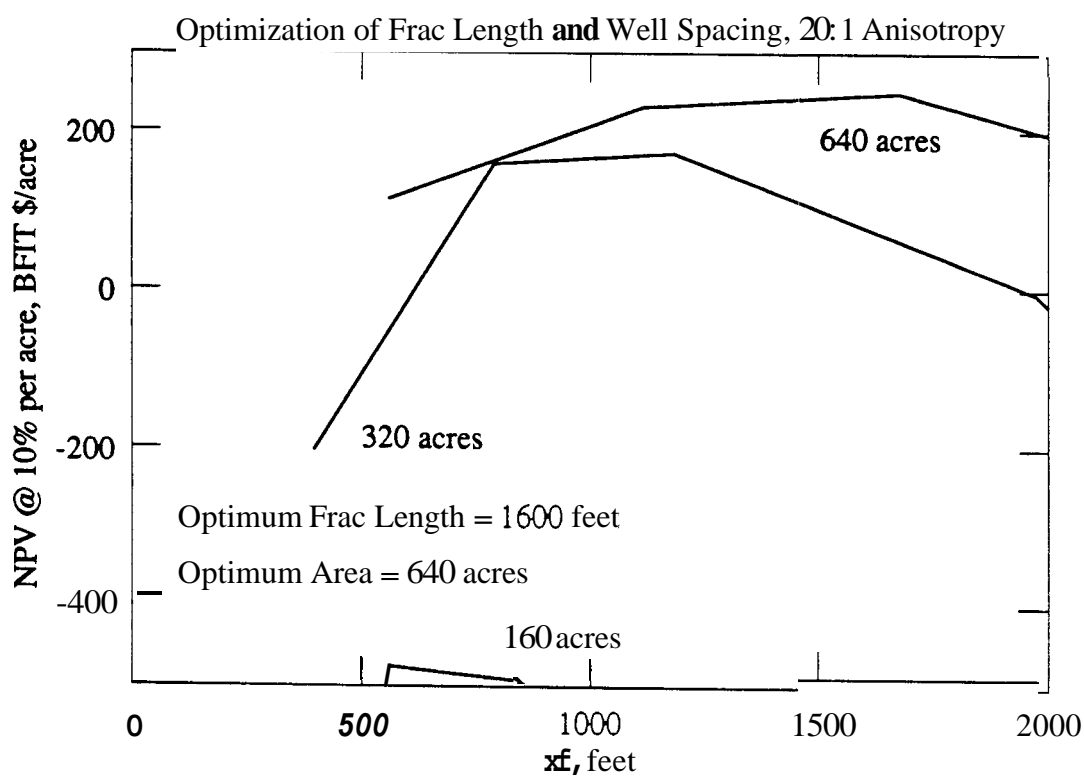


Figure 5.12: Economic Optimization Results With Permeability Anisotropy, Modified Well Spacing

fractured well. Any model of q_D as a function of t_{Dxf} can be used as input. A series of NPV values is calculated for varying fracture lengths and well spacings. Practical engineering applications are *always* economic in nature. Because a wide variety of technical and economic variables are involved in real applications, only example problems were used in this chapter. Those problems illustrated that, knowledge of fracture azimuth is important as fracture lengths approach well spacing. Knowledge of the magnitude and direction of permeability anisotropy is also important. These reservoir variables are not typically determined in most low permeability reservoirs.

The next chapter develops a geostatistical model for spatially correlated variations in permeability. This model is used to compare simulated performance of hydraulically fractured wells in heterogeneous reservoirs with the mathematical models developed for homogeneous models. The types of heterogeneities which make a significant impact on performance will be identified, and the economic model developed in this chapter will be extended to the heterogeneous systems.

Chapter 6

Reservoir Characterization Issues

Heterogeneity in reservoir variables reviewed. Methods of handling variability in reservoir permeability discussed. Local permeability anisotropy and anisotropies in correlation range. Kriging and conditional simulation approaches. Applications for hydraulically fractured wells, economic optimization, impact on interference testing.

6.1 Overview

Optimal development of oil and gas reservoirs requires integration of quantitative geological and geophysical analysis with appropriate flow models to assess alternative development and completion schemes and their relative economic values. Development plans are made early in the life of a reservoir, and may be nearly irreversible. Decisions about the type and quantity of reservoir characterization data to be obtained are critical. Sparse local conditioning data from logs, cores, and well tests are combined with expert interpretation of depositional environments, geophysical surveys, etc. to yield an estimate of the spatial distribution of reservoir variables.

Each new well and survey adds more data of varying quality and cost. Field development plans are constructed with a host of simplifying assumptions which may not incorporate all available expertise. One method for quantifying this expertise and

utilizing it for field development is **conditional simulation**. This method allows improved reservoir development by:

- generating equiprobable estimates of spatial distributions of reservoir variables,
- indicating where additional reservoir information is most valuable, and
- utilizing the whole array of reservoir information, even qualitative, or 'soft' interpretative information.

Optimization of fracture length and well spacing for low permeability gas reservoirs is used to demonstrate the power of this technique. This is a particularly attractive problem since it involves few 'process-related' risks which may dominate fluid displacement problems. Near well permeability is used as local conditioning data. Flow performance for gas wells with different fracture lengths is shown to be sensitive to geometric anisotropy, correlation length, and overall magnitude of heterogeneity. Optimization of fracture length and well spacing therefore depends on appropriate characterization of these features.

Simulation and economic optimization models are combined to illustrate a parametric solution for optimization of fracture length and well spacing as a function of various reservoir heterogeneities. Economic value of identifying and characterizing these parameters is quantified.

6.2 Effects of Reservoir Heterogeneities

One research topic of the Stanford Center for Reservoir Forecasting is optimal development of heterogeneous oil and gas fields. Low permeability reservoirs require hydraulic fracturing and are often 'infill drilled', with increased well densities to both accelerate recovery and increase ultimate recovery. Increased oil recovery from reservoirs being waterflooded has been frequently demonstrated; fewer examples of incremental gas recovery associated with infill drilling are published¹⁸².

Incremental gas recovery may be obtained by infill drilling, when permeability variations are large. Vertical hydraulic fractures intersect producing wells and are aligned

according to current stress states in the field. Typically, these stress directions remain fairly constant over distances typical of field sizes. Spatial correlation of permeability and porosity need not be related to hydraulic fracture direction. Two types of heterogeneities in low permeability reservoirs are addressed in this research:

- o anisotropy in permeability, and
- o spatial heterogeneities.

Permeability anisotropy can be related to small scale variations in rock properties as a result of microfractures, stress contrasts, deposition, and diagenesis. Microfracturing is believed to contribute significantly to total flow capacity in many low permeability reservoirs. Regardless of direction of microfractures, maximum permeability (due to *in situ* stresses) is typically in the direction parallel to the maximum compressive stress and the hydraulic fracture. This gives the unfortunate result of the minimum permeability feeding into the fracture ¹⁸⁰ .

Spatial heterogeneities arise from complex depositional histories, faulting, reworking, etc. Variations are most complex in the vertical direction. However, hydraulic fractures for most reservoirs below about 1,000 m. are vertical. Variations in vertical permeability are smoothed by commingled production into a long (\times 100–750 m.), narrow (\times 0.2 cm) fracture. Further work on commingled (multiple layer) heterogeneous systems is appropriate. Fractures have extremely high permeability compared to the formation. Fracture permeabilities are typically 10^3 – 10^9 times greater than formation permeability.

Areal heterogeneities in Permeability and porosity are more important for hydraulically fractured formations. If correlation range is small compared to hydraulic fracture length, spatial correlation should have little affect on well performance. Similarly, if the level of heterogeneity is small, essentially homogeneous behavior can be expected. An effective permeability anisotropy can be created by geometric anisotropies in correlation range. Both geometric anisotropy in correlation range and small scale permeability anisotropy may be present.

6.2.1 Dealing With Heterogeneities

Virtually every reservoir engineering text contains a discussion of Darcy's law and permeability. Most texts point out that actual petroleum reservoirs are quite heterogeneous, with some giving elaborate descriptions of actual reservoirs and core photomicrographs illustrating large and small scale heterogeneities. Nonetheless, each author at some point assumes something to the effect of '...uniform permeability k everywhere in the reservoir ...' to complete the derivation at hand. An assumption that an effective value for permeability can be obtained is common and can be useful for many simplified problems.

There are many practical limitations of this assumption. Difficulties associated with assumed homogeneity are most notable in fluid displacement projects. Interference and tracer tests can often reveal heterogeneities undetected by single well tests. It is widely recognized that reservoir heterogeneities affect oil recovery and well performance 38, 112, 143, 180, 238, 256, 260 . Stochastic approaches to representing heterogeneities have been quite popular 29, 68, 103, 142, 144, 231 . Geological literature is replete with discussions of heterogeneities. Leblanc 145, 146 presented an extensive bibliography of investigations which discussed impacts of environments of deposition and subsequent alterations on continuity and properties of sandstone formations. For examples of specific discussions of spatial heterogeneities effects on petroleum reservoir performance see Allen¹¹ , Lewis¹⁴⁸ , and Sharma²²⁷ . An excellent discussion of the general problem of estimating numerical grid block permeabilities is given by White 262 .

In many studies, permeability heterogeneities have been demonstrated to be far more critical to conditioning flow performance than have heterogeneities in porosity (ϕ) or porosity-compressibility product (ϕc_i) 13, 14, 22, 23, 123 .

Low permeability reservoirs may be more heterogeneous than higher permeability counterparts. Small scale microfracturing is often significant to production and extends anisotropically in space. Complex diagenesis, silica overgrowth, and precipitation in natural fractures are often associated with such systems.

Typical geological representations of porosity, thickness, etc. result in fairly smooth

contour maps (in the absence of large faults and reservoir boundaries). However, maps based on widely scattered data points, even if unbiased, rarely represent actual spatial variability. Important spatial variations in permeability, thickness, and rock properties are critical to fluid flow. Although kriging (for example) **can** generate a map which generates a minimum expected squared error, it fails to account for connectivity of extreme values. Kriging was not designed to estimate connectivity of high and low values, but rather to minimize squared estimation errors.

6.2.2 Some Historical Approaches

Dykstra-Parsons

The Dykstra-Parsons⁷⁴ approach has its historical significance in attempting to predict waterflood performance in the presence of multiple layers. This simple coefficient became a popular measure of heterogeneity. Determining this parameter was simple, requiring plotting the cumulative density function (cdf) of (typically) core-derived values of permeability on log probability paper. V_{DP} is calculated as

$$V_{DP} = \frac{k_{50\%} - k_{\sigma}}{k_{50\%}}$$

where $k_{50\%}$, is the median value of permeability and k_{σ} is the permeability value corresponding to a cumulative probability of either 15.9% or 84.1%, i.e., one standard deviation from the the median. Assymmetric probability density functions (pdf) can make the choice of the higher or lower value of the cdf an arbitrary decision. V_{DP} is always positive. If the data are log-normally distributed, all points will fall on the same straight line. The standard deviation of a log-normal distribution $\sigma_{\ln k}$ is related to V_{DP} by:

$$V_{DP} = 1 - \exp^{-\sigma_{\ln k}}$$

The use of core plugs typically results in a severe underestimation of V_{DP} due to sampling bias. Fractures and tight streaks are routinely not sampled in such measurements. Typical core results analyzed from productive reservoirs yield a majority of points which *do* fall on the straight line with departure occurring at low and high

permeability values. *Unfortunately, it is precisely these values and their spatial connectivity which condition reservoir flow.*

Effective Permeability

Methods to estimate effective permeability of heterogeneous media include analytic solutions for simple systems such as parallel or series flow of piecewise homogeneous systems and more complex approaches for stochastic distributions of permeability. Law¹⁴⁴ showed that for reservoirs with log-normal distributions of permeability, given mean and variance of the distribution one could predict an effective permeability. Warren and Price²⁵⁶ showed that geometric mean permeability was a good approximation to effective permeability for heterogeneous systems without spatial correlation; i.e., white noise. Smith and Freeze²³¹ included spatial correlation and demonstrated that geometric mean was no longer a satisfactory approximation. Gelhar and Axness⁹¹ and Gutjahr *et al.*¹⁰² showed approximations for multilog-normally distributed single phase flow with isotropic system with small variance.

Power Averaging

Jensen *et al.*¹²⁵ presented results which demonstrated that permeability data are frequently not simply log-normally distributed. They proposed a power series for effective permeability such that $(k_t)^p$ is normally distributed where k_t is effective permeability and p is an exponent whose range is $[-1,1]$. This approach was used to analyze core permeability data to determine representative values for p . They reported improved correlations of related parameters such as porosity when this method was used.

A power averaging method presented by Journel *et al.*¹³⁰ estimates effective vertical permeability k_v given a distribution of sand and shales with intrinsic permeabilities k_{ss} and k_{sh} respectively. For a given shale fraction, V_{sh} , vertical permeability is estimated as:

$$k_v = [V_{sh} k_{sh}^\omega + (1 - V_{sh}) k_{ss}^\omega]^{1/\omega}$$

Note that for limiting values of ω of -1, 0, and 1, harmonic, geometric, and arithmetic

means are given. As opposed to Jensen's approach which correlated core permeability values, Journel *et al.* correlated flow simulations for statistically heterogeneous systems with varying levels of V_{sh} . This model was extended by Desbarats⁶⁸ for shale fractions up to 90%. Deutsch^{69,130} extended the work of Desbarats to relate simulation block size and statistical anisotropy of the joint permeabilities.

6.3 Conditional Simulation

Kriging is an unbiased minimum error variance estimation technique. In this context, it is applied to estimating values (in space) of an incompletely known random variable. When two variables are jointly used for estimation, the method is known as cokriging. Kriging results in a minimum squared error. Spatial variance of estimated values is always less than or equal to the actual variance, resulting in maps which appear 'smoother' than reality. If, for example, a total gas in place resource estimate is desired, the kriged map may result in a 'best' estimate. However, flow properties are highly conditioned by fluctuations in permeability. These fluctuations should not be smoothed artificially.

Conditional simulation is a technique by which estimates of an unknown random variable may be deduced while retaining the heterogeneity (as expressed by the expected spatial variance) of the original field and honoring all data points which are known precisely. Conditional simulations reproduce the mean and covariance function while kriging reproduces only the mean¹²⁷. In this application, unconditional simulations are generated using the Turning Bands Method (TBM)¹²⁸. Data points which are known precisely are used to calculate local error in the unconditional simulation. These differences are kriged, with kriged errors being subtracted from the unconditional simulation. The result is a simulation which honors conditioning data, the input variogram, and maintains appropriate fluctuation patterns. The procedure for a conditional simulation of (e. g.) permeability is as follows:

- Estimate the permeability field by kriging.

- o Generate an unconditional random field with appropriate mean, variance, and covariance. Typical methods include LU decomposition 8, 67, 'nearest neighbors', turning bands, and indicator simulations 129.
- o Determine the unconditional simulation estimate of permeability at each point corresponding to a known value.
- o These estimates can then be kriged. Error estimates are the difference between kriging of known permeability points and permeability points from the unconditional simulation. This error is zero at the data points.
- o The unconditional simulation plus the error estimate is the conditional simulation. The procedure can be repeated as often as desired. The average of many conditional simulations will be equivalent to direct kriging from the known values.

6.3.1 Turning Bands Method

The conditional simulation method used to generate permeability distributions was the Turning Bands Method (TBM) in two dimensions as described by Mantoglou and Wilson 151. TBM was presented first by Journel 127 in three dimensions. Basically, the method involves transforming a two or three dimensional simulation into the sum of a series of one dimensional simulations. A random field with a specific covariance function and a zero mean is generated on a line. Points on the field to be simulated are projected normally onto the line. The covariance function for desired values, $C_2(x)$ must be related to that of the radial function, $C_1(r)$. This is accomplished either by:

- o Moving averages and Brooker's formula to obtain a weighting formula, \mathcal{B} such that $C_2(x) = \mathcal{F} \cdot \mathcal{F}^\psi$. Then, independent random numbers are drawn on each line and averaged as the convolution of \mathcal{F} and the random numbers.
- Using the Hankel transform to create appropriate radial spectral density functions,

$$f(\omega) = \frac{\omega}{\sigma^2} \int_0^\infty C_1(r) J_0(\omega r) dr$$

Rice's formula is used with $f(\omega)$ to generate the random field in the desired space. The final step is as in the moving average method.

Some useful radial spectral density functions include the exponential variogram, $\sigma^2 \exp^{-br}$ whose radial spectral density function is $\frac{\omega/b}{b[1+(\omega/b)^2]^{3/2}}$ and the Modified Bessel Function variogram, $\sigma^2 br K_1(br)$ whose radial spectral density function is $\frac{2(\omega/b)}{b[1+(\omega/b)^2]^2}$.

A more complete set can be found in Mantoglou and Wilson 151 .

6.4 Results

Geostatistical modelling has been used in three areas for this research:

1. **Hydraulically fractured wells in a heterogeneous closed square reservoir.** Sensitivity to reservoir heterogeneities are shown for a single hydraulically fractured well. Initially, completely unconditioned simulations were run and flow simulations conducted with a very high conductivity fracture ($(k_f b_f)_D \approx 2000$). Realization dependent permeabilities near the fracture made significant effects on well performance compared to the overall level of heterogeneity, correlation range, and geometric anisotropy. To demonstrate the sensitivity level to those three items, conditioning data of low variance and a desired mean were included in the near fracture region. This reduced realization dependent variations for a specific value of heterogeneity and correlation lengths.
2. **Two finite conductivity fractured wells in an 'infinite' media.** Motivation of this effort is comparison with a series of new analytic solutions for interference testing of hydraulically fractured wells in simply anisotropic reservoirs. Although not included here, results show when reservoir heterogeneities may be expected to influence such interference tests.
3. **Economic optimization of fracture length and well spacing.** Economic optimization is performed for fracture length and well spacing for homogeneous and heterogeneous cases. Optimal well spacing for heterogeneous cases is shown to generally require closer well spacing and shorter fractures than homogeneous cases. This is

due to a greater number of poorly drained areas in the heterogeneous case which do not encounter the hydraulic fracture. However, when substantial geometric anisotropies in the correlation range run normal to the hydraulic fracture and heterogeneity levels are high, optimal development indicates fewer wells with longer hydraulic fractures. This is due to greater than normal incremental recovery associated with increased hydraulic fracture length for this case.

6.4.1 Methodology

A 2000 by 2000 square foot grid was subdivided into 68 by 68 blocks. A quarter hydraulic fracture was added with the well origin at (0,0) and extending (typically) 1000 feet for fracture half-length (Figure 6.1). This symmetry treatment is perfect for homogeneous media; however, heterogeneities are almost certainly asymmetric. Sensitivities with a full scale fracture centered in a 4000 square foot grid yielded virtually identical results, so only quarter block results are given here.

Local grid refinement was required near the origin and the fracture tip to match the homogeneous solution. Ultimately, a fine grid was included for all fracture blocks near the fracture from the wellbore to five blocks past the fracture tip. Permeability values in the fine grid region were homogeneous and selected from conditional simulations for the block. Excellent agreement was obtained for both constant rate and constant pressure solutions. Very early time constant pressure solutions resulted in very high flow rates—a brief constant rate period was used in these times.

All simulations were done using a small, constant compressibility and constant viscosity. Conversion to gas problems requires appropriate time and pressure adjustments. Output rates and pressures have been converted to dimensionless quantities for comparison with analytic solutions.

6.4.2 Example Realizations

Figures 6.2–6.7 show a series of greyscale images of typical conditional simulation runs with varying correlation ranges. All have global means of approximately 10.0.

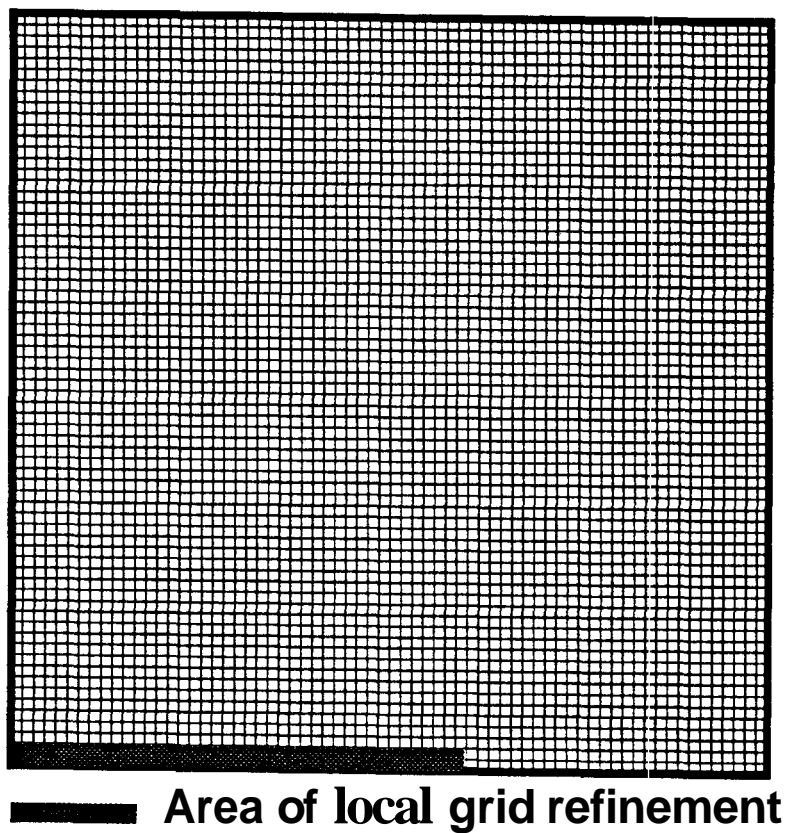


Figure 6.1: Simulation Grid for Heterogeneous Reservoir with a Hydraulically Fractured Well

In order to maintain approximately constant global means, a series of simulations was conducted until the desired mean was obtained. The simulation with correlation range of 2.0 approximates white noise (Figure 6.6). Conditioning data were specified near the wellbore and the hydraulic fracture.

Greyscale representations have been selected as being more visually informative than contour plots. For comparison, Figure 6.8 is a contour plot of the same information contained in Figure 6.7.

Range X Y, 34 34

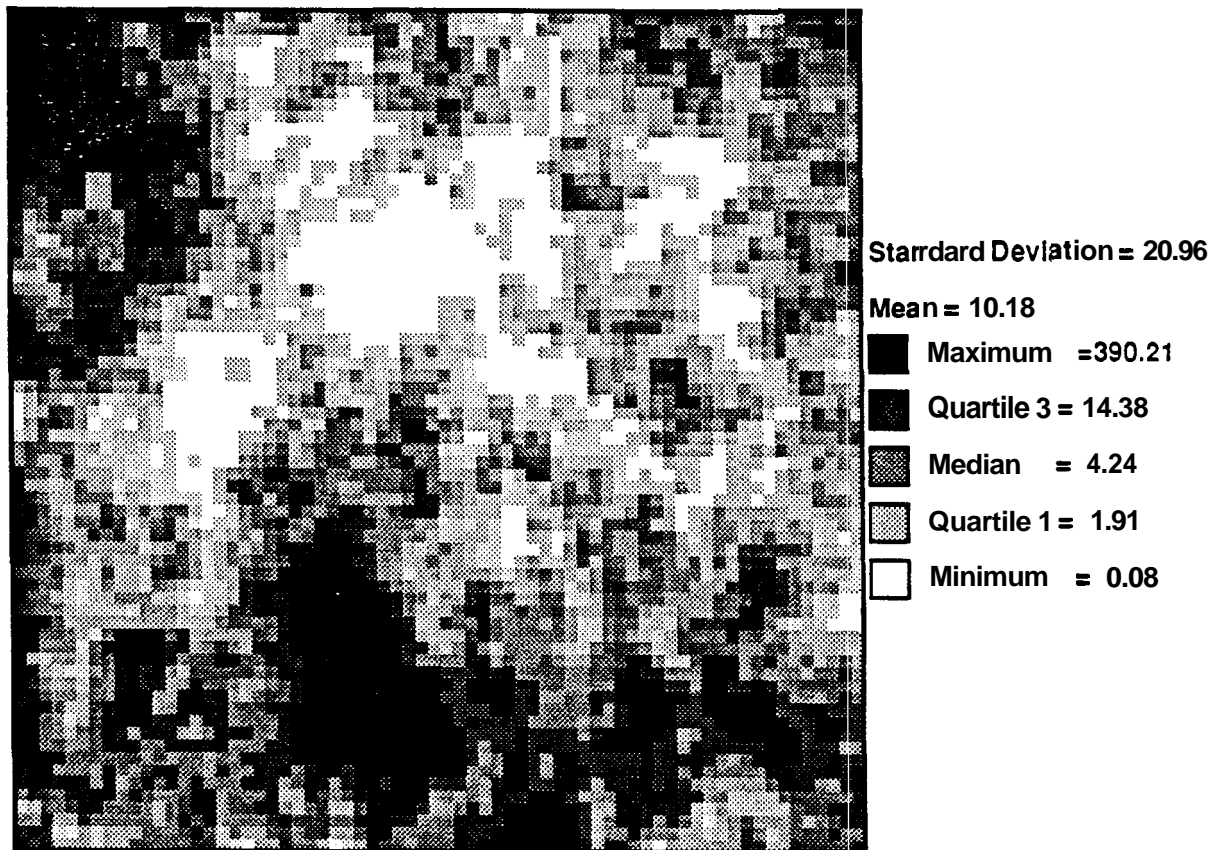


Figure 6.2: Conditional Simulation — Correlation Range= 34, Geometric Anisotropy = 1.0, $\sigma/m = 2.06$

Range X Y, 34 136

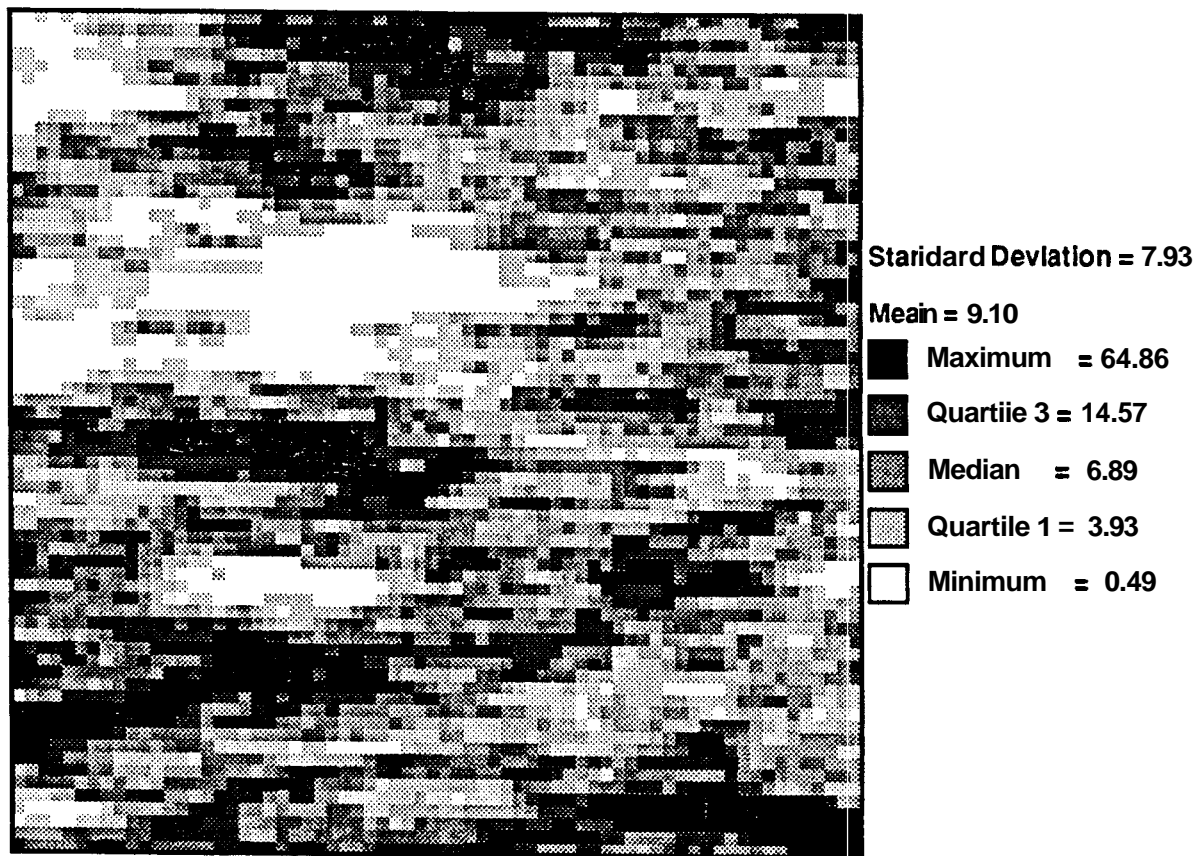


Figure 6.3: Conditional Simulation — Correlation range= 34. Geometric anisotropy= 4:1, $\sigma/m = 0.87$

Range X Y, 176 176

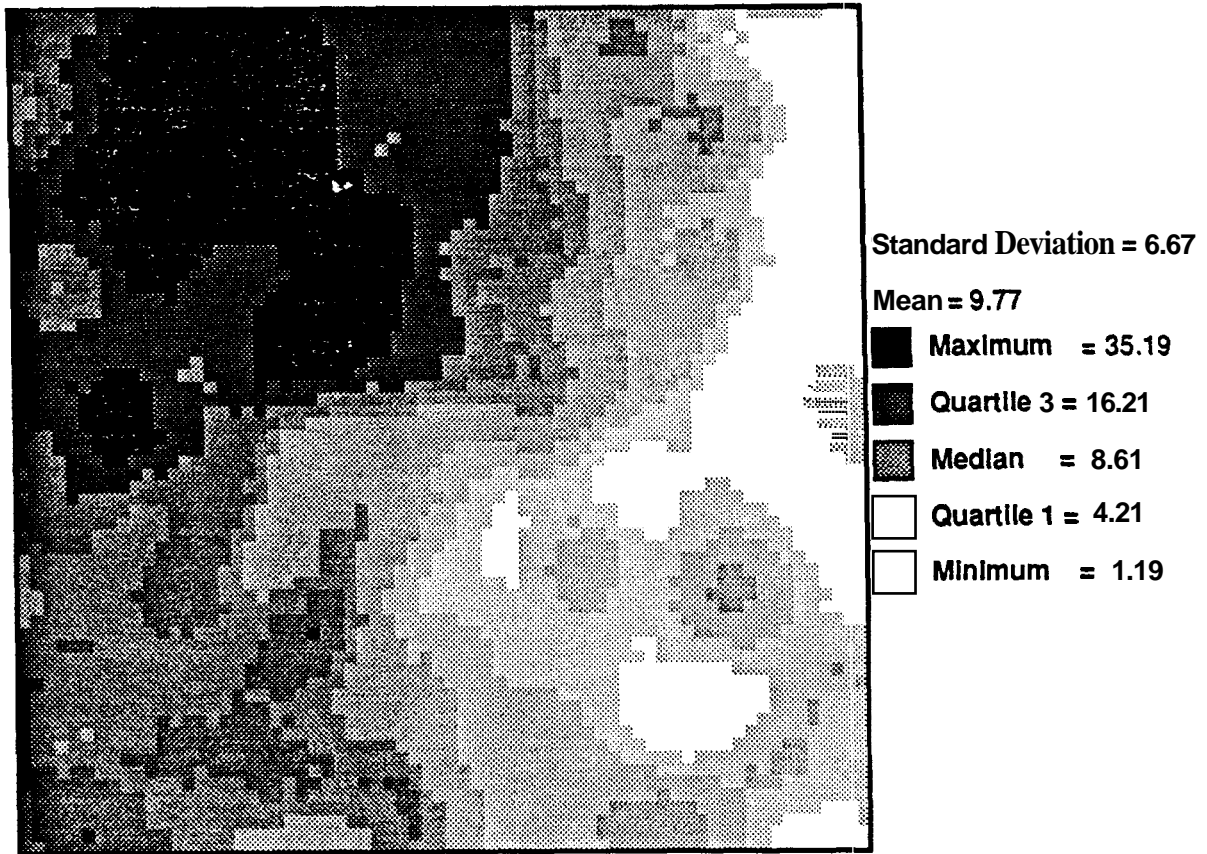


Figure 6.4: Conditional Simulation —Correlation range= 176, Geometric anisotropy = 1.0, $\sigma/m = 0.68$

Range X Y, 17 17

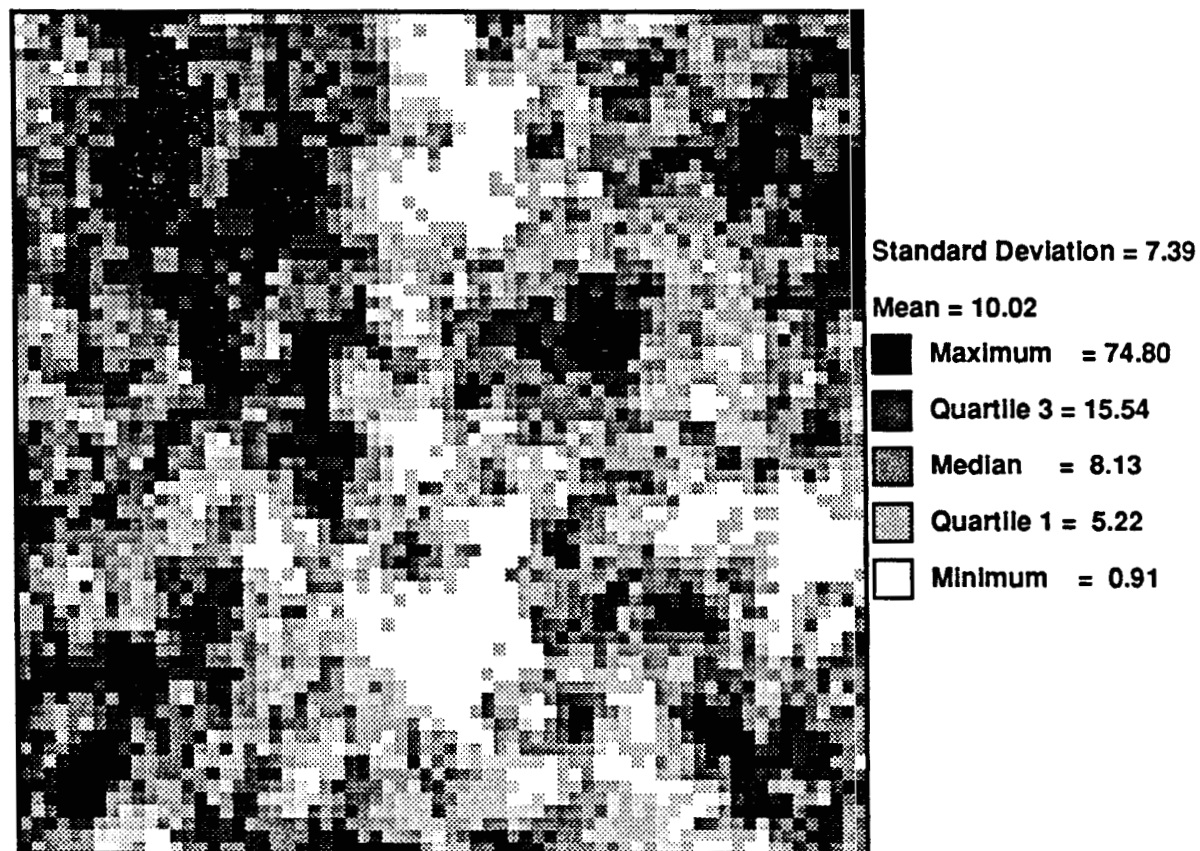


Figure 6.5: Conditional Simulation — Correlation range= 17, Geometric anisotropy = 1.0, $\sigma/m = 0.74$

Range X Y, 2 2

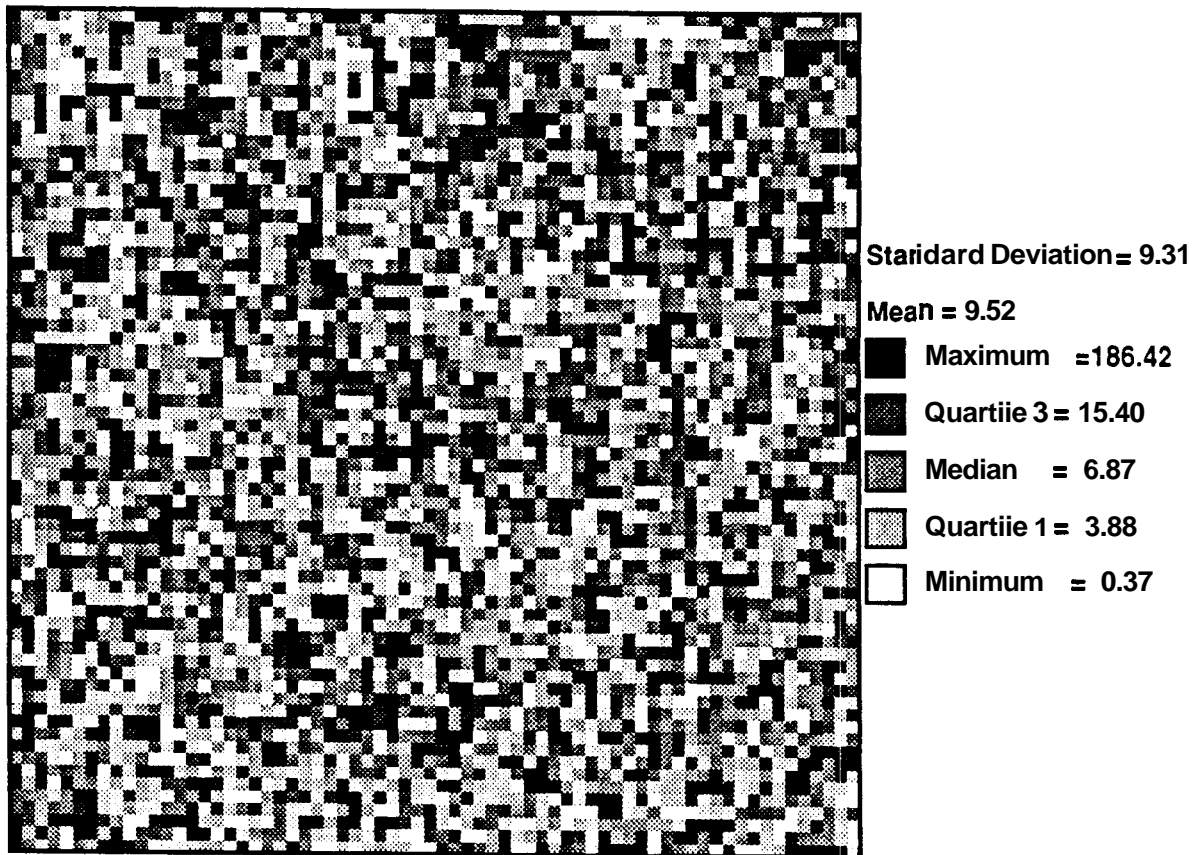


Figure 6.6: Conditional Simulation — Correlation range = 2, Geometric anisotropy = 1.0, $\sigma/m = 0.98$

Range X Y, 68 272

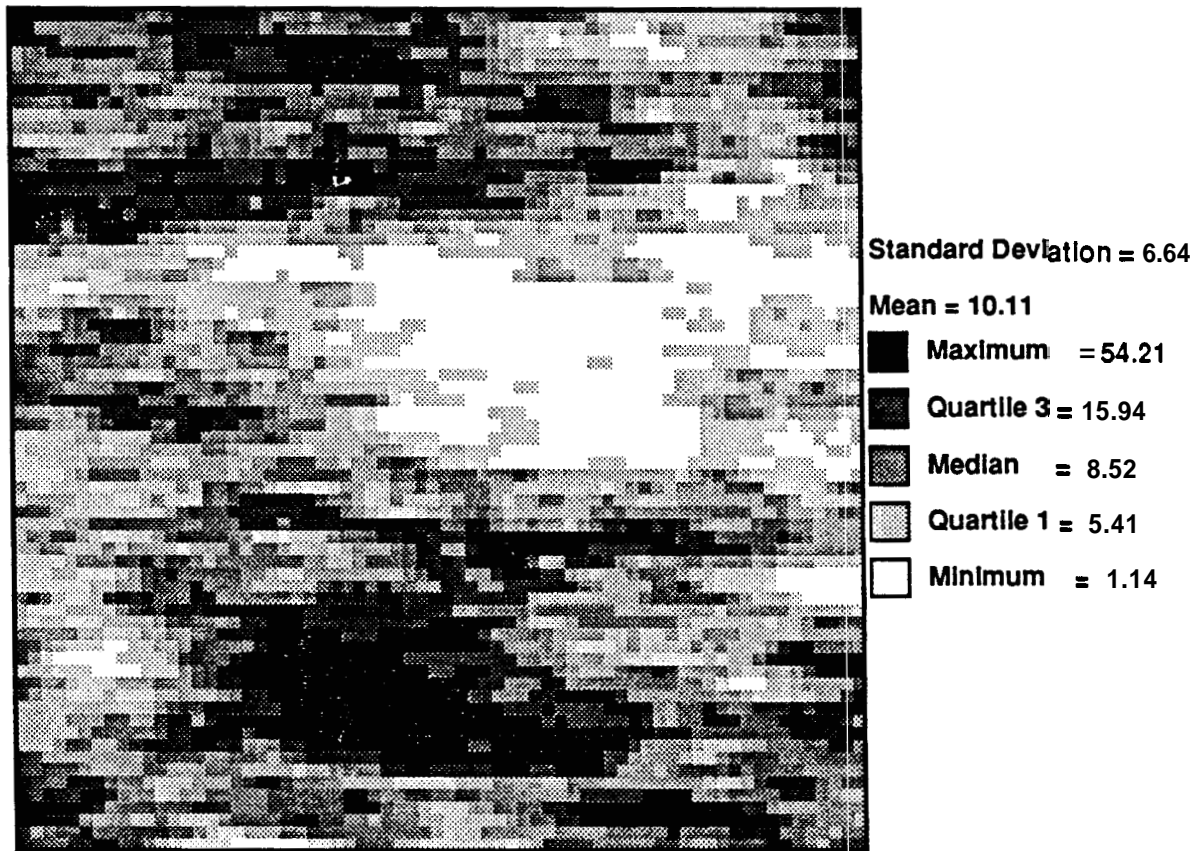


Figure 6.7: Conditional Simulation—Correlation range= 68, Geometric anisotropy = 4.0, $\sigma/m = 0.66$

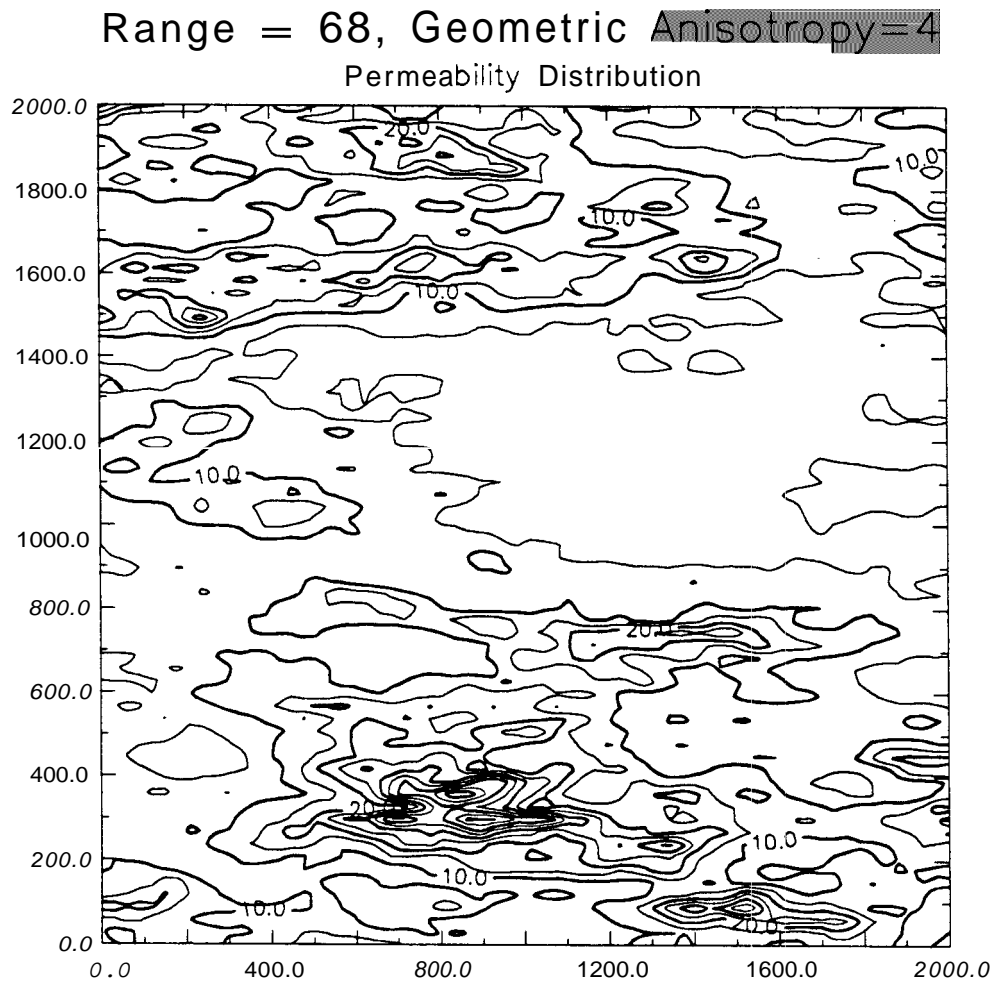


Figure 6.8: Conditional Simulation — Correlation range = 68, Geometric anisotropy = 4.0, $\sigma/m = 0.66$

6.4.3 Flow Simulation Results

Virtually all of the flow simulations based on permeability distributions developed as described in Section 6.3 resulted in pressure behavior at the wellbore which approximated the analytic solution for an infinite conductivity fracture in a closed rectangular reservoir. Largest variations in calculated flow rates or pressures were noticed when:

- a large anisotropy in the range was present ($> 4:1$),
- the overall level of heterogeneity was large ($\sigma/m > 1$), or
- the range in the fracture direction was between one-half and two times the fracture half-length.

Naturally, when the overall level of heterogeneity was quite low ($\sigma/m < 0.2$), the correlation range was unimportant. Spatial correlation is unimportant when variability is negligible! **Also**, very short correlation lengths required higher levels of heterogeneity to be noticeably different from the analytic solution. Figure 6.9 compares dimensional results of a homogeneous simulation with that of a case with white noise (uncorrelated variations) and $\sigma/m = 0.6-1.0$. The simulated and analytic cases virtually overlap for all realizations. Correlation lengths of less than about one-half of the fracture length were only significant for large levels of heterogeneity ($\sigma/m > 1$). When geometric anisotropy was less than about 4:1, the results of the flow simulations varied only slightly from the homogeneous case unless the correlation range was approximately equal to the fracture length and the heterogeneity level was large.

The remaining cases for simulation results will display the dimensionless flow rate q_D as a function of dimensionless time, t_{Dxf} . This allows simulation results for varying means to be normalized and for the generalization of results. Figure 6.10 shows the results of three similar cases. For each case, correlation length is 17 blocks, or one-half the fracture length and one quarter of the simulation size. **All** means have been normalized; heterogeneity levels range from $\sigma/m = 0.9-1.7$. Although the lowest value of σ/m is closest to the analytic solution, none of the three realizations pictured varies greatly from the analytic solution. Analyzing the dimensional results of

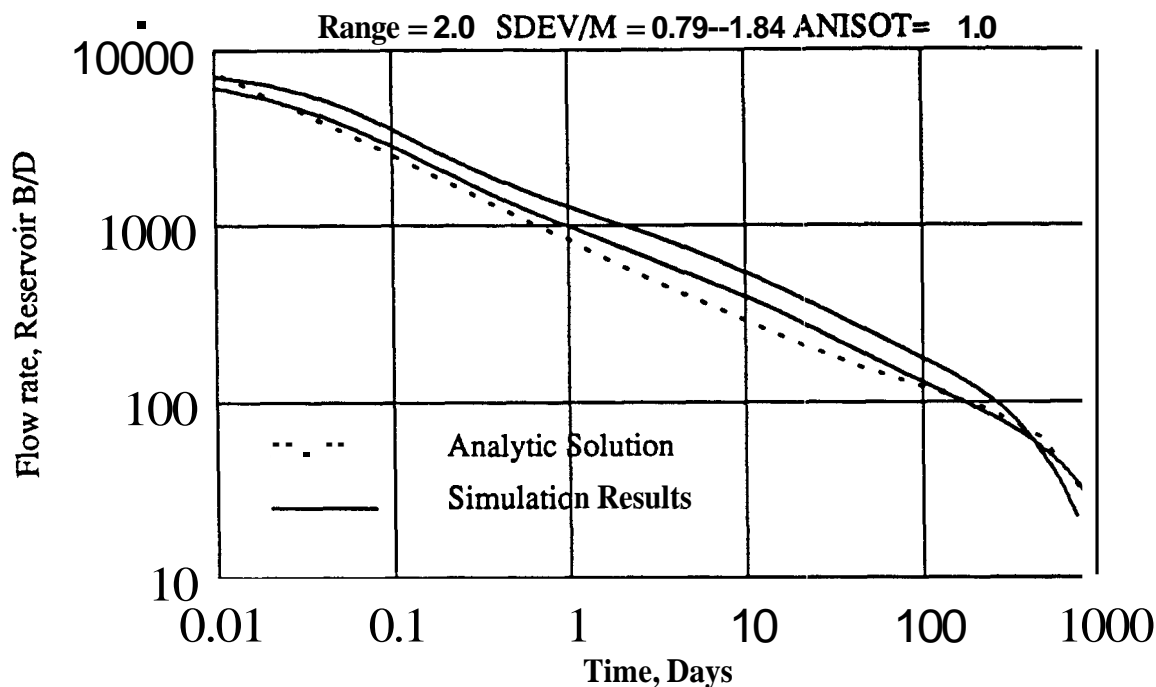


Figure 6.9: Conditional Simulation Results — WhiteNoise, $\sigma/m = 0.6-1.0$

these simulations gave estimated fracture lengths and x_e/x_f estimates within 10 % of the input values for the homogeneous cases. As σ/m exceeds 2.0, even uncorrelated heterogeneities result in large variances in flow behavior. The typical range of permeabilities realized for varying values of σ/m are given in Table 6.1. These values were obtained from one specific realization and only indicate general magnitudes.

Table 6.1: Example Permeability Variations (Log normal pdf)

σ/m	Minimum	Maximum
0.5	2.0	35.
1.0	1.5	50.
2.0	0.1	275.
4.0	0.01	1500.

However, as σ/m increases, mean permeability is held constant, and conditioning data near the well are near the mean, very high permeabilities may be concentrated in a small area. Much of the area will have permeabilities below the mean, so the

specific location of the very high permeability area(s) will mean significant realization dependent flow behavior. This will even hold true for white noise if the heterogeneity level is high enough. Erratically fractured reservoirs may have very high levels of heterogeneity; however, spatial correlation is almost sure to be present in such systems.

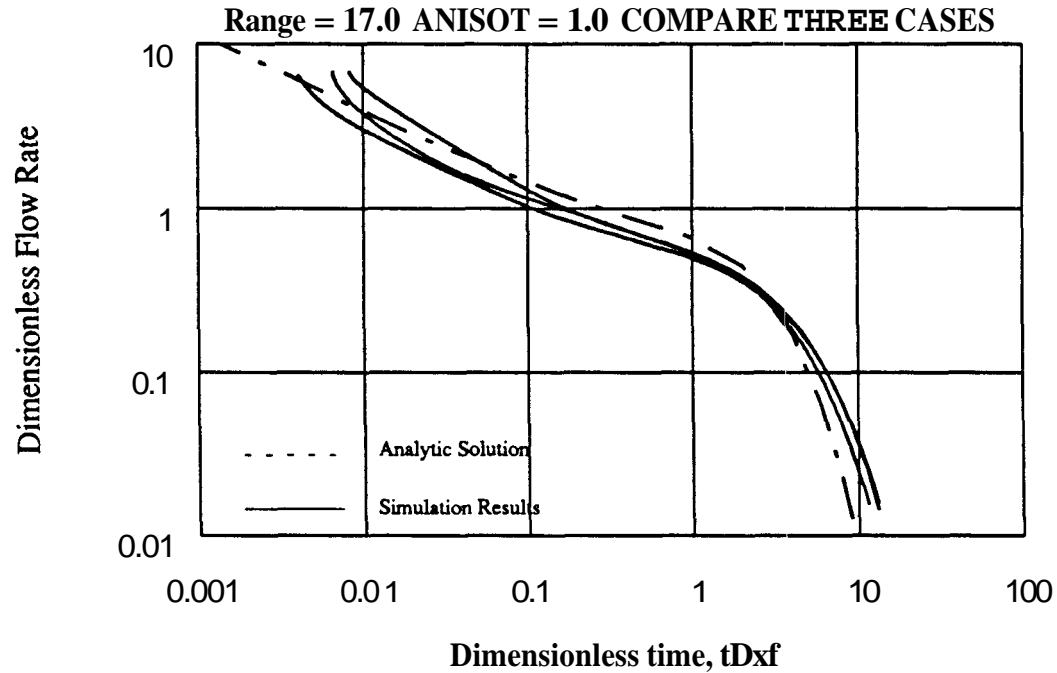


Figure 6.10: Three Flow Simulations With Correlation Range= 17, Varying σ/m

Figure 6.11 shows two simulations with σ/m varying from 0.6–1.0. This correlation range is quite long—three times the fracture length. Except when σ/m was greater than about 2.0, all flow simulations with very long correlation lengths were reasonably close to the analytic solution. Conventional analysis of these dimensional results gave parameter errors ranging from 5–18 %.

Figure 6.12 shows the combined results of six cases for a correlation length of 68 blocks, or two times the fracture length. As long as σ/m exceeded about 0.8, simulation results tended to vary substantially from the analytic solution for the homogeneous case. A substantial variation is defined as either an error of more than 20 % in calculated fracture length and permeability of the dimensional simulation results, or a correlation coefficient between the natural logarithms of q_D as a function

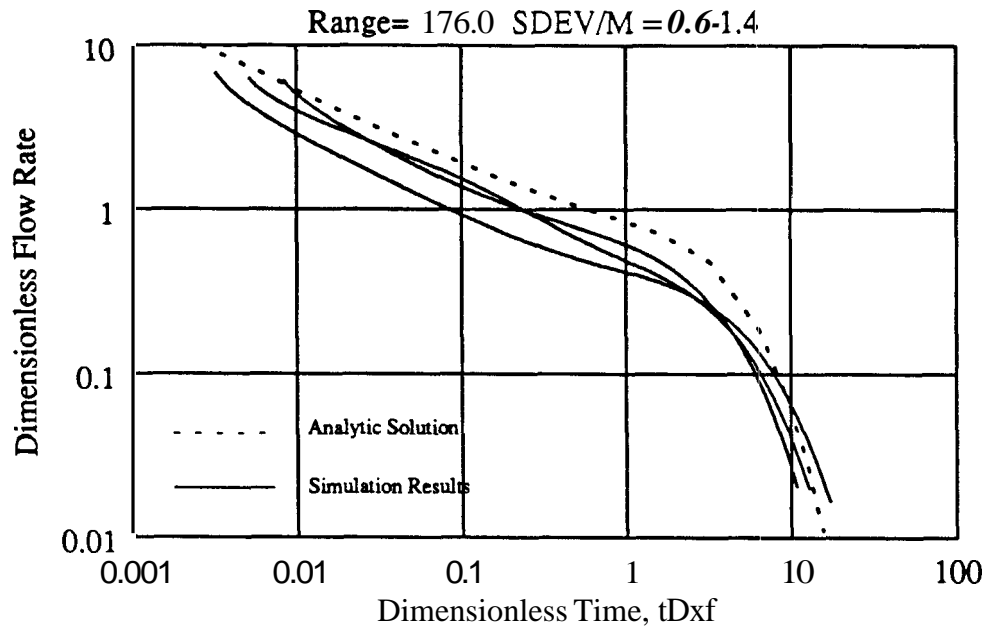


Figure 6.11: Two Flow Simulations With Correlation Range= 176, Varying σ/m

of $t_{D_{xf}}$ of less than 0.6 for the simulated case and analytic solutions.

Figure 6.13 compares four cases with correlation ranges of 68 in the direction of the fracture (\mathbf{x}) and 34 in the direction normal to the fracture (\mathbf{y}). This is referred to as a geometric anisotropy of 2.0. Results are identical to those determined for Figure 6.12. Small geometric anisotropies have little influence on results.

A correlation range of 34 blocks appears to be sufficient such that even modest heterogeneities can be significant. Figure 6.14 shows five cases without geometric anisotropies and a modest range in σ/m . Most cases are close to the analytic solution; however, the variability is much greater than observed for the short and long correlation lengths. Again, small values of anisotropy have little incremental effect (Figure 6.15–6.16). However, as the correlation length increases to large levels (10–20), most realizations were significantly altered (Figure 6.17–6.18). When the larger geometric anisotropies (10,20) are analyzed in a revised coordinate system, effects of geometric anisotropy can be reduced (Figure 6.19). The procedure for this renormalization is summarized in Section 6.4.4.

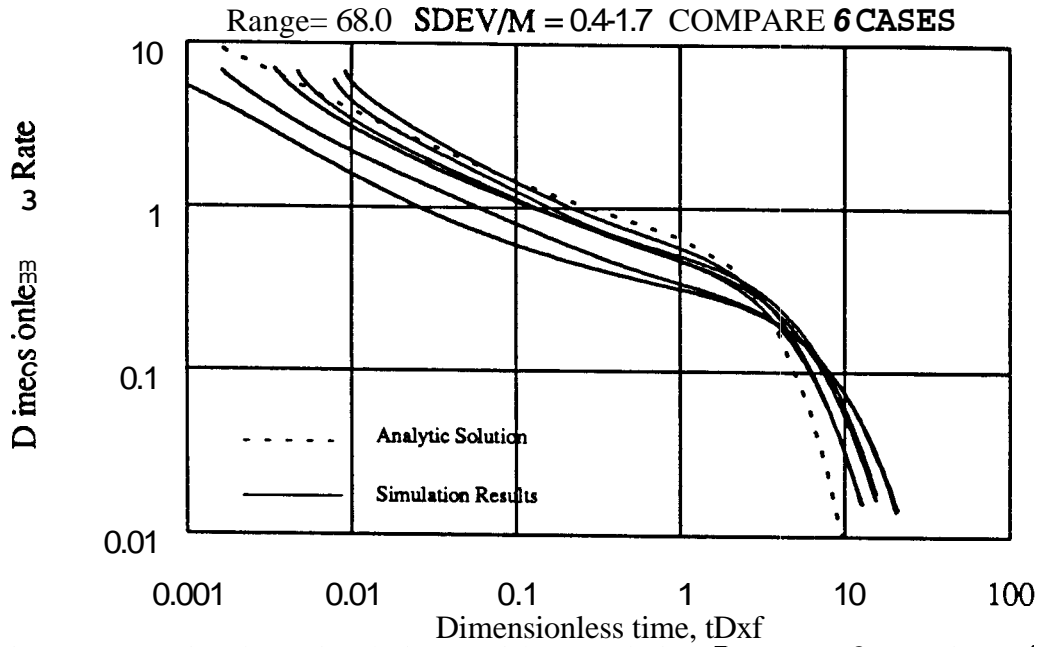


Figure 6.12: Six Flow Simulations With Correlation Range= 68, Varying σ/m

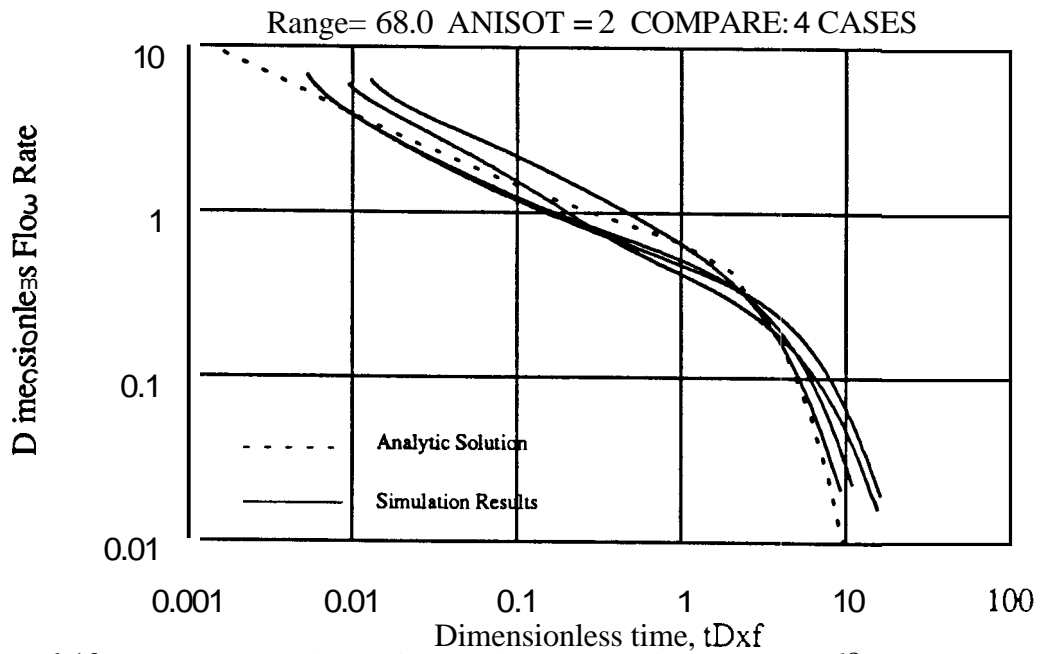


Figure 6.13: Three Flow Simulations With Correlation Range= 68, Small Geometric Anisotropy

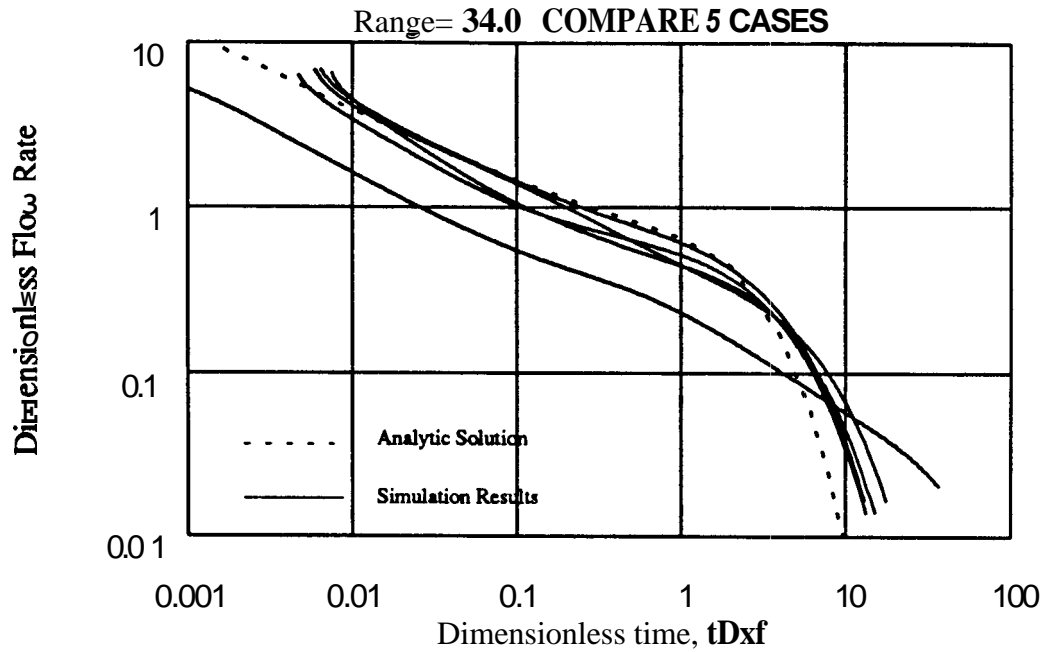


Figure 6.14: Five Flow Simulations With Correlation Range= 34, Varying σ/m

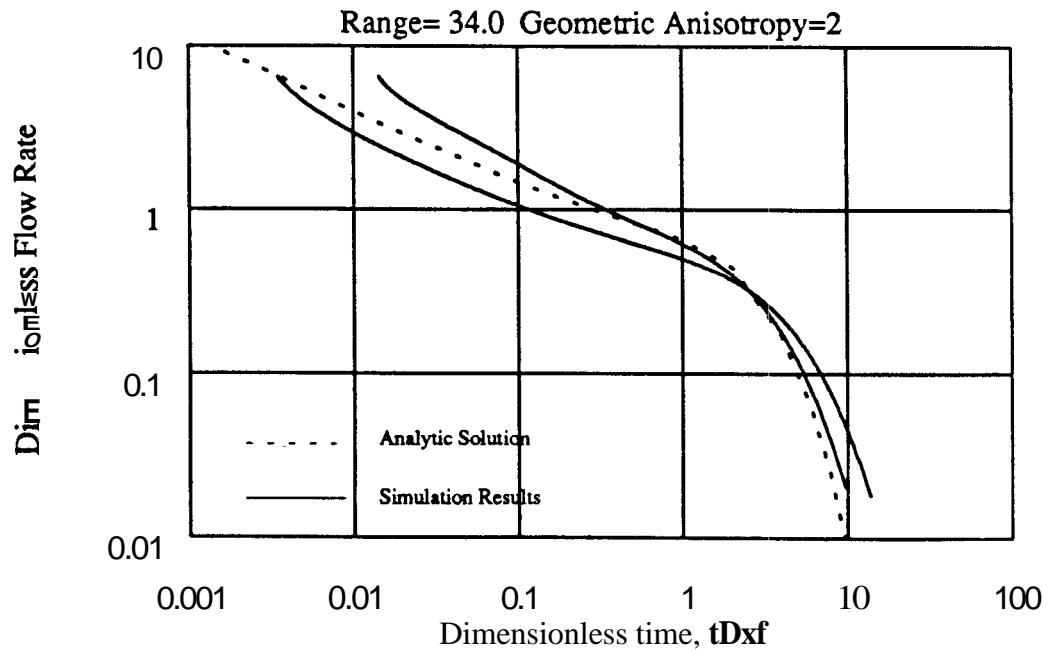


Figure 6.15: Flow Simulations With Correlation Range=34, Geometric Anisotropy=2

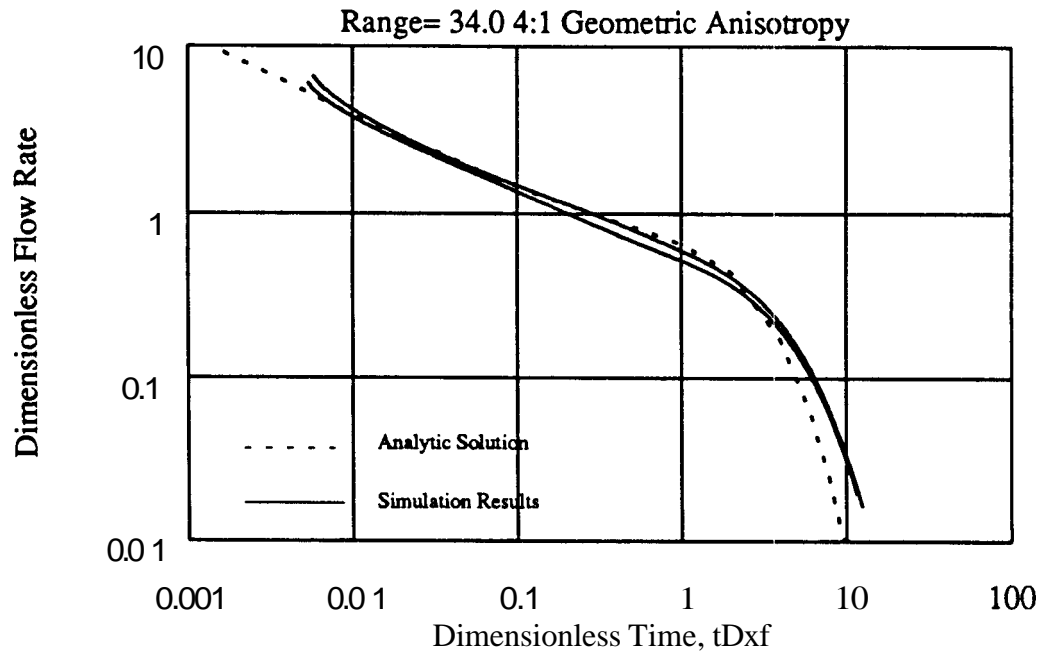


Figure 6.16: Flow Simulations With Correlation Range= 34, Geometric Anisotropy=4

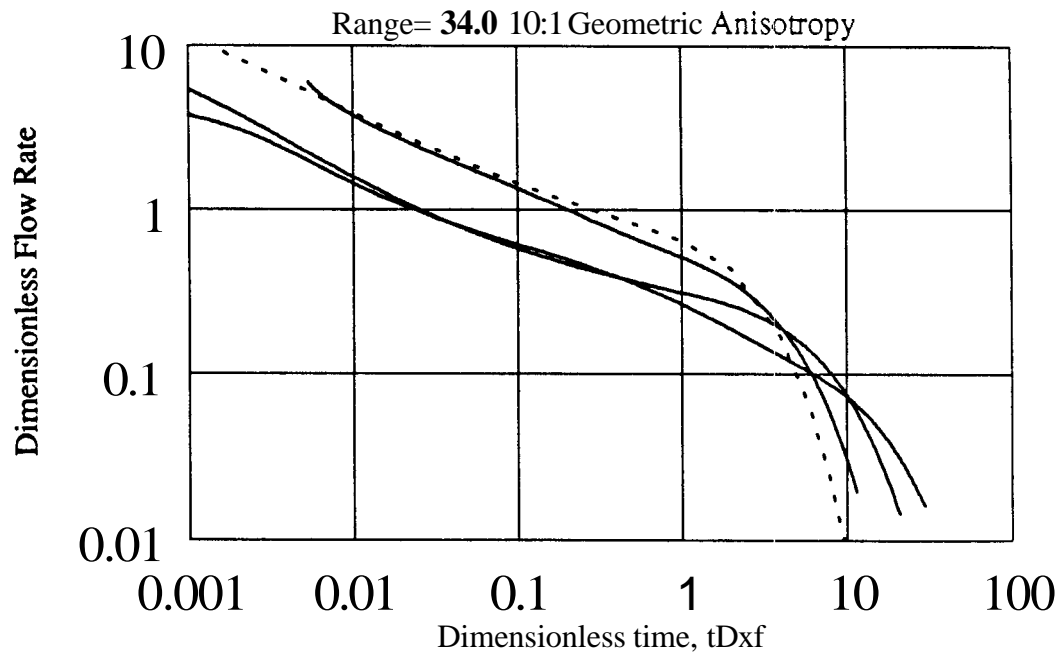


Figure 6.17: Flow Simulations With Correlation Range= 34, Geometric Anisotropy= 10

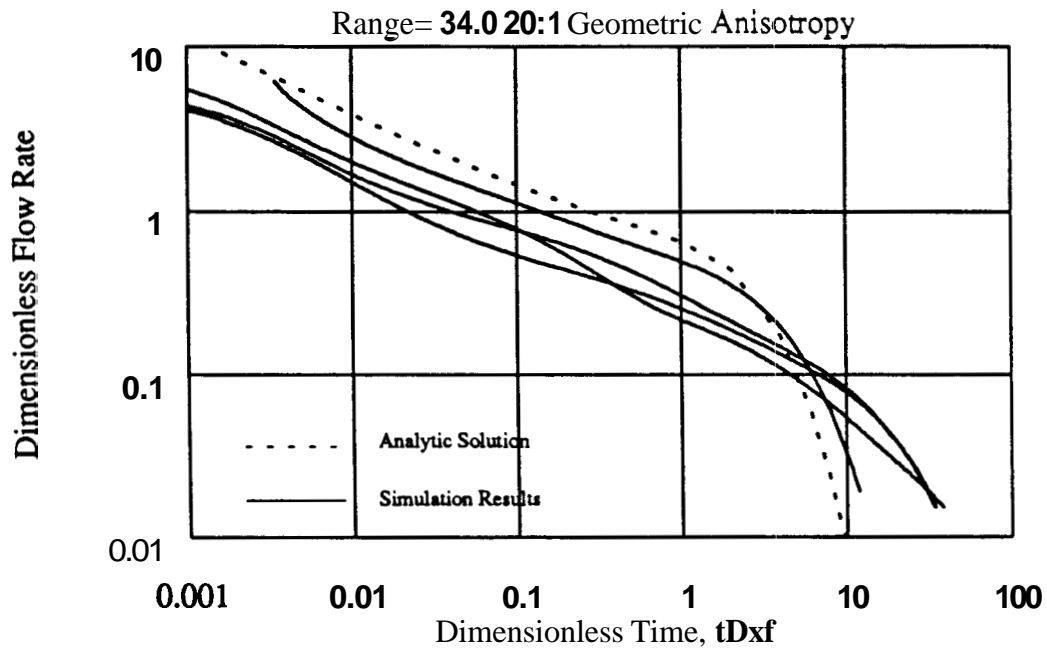


Figure 6.18: Flow Simulations With Correlation Range= 34, Correlation Range= 20

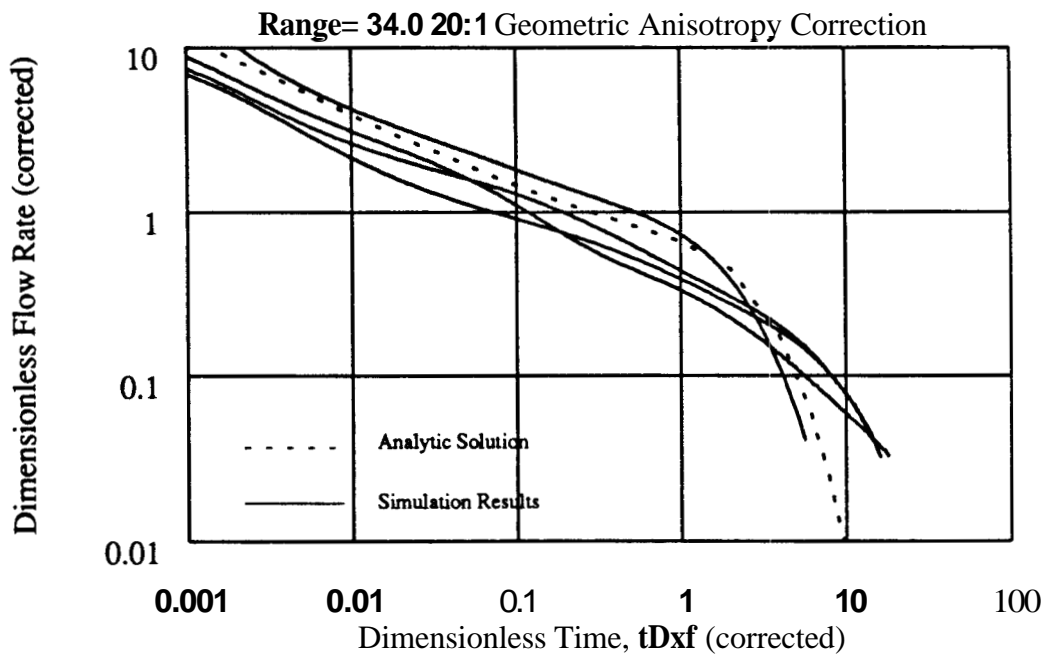


Figure 6.19: Flow Simulations With Correlation Range= 34, Geometric Correction for Correlation Range

Pressure Distributions

Even when wellbore pressures for heterogeneous cases are close to the analytic solution, pressure distributions in the formation vary significantly from one solution to the next. Figures 6.20 and 6.21 show pressure variations for two realizations. Figure 6.20 has a short correlation length and large values of σ/m . This case demonstrates little variability in space from the analytic solutions due to poor spatial correlation ($1/8 x_f$). Figure 6.21 has a correlation length equal to the fracture length and large heterogeneities ($\sigma/m = 2$). Figure 6.22 shows a perspective view of the same data. The variations from the homogeneous case are significant. Figure 6.23 shows a series of pressure distributions for a correlation length equal to the fracture length and $\sigma/m = 1.0$. In these figures, the shape of the pressure distributions in time are not simply elliptical.

Figures 6.24 and 6.25 give early and late time pressure contours for a homogeneous simulation. These can be compared with corresponding time pressure distributions for a moderate correlation length and a relatively low level of heterogeneity in Figures 6.26 and 6.27. Even modest levels of correlated heterogeneities result in severe alterations of drainage patterns.

6.4.4 Combined Anisotropies

Permeability anisotropies are common in low permeability reservoirs. Generally unfavorable results are associated with such anisotropies. Causes for permeability anisotropies are many, and have been reported on extensively ^{10, 259}. These include:

- o depositional variations in grain sizes and subsequent reorientation,
- o natural fractures which are dominantly oriented in one direction, and
- the current stress anisotropy which can cause minor permeability anisotropies without natural fractures, or larger anisotropies when the microfractures are opened preferentially parallel with the direction of maximum horizontal stress.

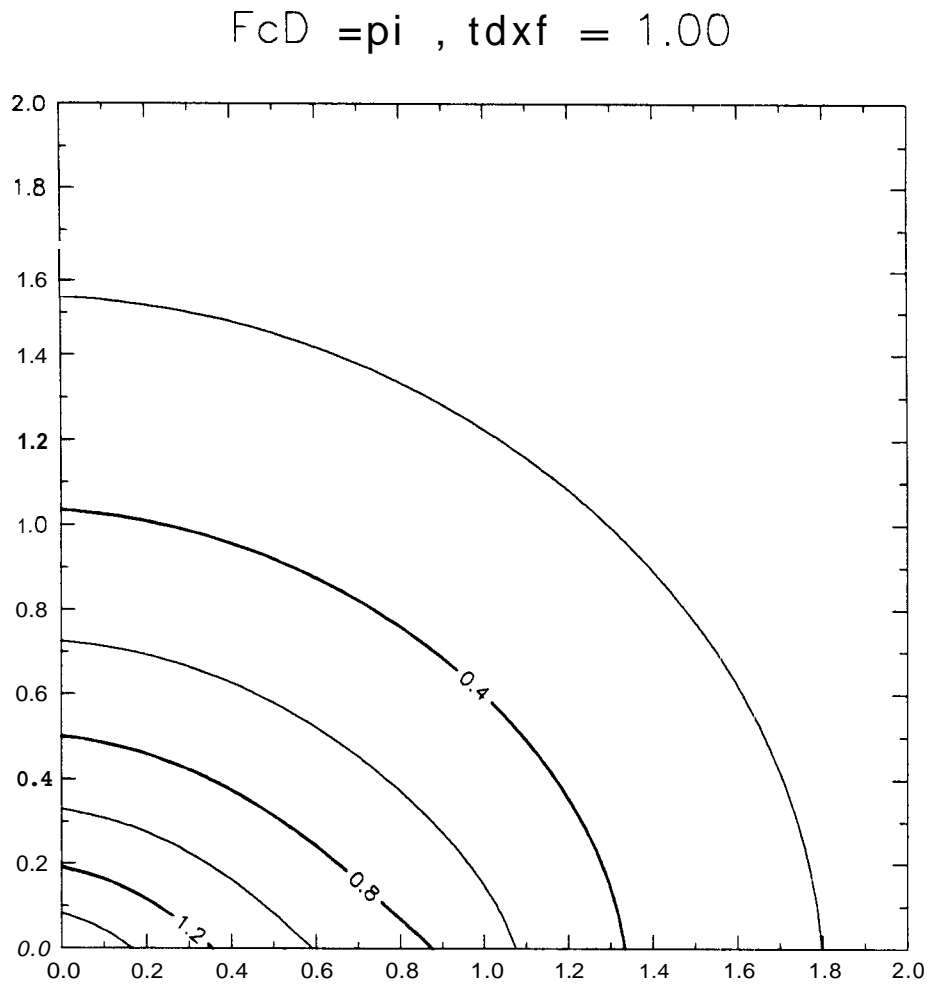


Figure 6.20: Contour Plot of Pressure Distribution for Short Scale Correlation and $\sigma/m = 2$

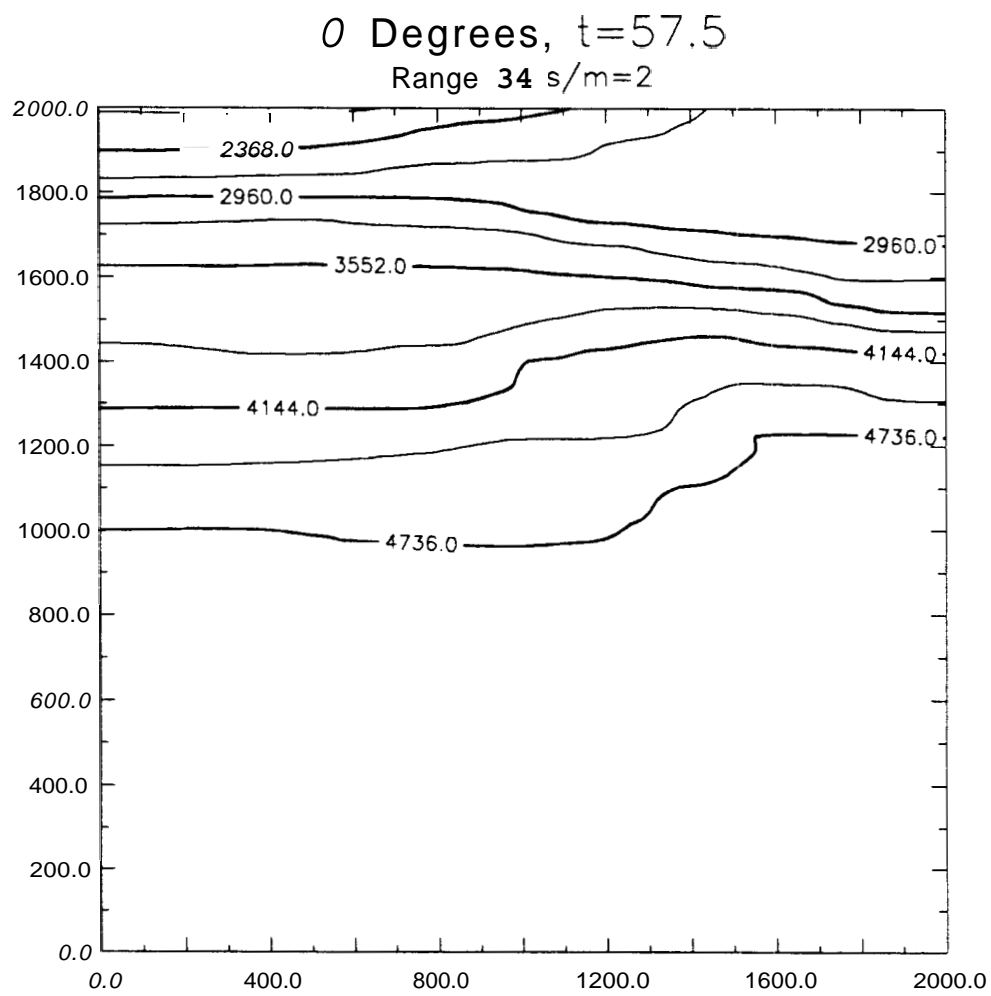


Figure 6.21: Contour Plot of Pressure Distribution for Medium Scale Correlation and $\sigma/m = 2$

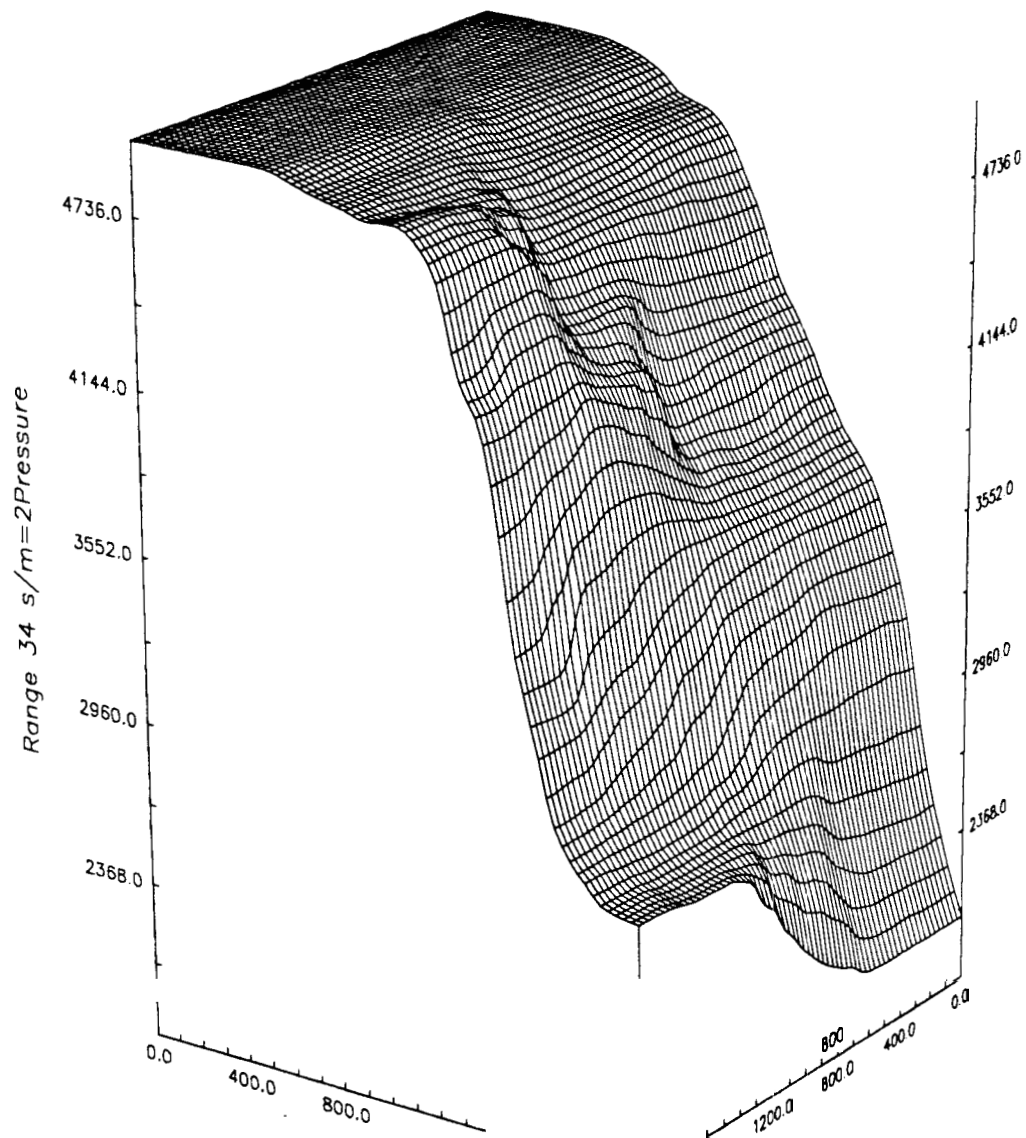


Figure 6.22: Perspective Plot of Pressure Distribution for Medium Scale Correlation and $\sigma/m = 2$

Pressure Distributions

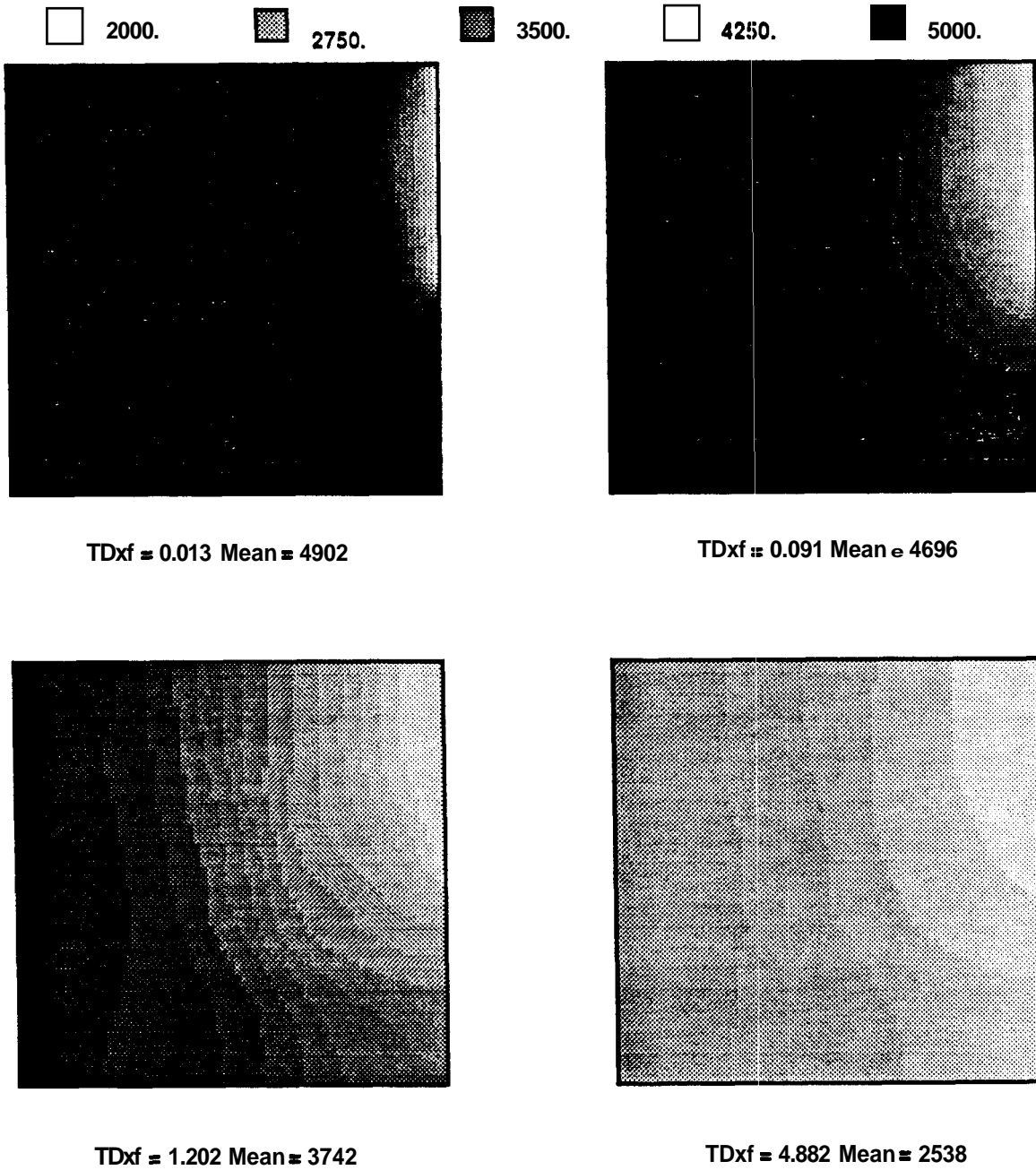


Figure 6.23: Greyscale Plot of Pressure Distribution for Moderate Scale Correlation and $a/m = 1$

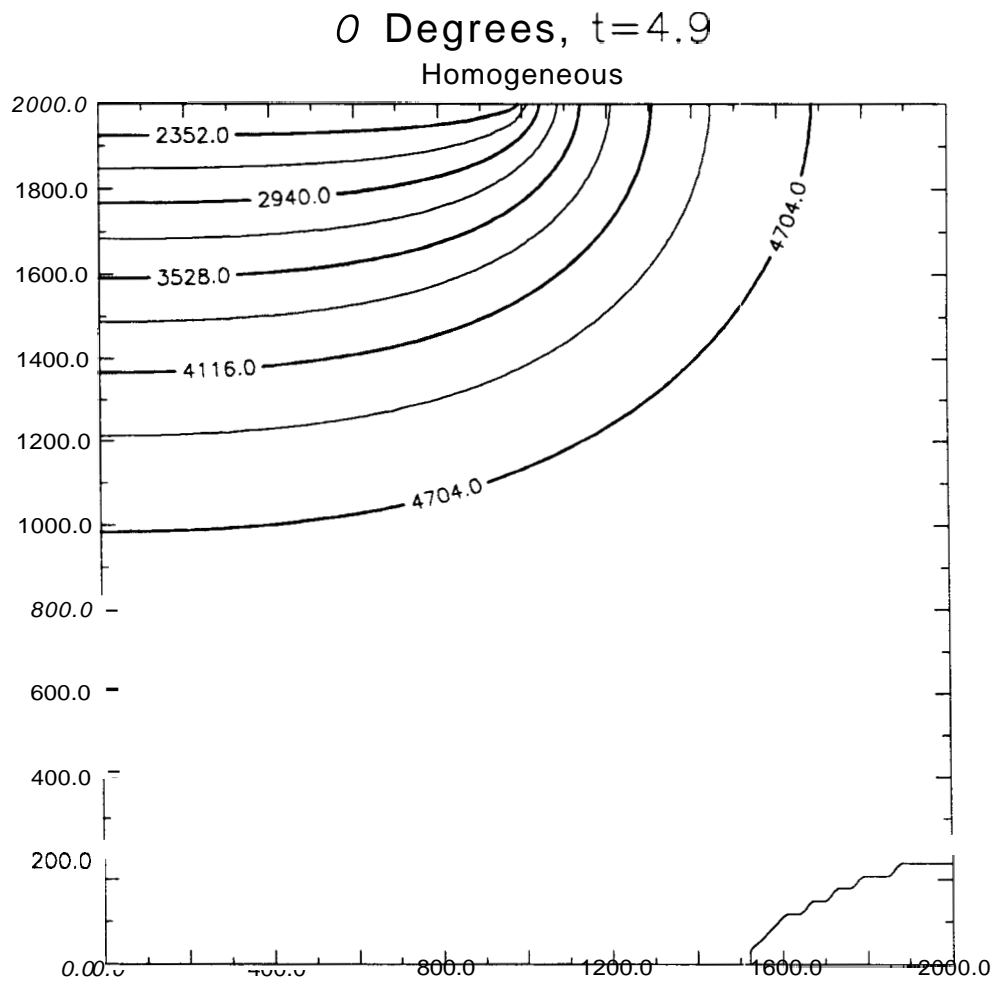


Figure 6.24: Early Time Pressure Distributions for Homogeneous Reservoir, $x_e/x_f = 2$

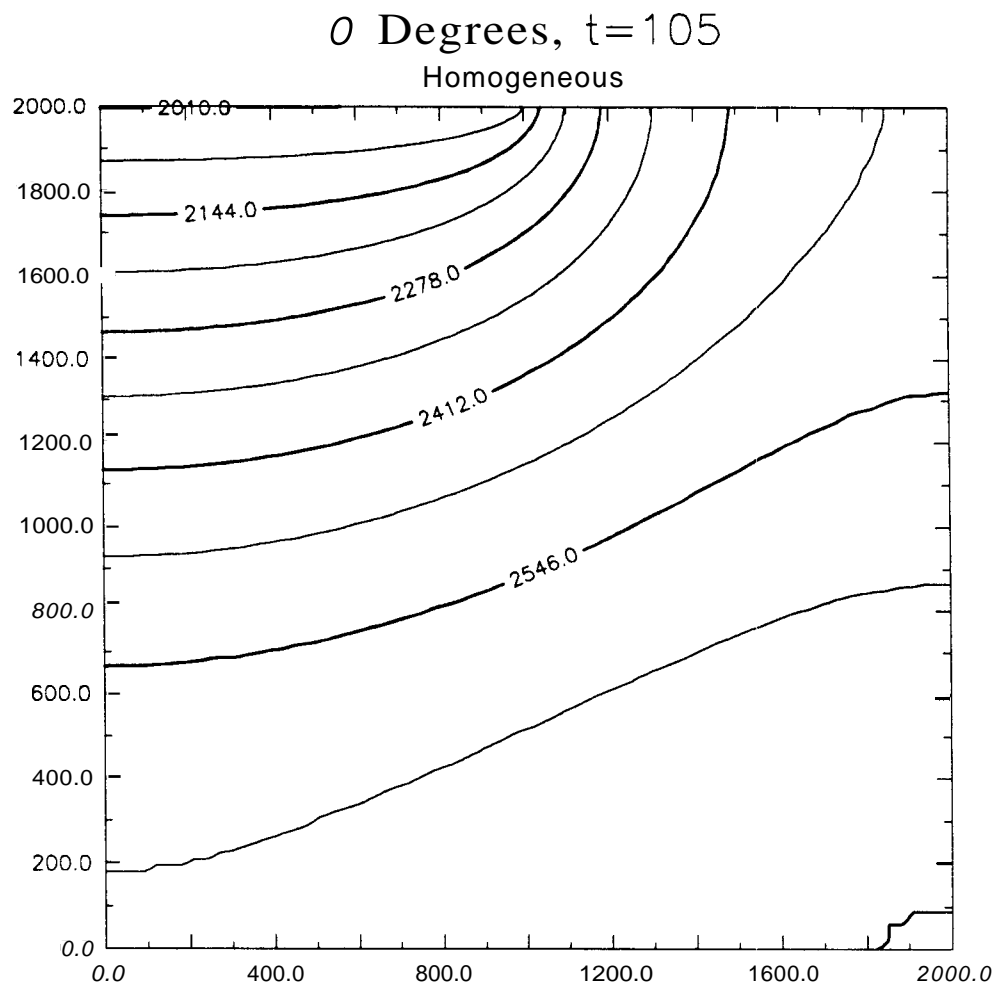


Figure 6.25: Late Time Pressure Distributions for Homogeneous Reservoir, $x_e/x_f = 2$

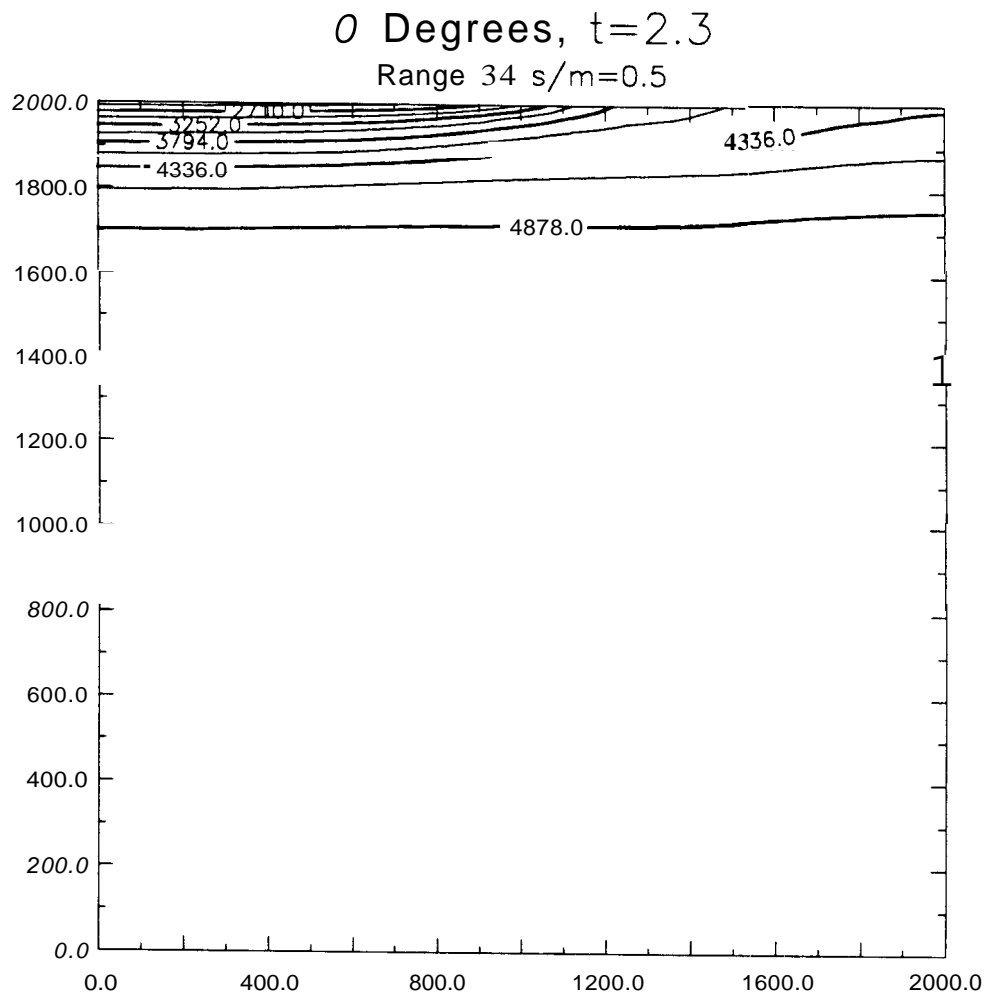


Figure 6.26: Early Time Pressure Distributions for Correlation Length= x_f , $a/m = 0.5$, $x_e/x_f = 2$

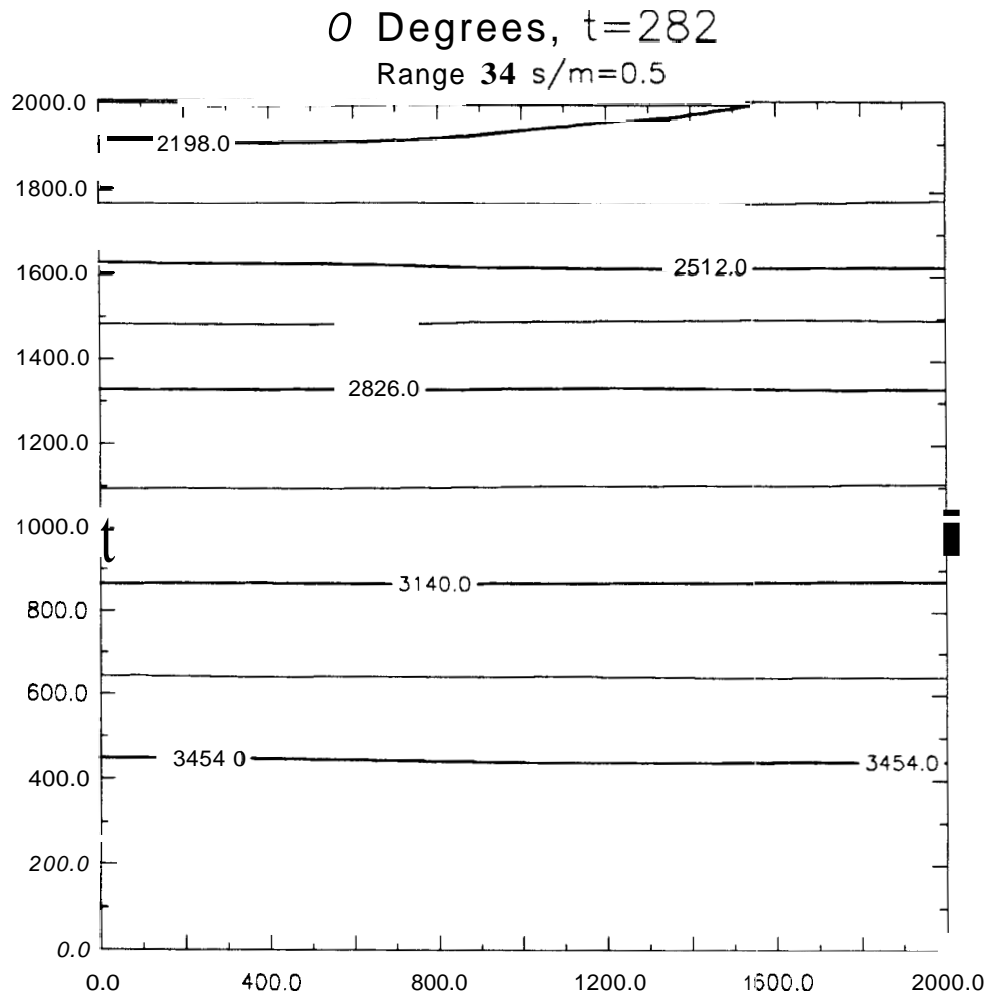


Figure 6.27: Late Time Pressure Distributions for Correlation Length= x_f , $\sigma/m = 0.5$, $x_e/x_f = 2$

Many problems can be handled by coordinate transforms^{75, 27} where the x and y axes are transformed as follows:

$$x' = x \sqrt{\frac{\bar{k}}{k_x}} = x \left(\frac{k_y}{k_x}\right)^{\frac{1}{4}} \quad (6.1)$$

$$y' = y \sqrt{\frac{\bar{k}}{k_y}} = y \left(\frac{k_x}{k_y}\right)^{\frac{1}{4}} \quad (6.2)$$

where the mean permeability \bar{k} is defined as:

$$\bar{k} = \sqrt{k_x k_y} \quad (6.3)$$

and the x and y axes are oriented along a major and minor permeability. The effective wellbore radius for an unfractured well can be shown to be:

$$r'_w = r_w \frac{\sqrt{k_y} + \sqrt{k_x}}{2k_x k_y^{\frac{1}{4}}} \quad (6.4)$$

when the major permeability axis is in the x -direction.

Presuming that the permeability is related to a current stress anisotropy, it can be seen that the fracture will propagate in the direction parallel with the maximum permeability and its reservoir response will be dominated in the transient flow period by the value of permeability perpendicular to the fracture, k_{min} . If the fracture was designed for the mean permeability, \bar{k} which could be obtained from a single well test, well performance would be overestimated. This is one of the reasons for fracture lengths obtained from well tests being shorter than the design calculations.

In the case of anisotropic permeability, the values of $t_{D,x}$ and p_D should have the values of permeability and fracture length replaced with \bar{k} and \bar{x}_f respectively, where:

$$\bar{x}_f = x_f \sqrt[4]{\frac{k_y}{k_x}} \quad (6.5)$$

The modification of fracture length for uniform flux fractures has been discussed by Branagan³⁴. Ben-Naceur and Economides²⁷ extended this quantitatively to include finite conductivity fractures with a revised definition of the dimensionless conductivity ratio originally defined by Agarwal⁶ as:

$$\bar{C}_r = \frac{k w_f \sqrt{\frac{k}{k_y}}}{\bar{k} x_f \sqrt{\frac{k}{k_x}}} = \frac{k w_f}{k_y x_f} \quad (6.6)$$

Figure 6.28 illustrates qualitatively how natural fractures give rise to anisotropic permeability parallel to the fracture azimuth. In this figure, the direction of the maximum horizontal compressive stress tends to close the fractures normal to it and allows those parallel to it to be open for fluid flow. Even if the original forces which created the joints and fractures are not the current ones, the net effect of current stresses will be to create anisotropic permeability which will be unfavorable for the hydraulically fractured well.

Figure 6.29 illustrates an experiment which shows the relative impact of both *geometric* anisotropy, i.e., different correlation ranges, and *local* anisotropies, i.e., differing values of k_x and k_y . The next series of flow simulations all use the same geostatistical realization for mean permeability distribution; the range is 34 blocks, $\sigma/m = 0.9$, and the geometric anisotropy is 4.0 (Figure 6.30). The realization with $k_x/k_y = 1$ is typical, and varies from the analytic solution only moderately. As k_x/k_y increases above 4 to 10, 50, and 100, a consistent displacement is observed. This shift is identical to that predicted by conventional theory. All of the local anisotropy effects can be converted to locally isotropic cases if k_x/k_y is known. Unfortunately, this cannot be done without multiple well interference tests. Comparing these realizations to the other heterogeneous cases clearly indicates that local anisotropy cannot be distinguished from many reservoir heterogeneities by a single well test. Determining k_x/k_y in an areally homogeneous reservoir is difficult enough. Without some understanding of the overall spatial correlation and heterogeneity of permeability, determining k_x/k_y from performance may be impossible. It must be kept in mind that these flow simulations and the analytic solutions represent the *entire* well life. Well tests rarely represent more than a few percent of this time range.

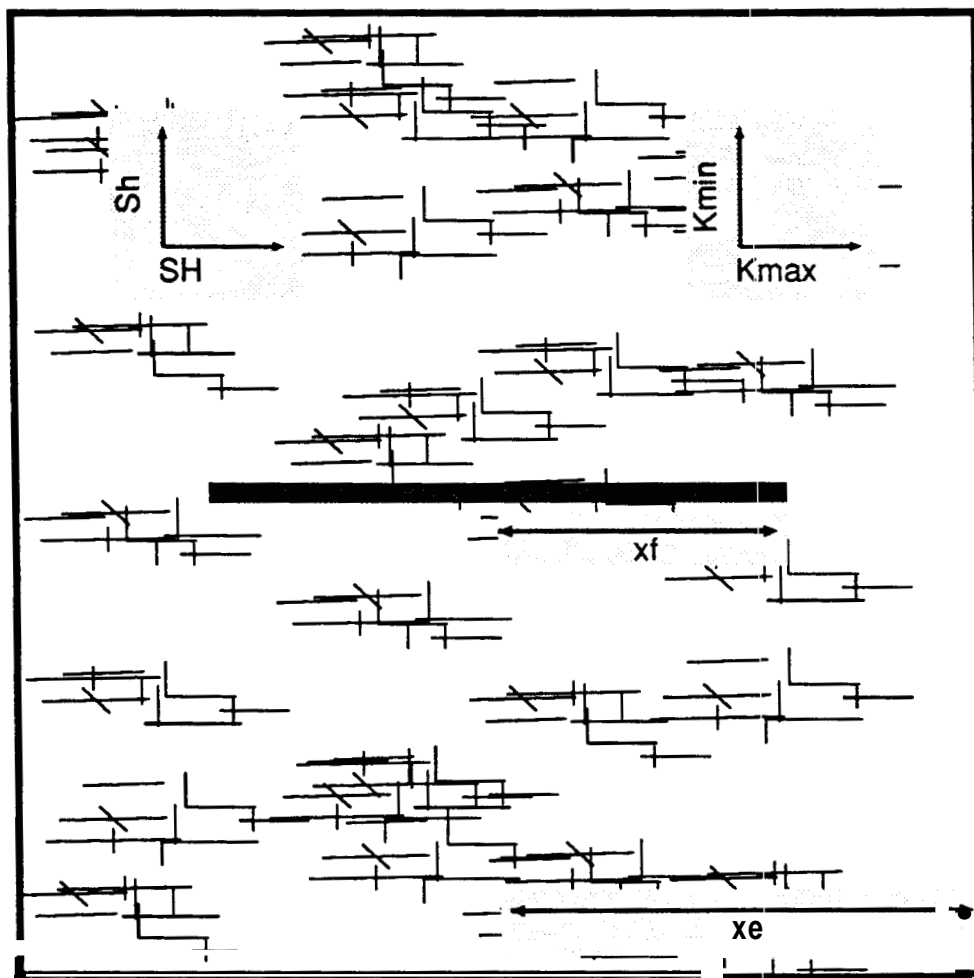


Figure 6.28: Conceptual Sketch of Natural Fracturing and Direction of *in situ* Stresses

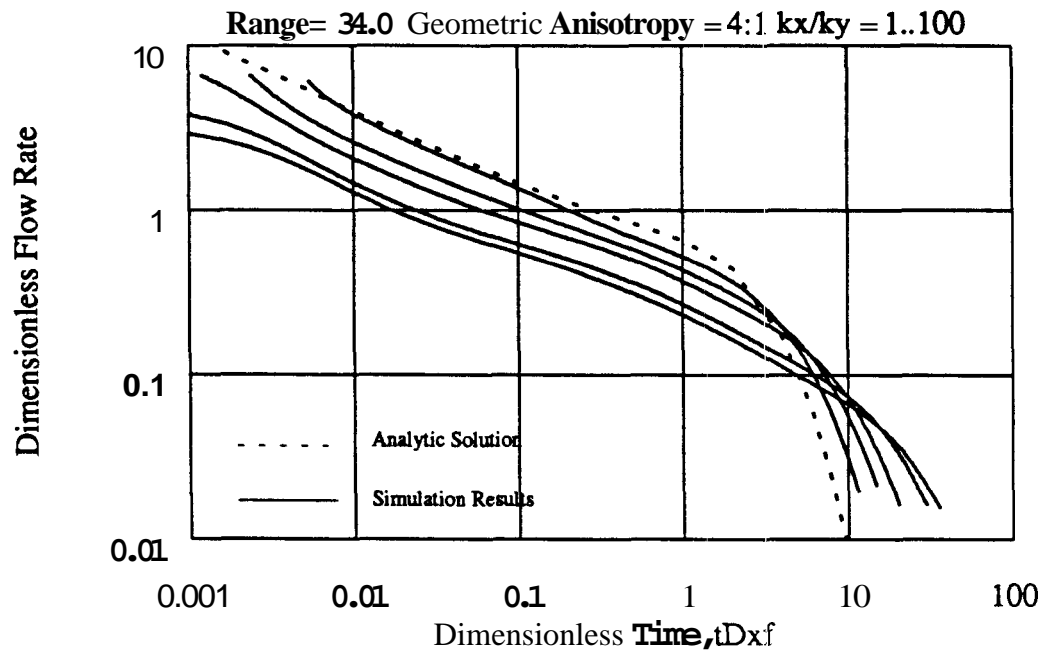


Figure 6.29: Flow Simulations With Correlation Range= 34, Local Anisotropies of $1 \leq k_x/k_y \leq 100$

6.4.5 Effects of Heterogeneities on Economic Optimization

Economic optimization for the heterogeneous cases is more complex than for the homogeneous case. Numerical simulation is required to generate the production forecast for each fracture length and well spacing. Larger areas must be simulated to account for fracture interaction. Because an economic optimum from the homogeneous case is already known, an initial estimate of the required fracture lengths and well spacings can be made. Each series of simulations applies to only *one* realization.

Figures 6.9–6.19 demonstrate when variability is most important and when flow simulations for heterogeneous cases will be close to the homogeneous forecasts. Additionally, the calculated early time production rates for each of these cases is usually *less* than the corresponding homogeneous case. This indicates that economic results will be *less* than indicated by the homogeneous case.

In the following example, a correlation range of 34 (equal to α_f) is used in the direction parallel to the fracture and 3.4 in the direction normal to the fracture.

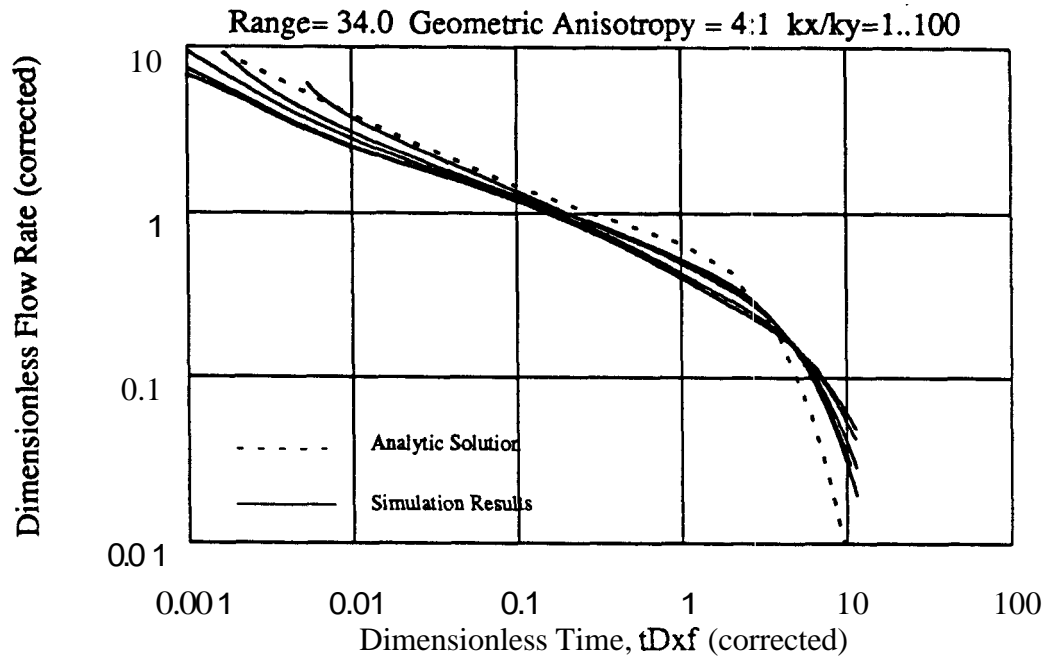


Figure 6.30: Flow Simulations With Correlation Range= 34, Adjusted for Local Anisotropy

Economic parameters from Table 5.2 are used. That case resulted in an optimum spacing of 160 acres and optimum fracture length of 400 feet (Figure 5.6). Further refinements of the case without spacing restrictions resulted in optimum values of 140 acres and 390 feet. The further refinement increased the NPV/acre by 1.5% to 587\$ /acre. The heterogeneous case indicated an economic optimum of 90 acres and 280 feet with a Net Present Value at 10% (NPV10) of 440\$ /acre. Using the indicated optimums from the homogeneous case (140 acres and 390 feet) resulted in a NPV10 of only 290 \$ /acre. For a moderate sized low permeability field of 2560 acres (four sections), the difference in NPV10 would be 384000\$.

For this specific example, accounting for reservoir heterogeneities would indicate that 10 more wells should be drilled in a 2560 acre field (28 compared to 18) with an additional capital cost of 4000000\$. This would be offset 2750000\$ by lower fracturing costs for all wells. The result would be an increase in NPV10 of 384000\$. However, the specific realization used to generate these production forecasts and economics is not the

actual distribution in the reservoir. In practice, a series of such realizations could be made, with economic optimizations for each case. The resulting optimal well **spacing** and fracture length should be estimated from the expected value of the realizations. Increased NPV compared to the homogeneous case would then be represented as a distribution.

If this distribution has a large variance, lower confidence should be attributed to the spacing and fracture length recommendations. This is because the optimum values are highly sensitive to the specific realization. This example demonstrates only *one* realization. Other examples with correlation lengths on the order of hydraulic fracture length have also resulted in lower economics and smaller recommended fracture lengths and well spacings.

6.5 Interference Testing

Relevant analytic research into interference between hydraulically fractured wells concentrates on two areas:

- o Pressure Transient Behavior—pressure responses at hydraulically fractured wells due to production at other wells. This can be used to elucidate fracture azimuth between producing wells, and combined interference effects on production.
- o Mechanical Interaction—how a propagating hydraulic fracture is affected by pressure drawdown (and accompanying reduction in stresses) due to production from a producing well. This is particularly important for infill drilling where **created** fracture lengths are large compared to interwell spacings. If differences in the principal components of horizontal compressive stress (S_H, S_h) is not much greater than net fracturing pressure and the infill well is aligned in the direction of S_H from the existing well, nonlinear growth of the infill well's hydraulic fracture and unequal wing lengths is predicted. When the infill well is aligned more than 20° from the existing well, little influence will be felt.

Geostatistical simulations have been reviewed for the first case with the goal of identifying how heterogeneities alter interference response. Analysis has demonstrated that certain theoretically possible measurements for the homogeneous case are impossible for reasonable heterogeneities in permeability. However, determination of fracture azimuth to within about 15° is generally possible.

Figures 6.31–6.32 compare interference tests in heterogeneous reservoirs with the analytic solutions derived in Chapter 4. Figure 6.31 shows simulation results for a reservoir with a heterogeneous reservoir with a moderate correlation length in permeability (one half of the fracture length and one quarter the interwell distance) and an intermediate level of overall heterogeneity ($\sigma/m = 1.0$). Modeled fracture azimuth is 30° . The overlay of the proposed type curve match does fit the 30° curve; however, variations are sufficiently large that the accuracy is ± 15 degrees. Both of the fractures have equal length and effectively infinite conductivity.

Figure 6.32 shows the result for a similar system with a 10:1 geometric anisotropy and the same level of heterogeneity. Interference results now fail to match any of the type curves. Realization dependent behavior affects the interference test more than it does the single well behavior. Because the direction of maximum continuity is in the direction parallel to the hydraulic fractures for this case, the variability in permeability between the wells is more pronounced.

6.5.1 Finite Conductivity Fractures

Interference models have been presented for infinite conductivity hydraulically fractured wells during the discussion on reservoir heterogeneities. Finite conductivity wells are less sensitive to reservoir heterogeneities at early times. During early times, the lower fracture conductivity behavior conditions the flow performance, essentially muffling some of the variability. However, all of the conclusions reached for the infinite conductivity fractures remain valid for the finite conductivity cases. The degree of variability at early times is decreased.

The simulation response of uncorrelated variations in permeability match the analytic solution for any value of fracture conductivity Figure 6.33 shows two cases with

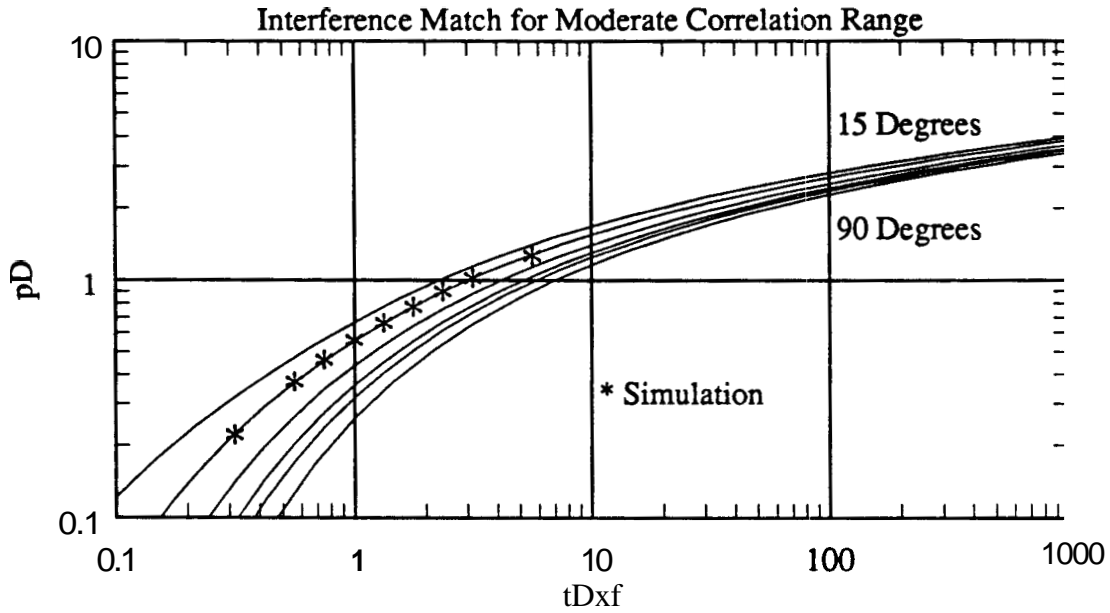


Figure 6.31: Interference Match in a Heterogeneous Reservoir, $r_D = 1, \theta = 30, a/m = 1.0$, Correlation Range= 17, Isotropic

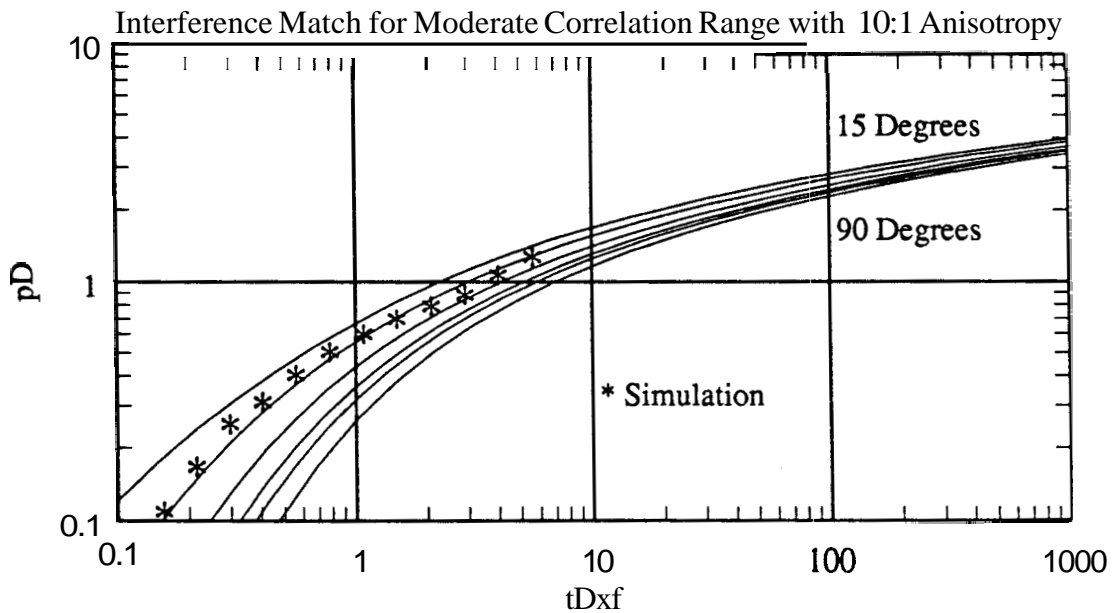


Figure 6.32: Interference Match in a Heterogeneous Reservoir, $r_D = 1, \theta = 30, \sigma/m = 1.0$, Correlation Range= 17, Geometric Anisotropy= 10:1

different fracture conductivities and the corresponding analytic solutions for a finite conductivity hydraulically fractured well in a closed reservoir. In each case, the correlation length of the permeabilities are equal to the fracture length, $x_e/x_f = 10/7$, and $\sigma/m = 1.1$. Both of the flow simulations represented in Figure 6.33 used the same

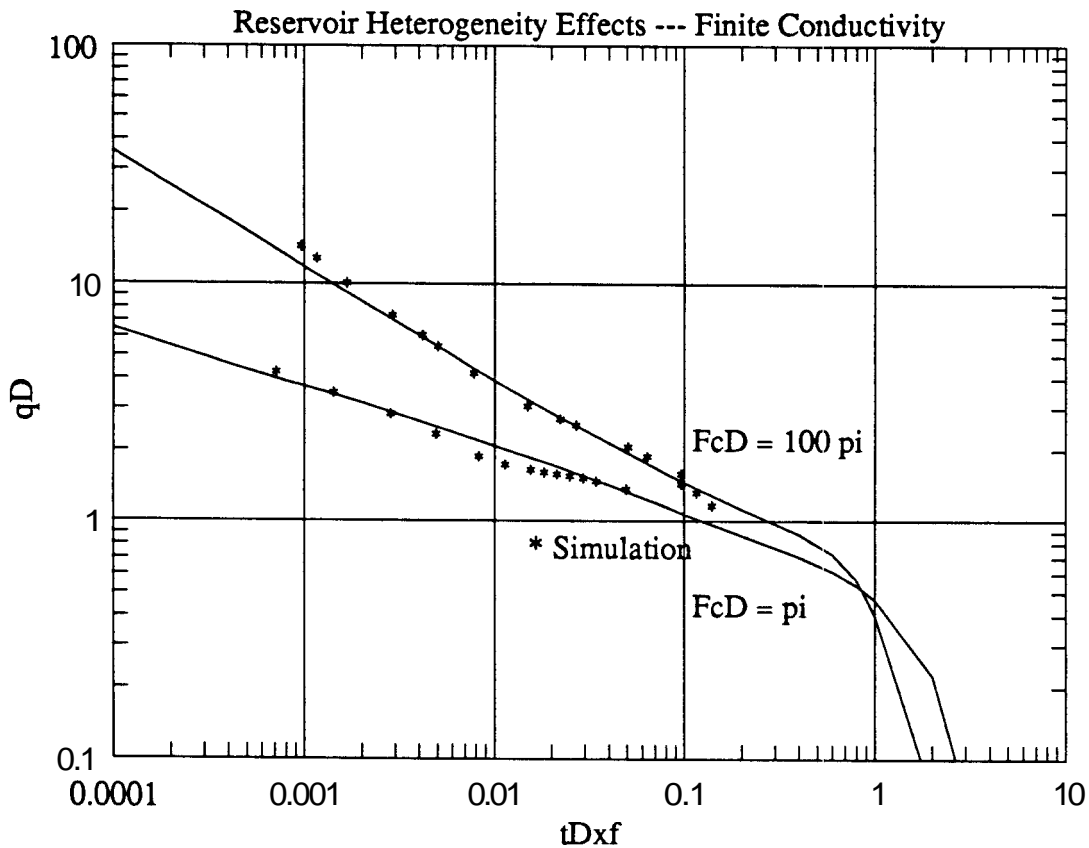


Figure 6.33: Effects of Finite Conductivity Fractures on Interference Tests in Heterogeneous Reservoirs

geostatistical realization for permeability distribution. Only the fracture permeability was varied. The heterogeneity effects are (in general) most substantial for the higher values of fracture conductivity.

6.6 Chapter Summary

The effects of correlated spatial heterogeneity on the flow behavior of hydraulically fractured wells has been demonstrated. The overall level of heterogeneity, spatial correlation range, and geometric anisotropy are all important. Correlation lengths of less than about one quarter of the fracture length do not appear important. When heterogeneity levels are **low** ($\sigma/m \leq 0.5$), the permeability field is relatively homogeneous and flow performance matches the homogeneous case. For larger levels of heterogeneity, variations in flow performance are realization dependent; the results from each geostatistical simulation vary significantly. Correlation range in the direction of the hydraulic fracture is particularly important. When the correlation range in the fracture direction is large compared to the fracture, the correlation in the normal direction is unimportant.

Geometric anisotropies are shown to have effects similar to permeability anisotropies. Correlated heterogeneities are shown to have generally unfavorable effects on performance. The economic value of characterizing reservoir heterogeneities was demonstrated with an example case.

Chapter 7

Summary and Recommendations

*Summary of results. Conclusions for each specific area of investigation.
Recommendations for further study.*

7.1 Summary of Results

Results have been presented for several problems dealing with hydraulically fractured wells. First, problems of determining hydraulic fracture azimuth were reviewed. Methods ranging from direct observation methods to indirect inference are available to predict *in situ* stress directions. These vary greatly in cost, accuracy, and ease of use. At shallow depths, direct observation using inflatable cameras or borehole video viewers is possible. Surface tilts can be used inexpensively at such depths. At greater depths, other geophysical techniques and cores are currently more attractive. As a first indication, wellbore eccentricity (as caused by stress induced spalling) gives an inexpensive measure with an accuracy ranging from ± 5 to 15° . Core methods have been frequently reported to have significant errors. However, incremental costs for core analysis is small, and cores can provide other worthwhile reservoir information. The choice of tests to determine the directions of S_H and S_h (and consequently, fracture azimuth) depend on the specific application. The stress directions determined must be integrated into the appropriate geological model to be valid.

A model of hydraulic fracture interference was developed for uniform flux fractures. Essentially no influence on the producing wells was observed, and as long as the uniform flux approximation is valid, fracture azimuth is unimportant. The uniform flux approximation is not good for many finite conductivity fractures, even in infinite media. When two fractures are sufficiently close to interfere with each other, the uniform flux model is even less applicable.

Laplace space formulations of several interference problems were developed. These included:

- o Interference between a finite conductivity or infinite conductivity hydraulically fractured active well and a line source observation well;
- o Interference at a line source well due to a nearby finite conductivity or infinite conductivity hydraulic fracture — either an active or observation well, or a natural fracture.
- o Interference between two finite conductivity or infinite conductivity hydraulically fractured wells. Either or both wells can be producers, with either constant pressure or constant rate constraints.
- For the case of two hydraulically fractured wells, either well can have skin effect or wellbore storage. The reservoir can be modeled as having either isotropic or anisotropic permeability. Natural fracture models may also be used.

Effects of interwell distance and azimuth were reviewed in detail. Effects of fracture lengths and fracture conductivities were also presented. The effects of fracture azimuth in a closed system were also studied and shown to be more substantial than in the uniform flux case.

Economic optimization of hydraulic fracture length and well spacing was presented. The value of knowing fracture azimuth and of knowing permeability anisotropy was presented for example cases. The effects of reservoir heterogeneities on the optimal fracture length and well spacing were also presented. Spatial variations in permeability were shown to have significant effects on reservoir performance for hydraulically fractured wells. This is particularly true when the correlation length of the

heterogeneity is on the order of the fracture, when overall heterogeneities are large, and when significant geometric anisotropies are present.

7.2 Conclusions

Conclusions are summarized by topic, including:

- Interference testing of finite conductivity wells,
- Optimization of fracture length and well spacing, and
- Effects of reservoir heterogeneities.

Recommendations for further work are given in Section 7.3.

7.2.1 Interference Testing for Finite Conductivity Wells

1. Vertical finite conductivity hydraulic fractures at observation wells have a significant impact on observation well response. Fractures at the active well also influence observation well response. Most significant effects are for $r_D < 3$.
2. Hydraulic fracture conductivity at the observation well has a small impact on the response. However, fracture conductivity at the active well is important in the response and significant errors in azimuth estimation can occur when fracture conductivity is neglected at the active well. Nothing in the shape of the observation well response indicates the conductivity of the active well. Since it is necessary to know both hydraulic fracture lengths in practice, the fracture conductivities and lengths for both wells must be determined independently.
3. Different fracture lengths at observation and active wells alter the duration and magnitude of fracture interference. For values of $\Lambda_{[AO]} = x_{fa}/x_{fo}$ greater than 1.0, accounting for the active well fracture is necessary for values of r_D that are greater than when $\Lambda_{[AO]} = 1$. For $\Lambda_{[AO]} < 0.5$, the active well can be approximated as a line source well with little loss of accuracy for large values of

$(k_f b_f)_D$. Lower fracture conductivities at the active well are better approximated by a line source response using an effective wellbore radius including the pseudo-steady state skin effect.

4. For a fixed value of r_D , the observation well response is insensitive to azimuth for $\theta > 50^\circ$. Sensitivity to fracture azimuth is essentially independent of fracture conductivity for practical cases.
5. Interference response at the active well is much less pronounced than at the observation well. Sensitivity to fracture azimuth is only present for small angles and nearby wells. Except for values of $r_D < 1$, this effect can be neglected for active wells.
6. Active and observation well fluxes vary dramatically for interference cases from typical models.
7. Constant pressure production at the active well can be interpreted at the observation well by a combination of conventional techniques and these results.

7.2.2 Optimization of Fracture Length and Well Spacing

1. Coupling economics with reservoir engineering can be accomplished for a given set of economic parameters. Optimum fracture length and well spacing can be determined for many alternatives.
2. Hydraulic fracture azimuth becomes important in determining optimum fracture length and well spacing whenever azimuth is important in well performance as concluded in the prior series of conclusions (Section 7.2.1).
3. The primary mechanism for increasing Net Present Value (NPV) by knowing fracture azimuth is delaying interwell interference. This applies when the created fracture lengths are large compared to interwell distances.

4. The primary mechanism for improved NPV by knowing the direction of permeability anisotropy is modification of fracture length and well spacing. Fracture azimuth must be known to utilize the permeability anisotropy information.
5. Reservoir heterogeneities can significantly alter the optimal fracture length and well spacing. This methodology provides a quantitative framework for estimating the value of determining the value of characterizing reservoir heterogeneities.

7.2.3 Effects of Reservoir Heterogeneities

1. Correlated spatial variability in permeability effects hydraulically fractured well performance. No 'effective permeability' mechanism can be substituted for flow simulations of realizations of conditioned random fields.
2. Overall magnitude, correlation length, and geometric anisotropy of permeability heterogeneity each contribute to a well performance which may be significantly different from that of the homogeneous case.
3. Correlation lengths of less than about one fourth of the hydraulic fracture half length have minimal effect on performance, except for very high levels of heterogeneity. Uncorrelated permeability variations, or white noise, has negligible performance effects unless the heterogeneity level is extremely large.
4. Heterogeneity level is less important than correlation range in its effects on performance. When the level is low ($\sigma/m < 0.5$), correlation length is unimportant because the permeability field is fairly homogeneous. Values of $\sigma/m > 2$ have major effects on performance, for any significant correlation length.
5. Correlation lengths on the scale of the hydraulic fracture length are most important. The correlation length in the direction of the hydraulic fracture is also important. When the direction of maximum continuity parallels the hydraulic fracture, the correlation length in the normal direction has a secondary impact.

6. When heterogeneity levels are large, geometric anisotropies magnify the impact of correlation length. This is most noticeable in interwell interference.
7. Geometric anisotropies have effects similar to local permeability anisotropies. Correlations designed for analyzing the local anisotropy cases may also be used for the cases of geometric anisotropy.
8. Reservoir heterogeneities are important for reservoir management decisions for single phase hydraulically fractured wells. Observations include:
 - (a) Critical ranges of heterogeneities for economic impact are the same as those that affect performance.
 - (b) The value of characterizing reservoir heterogeneities may be quantified. Comparing results of optimal development plans for a given set of heterogeneities with the results of plans from a homogeneous analysis can be used. If identical fracture lengths and well spacings are obtained over a wide range of reasonable heterogeneities, no significant value is obtained from the characterization effort. If different reservoir management decisions are indicated, these can be simulated on another realization compared to the proposed decisions from the homogeneous case. The difference in resulting NPVs is the estimated economic value of reservoir characterization.
 - (c) When the direction of maximum principal continuity is in the direction of maximum compressive stress, optimal fracture lengths and well spacings are both *smaller* than would be indicated for the homogeneous case.

Heterogeneity in permeability for low permeability and gas reservoirs has been infrequently characterized. Correlation lengths of permeability probably range from tens to hundreds of meters by inference from reported outcrop studies and higher permeability oil reservoirs. This is the same scale as typical hydraulic fracture lengths; therefore, the issue of reservoir characterization for low permeability reservoirs is of substantial practical concern.

7.3 Récommendations for Further Study

1. Solve the mechanical interaction problem.—Several Stanford researchers in Geophysics, Geology, and Applied Earth Sciences are working on closely related problems dealing with hydraulic fracturing or natural fractures. Quantification of mechanical interaction is important when the angle and distance between wells is small. This will also be important for attempts to **link** wells by hydraulic fracturing, such as for waterflooding anisotropic reservoirs, geothermal applications such as the ‘Hot Dry Rock’ project, and well control operations.
2. Extend heterogeneity **work** to two phase systems.—Impacts of spatial characterization will be important for fluid displacement projects including waterflooding and Enhanced Oil Recovery. Quantification of the economic value of such efforts could spur more efforts in characterization, increasing project profitability and ultimate product recoveries.
3. Extend characterization **work** to three dimensions.—Two dimensional models were used for the hydraulically fractured case because the wide areas of the fracture face tend to average variability in the vertical dimension for near well flow. Fluid displacement projects will be more sensitive to such variations. While conditional simulations will still be useful, a technique such as **3D** Indicator simulation will probably be more practical than the turning bands method.

Appendix A

Fracture Interaction Issues

Hydraulic fracturing and rock mechanics. Potential interference between stress changes due to production from an existing hydraulically fractured well and the propagation direction and wing length of an infill well's hydraulic fracture. Advantages and disadvantages of interference. Potential solutions described.

A.1 Mechanical Interaction of Hydraulic Fractures

The motivation of this area of research comes from field observations of infill drilling low permeability reservoirs. In numerous instances when the design fracture length was a large fraction of the interwell distance, pressure or fluid communication has occurred with existing hydraulically fractured wells. In some fields, it is common to shut in offset wells for a few days before a hydraulic fracture treatment to avoid such problems. It is unlikely that more than a small fraction of these cases could be explained by the chance intersection of what are thought to be parallel fracture planes. It has been widely speculated that the hydraulic fracture being generated actually curves in the presence of the pore pressure drawdown due to previous wells. Unfortunately, most documented cases are in fields which have numerous natural fissures and are highly anisotropic. The resulting performance of the wells will generally

be less than anticipated. Since potential damage to one or the other wells may result, this area has received little attention.

The study of the interaction of cracks in solids has an extensive following in diverse fields. In Earth sciences, natural fractures occur on many scales and appear to follow similar principles. Poroelastic effects can often be neglected in such efforts as the time scale for fracture extension is usually long compared to that for pressure diffusion²⁰⁷. In hydraulic fracturing, the entire process occurs in a few hours and poroelastic effects will almost always be substantial^{54, 55}. Primary questions include:

- o What are the effects of a region of pressure depletion on the earth stresses?
- o To what extent will these alter the direction and extent of hydraulic fracture propagation?

A.1.1 Earth Stress Effects

The stresses which are important for fracture growth are the *total* stresses, not just the net effective stress. Total stresses for a poroelastic medium are a function of pressure distributions everywhere. Except for overpressured reservoirs and friable sands, these effects are routinely neglected in pressure transient problems. However, the stress distribution must be known in order to predict fracture growth. Solving the total stress distributions in poroelastic media due to production or injection from a hydraulically fractured well is required to know the stress distributions. There are three possible solution methods that have been identified and will be briefly described:

- Use a finite element model. This procedure requires a large simulation effort and is computationally intensive. Since the stress distributions are actually just the input to the fracture propagation work, it is desirable to minimize the effort required for such input generation.
- o Approximate the stresses with a series of Eshelby transformation strains^{83, 41}. Although Eshelby transformation strains are useful for modeling the stress effects caused by an inclusion of material inhomogeneity, their superposition in space

to determine stress distributions requires *a priori* knowledge of these stresses. One approach might be correlating finite element model results with those of the inclusion approximations.

- Solve the problem analytically. The stresses in space due to a line source well are known analytically and can be expressed using Green's functions. Known fluxes from previous solutions of the finite conductivity fracture performance models could be used to determine the stresses due to an entire fracture.

A.1.2 Predicting Fracture Growth

Virtually all fracture models in existence assume linear fracture growth. One exception is the work of Narendran 193–191 and its extension by Chin 41, 42 at the Massachusetts Institute of Technology. Their model predicts curvilinear growth and has been provided to the Stanford Center for Reservoir Forecasting on the MIT Resource Extraction Laboratory's computer system. The program assumes Mode I stress type at the fracture tip, i. e. $K_{II} = 0$. This criterion may be used to determine the path taken by an extending fracture. Although numerous runs have been completed, results are not presented in this dissertation. Results are interesting and warrant further study.

Appendix B

Calculation Improvements

B.1 Improving Solution Performance

Several methods can be used to decrease the number of computations for solving Equation 4.21. These include:

1. Methods to speed the matrix solution.
2. Methods to reduce the number of calculations required to fill the matrix.
3. Methods to eliminate matrix calculations entirely.

B.1.1 Reducing Matrix Order

Most of the matrices have a form which resemble:

$$\begin{vmatrix} A_{11} & A_{12} & A_{13} & 1 \\ A_{21} & A_{22} & A_{23} & 1 \\ A_{31} & A_{32} & A_{33} & 1 \\ 1 & 1 & 1 & 0 \end{vmatrix} \begin{vmatrix} q_1 \\ q_2 \\ q_3 \\ p \end{vmatrix} = \begin{vmatrix} x_{D1} \\ x_{D2} \\ x_{D3} \\ 1 \end{vmatrix} \quad (\text{B.1})$$

For this example case, $j = i = 3$, and the j equations are used to solve the case of

$$\bar{p}_{wD}(s) + \sum_{i=1}^3 A_{ij} \cdot x_{Di} \quad (\text{B.2})$$

for $i = 1, 3$. The fourth equation arises directly from a flow constraint that:

$$\sum_{i=1}^n q_i = 1 \quad (\text{B.3})$$

For clarity, these terms are always separated in the main text. In practice, the matrix order is reduced by including the constraint of Equation B.3 in the matrix. This has the combined advantages of decreasing storage requirements, decreasing computation time, and removing zero (0) terms from the main diagonal. Rewriting Equation B.3 for the case of $j = 3$:

$$q(3) = 1 - \sum_{i=1}^2 q(i) = 1 - q(1) - q(2) \quad (\text{B.4})$$

Substituting into the equations and removing extraneous nomenclature:

$$\begin{aligned} A_{11}q_1 + A_{12}q_2 + A_{13}(1 - q_1 - q_2) + P &= x_1 \\ A_{21}q_1 + A_{22}q_2 + A_{23}(1 - q_1 - q_2) + P &= x_2 \\ A_{31}q_1 + A_{32}q_2 + A_{33}(1 - q_1 - q_2) + P &= x_3 \end{aligned} \quad (\text{B.5})$$

Gathering like flux terms:

$$\begin{aligned} (A_{11} - A_{13})q_1 + (A_{12} - A_{13})q_2 + P &= x_1 - A_{13} \\ (A_{21} - A_{23})q_1 + (A_{22} - A_{23})q_2 + P &= x_2 - A_{23} \\ (A_{31} - A_{33})q_1 + (A_{32} - A_{33})q_2 + P &= x_3 - A_{33} \end{aligned} \quad (\text{B.6})$$

This can be expressed in the reduced matrix form as:

$$\begin{vmatrix} (A_{11} - A_{13}) & (A_{12} - A_{13}) & 1 \\ (A_{21} - A_{23}) & (A_{22} - A_{23}) & 1 \\ (A_{31} - A_{33}) & (A_{32} - A_{33}) & 1 \end{vmatrix} \begin{vmatrix} q_1 \\ q_2 \\ P \end{vmatrix} = \begin{vmatrix} x_{D1} - A_{13} \\ x_{D2} - A_{23} \\ x_{D3} - A_{33} \end{vmatrix} \quad (\text{B.7})$$

The final value of the flux is solved by substitution into Equation B.3.

B.1.2 Reducing Matrix Building Requirements

Depending on the value of s , the time required to calculate all of the matrix components in a matrix such as 4.21 may take 20–40 % of the total computation time,

if done in a 'brute force' manner. Numerous simplifications accelerate matrix filling, including:

- o Many of the terms which are added to the main A_{ij} terms are independent of s . These can be calculated once and added again for each Stehfest step. This requires a small increase in the total storage requirements.
- Integral evaluation for the integrals of the form $\int_0^x K_0(u)du$ are replaced by $\pi/2$ for values of x greater than 20.
- o The $n \times n$ matrix components which require integral evaluation have only $2n - 1$ integrals. The first column and row contain the required values.
- o values of $[k_f b_f]_{AO} = 1$, or $\Lambda_{[AO]} = 1$ reduce the required number of calculations because many interference terms becomes identical.

B.1.3 Early and Late Time Approximations

At very early times, interference terms are negligible. For the interference case with finite conductivity wells, Equation 4.21 may be reduced in size by 75%. At such early times, the active and observation wells behave independently, and infinite acting solutions apply. Duration of this time may be observed from Figures 4.14-4.28 to depend on δ and r_D . Typical values for the end of the infinite acting period range from $t_{Dxf} = 0.01-0.1$.

At late times, flux distributions for both wells stabilize at dimensionless times on the order of $t_{Dxf}/r_D^2 > 10$. These flux distributions can be retained to calculate wellbore pressures at the active and observation wells directly. This may be done either in the Laplace or real space formulations. At late times, the active well pressure response may be approximated by a line source well with an effective wellbore radius. The 'skin' associated with the effective wellbore radius arises both from the value of $(k_f b_f)_D$ and the distance and angle to the interference well.

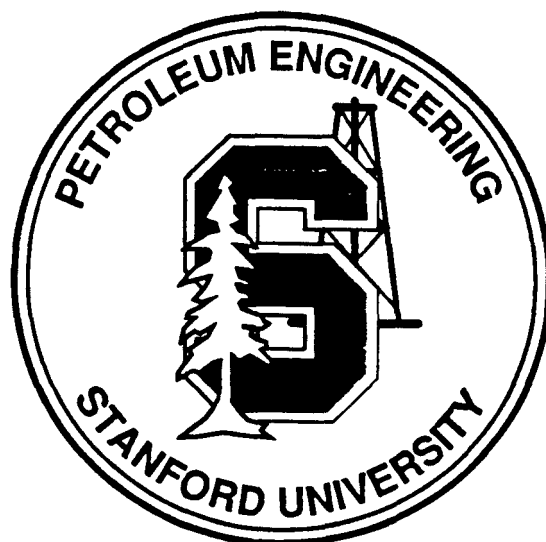
Colophon

The colophon of a book is a traditional embellishment of the last page. It contains a printer's mark or enscription, date, location, and related information regarding publication. The word is from the Greek, either:

κολοφων for the peak, or completion, or

κολοφως the furthest island in the Greek chain of islands.

This dissertation has **been** prepared according to the guidelines promulgated by the Office of Graduate Studies at Stanford University. The document was prepared using **L^AT_EX** on the Petroleum Engineering Department's VAX 11/750, Apollo 4000, and Apollo 590 computers. Graphs were prepared using **GRAPH** (a Stanford graphics package) and **GRIDCON** (a Dynamic Graphics product). Other figures were written directly in **PostScript**. Most calculations were done on the School of Earth Sciences Gould 1080 or Apollo 10000 computers. Extensive use of IMSL subroutines simplified programming efforts. Numerical flow simulations were done using the Computer Modeling Group's **IMEX** software. Petroland's **AUTOMATE** was used for pressure transient solutions. Equation references from Abramowitz and Stegun's Handbook ⁴ are cited in boldface. Program names are typically given in **sans serif** font.



Bibliography

- [1] A. A. Abdel-Mota'al, "*Detection and Remedy of Behind Casing Communication During Well Completion*", SPE 11498, presented at the SPE Middle East Oil Technical Conference held in Manama, Bahrain, March, 1983.
- [2] E. O. Abobise and D. Tiab, "*Determining Fracture Orientation and Formation Permeability From Pulse Testing*", SPE 11027, presented at the 57th Annual Meeting of the Society of Petroleum Engineers held in New Orleans, LA, September, 1982.
- [3] I. S. Abou-Sayed and C. M. Pearson, "*Evaluation of Fracturing Results in Deviated Wellbore Through Onsite Pressure Measurement and Post-Fracture Temperature Survey*", SPE 13616, presented at the 60th Annual Meeting of the Society of Petroleum Engineers held in Las Vegas, NV, September, 1985.
- [4] M. Abramowitz and I. A. Stegun, *Handbook of Mathematical Functions*, Dover Publications, ninth edition, (1970).
- [5] R. Agarwal, R. Al-Hussainy, and H. J. Ramey Jr., "*An Investigation of Wellbore Storage and Skin Effects in Unsteady Liquid Flow : 1. Analytical Treatment*", *Society of Petroleum Engineers Journal*, 279-290, (September 1970).
- [6] R. G. Agarwal, R. D. Carter, and C. B. Pollock, "*Evaluation and Prediction of Performance of Low-Permeability Gas Wells Stimulated by Massive Hydraulic Fracturing*", *Journal of Petroleum Technology*, 362-372, (March 1979).

- [7] U. Ahmed, J. F. Schatz, A. S. Abou-Sayed, and A. H. Jones:, ‘*Step By Step Approach to Hydraulic Fracture Treatment Design, Implementation, and Analysis for Tight Gas Sands*’, SPE 10829, presented at the Unconventional Gas Recovery Symposium held in Pittsburgh, PA, May, 1982.
- [8] F. G. Alabert:, “*The Practice of Fast Conditional Simulaiions Through the LU Decomposition of the Covariance Matrix*”, *Mathematical Geology*, 19(5):369–385, (1987).
- [9] J. N. Albright and C. F. Pearson:, “*Acoustic Emissions as a Tool for Hydraulic Fmcture Location: Experience at the Fenton Hill Hot Dry Rock Site*”, *SPE Journal*, 525–530, (August 1982).
- [10] W. G. Alexander:, “*Geologic Controls on Producibility at Clear Creek Field, Uinta County, Wyoming*”, SPE 15528, presented at the Annual Meeting of the Society of Petroleum Engineers held in New Orleans, LA, October, 1986.
- [11] O. A. Allen:, “*A Practical Approach to Defining Reservoir Heterogeneity*”, SPE 3608, presented at the 46th Annual Meeting of the Society of Petroleum Engineers held in New Orleans, LA, October, 1971.
- [12] T. O. Anderson and E. J. Stahl:, “*A Study of Induced .Fracturing Using an Instrumental Approach*”, *Journal of Petroleum Technology*, 14:261–267, (February 1967).
- [13] U. G. Araktingi and F. M. Orr Jr.:', “*Viscous Fingering in Heterogeneous Porous Media*”, SPE 18095, presented at the 63rd Annual Meeting of the Society of Petroleum Engineers held in Houston, TX, October, 1988.
- [14] A. Arya, T. A. Hewett, R. Larson, and L. W. Lake:, “*Dispersion and Reservoir Heterogeneity*”, SPE 14364, presented at the 60th Annual Technical Conference and Exhibition held in Las Vegas, NV, September, 1985.
- [15] E. A. Babcock:, “*Measurement of Subsurface Fractures from Dipmeter Logs*”, *AAPG Bulletin*, 62(7):1111–1126, (July 1978).

- [16] B. Barker and H. J. Ramey Jr., “*Transient Flow to Finite Conductivity Vertical Fractures*”, SPE 7489, presented at the 53rd Annual Meeting of the Society of Petroleum Engineers held in Houston, TX, October, 1978.
- [17] B. A. Barna and J. T. Patton:, “*Permeability Damage **from** Drilling Fluid Additives*”, SPE 3830, presented at the Rocky Mountain Regional Meeting held in Denver, CO, April, 1972.
- [18] C. A. Barton, M. D. Zoback, and K. L. Burns:, “*In-Situ Stress Orientation and Magnitude at the Fenton Geothermal Site, New Mexico Determined **from** Wellbore Breakout*”, *Geophysical Research Letters*, 15(5):467–470, (May 1987).
- [19] A. S. Batchelor, R. Baria, and K. Hearn:, “*Monitoring the Effects of Hydraulic Stimulation by Microseismic Event Location: A Case Study*”, SPE 12109, presented at the 58th Annual Meeting of the Society of Petroleum Engineers held in San Fransisco, CA, 1983.
- [20] M. L. Batzle, G. Simmons, and R. G. Hipkin:, “*Microcrack Closure Under Stress: Direct Observations*”, *J. Geophys. Res.*, 85:7072–7090, (1980).
- [21] J. Bear:, (1987), Personal communication at Stanford University.
- [22] J. Bear:, *Dynamics of Fluids in Porous Media*, American Elsevier, New York, (1972).
- [23] S. H. Begg and R. R. Carter:, “*Assigning Effective Values to Simulator Grid-Block Parameters Heterogeneous Reservoirs*”, SPE 16754, presented at the 62nd Annual Meeting of the Society of Petroleum Engineers held in Dallas, TX, September, 1987.
- [24] R. M. Beirute:, “*All Purpose Cement-Mud Spacer*”, SPE 5691, presented at the SPE Formation Damage Symposium held in Houston, TX, 1976.
- [25] J. S. Bell and D. I. Gough:, “*Northeast-Southwest Compressive Stress in Alberta: Evidence **from** Oil Wells*”, *Earth Planetary Science Letter*, 45:475–482, (1979).

- [26] F. Ben Marek:, “*Permeability Loss During Depletion of Reservoirs*”, SPE 8433, presented at the 54th Annual Meeting of the Society of Petroleum Engineers held in Las Vegas, NV, March, 1979.
- [27] K. Ben-Naceur and M. J. Economides:, “*Production from Naturally Fissured Reservoirs Intercepted by a Vertical Hydraulic Fracture*”, SPE 17425, presented at the SPE California Regional Meeting held in Long Beach, CA, March, 1988.
- [28] C. O. Bennett, N. D. Rosato, and A. C. Reynolds Jr.:', “*Influence of Fracture Heterogeneity and Wing Length on the Response of Vertically Fractured Wells*”, SPE 9886, presented at the SPE/DOE Symposium on Low Permeability Gas Reservoirs held in Denver, CO, May, 1981.
- [29] D. W. Bennion:', *A Stochastic Model for Predicting Variations in Reservoir Rock Properties*, PhD thesis, Penn. State U., (1965).
- [30] L. K. Blacker:', “*An Analysis of Rate Sensitive Skin in Oil Wells*”, SPE 11187, presented at the 57th Annual Meeting of the Society of Petroleum Engineers held in New Orleans, LA, March, 1982.
- [31] T. L. Blanton:', “*An Experimental Study of Interaction Between Hydraulically Induced and Pre-Existing Fractures*”, SPE 10847, presented at the SPE Unconventional Gas Recovery Symposium held in Pittsburgh, PA, May, 1982.
- [32] T. L. Blanton:', “*A Field Test of the Strain Recovery Method of Stress Determination in Devonian Shales*”, SPE 12304, presented at the SPE Eastern Regional Meeting held in Champions, PA, 1983.
- [33] T. L. Blanton:', “*The Relation Between Recovery Deformation and In Situ Stress Magnitudes*”, SPE 11624, presented at the SPE Symposium on Low Permeability Gas Reservoirs held in Denver, CO, March, 1983.
- [34] P.T. Branagan, C. L. Cippola, and S. J. Lee:', “*Designing and Evaluating Hydraulic Fracture Treatments in Naturally Fractured Reservoirs*”, SPE 16434,

presented at the SPE/DOE Symposium on Low Permeability Gas Reservoirs held in Denver, CO, 1987.

- [35] K. E. Brown and J. F. Lea:, “*NODAL Systems Analysis for Oil and Gas Wells*”, *Journal of Petroleum Technology*, 1751–1763, (October 1985).
- [36] R. O. Brown, J. M. Forgotson, and J. M. Forgotson Jr.:', “*Predicting the Orientation of Hydraulically Created Fractures in the Cotton Valley Formation of East Texas*”, SPE 9269, presented at the 55th Annual Meeting of the Society of Petroleum Engineers held in Dallas, TX, September, 1980.
- [37] H. G. Byars and B. R. Gallop:', “*Injection Water + Oxygen = Corrosion and/or Well Plugging Solids*”, SPE 4253, presented at the Symposium on the Handling of Oilfield Waters held in Los Angeles, CA, December, 1972.
- [38] W. T. Cardwell and R. L. Parsons:', “*Average Permeabilities of Heterogeneous Oil Sands*”, *Transactions of the AIME*, 160:32–42, (1945).
- [39] H. C. Carslaw and J. C. Jaeger:', *Conduction of Heat in Solids*, Clarendon Press, Oxford, (1959).
- [40] P. Charlez, K. Saleh, and D. Despax:', “*The Fracmeter: A New Numerical Method to Evaluate the State of Stress and the Elastic Properties of Rocks*”, In *Proceedings of the 5th Middle East Oil Show*, pages 703–708, Society of Petroleum Engineers, Richardson, TX, (March 1987).
- [41] C. J. Chin:', *Simulation of Fractures Growing in Thermal or Pore-Pressure Induced Stress Fields*, Master’s thesis, Mass. Inst. of Tech., (January 1985).
- [42] C. J. Chin and M. P. Clary:', *Stresses In and Around Homogeneous Inclusions*, UFRAC Report REL-86-2, Mass. Inst. of Tech., (March 1986).
- [43] S. A. Christianovich and Yu. P. Zheltov:', “*Formation of Vertical Fractures by Means of Highly Viscous Fluids*”, In *Proceedings of the 4th World Petroleum Congress*, (1955).

- [44] H. Cinco-L., "Evaluation of Hydraulic Fracturing by Transient Pressure Analysis Methods", SPE 10043, presented at the SPE Intl. Petr. Exhibition and Tech. Symposium held in Beijing, China, March, 1982.
- [45] H. Cinco-L., H. J. Ramey Jr., and F. G. Miller., "Pseudoskin Factors for Partially Penetrating or Directional Wells", SPE 5589, presented at the 50th Annual Meeting of the Society of Petroleum Engineers held in Dallas, TX, 1975.
- [46] H. Cinco-L., H. J. Ramey Jr., and F. G. Miller., "Unsteady-State Pressure Distribution Created by a Well With an Inclined Fracture", SPE 5591, presented at the 50th Annual Meeting of the Society of Petroleum Engineers held in Dallas, TX, October, 1975.
- [47] H. Cinco-L. and F. Samaniego-V., "Determination of the Orientation of a Finite Conductivity Vertical Fracture by Transient Pressure Analysis", SPE 6750, presented at the 52nd Annual Meeting of the Society of Petroleum Engineers held in Denver, CO, October, 1977.
- [48] H. Cinco-L. and F. Samaniego-V., "Transient Pressure Behavior for a Well with a Finite Conductivity Vertical Fracture", *Society of Petroleum Engineers Journal*, 253-264, (August 1978).
- [49] H. Cinco-L., F. Samaniego-V., and A. N. Dominguez., "Unsteady-State Flow Behavior for a Well Near a Natural Fracture", SPE 6019, presented at the 51st Annual Meeting of the Society of Petroleum Engineers held in New Orleans, October, 1976.
- [50] H. Cinco-Ley and H. Z. Meng., "Pressure Transient Analysis of Wells With Finite Conductivity Vertical Fractures in Double Porosity Reservoirs", SPE 18172, presented at the 63rd Annual Meeting of the Society of Petroleum Engineers held in Houston, TX, October, 1988.
- [51] H. Cinco-Ley, H. J. Ramey Jr., F. Samaniego, and F. Rodriguez., "Behavior of Wells with Low-Conductivity Vertical Fractures", SPE 16776, presented at the

62nd Annual Meeting of the Society of Petroleum Engineers held in Dallas, TX, September, 1987.

- [52] J. A. Clark:, "*Prediction of Hydraulic Fracture Azimuth through Geological, Core and Analytical Studies*", SPE 11611, presented at the SPE/DOE Symposium on Low Permeability ~~Gas~~ Reservoirs held in Denver, CO, March, 1983.
- [53] J. B. Clark:, "*A Hydraulic Process for Increasing the Productivity of Oil Wells*", *Trans., AIME*, 186(1), (1949).
- [54] M. P. Cleary:, "*The Engineering of Hydraulic Fractures—State of the Art and Technology of the Future*", *Journal of Petroleum Technology*, 40:1(17260):13-21, (January 1988).
- [55] M. P. Cleary, S. K. Wong, V. M. Narendran, and A. Settari:, *General Solutions for Unsymmetric Unidirectional Fracture Propagation in Reservoir Structures*, Rept. of Res. in Mech. Matls. REL-82-10, Dept. of Mech. Engr., Mass. Inst. of Tech., (September 1982).
- [56] A. C. Correa and H. J. Ramey Jr.:', "*Application of the Unit Step Function to Unusual Well Test Problems*", SPE 18156, presented at the 63rd Annual Meeting of the Society of Petroleum Engineers held in Houston, TX, October, 1988.
- [57] J. W. Cox:, "*Long Axis Orientation in Elongated Boreholes and Its Correlation with Rock Stress Data*", 24th Annual SPWLA Logging Symposium and 9th CWLS Formation Evaluation, (June 1983).
- [58] S. Crampin:, "*Evaluation of Anisotropy by Shear- Wave Splitting*", *Geophysics*, 1(50):145-152, (January 1985).
- [59] S. Crampin:, "*A Review of Wave Motion in Anisotropic and Cracked Media*", *Wave Motion*, (3):343-391, (1981).

- [60] S. Crampin, E. M. Chesnokov, and R. G. Hipkin:, “*Seismic Anisotropy - The State of the Art*”, Proc. of the First Intl. Workshop on Seismic Anisotropy, (1984).
- [61] P. B. Crawford and R. E. Collins:, “*Estimated Effects of Vertical Fractures on Secondary Recovery*”, *Transactions of the AIME*, 201:192-196, (1959).
- [62] C. W. Crowe and S. S. Minor:, “*Acid Corrosion Inhibitor Adsorption and Its Effect on Matrix Stimulation Results*”, SPE 10650, presented at the SPE Formation Damage Symposium held in Lafayette, LA, 1982.
- [63] W. C. Cunningham and D. K. Smith:, “*Effect of Salt Cement Filtrate on Sub-surface Formations*”, *J. Petr. Tech.*, 259-264, (March 1968).
- [64] J. Van Dam:, “*Planning of Optimum Production for a Natural Gas Reservoir*”, *Journal of the Institute of Petroleum*, 54(531):55-67, (March 1968).
- [65] A. A. Daneshy, G. L. Slusher, P. T. Chisolm, and D. A. Magee:, “*In-Situ Stress Measurements During Drilling*”, *Journal of Petroleum Technology*, (13227):891-898, (August 1986).
- [66] D. R. Davies and T. O. H. Kulper:, “*Fracture Conductivity in Hydraulic Fracture Stimulation*”, *J. Petr. Tech.*, 40:5(17655), (May 1988).
- [67] M. Davis:, “*Production of Conditional Simulations via the LU Triangular Decomposition of the Covariance Matrix*”, *Mathematical Geology*, 19(2):91-98, (1987).
- [68] A. J. Desbarats:, *Stochastic Modeling of Flow in Sand-Shale Sequences*, PhD thesis, Stanford University, Stanford, CA, (1987).
- [69] C. V. Deutsch:, *A Probabilistic Approach to Estimate Effective Absolute Permeability*, Master's thesis, Stanford University, Stanford, CA, (March 1987).

- [70] T. L. Dobecki:, “*Hydraulic Fracture Orientation Using Passive Borehole Seismic~*”, SPE 12110, presented at the 58th Annual Meeting of the Society of Petroleum Engineers held in San Fransisco, CA, 1983.
- [71] T. Doe, K. Ingevald, L. Strindell, B. Haimson, and H. ~~Caarlson:~~, *Rock Mechanics From Research to Application*, chapter Hydraulic Fracturing and Overcoming Stress Measurements in a Deep Borehole at the Strata Test Mine, Sweden, pages 403–408, Mass. Inst. of Tech., Cambridge, MA, (June 1981).
- [72] D. A. T. Donohue, J. T. Hansford, and R. A. Burton:., “*The ~~Et~~ of Induced Vertically-Oriented Fractures on Five-Spot Sweep Efficiency*”, *Society of Petroleum Engineers Journal*, (1948):260–268, (September 1968).
- [73] A. B. Dyes, C. E. Kemp, and B. H. Caudle:., “*Effect of Fractures on Sweep-Out Pattern*”, *Transactions of the AIME*, 213:245–249, (1958).
- [74] H. Dykstra and R. L. Parsons:., *Secondary Recovery of Oil in the United States*, chapter The Prediction of Oil Recovery by Waterflooding, pages 160–174, API, (1950).
- [75] R. C. Earlougher Jr.:., *Advances in Well Test Analysis, Monograph Series 5*, Society of Petroleum Engineers of AIME, Dallas, TX, first edition, (1977).
- [76] B. A. Eaton and M. Smithey:., “*Formation Damage from Completion and Workover Fluids*”, SPE 3707, presented at the California Regional hfeeting held in Los Angeles, CA, 1971.
- [77] M. J. Economides and K. G. Nolte:., *Reservoir Stimulation*, Schlumberger Educational Services, Houston, TX, (1987).
- [78] S. Ekies, N. Hadinoto, and R. Raghavan:., “*Pulse-Testing of Vertically Fractured Wells*”, SPE 6751, presented at the 52nd Annual Meeting of the Society of Petroleum Engineers held in Denver, CO, 1977.

- [79] M. P. Ekstrom, Dahan, C. A., Min-Yi Chen, P. M. Lloyd, and D.J. Rossi:, "*Formation Imaging with Microelectrical Scanning Arrays*", 27th SPWLA Logging Symposium BB, (1986), Houston, TX.
- [80] J. L. Elbel:, "*Designing Hydraulic Fracturing for Efficient Reserve Recovery*", SPE 15231, presented at the SPE Unconventional Gas Symposium held in Louisville, KY, May, 1986.
- [81] L. F. Elkins and A. M. Skov:, "*Determination of Fracture Orientation from Pressure Interference*", *Transactions of the AIME*, 219:301-304, (1960).
- [82] J. R. Erickson and R. K. Waddell:, *Identification and Characterization of Hydrologic Properties of Fractured Tuff Using Hydraulic Tracer Tests, Test Well USW H-4*, Technical Report USGS/WRI-85-4066, USGS, Denver, CO, (1985).
- [83] J. D. Eshelby:, "*The Determination of the Elastic Field of an Ellipsoidal Inclusion and Related Problems*", *Proceedings, Royal Society*, 241:376-396, (1957).
- [84] M.A. Evans:, *Fractures in Oriented Cores from the Appalachian Basin*, Technical Report DOE/ET/12138-1341-Vol. 1, West Virginia University, Morgantown, WV, (January 1980).
- [85] M. J. Fetkovich and M. E. Vienot:, "*Shape Factor, $C(A)$, Expressed as a Skin, $S(C(A))$* ", (1984), SPE 13304.
- [86] R. J. Finley and J. C. Lorenz:, "*Significance of Drilling and Coring-Induced Fractures in Mesa Verde Core, Northwestern Colorado*", *American Association of Petroleum Geologist's Bulletin*, 71(5):556, (May 1987).
- [87] C. D. Fraser and B. E. Pettit:, "*Results of a Field Test to Determine the Type and Orientation of a Hydraulically Induced Formation Fracture*", *Journal of Petroleum Technology*, 463-466, (May 1962).
- [88] K. H. Frohne and C. A. Komar:, "*Offset Well Test: An Engineering Study of Devonian Shale Production Characteristics*", Intersociety Energy Conversion Engineering Conference held at Los Angeles, CA, (August 1982), 829177.

- [89] K. H. Frohne and J. C. Mercer:, “*Fmctured Shale Gas Reservoir Performance Study – An Offset Well Interference Field Test*”, *Journal of Petroleum Technology*, 36:2(SPE 11224):291–300, (February 1984).
- [90] E. I. Gal’perin:, “*The Polarization Method of Seismic Exploration*”, English translation(1984) D. Reidel Publishing Co., Nedra, Moscow, (1977).
- [91] L. W. Gelhar and C. L. Axeness:, “*Three-Dimensional Stochastic Analysis of Macmdispersion in Aquifers*”, *Water Resources Research*, 19(1):161–180, (February 1983).
- [92] D. T. Georgi:, “*GeometricalAspects of Borehole Images*”, 26th SPWLA Logging Symposium, (June 1985).
- [93] D. I. Gough and J. S. Bell:, “*Stress Orientations from Oil-Well Fractures in Alberta and Texas*”, *Canadian Journal of Earth Sciences*, 18:638–645, (1981).
- [94] K. W. Griffin:, “*Induced Fracture Orientation Determination in the Kuparuk Reservoir*”, SPE 14261, presented at the 60th Annual Meeting of the Society of Petroleum Engineers held in Las Vegas, NV, September, 1985.
- [95] A. C. Gringarten and H. J. Ramey Jr.:', “*Unsteady State Pressure Distributions Created by a Well With a Single-Infinite Conductivity Vertical Fractum*”, *Society of Petroleum Engineers Journal*, 347–360, (August 1974).
- [96] A. C. Gringarten and H. J. Ramey Jr.:', “*Unsteady-State Pressure Distributions Created by a Well With a Single Infinite-Conductivity Horizontal Fracture*”, *Society of Petroleum Engineers Journal*, 413–426, (August 1974).
- [97] A. C. Gringarten and H. J. Ramey Jr.:', “*The Use of the Point Source and Green’s Functions in Solving Unsteady-Flow Problems in Reservoirs*”, *Society of Petroleum Engineers Journal*, (October 1973).
- [98] A. C. Gringarten, H. J. Ramey Jr., and R. Raghavan:', “*Applied Pressure Analysis for Fractumd Wells*”, *Journal of Petroleum Technology*, 887–892, (July 1975).

- [99] A. C. Gringarten, H. J. Ramey Jr., and R. Raghavan:, “*Pressure Analysis for Fractured Wells*”, SPE 4051, presented at the **47th** Annual Meeting of the Society of Petroleum Engineers held in San Antonio, TX, October, 1972.
- [100] M. S. Gulati and G. P. Maly:, “*Thin-Section and Permeability Studies Call for Smaller Gravels in Gravel-Packing*”, *J. Petr. Tech.*, 107–112, (January 1975).
- [101] K. H. Guppy, H. Cinco-L., H. J. Ramey Jr., and F. Samaniego-V.:', “*Non-Darcy Flow in Gas Wells With Finite Conductivity Vertical Fractures*”, SPE 8281, presented at the 54th Annual Meeting of the Society of Petroleum Engineers held in Las Vegas, NV, September, 1979.
- [102] A. L. Gutjahr and L. W. Gelhar:, “*Stochastic Models of Subsurface Flow: Infinite Versus Finite Domains and Stationarity*”, *Water Resources Research*, 17(2):337–350, (1981).
- [103] H. H. Haldorsen and C. J. MacDonald:, “*Stochastic Modeling of Underground Reservoir Facies (SMURF)*”, SPE 16751, presented at the 62nd Annual Meeting of the Society of Petroleum Engineers held in Dallas, TX, September, 1987.
- [104] K. S. Hansen and W. R. Purcell:, “*Earth Stress Measurements in the South Belridge Oil Field, Kern County, California*”, SPE 15641, presented at the 61st Annual Meeting of the Society of Petroleum Engineers held in New Orleans, LA, October, 1986.
- [105] J. T. Hansford and D. A. T. Donahue:, “*The Relation of Multi-Well Vertical Fractures to Five-Spot Sweep Efficiency at Breakthrough*”, *Prod. Monthly*, 31(2), (1967).
- [106] J. M. Hanson:, *Evaluation of Subsurface Fracture Geometry Using Fluid Pressure Response to Solid Earth Tidal Strain*, Technical Report UCID-20156, Lawrence Livermore National Lab, (September 1984).

- [107] J. M. Hanson and L. B. Owen:, “*Fracture Orientation by the Solid Earth Tidal Strain Method*”, SPE 11070, presented at the 57th Annual Meeting of the Society of Petroleum Engineers held in New Orleans, LA, September, 1982.
- [108] M. E. Hanson, G. D. Anderson, R. L. Schaffer, D. N. Montan, B. Haimson, M. P. Cleary, and J. Riccio:, *LLL Gas Stimulation Program Quarterly Progress Report January through March, 1978*, Technical Report DOE/BC/10003-22, CER Corp., Las Vegas, NV, (May 1981).
- [109] E. Hardin and M. N. Toksoz:, “*Detection and Characterization of Fractures From Generation of Tube Waves*”, In *Transactions of the 26th SPWLA Logging Symposium*, SPWLA, Houston, TX, (June 1985).
- [110] C. M. Hart:, *Multiwell Experiment: Fracture Diagnostics*, Technical Report SAND-85-2401C, Sandia National Labs, Albuquerque, NM, (November 1985).
- [111] D. Hassan:, “*A Method for Predicting Fracture Azimuth and the Implications Thereto Improve Hydrocarbon Recovery*”, 33rd Annual CIM Petroleum Soc. Technical Meeting held at Calgary, Canada, (June 1983), CIM 82-33-19.
- [112] T. A. Hewett:, “*Fractal Distributions of Reservoir Heterogeneity and Their Influence on Fluid Transport*”, SPE 15386, presented at the 61st Annual Technical Conference and Exhibition held in New Orleans, LA, October, 1986.
- [113] S. P. Hichman and R. D. Barree:, “*Productivity Loss in Gas Condensate Reservoirs*”, SPE 14023.
- [114] S. H. Hickman, J. H. Healy, and M. D. Zoback:, “*In Situ Stress, Natural Fracture Distribution, and Borehole Elongation in the Auburn Geothermal Well*”, *J. Geophys. Res.*, (90):5497-5512, (1985).
- [115] S. A. Holditch, J. W. Jennings, and S. H. Neuse:, “*The Optimization of Well Spacing and Fracture Length in Low Permeability Gas Reservoirs*”, SPE 7496,

- presented at the 53rd Annual Meeting of the Society of Petroleum Engineers held in Houston, TX, October, 1978.
- [116] S. A. Holditch and W. L. Laufer:, “*The Analysis of Fractured Gas Wells Using Reservoir Simulation*”, SPE 7473, presented at the 53rd Annual Meeting of the Society of Petroleum Engineers held in Houston, TX, October, 1978.
- [117] S. A. Holditch, B. M. Robinson, and W. S. Whitehead:, “*Pre-Fracture and Post-Fracture Formation Evaluation Necessary to Characterize the Three-Dimensional Shape of a Hydraulic Fracture*”, SPE 14086, presented at the SPE International Meeting on Petroleum Engineering held in Beijing, China, 1986.
- [118] M. M. Honarpour, K. R. McGee, N.L. Maerefat, and B.Sharma:., “*Detailed Core Description of a Dolomite Sample from the Upper Madison Limestone Group*”, SPE 15174, presented at the SPE Rocky Mountain Regional Meeting held in Billings, MT, May, 1986.
- [119] D. R. Horner:, “*Pressure Buildup in Wells*”, In E. J. Brill, editor: ,*Proceedings*, Third World Petroleum Congress, Leiden, (1951).
- [120] O. P. Houze, R. N. Horne, and H. J. Ramey Jr.:., “*Infinite Conductivity Vertical Fracture in a Reservoir with Double Porosity Behavior*”, SPE 12778, presented at the SPE California Regional Meeting held in Long Beach, CA, April, 1984.
- [121] M. K. Hubbert and J. Riccio:, *Natural and Induced Fracture Orientation*, Technical Report DOE/BC/10003-22, CER Corp., Las Vegas, NV, (May 1981).
- [122] M. K. Hubbert and D. G. Willis:, “*Mechanics of Hydraulic Fracturing*”, *Trans., AIME*, 210:153-168, (1957).
- [123] M. R. Islam and A-E. K. Delhomme:., “*Reservoir Description of a Complex Heterogeneous Reservoir for Numerical Simulation Study*”, SPE 18312, presented at the 63rd Annual Meeting of the Society of Petroleum Engineers held in Houston, TX, October, 1988.

- [124] K. E. Brown *et al.*, *Technology of Artificial Lift Methods*, PennWell Publishing, Tulsa, OK, (1984).
- [125] J. Jensen:, *A Statistical Study of Reservoir Permeability Distributions*, PhD thesis, The Univ. of Texas at Austin, (1986).
- [126] D. H. Johnston:, “*VSP Detection of Fracture-Induced Velocity Anisotropy*”, *American Association of Petroleum Geologist’s Bulletin*:, 71(5):573, (June 1987).
- [127] A. G. Journel:, “*Geostatistics for Conditional Simulation of Orebodies*”, *Economic Geology*, 69(5):673–687, (1974).
- [128] A. G. Journel:, *Simulations Conditionnelles: Theorie et Pratique*, PhD thesis, University of Nancy, (1974).
- [129] A. G. Journel and F. G. Alabert:, “*Focusing on Spatial Connectivity of Extreme-Valued Attributes: Stochastic Indicator Models of Reservoir Heterogeneities*”, SPE 18324, presented at the 63rd Annual Meeting held in Houston, TX, October, 1988.
- [130] A. G. Journel, C. V. Deutsch, and A. J. Desbarats:, “*Power Averaging for Block Effective Permeability*”, SPE 15128, presented at the 56th California Regional Meeting held in Oakland, CA, 1986.
- [131] W. J. Karplus:, *Analog Simulation*, McGraw-Hill, New York, (1958).
- [132] J. Kikani and R. N. Horne:, “*Pressure Transient Analysis of Arbitrary Shaped Reservoirs With the Boundary Element Method*”, SPE 18159, presented at the 63rd Annual Meeting of the Society of Petroleum Engineers held in Houston, TX, October, 1988.
- [133] G. E. King, A. Anderson, and M. Bingham:, “*A Field Study of Underbalanced Pressures Necessary to Obtain Clean Perforations Using Tubing Conveyed Perforating*”, (1985), SPE 14321.

- [134] J. A. Klotz, R. F. Krueger, and D. S. Pye:, “*Effect of Perforation Damage on Well Productivity*”, *J. Petr. Tech.*, **1303–1314**, (November **1974**).
- [135] J. A. Klotz, R. F. Krueger, and D. S. Pye:, “*Maximum Well Productivity in Damaged Formations Requires Deep, Clean Perforations*”, SPE **4792**, presented at the SPE Formation Damage Symposium held in New Orleans, LA, **1974**.
- [136] C. A. Komar et al.:', “*Delineating a Subsurface Fracture System in a Petroleum Reservoir — An Experiment*”, *Journal of Petroleum Technology*, **531–37**, (May **1973**).
- [137] C. A. Komar, W. K. Overbey Jr., R. L. Rough, and W. G. Lambert:', “*Factors that Predict Fracture Orientation in a Gas Storage Reservoir*”, *Journal of Petroleum Technology*, **57(5):546–550**, (**1971**).
- [138] C. A. Komar and L. Z. Shuck:', “*Pressure Responses From Induced Hydraulic Fractures in Adjacent Wells Within a Petroleum Reservoir: An Experiment*”, *Journal of Petroleum Technology*, **951–53**, (August **1975**).
- [139] F. Kuchuk:', *Transient Flow in Elliptical Systems*, PhD thesis, Stanford U., Stanford, CA, (May **1978**).
- [140] F. Kuchuk and W. E. Brigham:', “*Transient Flow in Elliptical Systems*”, *Journal of Petroleum Technology*, (7488):**401–410**, (December **1979**).
- [141] L. L. Lacy:', “*Comparison of Hydraulic Fracture Orientation Techniques*”, SPE **13225**, presented at the **59th** Annual Technical Conference and Exhibition of the SPE of AIME held in Houston, TX, September, **1984**.
- [142] M. E. Lambert:', *A Statistical Study of Reservoir Heterogeneity*, Master's thesis, The Univ. of Texas at Austin, (**1981**).
- [143] T. J. Lasseter, J. R. Waggoner, and L. W. Lake:', *Reservoir Characterization*, chapter Reservoir Heterogeneities and Their Influence on Ultimate Recovery, pages **545–560**, Academic Press, New York, (**1986**).

- [144] J. Law:, “A Statistical Approach to the Interstitial Heterogeneity of Sand Reservoirs”: *Transactions of the AIME*, 155:202–222, (1944).
- [145] R. J. LeBlanc Sr.:', “Distribution and Continuity of Sandstone Reservoirs – Part I”, *J. Petr. Tech.*, 776–792, (July 1977).
- [146] R. J. LeBlanc Sr.:', “Distribution and Continuity of Sandstone Reservoirs – Part II”, *J. Petr. Tech.*, 793–804, (July 1977).
- [147] R. F. Lemon and H. J. Patel:', “Effects of Fracture and Reservoir Parameters on Recovery from Low Permeability Gas Reservoirs”, SPE 5111, presented at the 49th Annual Meeting of the Society of Petroleum Engineers held in Houston, TX, October, 1974.
- [148] J. J. M. Lewis:', “Outcrop-Derived Quantitative Models of Permeability Heterogeneity for Genetically Different Sand Bodies”, SPE 18153, presented at the 63rd Annual Meeting of the Society of Petroleum Engineers held in Houston, TX, October, 1988.
- [149] T. E. Libson, H. L. Vacca, and D. N. Meehan:', “Stratton Field, Texas Gulf Coast: A Successful Cased-Hole Re-Evaluation of an Old Field to Determine Remaining Reserves and Increase Production Level”, *Journal of Petroleum Technology*, 37(1):105–123, (January 1985).
- [150] S. Locke:', “An Advanced Method for Predicting the Productivity Ratio of a Perforated Well”, SPE 8804, presented at the SPE Formation Damage Symposium held in Bakersfield, CA, January, 1980.
- [151] A. Mantoglou and J. L. Wilson:', “The turning bands method for simulation of random fields using line generation by a spectral method”, *Water Resources Research*, 21(5):577–583, (1982).
- [152] R. P. McCann, R. G. Hay, L.C. Bartel, and J. Riccio:', *Massive Hydraulic Fracture Mapping and Characterization Program—First Annual Report*, Technical Report DOE/BC/10003-22, CER Corp., Las Vegas, NV, (May 1981).

- [153] B. W. McDaniel:, “*Conductivity Testing of Proppants at High Temperature and Stress*”, SPE 15067, presented at the 1986 California Regional Meeting held in Oakland, CA, April, 1986.
- [154] J. D. McLennann and J. C. Roegiers:, “*How Instantaneous are Instantaneous Shut-In Pressures?*”, SPE 11064, presented at the 57th Annual Meeting of the Society of Petroleum Engineers held in New Orleans, LA, September, 1982.
- [155] H. O. McLeod, Jr.:', “*The Effects of Perforating Conditions on Well Performance*”, SPE 10649, presented at the SPE Formation Damage Symposium held in Lafayette, LA, March, 1982.
- [156] D. N. Meehan:, “*Calculator Program Simplifies Hyperbolic Decline Curve Analysis*), *Oil and Gas Journal*, 79(18):247-250, (May 1981).
- [157] D. N. Meehan:, “*Calculator Simplifies Real Gas Potential Applications*”, *Petroleum Engineer International*, 55(10):70-74, (August, 1983).
- [158] D. N. Meehan:, “*A Correlation for Water Compressibility*”, *Petroleum Engineer International*, 52(13):125-126, (November 1980).
- [159] D. N. Meehan:, “*A Correlation for Water Viscosity*”, *Petroleum Engineer*, 117-118, (July 1908).
- [160] D. N. Meehan:, “*Crude Oil Viscosity Correlation*”, *Oil and Gas Journal*, 78(45):214-216, (Novenber 1980).
- [161] D. N. Meehan:, “*Decline Curve Confusion*”, *Oil and Gas Journal*, 80(17):59, (April 1982).
- [162] D. N. Meehan:, “*Enhanced Oil Recovery - Miscible Methods*”, *Sigma Four*, (8):16-17, (May 1981).
- [163] D. N. Meehan:, “*Enhanced Oil Recovery - Overview*”, *Sigma Four*, (7):5-7, (July 1980).

- [164] D. N. Meehan:, “*Enhanced Oil Recovery – Thermal Recovery Methods*”, *Sigma Four*, (9), (July 1981).
- [165] D. N. Meehan:, “*Exponential, Harmonic Declines Programmed for Calculators*”, *Oil and Gas Journal*, 95–100, (May 1980).
- [166] D. N. Meehan:, “*Forecast Made Easier for Developed Waterfloods*”, *Oil and Gas Journal*, 78(27):114–124, (July 1980).
- [167] D. N. Meehan:, “*Gas Composition Gives Pseudocritical Values*”, *Oil and Gas Journal*, 78(49):112–114, (December 1980).
- [168] D. N. Meehan:, “*Gas Well Performance Predicted*”, *Oil and Gas Journal*, 78(33):129–130, (August 1980).
- [169] D. N. Meehan:, “*GOR Change Estimated for Condensate Reservoirs*”, *Oil and Gas Journal*, 78(29):72–73, (July 1980).
- [170] D. N. Meehan:, “*Hyperbolic Oil Production Decline Analysis Programmed*”, *Oil and Gas Journal*, 52–56, (June 1980).
- [171] D. N. Meehan:, “*Improved Oil PVT Property Correlations*”, *Oil and Gas Journal*, 78(43):64–71, (October 1980).
- [172] D. N. Meehan:, *A Laboratory Study of Water Immobilization for Enhanced Oil Recovery*, Master’s thesis, University of Oklahoma, Norman, OK, (1976).
- [173] D. N. Meehan:, “*Multiwell Production Forecast by Calculator*”, *Oil and Gas Journal*, 78(25):152–154, (June 1980).
- [174] D. N. Meehan:, “*Petroleum Fluids Pac Solves Engineering Problems*”, *Petroleum Engineer International*, 54(1):104–109, (January 1982).
- [175] D. N. Meehan:, “*Program Determines Gas Constants*”, *Oil and Gas Journal*, 78(47):140–141, (November 1980).

- [176] D. N. Meehan:, “*Program for HP 67/97 Calculator Used to Find Hyperbolic Exponent*”, *Oil and Gas Journal*, 79(19):120–122, (May 1981).
- [177] D. N. Meehan:, “*Pseudotime Function Improves Gas Well Test Analysis*”, *Petroleum Engineer International*, 55(12):60–62, (October 1983).
- [178] D. N. Meehan:, “*Stabilized Flow Coefficient Calculated for Gas Wells*”, *Oil and Gas Journal*, 78(31):53–54, (August 1980).
- [179] D. N. Meehan:, “*Three New Programs Aid Decline Curve Analysis by Calculator*”, *Oil and Gas Journal*, 79(16):90–96, (April 1981).
- [180] D. N. Meehan, R. N. Horne, and K. Aziz:, “*The Effect of Reservoir Heterogeneity and Fracture Azimuth on Optimization of Fracture Length and Well Spacing*”, SPE 17606, presented at the SPE International Meeting on Petroleum Engineering held in Tianjin, China, November, 1988.
- [181] D. N. Meehan and W. K. Lyons:, “*Calculations Programmable for Gas Compressibility*”, *Oil and Gas Journal*, 77(41):74–78, (October 1979).
- [182] D. N. Meehan and B. F. Pennington:, “*Numerical Simulation Results in the Carthage Cotton Valley Field*”, *Journal of Petroleum Technology*, 34(9838):189–198, (January 1982).
- [183] D. N. Meehan and E. J. Schell:, “*An Analysis of Rate Sensitive Skin in Gas Wells*”, SPE 12176, presented at the Annual Meeting of the Society of Petroleum Engineers held in San Francisco, CA, September, 1983.
- [184] D. N. Meehan and E. L. Vogel:, *HP-41 Reservoir Engineering Manual*, PennWell Publishing, Tulsa, OK, first edition, (June 1982).
- [185] H-Z. Meng and K. E. Brown:, “*Coupling of Production Forecasting, Fracture Geometry Requirements and Treatment Scheduling in the Optimum Hydraulic Fracture Design*”, (1987), SPE 16435.

- [186] N. Morita, K. E. Gray, F. A. A. Srouji, and P. N. Jogi:, “*Rock Property Change During Reservoir Compaction*”, SPE 13099, presented at the 59th Annual Meeting of the Society of Petroleum Engineers held in Houston, TX, 1984.
- [187] N. A. Mousli, R. Raghavan, H. Cinco-L., and F. Samaniego-V.:', “*The Influence of Vertical Fractures Intercepting Active and Observation Wells on Interference Tests*”, *Society of Petroleum Engineers Journal*, 933–944, (December 1982).
- [188] M. Much and G. S. Penny:', “*Long-Term Performance of Proppants Under Simulated Reservoir Conditions*”, SPE 16415, presented at the Low Permeability Reservoirs Symposium held in Denver, CO, May, 1987.
- [189] T. W. Muecke:', “*Formation Fines and Factors Controlling Their Movement in Porous Media*”, *J. Petr. Tech.*, 144–150, (February 1979).
- [190] M. Muskat:', *The Flow of Homogeneous Fluids Through Porous Media*, J. W. Edwards, Inc., Ann Arbor, Michigan, (1946).
- [191] V. M. Narendran:', *Analysis of the Growth and Interaction of Multiple Plane Hydraulic Fractures*, PhD thesis, Mass. Inst. of Tech., (March 1986).
- [192] V. M. Narendran and M. P. Cleary:', “*Analysis of Growth and Interaction of Multiple Hydraulic Fractures*”, SPE 12272, presented at the Reservoir Simulation Symposium held in San Fransisco, CA, November, 1983.
- [193] V. M. Narendran and M. P. Cleary:', “*Elastostatic Interaction of Multiple Arbitrarily Shaped Cracks in Plane Inhomogenous Regions*”, *Eng. Frac. Mech.*, (1983).
- [194] S. Nelmat-Nasser and H. Horii:', “*Compression-Induced Non-Planar Crack Extension with Applications to Splitting, Exfoliation, and Rockburst*”, *J. Geophys. Res.*, 87:6805–6821, (1982).
- [195] A. B. Newman:', “*Heating and Cooling Rectangular and Cylindrical Solids*”, *Industrial and Engineering Chemistry*, 28:545, (May 1936).

- [196] K. G. Nolte and M. B. Smith:, “*Interpretation of Fracturing Pressure Decline*”, *Journal of Petroleum Technology*, **1761–1775**, (September **1981**). .
- [197] A. S. Odeh:, “*Steady-State Flow Capacity of Wells with Limited Entry to Flow*”, *SPE Journal*, **43–51**, (March **1968**).
- [198] D. S. Oliver:, “*Pressure Transients Caused By Fracturing*”, SPE **12735**, presented at the SPE California Regional Meeting held in Long Beach, CA, April, **1984**.
- [199] O. Olsson, L. Falk, E. Sandberg, S. Carlsten, and K. A. Magnusson:, *In Situ Experiments in Granite Associated With the Disposal of Radioactive Waste*, Report to the Nuclear Energy Agency, Swedish Geological Company, Uppsala, Sweden, (June **1985**).
- [200] P. Papatzacos:, “*Exact Solutions for Infinite-Conductivity Wells*”, *SPE Reservoir Engineering*, (**13846**):217–226, (May **1987**).
- [201] E. S. Pasternak and G. P. Goodwill:, “*Applications of Digital Borehole Televiewer Logging*”, **24th** Annual SPWLA Symposium, (June **1983**).
- [202] J. T. Patton:, “*Well Damage Hazards Associated with Conventional Completion Fluids*”, SPE 13800, (**1985**).
- [203] W. L. Penberthy Jr. and B. J. Cope:, “*Design and Productivity of Gravel Packed Completions*”, SPE **8428**, presented at the **54th** Annual Meeting of the Society of Petroleum Engineers held in Las Vegas, NV, **1979**.
- [204] A. E. Pierce, S. Vela, and K. T. Koonce:, “*Determination of the Compass Orientation and Length of Hydraulic Fractures by Pulse Testing*”, *Journal of Petroleum Technology*, **1433–1438**, (December **1975**).
- [205] R. A. Plumb and S. H. Hickman:, “*Stress-Induced Borehole Elongation: A Comparison Between the Four Arm Dipmeter and the Borehole Televiewer in*

- the Auburn Geothermal Well*”, *Journal of Geophysical Research*, 90:5513–5521, (1985):
- [206] R. A. Plumb and S. M. Luthi:, “*Application of Borehole Images to Geologic Modeling of an Eolian Reservoir*”, SPE 15487, presented at the 61st Annual Meeting of the Society of Petroleum Engineers held in New Orleans, LA, October, 1986.
- [207] D. D. Pollard and A. Aydin:, “*Progress in Understanding Jointing Over the Past Century*”, *The Geological Society of America Bulletin*, (March 1988).
- [208] A. W. M. El Rabaa and D. L. Meadows:, “*Laboratory and Field Applications of the Strain Relaxation Method*”, SPE 15072, (June 1986).
- [209] R. Raghavan, G. C. Cady, and H. J. Ramey Jr.:', “*Well Test Analysis for Vertically Fractured Wells*”, *Journal of Petroleum Technology*, 1014–1020, (August 1972).
- [210] H. J. Ramey Jr.:', “*Interference Analysis for Anisotropic Formations — A Case History*”, *Journal of Petroleum Technology*, 1290–1298, (October 1975).
- [211] H. J. Ramey Jr.:', “*Non-Darcy Flow and Wellbore Storage Effects in Pressure Buildup and Drawdown of Gas Wells*”, *Journal of Petroleum Technology*, 223–233, (February 1965).
- [212] H. J. Ramey Jr.:', “*Practical Use of Modern Well Test Analysis*”, SPE 5875, presented at the SPE California Regional Meeting held in Long Beach, CA, April, 1976.
- [213] H. J. Ramey Jr., B. Barker, N. Arihara, M. L. Mao, and J. K. Marques:', “*Pressure Transient Testing of Hydraulically Fractured Wells*”, In *Proceedings, American Nuclear Society, Colorado School of Mines, Golden, CO*, (April 1977).
- [214] H. J. Ramey Jr. and W. M. Cobb:', “*A General Pressure Buildup Theory for a Well in a Closed Drainage Area*”, *Journal of Petroleum Technology*, 1493, (December 1971).

- [215] N. K. Ren and J. C. Roiegers:, “*Differential Strain Curve Analysis—A New Method of Determining In-Situ Stress State from Rock Core Measurements*”, In *Proceedings*, International Society Rock Mechanics Congress, Melbourne, Australia, (April 1983).
- [216] J. Riccio:, *Preliminary Determination of the Spatial Geometry of Four Hydraulic Fractures at TES1: Site 17 Rock Springs, Wyoming*, Technical Report DOE/BC/1000/BC/10003-22, CER Corp., Las Vegas, NV, (May 1981).
- [217] L. F. Richardson:, “*The Deferred Approach to the Limit*”, *Transactions of the Royal Society of London*, A(226):299-361, (1927).
- [218] J. L. Rike:, “*The Relationship Between Clean Fluids and Effective Completions*”, SPE 9426, presented at the 55th Annual Meeting of the Society of Petroleum Engineers held in Dallas, TX, September, 1980.
- [219] L. P. Roodhart, T. O. H. Kuiper, and D. R. Davies:, “*Proppant Pack and Formation Impairment During Gas Well Hydraulic Fracturing*”, SPE 15629, presented at the 1986 SPE Annual Meeting held in New Orleans, LA, October, 1986.
- [220] P. Saksä:, *Radiometric, Electrical, and Acoustic Geophysical Borehole studies of the Loviisa Power Plant Site in 1983*, Technical Report JT-84-02, Voimayhtöiden Ydinjätetoimikunta, Helsinki, Finland, (January 1984).
- [221] J. P. Sarda:, “*Well-Linking by Hydraulic Fracturing: Problem of Hydraulic Fracture Orientation*”, *Bull. Soc. Geol. (France)*, 26:5:827-831, (1984).
- [222] C. L. Schuster:, “*Detection Within the Wellbore of Seismic Signals Created by Hydraulic Fracturing*”, SPE 7448, presented at the 53rd Annual Meeting of the Society of Petroleum Engineers held in Houston, TX, 1978.
- [223] P. P. Scott Jr., W. G. Bearden, and G. C. Howard:, “*Rock Ruptures as Affected by Fluid*”, *Transactions of the AIME*, 198:111, (1953).

- [224] A. Settari:, “*Simulation of Hydraulic Fracturing Processes*”, *Society of Petroleum Engineers Journal*, 487–500, (December 1980).
- [225] A. Settari and M. P. Cleary:, “*Development and Testing of a Pseudo-Three-Dimensional Model of Hydraulic Fracture Geomety (P3DH)*”, SPE 10505, presented at the Sixth SPE Reservoir Simulation Symposium held in New Orleans, LA, January, 1982.
- [226] A. Settari and H. S. Price:, “*Three-Dimensional Simulation of Hydraulic Fracturing*”, *Journal of Petroleum Technology*, 1177–1190, (July 1984).
- [227] B. Sharma, M. M. Honarpour, and M. J. Szpakiewicz:, “*Critical Heterogeneities in a Barrier Island Deposit and Their Influence on Primary Waterflood and Chemical EOR Operations*”, SPE 16749, presented at the 62nd Annual Meeting of the Society of Petroleum Engineers held in Dallas, TX, September, 1987.
- [228] R. W. Siegfried and G. Simmons:, “*Characterization of Oriented Cracks with Differential Strain Analysis*”, *J. Geophys. Res.*, 83:1269–1278, (1978).
- [229] G. Simmons, R. W. Siegfried, and M. Feves:, “*Differential Strain Analysis: A New Method for Examining Cracks in Rocks*”, *J. Geophys. Res.*, 79:4383–4385, (1974).
- [230] J. P. Simpson:, “*The Drilling Mud Dilemma-Recent Examples*”, *J. Petr. Tech.*, 201–206, (February 1985).
- [231] L. Smith and R. A. Freeze:, “*Stochastic Analysis of Steady-State Groundwater Flow in a Bounded Domain*”, *Water Resour. Res.*, 15(6):1543–1559, (1979).
- [232] M. B. Smith:, “*Est of Fracture Azimuth on Production with Application to the Wattenberg Gas Field*”, SPE 8298, presented at the 54th Annual Meeting of the Society of Petroleum Engineers held in Las Vegas, NV, September, 1979.
- [233] M. B. Smith, G. B. Holman, C. R. Fast, and R. J. Covlin:, “*The Azimuth of Deep, Penetrating Fractures in the Wattenberg Field*”, *Journal of Petroleum Technology*, (6092):185–193, (February 1978).

- [234] M. B. Smith and J. Riccio:, *Est* of Fracture Azimuth on Production with Application to the Wattenberg Gas Field, Technical Report DOE/BC/10003-22, CER Corp., Las Vegas, NV, (May 1981).
- [235] G. G. Sorrells and C. C. Mulcahy:, "Advances in the Microseismic Method of Hydraulic Fracture Azimuth Estimation", SPE 15216, presented at the SPE Unconventional Gas Symposium held in Louisville, KY, 1986.
- [236] H. Stehfest:, "Algorithm 368: Numerical Inversion of the Laplace Transform", *Communication of the A. C. M.*, 1(13), (August 1970).
- [237] J. M. Stock, J. H. Healy, S. H. Hickman, and Zoback M. D.:', "Hydraulic Fracturing Stress Measurements at Yucca Mountain, Nevada and Relationship to the Regional Stress Field", *Journal of Geophysical Research*, 90:8691-8706, (1985).
- [238] T. D. Streltsova:, *Well Testing in Heterogeneous Formations*, John Wiley & Sons, New York, first edition, (1988).
- [239] F. Strickland and N. Ren:', "Predicting the In Situ Stress for Deep Wells Using the Differential Strain Curve Analysis", SPE 8954, presented at the Unconventional Gas Recovery Symposium held in Pittsburgh, PA, 1980.
- [240] G. O. Suman Jr.:', "Perforations-A Prime Source of Well Performance Problems", *J. Petr. Tech.*, 399-411, (April 1972).
- [241] T. J. Taylor:', "Interpretation and Application of Borehole Televiewer Surveys", 24th Annual SPWLA Symposium, (June 1983).
- [242] L. W. Teufel:', "Determination of In Situ Stress from Anelastic Strain Recovery Measurements of Oriented Core", SPE 11649, presented at the SPE Symposium on Low Permeability Reservoirs held in Denver, CO, March, 1983.
- [243] L. W. Teufel:', "In Situ Stress Measurements in Inclined Holes in the North Sea: Application to Water Flooding and Enhanced Oil Recovery", SPE 13986,

presented at the European Offshore Conference held in Aberdeen, September, 1985.

- [244] L. W. Teufel:, “*In-Situ Stress State on the Mounds Test Well as Determined by the Anelastic Strain Recovery Method*”, SPE 13896, presented at the 1985 SPE/DOE Symposium on Low Permeability Gas Reservoirs held in Denver, CO, May, 1985.
- [245] L. W. Teufel:, “*Prediction of Hydraulic Fracture Azimuth from Anelastic Strain Recovery Measurements of Oriented Core*”, In *Proceedings of the 23rd U. S. National Rock Mechanics Symposium*, (1982).
- [246] L. W. Teufel, C. M. Hart, and A. R. Sattler:, “*Determination of Hydraulic Fracture Azimuth by Geophysical Geological, and Oriented-Core Methods at the Multiwell Experiment Site, Rifle, CO*”, SPE 13226. presented at the 59th Annual Technical Conference and Exhibition of the SPE of AIME held in Houston. TX, September, 1984.
- [247] J. K. Tison, R. G. Agarwal, M. J. Rosepiler. and B. W. Schlotman:, “*A Method for Selecting Potential Infill Locations in the East Texas Cotton Valley Gas Play*”, SPE 11022, presented at the 57th Annual Technical Conference and Exhibition held in New Orleans, LA, September, 1982.
- [248] A. Uraiet, R. Raghavan, and G. W. Thomas:, “*Determination of the Compass Orientation of a Vertical Fracture by Interference Tests*”, *Journal of Petroleum Technology*, 73–80, (January 1977).
- [249] C. P. J. W. van Kruysdijk:, “*Semianalytical Modeling of Pressure Transients in Fractured Reservoirs*”, SPE 18169, presented at the 63rd Annual Meeting of the Society of Petroleum Engineers held in Houston, TX, October, 1988.
- [250] R. W. Veatch Jr.:', “*Overview of Current Hydraulic Fracturing Design and Treatment Technology – Part 1*”, *Journal of Petroleum Technology*, 677–687, (April 1983).

- [251] R. W. Veatch Jr., "Overview of Current Hydraulic Fracturing Design and Treatment Technology - Part 2", *Journal of Petroleum Technology*, 853-864, (May 1983).
- [252] J. L. Ventura:, "Slator Ranch Field Optimization Study", *Journal of Petroleum Technology*, 37:8(12816):1251-1262, (July 1983).
- [253] O. J. G. Vetter and R. C. Phillips:, "Prediction of Deposition of Calcium Sulfate Scales Under Down-Hole Conditions", *J. Petr. Tech.*, 1299-1308, (October 1970).
- [254] N. R. Warpinski, J. A. Schmidt, and D. A. Northrop:, "In Situ Stresses: The Predominant Influence on Hydraulic Fracture Containment", *Journal of Petroleum Technology*, 34:653-664, (March 1982).
- [255] N. R. Warpinski and L. W. Teufel:, "In Situ Stresses in Low Permeability, Nonmarine Rocks", SPE 16402, presented at the SEE Symposium on Low Permeability Gas Reservoirs held in Denver, CO, May, 1987.
- [256] J. E. Warren and H. S. Price:, "Flow in Heterogeneous Porous Media", *Society of Petroleum Engineers Journal*, 153-169, (September 1961).
- [257] R. A. Wattenbarger and H. J. Ramey Jr.:', "Gas Well Testing With Turbulence, Damage and Wellbore Storage", *Journal of Petroleum Technology*, 877-887, (August 1968).
- [258] R. A. Wattenbarger and H. J. Ramey Jr.:', "Well-Test Interpretation of Vertically Fractured Gas Wells", *Journal of Petroleum Technology*, 625-632, (May 1969).
- [259] N.L. Watts, D. Ellis, A. P. Heward, G. Maier, and G. P. Mark.:', "Geologic Input to Enhanced Oil Recovery Project Planning in south Oman Watts", *American Association of Petroleum Geologist's Bulletin*, 70(5):661, (May 1986).
- [260] K. J. Weber.:', *Reservoir Characterization*, chapter How Heterogeneity Affects Oil Recovery, pages 487-544, Academic Press, (1986).

- [261] R. V. Westermarck and P. Scholes:, “*Fracture Identification in Openhole from a Cement Evaluation Tool*”, SPE California Regional Meeting, Ventura, CA, pp.601-607, (April 1987).
- [262] C. D. White:, *Representation of Heterogeneity for Numerical Reservoir Simulation*, PhD thesis, Stanford University, Stanford, CA, (1987).
- [263] C. D. White and R. N. Horne:, “*Computing Absolute Transmissibility in the Presence of Fine-Scale Heterogeneity*”, SPE 16011, presented at the Ninth SPE Reservoir Simulation Symposium held in San Antonio, TX, February, 1987.
- [264] R. Wiley:, “*Borehole Televiewer-Revisited*”, 21st Annual SPM’LA Symposium. (1980), HH.
- [265] C. M’ittrisch and J. P. Sarda:, “*New Method for Determining the Direction of a Hydraulic Fracture*”.
- [266] hl. D. Wood:, “*Method of Determining Change in the Subsurface Due to Applications of Fluid Pressure to the Earth*”, U. S. Patent 4,271,696, (June 1981).
- [267] M. D. Wood:, *Preliminary Report*, Technical Report Contract E(49-18)-2257, ERDA, (May 1976).
- [268] J. Zemanek and R. L. Caldwell:, “*The Borehole Televiewer-A New Logging Concept for Fracture Location and Other Types of Borehole Inspection*”, *J. Petr. Tech.*, (June 1969).
- [269] M. D. Zoback, D. Moos, L. Mastin, and R. N. Anderson:, “*Well Bore Breakouts and In Situ Stress*”, *J. Geophys. Res.*, 90:5523-5530, (1985).
- [270] hl. D. Zoback, D. Moss: B. Coyle, and R. W. Anderson:, “*In-Situ and Physical Property Measurements in Appalachian Site Survey Holes*”, *American Association of Petroleum Geologists Bulletin*, 70:666, (1986).